ION GENERATION, ELECTRON ENERGY DISTRIBUTIONS, AND PROBE MEASUREMENTS IN A LOW PRESSURE ARC

by

SOL AISENBERG

B.S., Brooklyn College

(1951)

SUBMITTED IN PARTIAL FULFILLMENT OF THE REQUIREMENTS FOR THE DEGREE OF DOCTOR OF PHILOSOPHY

at the

MASSACHUSETTS INSTITUTE OF TECHNOLOGY

May 1957

Signature of Author . . . . . .
Department of Physics, May 13, 1957

Certified by . . . . . .
Thesis Supervisor

Accepted by . . . . . .
Chairman, Departmental Committee on Graduate Students

Physics
Thesis
1957

ION GENERATION, ELECTRON ENERGY DISTRIBUTIONS, AND PROBE MEASUREMENTS IN A LOW PRESSURE ARC

by

Sol Aisenberg

Submitted to the Department of Physics on May 13, 1957 in partial fulfillment of the requirements for the degree of Doctor of Philosophy.

ABSTRACT

A series of Langmuir probe measurements have been made on the plasma of a low pressure mercury arc in order to obtain information about some of the fundamental processes in the plasma. It is shown that the actual ionziation is many times larger than the direct ionization, and that the effect of the electron drift velocity on the direct ionization is negligible. The results of this research plus the limited information available in the literature indicate that the metastable density is independent of the electron density, and that the cumulative ionization is a linear function of the electron density and not a quadratic one. The effective cross-section for ionization of the 6^3P states is calculated to be at least 9.0 times larger than that for the ground state. The mobility of the electrons in the plasma was measured and it is found that the effective cross-section for slow electrons in the plasma is essentially constant with an average value of 42×10^{-16} cm^2. The ambipolar diffusion coefficient and the ambipolar mobility coefficient are determined as a function of E/p_o for an active plasma. With the aid of a specially developed theory for ion mobility and diffusion in a strong nonuniform electric field, the mobility and longitudinal diffusion coefficients are calculated for Hg ions in the plasma. The effective cross-section for Hg ions is found to increase from 31 to 104×10^{-16} cm^2 as the ion energy is increased from 0.44 to 1.37 electron volts. There is reasonable agreement with the limited data of others. The theories and methods developed can be used for the measurement of ion cross-section in other gases. A study is made of the collection of positive ions by a negative probe for comparison with theory. Several new experimental techniques are introduced. The partial pressures of the residual gases in the arc were in the 10^{-8} to 10^{-7} mm Hg range and were measured while the arc was in operation in the water bath. The probe potential was supplied by a specially designed low impedance voltage source featuring a high degree of negative feedback. A new method is developed to permit the change of probe work-function to be directly recorded as a function of time, and may prove useful in future experiments.

Thesis Supervisor: W. B. Nottingham

Title: Professor of Physics

Table of Contents

Table of Figures

Appendix

I. Theory of Probe Measurements

A. Introduction

The theory of probe measurements of arc plasmas was first developed by Langmuir and Mott-Smith[1, 2, 3] and made possible the determination of many of the fundamental properties of the plasma[4, 5]. The Langmuir probe method is very powerful because it yields the plasma potential V_p, the electron temperature T_-, (for the range of electron energies where the electron velocity distribution is Maxwell-Boltzmann), and the electron density n_-. Because of the low potential gradients existing in the plasma (of the order of 1 volt per centimeter) the ion and electron densities are very closely equal in the plasma (to within about 0.001 per cent) and therefore the Langmuir probe measurements will also yield the plasma ion densities n_+.

The basic theory of the Langmuir probe method is as follows. When the probe potential is slightly positive with respect to the plasma potential, the current to the probe i_p, is predominantly electron current and is relatively independent of the probe potential. For a spherically symmetric electron velocity distribution, the saturation electron current density J_{-s}, is equal to the random electron current density and is thus proportional to the product of the electron density n_-, and the average electron velocity $\langle v_- \rangle$. As the probe potential is made negative with respect to the plasma potential, the electron current to the probe is reduced because of the retarding field acting on the electrons, and the ion current is increased until the probe current is predominantly ion current and is again relatively independent of the probe potential. The electron current i_-, is found from the probe current i_p, and the

extrapolated ion current i_+, and is used to determine the electron temperature and the electron density. For the case where the electron velocity distribution is Maxwell-Boltzmann (M-B), a plot of $\log_{10} i_-$ vs the collector potential V_c, will be linear with a slope $d\log_{10} i_-/dV_c$ equal to $2.303\, q/kT_-$ where q/k is the ratio of the electron charge to Boltzmann's constant and is equal to 11,606 degrees absolute per volt. The plasma potential V_p, is usually taken as the intersection (on the semilogarithmic plot) of the saturation electron current extrapolation and the extrapolation of the linear part of the retarding potential plot. The average electron velocity $\langle v_- \rangle$ found from the electron temperature is used to calculate the electron density.

B. Current density to a planar retarding probe

A useful expression will be given for the electron current density J_-, to a retarding planar probe for a common class of distribution functions. In general:

$$J_- = q \int_{v_o}^{\infty} \int_{-\infty}^{\infty} \int_{-\infty}^{\infty} v_x f(\vec{v})\, dv_y\, dv_z\, dv_x \qquad \text{(I-1)}$$

where J_- is the electron current density in the +x direction (charge per unit area per unit time), v_x is the electron velocity in the x direction, and $f(\vec{v})$ is the density of electrons in phase space. The velocity v_o is defined by: $m_- (v_o)^2/2 = qV$ where m_- and q are the electron mass and charge, and $V(V > 0)$ is the retarding potential of the probe with respect to the plasma. This expression states that only electrons with velocities in the +x direction that are larger than v_o will be able to overcome the retarding potential and be collected. For the case of a spherically symmetric velocity distribution function (or for the leading

spherically symmetric term of the spherical harmonic expansion in velocity space), $f(\vec{v}) = f_o(v)$ where $v^2 = v_x^2 + v_y^2 + v_z^2 = v_x^2 + v_r^2$, and the multiple integral may be reduced by change of variable and integration by parts to the relatively simple expression:

$$J_- = \frac{q}{4} \int_{v_o}^{\infty} v \left(1 - \frac{v_o^2}{v^2}\right) f_o(v)\, 4\pi v^2\, dv \qquad \text{(I-2)}$$

When there is no retarding field, then $v_o = 0$, and the saturation or random current density for an arbitrary spherically symmetric distribution function is thus shown to be:

$$J_s = q\, \frac{n \langle v_- \rangle}{4} \qquad \text{(I-3)}$$

where $\langle v_- \rangle$ is the velocity averaged over the distribution function. The distribution function averaging operator is defined by:

$$\langle A \rangle = \frac{1}{n} \int_{-\infty}^{\infty} \int_{-\infty}^{\infty} \int_{-\infty}^{\infty} A f(\vec{v})\, dv_x\, dv_y\, dv_z \qquad \text{(I-4)}$$

If the distribution function is of the general form $f(v) = A \exp(-B v^s)$, the integral may be expressed in closed form in terms of incomplete gamma functions. There are, however, two important distribution functions, the Maxwell-Boltzmann distribution ($s = 2$), and the Druyvesteyn distribution[6, 7, 8] ($s = 4$), which yield values of J_- that can be expressed in terms of exponential functions and error functions.

C. Probe current for the case of a Maxwell-Boltzmann distribution and for a Druyvesteyn distribution

A M-B distribution function:

$$f(v) = n_- \left(\frac{m_-}{2\pi k T_-}\right)^{3/2} \exp\left(\frac{-m_- v^2}{2 k T_-}\right) \qquad \text{(I-5)}$$

gives the following result for the current density to the probe:

$$J_- = q \frac{n_-}{4} \left(\frac{8}{\pi} \frac{q}{m_-} \frac{k T_-}{q}\right)^{1/2} \exp\left(-\frac{q V}{k T_-}\right) \qquad \text{(I-6)}$$

where the constant $(8q/\pi m_-)^{1/2}$ is equal to 6.693×10^5 (meters/second)/(electron volt)$^{1/2}$. Thus a measurement of the current to the probe and the saturation electron current density, plus the value of the electron temperature obtained from the slope of the retarding potential plot will permit the determination of n_-. The M-B distribution is the one which results when the electron-electron interactions are predominant and when the effect of the field, gas atoms, ions, and boundaries can be neglected.

On the other hand, the Druyvesteyn distribution[6, 7, 8] is the leading term of the solution (in spherical harmonic form in velocity space) of the Boltzmann transport equation, and corresponds physically to the following assumptions: 1. electrons move under the influence of the field in the gas; 2. electron-electron and electron-ion interactions are negligible in comparison with the electron-gas interactions; 3. electron-gas collisions are elastic; 4. gas temperature is low compared to the electron temperature; 5. electron mean free path is

independent of electron velocity (hard sphere model for gas atoms). Some of these assumptions are of course subject to question: inelastic collisions occur for high energy electrons, and the electron cross-section in Hg is quite velocity dependent for the faster electrons. In addition, since the electron-electron interactions for slow electrons are much stronger than for fast electrons[9], it is expected that the slow electrons will tend toward a M-B distribution. The theoretical normalized retarding potential plot for the D-D (Fig. VI-1) will show the extreme case when the processes leading to a D-D are predominant.

The D-D is given by:

$$f(v) = \frac{n_-}{\pi\,\Gamma\left(\frac{3}{4}\right)}\left(\frac{\Gamma\left(\frac{5}{4}\right)}{\Gamma\left(\frac{3}{4}\right)}\right)^{3/2}\left(v_{rms}\right)^{-3}\exp\left[-\left(\frac{\Gamma\left(\frac{5}{4}\right)}{\Gamma\left(\frac{3}{4}\right)}\right)^{2}\frac{v^4}{v_{rms}^4}\right] \qquad \text{(I-7)}$$

where $\Gamma(k)$ is the complete gamma function, n_- is the electron density in configuration space, and v_{rms} is the root-mean-square velocity corresponding to the average energy of the distribution function. It should be noted that the number of high energy electrons drop off much faster for the D-D than for the M-B distribution.

The probe current density corresponding to the D-D is given in normalized form by:

$$\frac{J(D\text{-}D)}{J_{sat}} = \exp\left(-y_o^2\right) - (\pi)^{1/2}\, y_o\, \operatorname{erfc} y_o \qquad \text{(I-8)}$$

where $y_o = \left[\Gamma(5/4)/\Gamma(3/4)\right] V/\bar{V} = 0.7397\ V/\bar{V}$, $\bar{V}$ is the average energy of the D-D in electron volts, V is the retarding potential, and

$$\operatorname{erfc} y_o = 1 - \operatorname{erf} y_o = 1 - 2(\pi)^{-1/2}\int_0^{y_o} e^{-t^2}\,dt \qquad \text{(I-9)}$$

The value of the saturation current density for the D-D is given by:

$$J_{SAT} = q \frac{n_-}{4} \frac{v_{rms}}{\left(\Gamma\left(\frac{3}{4}\right)\Gamma\left(\frac{5}{4}\right)\right)^{1/2}} \qquad \text{(I-10)}$$

The ratio of saturation current for the D-D to the saturation current for the M-B distribution of the same electron density and same average energy is equal to 1.030. For the purpose of comparison with each other and with experiment, normalized probe curves for both distributions are given in Fig. VI-1.

D. Method for the direct determination of the distribution function from probe measurements

It was shown by Druyvesteyn[10] (and earlier by Mott-Smith and Langmuir[3] for a spherical collector) that there is a simple relationship between the distribution function f(v), and the second derivative (with respect to the retarding potential V) of the electron current to a retarding planar, cylindrical or spherical probe. This relationship can be obtained from Eq. I-2 by double differentiation with respect to the potential V which is implicitly contained in the definition of v_o. The result is:

$$\frac{d^2 J_-}{dV^2} = 2q\left(\frac{q}{m_-}\right)^2 f(v) \qquad \text{(I-11)}$$

Numerical or graphical differentiation of the J_- vs V data will yield very inaccurate results because the process of differentiation will magnify the relative effects of any small errors or fluctuations, and a second differentiation will further increase the uncertainty. The

use of more than three points in the determination of d^2J_-/dV^2 will reduce the error but not appreciably. Medicus[11] has recently developed a convenient graphical method for determining the distribution function from very accurate probe data but his method does not prevent an amplified error in the second derivative. Direct measurement of the second derivative is possible through the use of harmonic analysis but it is necessary to separate electrically the electron current from the ion current if the high energy electrons are of interest. The theory of the determination of the distribution function through harmonic analysis will be developed in Chapter VI along with a discussion of the limitations of the various methods plus suggestions for an improved method. In the present research the distribution function was not measured.

E. Utilization of the probe measurements

The basic data obtained from the probe measurements consist, in part, of a set of electron densities, electron temperatures, plasma potentials, and probe currents for each probe at a given value of bath temperature T_b, and arc current I_z. This data will yield the average electron density $\overline{n_-}$, (averaged over a cross-section of the cylindrical plasma) provided that a reasonable representation can be assumed for the radial electron density distribution. The basic data will also give the axial potential gradient E_z, and the total ionization per unit volume. This total ionization can be compared with the computed direct ionization to demonstrate that the total ionization is much larger than the direct ionization component. Information can be obtained about the dependence of the total ionization upon the electron temperature and the electron density.

The electron and ion mobilities will also be calculated in Chapter V. Knowledge of the axial current density J_z, and the axial potential gradient E_z, plus the average electron density will yield the values of the electron mobility μ_-, as a function of the discharge parameters and will also give the equivalent cross-section for scattering of slow electrons in mercury. If the requirements for ambipolar diffusion are assumed to be approximately satisfied, the ambipolar diffusion coefficient D_a, can also be calculated.

If the radial electron density distribution can be assumed accurately enough, the radial density gradient at the plasma edge can be calculated from the measured electron density at the center n_{-o}, and from the measured electron density at the plasma edge n_{-w}. The radial potential gradient E_r, can then be calculated from the electron temperature and the Boltzmann density distribution law relating the potential and the density. This value of E_r in conjunction with the ion density and the ion current to the wall at floating potential will give information about the motion of ions in the plasma. A simple model for ion flow in strong electric fields will permit the calculation of the ion mobility and the diffusion coefficient.

From the measured retarding potential plots, information can be obtained about a dimensionless form of the retarding potential plots. The mechanism of ion collection by a negative probe will also be investigated.

Chapter II will describe the experimental conditions and the precautions used in making the measurements. Chapter III will present the basic results and will show some of the corrections necessary before the arc parameters are specified.

II. Apparatus and Measuring Technique

A. Discharge tube and water bath

The probe measurements were made in the plasma of a low pressure mercury arc in a pyrex envelope. An auxiliary arc (with a current I_v of about 5 amps) was produced between a mercury pool cathode and a vertical anode. The main arc in the horizontal side arm (which carried a current I_z of about 5 amps) supplied the plasma to be measured. The use of the side arm helped to isolate the plasma from the effects of the jets of mercury vapor given off by the cathode spot and from the high energy electrons produced by the potential drop across the cathode sheath. The anodes are hollow nickel cylindrical cans mounted on 80 mil tungsten rod with the open ends facing towards the plasma. Hollow anodes were used instead of disk anodes to minimize the effects of fluctuating anode spots. The horizontal arm consisted of a pyrex cylinder of 5.5 cm inside diameter with a wall thickness of 0.24 cm. The horizontal plasma was about 38 cm long. Figure II-1a shows the discharge tube in more detail.

The mercury vapor pressure was controlled through immersion of the complete discharge tube in a constant temperature water bath. The mercury pressure in the arc is thus the vapor pressure of clean mercury at this bath temperature with a small correction of 1 to 2 degrees C because of the thermal drop in the pyrex wall. The bath temperature was varied from 25.1°C to 62.6°C to within 0.1°C which corresponds to a vapor pressure uncertainty of about 0.8 per cent. This control was obtained through the use of copper cooling coils with circulating cold water, plus a mercury thremoregulator controlling immersion heaters totaling 2 kilowatts. Two stirrers were used to

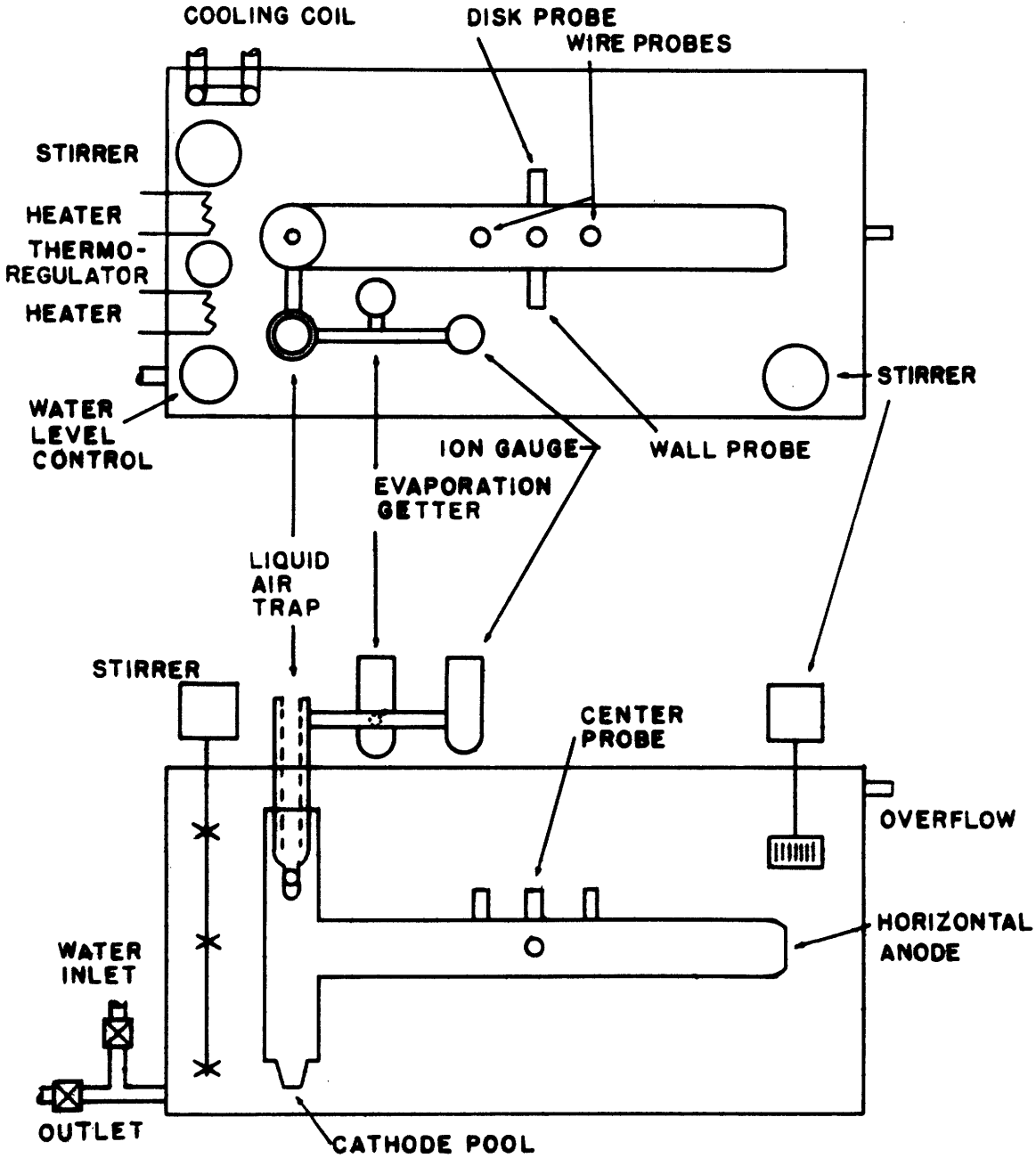

Fig. II-1

Tube and water bath

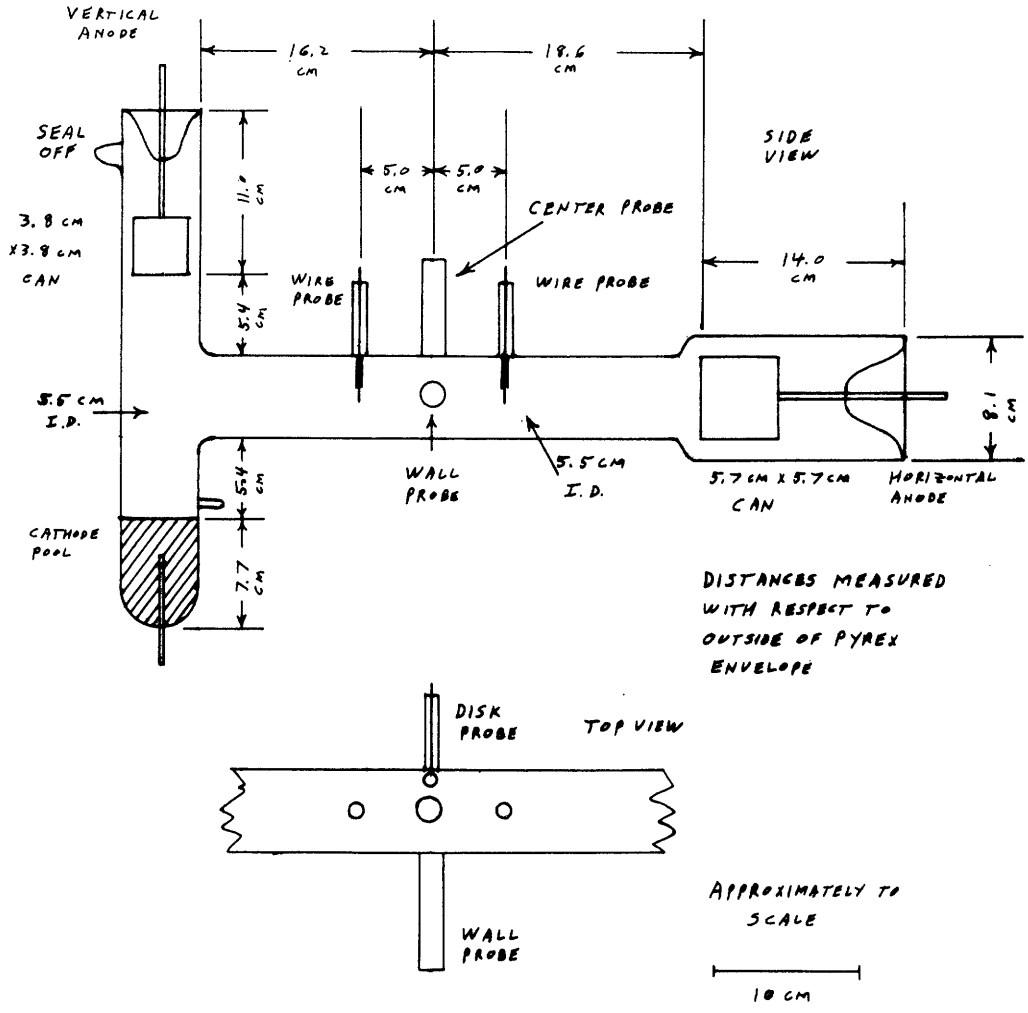

Fig. II-1a

Detailed drawing of discharge tube

keep the water in strong motion so as to reduce thermal gradients and to keep the bath temperature uniform. More information about the tube and bath is available in Fig. II-1.

B. Auxiliary equipment used to monitor and measure low residual gas pressures

A novel feature which was added to the usual discharge tube was a re-entrant liquid air trap in series with a Bayard-Alpert[12] type ionization gauge, and an "evaporated metal" getter tube. The liquid air trap permitted the mercury vapor component to be frozen out so that the ionization gauge could measure the partial pressure of the non-condensable residual gases while the discharge tube was on the vacuum system and also while the discharge tube was in operation in the water bath. In addition, the liquid air trap served to "pump" any condensable gases in the arc and thus helped to improve the vacuum. The tubulation connecting the trap and the tube was built with two slight constrictions, one before and one after a well designed to contain some mercury. This supply of mercury between the tube and the trap served to reduce the mercury pumping action of the trap. Unfortunately, the liquid air trap needed refilling about every four hours and even more frequently if a virtual leak was to be avoided. A re-entrant liquid air trap was necessary in order to prevent the trap from filling with mercury. The bottom of the trap was connected to the discharge tube so that the consensed mercury could return by gravity flow to the main tube whenever the trap was allowed to warm up. The liquid air was introduced at least 6 hours before measurements were made.

A specially designed ionization gauge control circuit (M.I.T. Research Laboratory of Electronics drawings number D-1607-1, A-1608-1 and A-1609-1) was used with the ionization gauge to measure the residual gas pressure and to display it on a 1 milliampere chart recorder. This procedure made the history of the background pressure available to aid in the vacuum processing of the tube and also permitted the anticipation of a virtual leak due to the lowering of the liquid air level. An overpressure protector was used to prevent the burnout of the ionization gauge filaments as a result of the loss of liquid air.

The getter tube contained 10 mil filaments of Mo, Ta, and W which were used to evaporate clean metal surfaces on the pyrex walls for the absorption of contaminating gases. The evaporation filaments were operated with current pulses of about 1 second duration every 6 seconds in order to reduce the heating of the filament supports and the consequent evolution of unwanted gas. The ionization gauge cleanup helped to remove residual gases in addition to the cleanup of the discharge tube itself.

As a result of all these inovations and precautions, it was possible to make measurements in a mercury plasma with a known residual gas pressure ranging from about 4×10^{-8} mm Hg to 4×10^{-7} mm Hg (nitrogen equivalent). If better vacuum is desired in future experiments, it is suggested that a vacuum system be connected to the discharge tube while it is in the water bath.

C. Probes

Five probes were built into the discharge tube: two tungsten wire probes and three tantalum planar probes. The wire probes

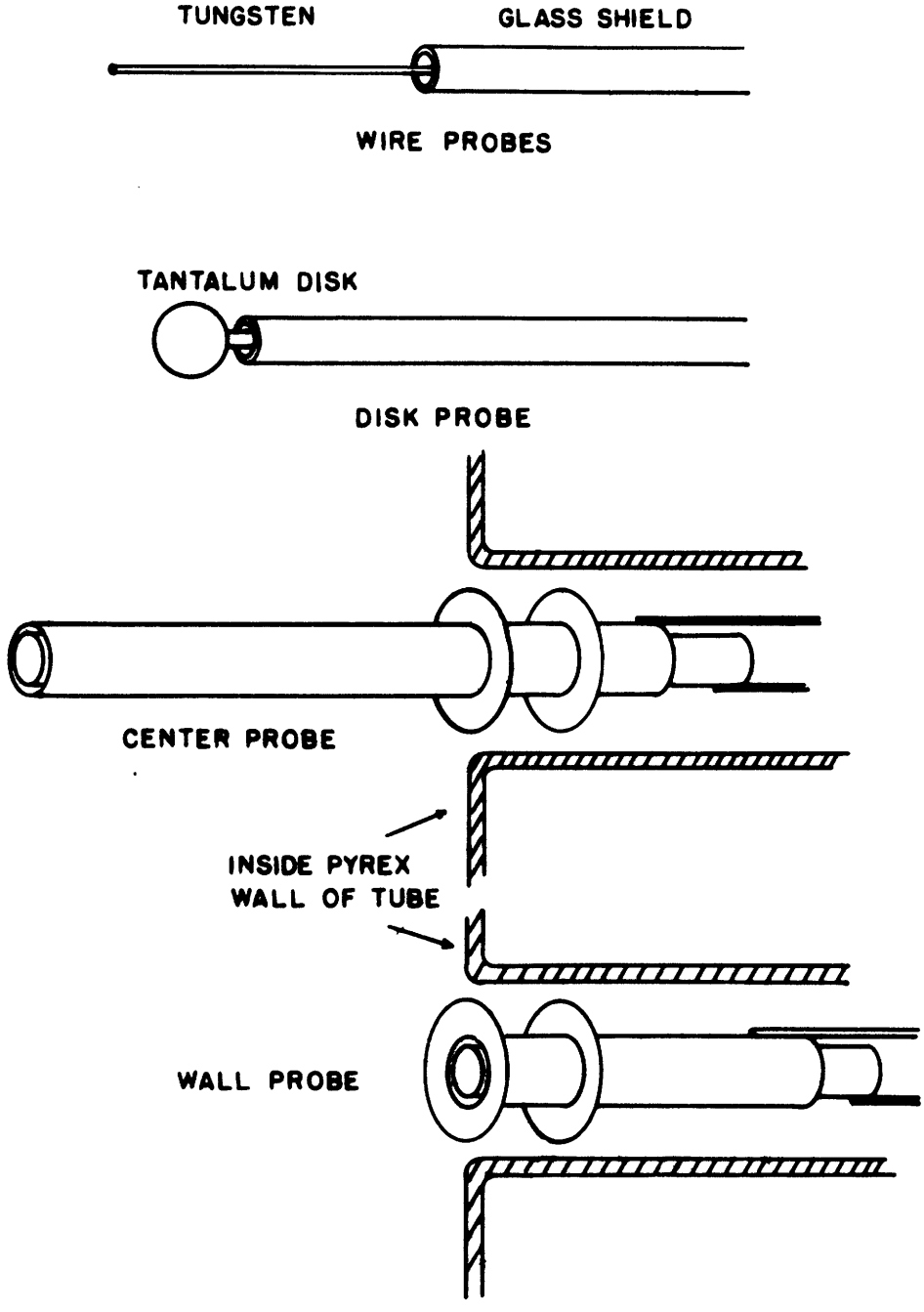

Fig. II-2

Probes

consisted of 29 mil diameter W wire with glass tubing shielding all but 0.98 cm. They were mounted in the center of the horizontal cylinder with a 10 cm separation in the axial direction and with the probe axis coincident with a diameter of the cylinder. Since the radial potential and charge density gradients are small at the center of the discharge tube, the wire probes were in a uniform region. An alternate way of positioning the wire probes would be to mount them with their axis coincident with the cylinder axis. In this way, the effect of the axial drift electron current would be reduced, but the effect of the axial potential gradient (which is about 0.3 volts/cm) would result in rounding of the retarding potential plot near plasma potential and would cause considerable uncertainty in the measured axial potential gradient.

The disk probe consisted of a disk of 3 mil tantalum sheet about 4 mm diameter, mounted on 30 mil tungsten wire with a glass shield around the wire to limit the collection area to both sides of the disk only. In order to eliminate the effects of axial and radial drift currents, the plane of the disk is located in a plane defined by the cylinder axis and a diameter. The center of the disk is located about 6 mm in from the inner wall of the tube.

The center probe is somewhat more complicated and is illustrated in Fig. II-2. It was mounted in the center of the cylinder with its plane located in the plane determined by the cylinder axis and a diameter. This probe was originally designed and constructed to permit the ion and electron components of the probe current to be separately measured, and consists of three concentric cylinders of 3 mil Ta sheet, plus a 30 mil W wire mounted axially. The outermost cylinder acts as a

shield while the next innermost cylinder supports a disk of about 4 mm diameter with a 23 mil hole punched in it. The next smallest cylinder and the W wire are situated within these two cylinders and are designed to permit a transverse electric field to separate the ions and electrons passing through the hole in the disk face. The alignment of the concentric cylinders was somewhat of a problem because of the small radial separations (about 25 mils) and because the clearance of the two innermost cylinders could not be checked visually. This problem was solved by using aluminum foil spacers to maintain the required clearance during assembly and then disolving the aluminum out with hydrochloric acid.

Maintenance of this separation was more difficult because the large length of the cylinders made it possible for a small angular displacement of about 1 degree at the press to cause a short circuit. Unfortunately a short circuit did occur between the wire and the next cylinder after the tube had been processed and was in operation in the water bath. Such a possibility had been anticipated, however, and therefore the probe was designed to permit its use as a regular planar probe in spite of such a short circuit.

The wall probe is the same as the center probe except that the two innermost elements were not included, and the probe is mounted with its face flush with the tube wall. The cylinders were made on the same mandrils and the face disks were punched with the same jewelers punch.

The Ta probe elements were cleaned and degassed in the usual ways and then were preoutgassed by electron bombardment with

1,000 volt electrons until the pressure was 10^{-9} mm Hg. They were then sealed off under vacuum to keep them gas free until just before assembly. The areas of the probes are listed below for reference.

Probe	Area
wire probes	0.227 cm^2
disk probe (both faces)	0.280 cm^2
center face probe	0.137 cm^2
wall face probe	0.137 cm2

D. Vacuum Processing

After the pyrex envelope was cleaned and the probes were sealed in, the discharge tube was sealed on the vacuum system along with two mercury stills. The tube and the smaller still were baked at 450°C while the larger still outside the oven and its charge of triple distilled clean mercury were torched out. Mercury from the outer still was then distilled over into the smaller still and the outer still was then sealed off. Some mercury from the inner still was then distilled over into the discharge tube and the arc was started with a high voltage sparker.

The anodes were operated at overload currents until the anodes were red hot. The probe elements were heated white hot by electron bombardment by connecting them in series with current limiting resistors to a high voltage, high current dc line. The ionization gauge elements were again outgassed by electron bombardment, and the evaporation filaments were again outgassed and slightly evaporated. This outgassing procedure was repeated several times until the

pressure with the arc in operation was in the 10^{-9} mm Hg range as measured with the ionization gauge. The glass sealoff constriction was preoutgassed and softened in preparation for sealoff of the discharge tube. After sealoff and after some pulsed operation of the evaporation getter filaments, the residual pressure was about 10^{-7} mm Hg with the arc in normal operation. Continued operation of the arc and the ionization gauge resulted in slow cleanup of the residual gases and reduced the pressure to as low as 4×10^{-8} mm, although subsequent electron bombardment of the tantalum probes resulted in temporary increases of pressure to about 4×10^{-7} mm. This evolution of gas was somewhat unavoidable since the press leads and part of the probe cylinders could only be slightly outgassed by heat conduction from parts of the probe that are subject to electron bombardment.

E. Voltage source for retarding potential measurements

A novel and convenient source of retarding potential was designed and used. The principle of operation is illustrated in Fig. II-3. The desired retarding potential (with respect to the horizontal anode) was selected by a Leeds and Northrup voltage divider (accurate to 0.1 per cent) from a stabilized set of batteries. This selected retarding potential (plus a feedback voltage derived from the probe potential) was fed into the grid circuit of a specially designed high gain battery operated dc amplifier with a drift of less than 0.1 millivolt per hour. The output of the amplifier drives a cathode follower (composed of four 6AS7's in parallel) which supplies the probe potential at a current of up to one ampere. As a result of

the negative feedback and the high gain, the retarding potential will be within 0.01 per cent $\pm$ 3 millivolts of the retarding potential selected on the voltage divider, and the output impedance of the cathode follower will be less than approximately 5 milliohms. A small correction, however, must be made for the voltage drop across the probe current meter.

F. Measuring technique and electron bombardment of the probe

In order to avoid the contact potential changes associated with a contaminated probe surface[13, 14, 15, 16], the probe was cleaned before each current reading (or at least made reproducibly dirty) by heating it by electron bombardment before each reading. An electronic timer was used to make the bombardment operation semi-automatic and reproducible in time, and a series resistor and a high voltage source provided in effect a constant current source for the bombardment current.

The time for each probe current measurement was about 15 seconds. This included bombarding the probe for 5 seconds (meanwhile changing the retarding potential to the next value), reading the probe current meter two seconds after the probe current was automatically switched into the measuring circuit, recording the data and comparing the probe current with check points to insure that the arc had not drifted.

The bombardment current drawn by the probe was about 10 per cent (or less) of the horizontal arc current I_z. If in the future it is desired to avoid the possible disturbance of the plasma by the

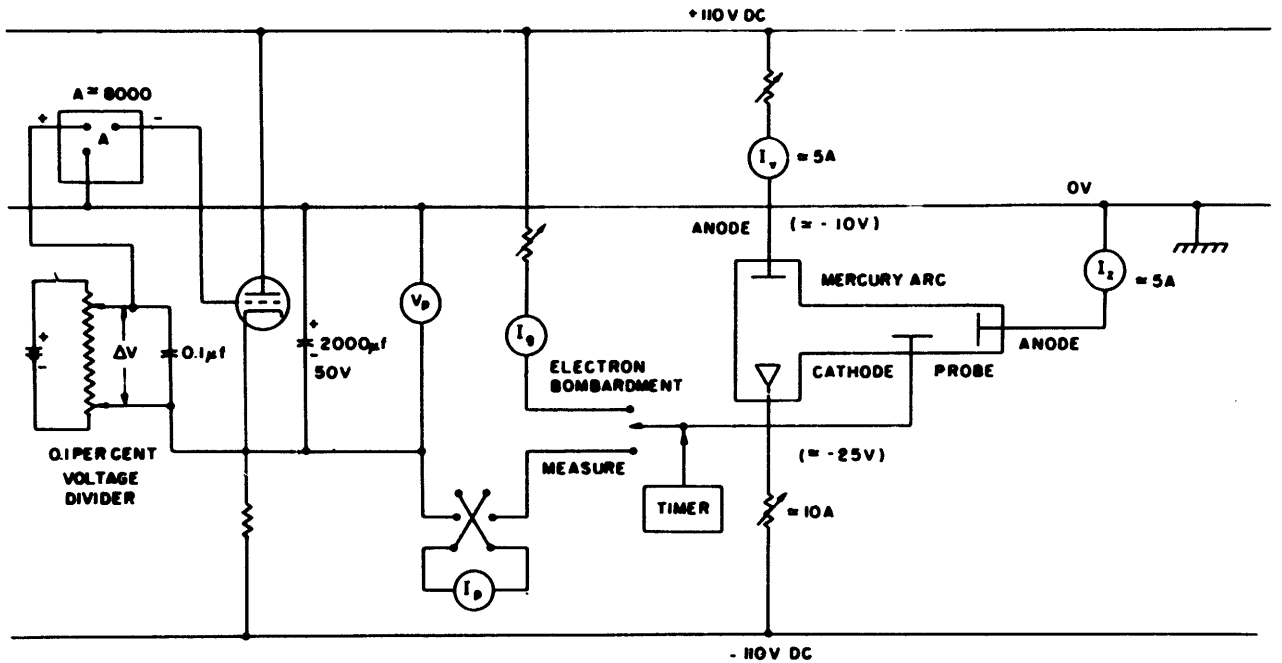

Fig. II-3

Mounting circuit

bombardment current drain, the probe can be constructed in wire or hairpin form to permit probe cleaning by the passage of external heating current pulses. There is no doubt about the need for cleaning the probe surface reproducibly before each current reading if accurate results are desired.

G. Change of probe work-function

An interesting method was developed to permit the change of probe work-function to be directly recorded to within a few millivolts. A value of electron probe current was selected (usually slightly more than the ion current at floating potential), and this current was supplied by a constant current source (usually the ion current). A specially designed low drift high impedance recording dc millivoltmeter was connected between the probe and a very stable low impedance voltage supply which was set to the probe potential. In this way, the recording millivoltmeter acted as an expanded scale voltmeter. Since the dynamic impedance of the electron current source was quite low ($dV/di_- = kT/qi_- \sim 10^3$ OHMS) compared to the input impedance of the millivoltmeter, the change of work-function appeared across the millivoltmeter to within a few millivolts.

The probe surface was cleaned by electron bombardment and the change of contact potential was recorded as a function of time. A typical plot is given in Fig. II-4 for both W and Ta probes. The probes of the same material have the same behavior indicating that the change of contact potential is largely determined by the probe material. The non-monotonic behavior of the change of work-function can be ascribed to the presence of the residual gases in

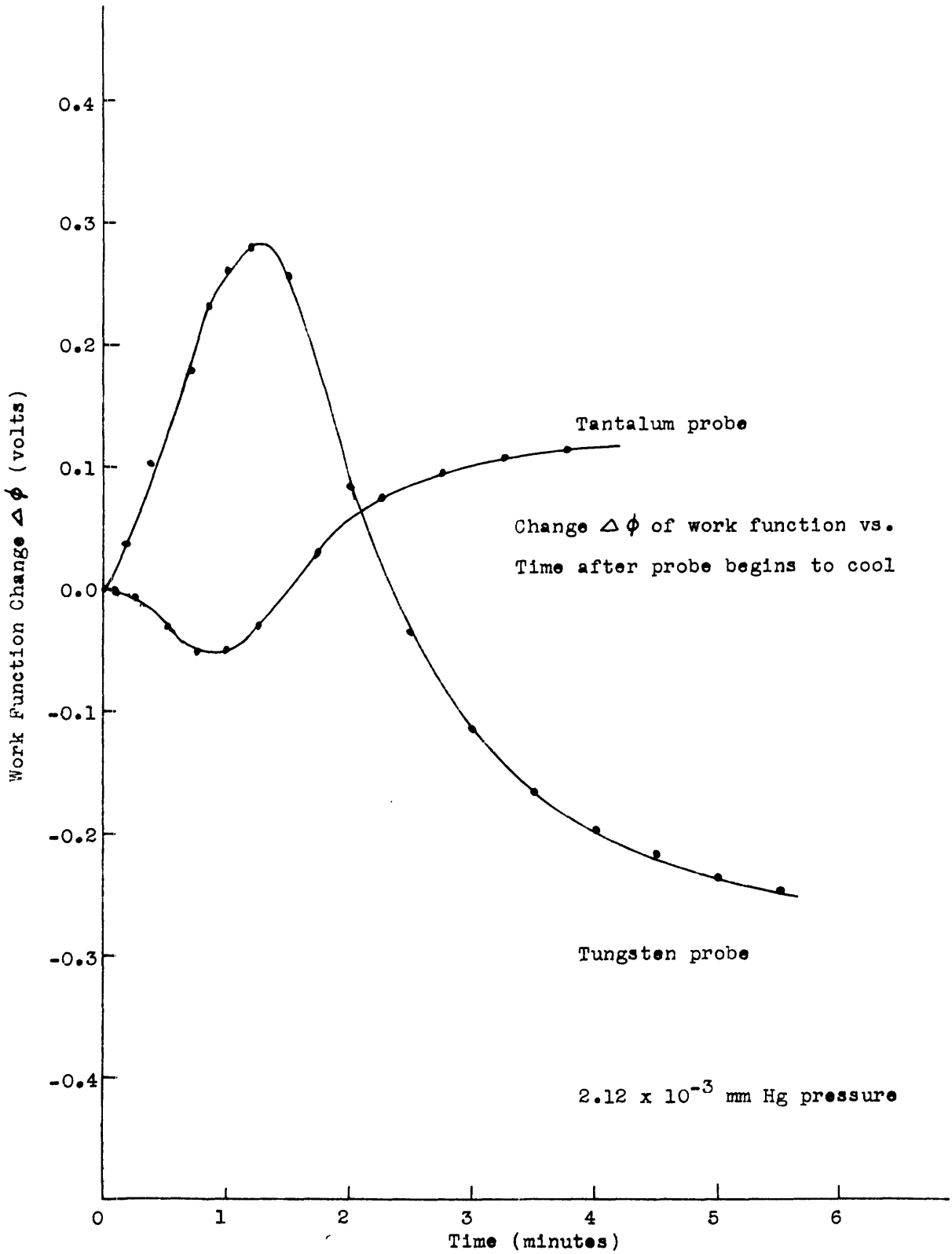

Fig. II-4

Work function change

addition to the mercury on the probe surface.

Since mercury is electropositive, it should reduce the work-function of a clean metal surface although it is questionable how it would effect the work-function of a dirty surface. Various gases will influence different surfaces in different ways. Typical values of reported work-function changes are given below.

Surface	Gas	Change (volts)	Source
W	oxygen	+ 1.70	(17)
		+ 1.20	(18)
	nitrogen	- 0.35	(18)
	hydrogen	- 0.85	(18)
Ta	oxygen	increase	(19)
	nitrogen	decrease	(19)
	hydrogen	decrease	(19)
Ag	oxygen	+ 1.0, + 1.4	(18)
	nitrogen	- 0.1, - 0.2	(18)
	hydrogen	- 0.3	(18)
Pt	oxygen	+ 1.19	(20)
	hydrogen	- 1.15	(20)

For the case of the tungsten probes in this experiment, the initial increase is probably related to the absorption of oxygen (or other electronegative gas), while the later increase can be explained as the formation of mercury on the dirty tungsten surface. Apparently it takes longer for the mercury to deposit in spite of the much larger concentration because of the thermal time lag of the cooling probe and the strong dependence of the mercury condensation upon the probe temperature. Heating the same tungsten probe hotter or for a longer time makes the decreasing part occur slightly later, indicating that it is related to the cooling of the probe structure.

In addition, the decrease in the work-function can be drastically hastened by operating the probe an additional 10 volts negative with respect to the plasma (for about 10 seconds), thus increasing the energy of the bombarding mercury ions and thereby increasing the number of mercury atoms sticking to the probe. In addition, if the probe was not heated very hot, only the later, decreasing part of the work-function change was observed. These factors demonstrate that the decrease in work-function is related to the presence of mercury on the probe.

The tungsten probe temperature was over 2400^{o}K, as calculated from equilibrium between electron bombardment energy input, thermal conduction loss, and radiated energy loss, and also as calculated from the observed electron emission from the hot probe. As a result of this high temperature, the W probe surface can be assumed to be quite clean just after bombardment.

Since the probe current determines the probe temperature and therefore the amount of mercury on the probe surface, it can be seen that the decreasing part of the change of work-function will not be observed at the higher probe currents. On the other hand, if the residual gas pressure is high enough (in other experiments), the recontamination by the residual gases will not be observable particularly if it follows closely the cooling of the probe. For this experiment, the W probes were heated hot enough to insure clean surfaces. In addition, direct measurement showed that the residual gas pressure was about 10^{-7} mm Hg, and the time calculated for the formation of a monolayer of oxygen at this pressure was about 40 seconds. As a result of the clean probe and low residual gas pressure, it was possible to observe changes of work-function

that are non-monotonic.

Two other experimenters who report the use of electron bombarded probes for plasma measurements were Howe[15] and Easley[14], but unfortunately they do not agree on the sign of the change of work-function (by mercury) and they do not specify the experimental conditions well enough to resolve the difference without some assumptions about their experiment. Howe used probes of unspecified material (either W or Ta) in a mercury arc and observed a monotonic decrease in work-function, while Easley used W probes in mercury-argon and mercury-krypton mixtures and observed an increase in work-function (a decrease in probe current) of several tenths of a volt. If it is assumed that the data given by Howe for the change of work-function is for a W probe, then it can be seen that Howe's data is just a limiting case of the results of this experiment and corresponds to either high residual gas pressure, or to a probe that was not heated enough. For the case of Easley, since her value of the difference of work-function is taken from the shift of the retarding potential plots for measurements taken with clean and dirty probes, and since the "body" of the "dirty probe" curve corresponds physically to large electron currents and to a hot probe, there will be little mercury on the surface and the uncompensated electronegative gases on the probe surface will give a larger work-function for the dirty probe than for the bombarded probe. It should be noted, however, that the dirt on the probe is not mercury. With this interpretation, Easley's results are in agreement with the present results and with Howe's results.

The behavior of the Ta work-function is somewhat different but

can be understood if it is realized that it is quite difficult to clean Ta surfaces. It seems that hot Ta dissolves or absorbs the surface layer which reappears upon cooling[21]. Apparently the electropositive components appear on the surface first and reduce the work-function until the oxygen overcomes this effect and produces a net increase in work-function. When the dirty Ta probe is operated about 10 volts negative with respect to the floating potential for about 10 seconds, it is observed that the work-function decreases considerably. Apparently mercury atoms on the surface of a dirty probe will not reduce the work-function appreciably but when mercury ions are driven into the probe to penetrate the surface layers they will reduce the work-function.

It is suggested that this combination of a high impedance, expanded scale recording millivoltmeter and a constant current source be used in future experiments to investigate changes of work-function.

In any event, the measurements of the change of work-function of W and Ta that were made with the aid of the recording millivoltmeter, and with a triggered sweep oscilloscope (Dumont 304-H) and a recording camera (for time in the millisecond range), plus the direct knowledge of the low residual pressure, make it evident that whatever the detailed mechanism of the change of work-function, accurate measurements may be made (under the conditions of this research) if the probe currents are read within a few seconds of the time that the probe is cleaned by electron bombardment. Clean probes are not really necessary, but probes with reproducible work-functions are required. If the electrons have a characteristic temperature of about 1 electron volt, and if one per cent accuracy in electron current is required, it can be seen that a change

of 10 millivolts in probe work-function can be tolerated. Rapid reading of the probe current reduced the drift, and in addition, the readings were always made after a constant short time interval so that the error due to drift of probe potential is a second order effect. This technique was developed because such exotic equipment as a high speed electronic recorder was not available. Wehner and Medicus[16] used an x-y plotter to quickly take the retarding potential plot within 2 or 3 seconds after the probe was cleaned by bombardment. This high speed technique also improves the apparent stability of the arc because it has less chance to change in such a short time interval.

H. Stability of the arc and the reproducibility of the measurements

The state of the arc is primarily determined by two externally controlled parameters. The water bath temperature determines the vapor pressure of the mercury (with allowance for the small thermal drop in the tube wall), and the arc current determines the power input. For a given tube of a given geometry and gas composition, the internal quantities are uniquely determined by these two parameters. Regulation of the vapor pressure was satisfactory since the bath temperature was stable to $\pm$ 0.1°C which corresponds to an uncertainty of 0.8 per cent in the vapor pressure for bath temperatures above 20°C. The situation was somewhat more difficult for the arc current since it required a constant current source of up to 10 amperes for both anodes, and this made it necessary to use a 220 volt dc line which was not as stable as desired because of the varying load placed upon it by other users.

Since the majority of the arc current fluctuations was about

1 per cent with occasional ones of up to 5 per cent, a special technique was developed to eliminate the effects of these large changes. Measurements were made in the late evening and early morning (between 12 a.m. and 6 a.m.) when the laboratory was deserted. Precautions were taken so that if a large change of arc conditions occurred it would be detected without the loss of more than 5 measurements. This was done by first taking (for each probe characteristic) a sequence of probe measurements at one volt intervals, progressing toward a more negative probe. This sequence of measurements was then repeated with an interval of 0.2 volts (less dense in the saturation region) and was compared with the previous sequence to check the stability at every fifth measurement. In this way, a total of 5,159 points were obtained of which 25 per cent were check points with an average magnitude of deviation of 0.7 per cent for these points.

An additional factor which contributed to the arc instability was the erratic motion of the cathode spot which raced about the surface of the mercury pool. This spot could have been made stationary by a short section of tungsten rod extending above the surface of the cathode pool. There was a deplorable tendency for the arc to go out probably because of short transients in the dc line. Since the arc had to be reignited with a high voltage sparker, it was necessary to drain the water tank, start the arc, fill the water tank and re-establish the bath temperature and the arc stability. This process involved about 4 hours and was a great inconvenience. It is suggested that in future experiments of this kind, an auxiliary filament be built into the discharge tube near the

mercury cathode to provide a short burst of electron emission for the re-ignition of the arc without the need to drain the tank. In addition, the use of electronic regulators for the dc line is indicated.

III. Basic Experimental Data

A. Retarding potential plots

The fundamental data obtained from the experiments takes the form of probe current i_p, as a function of probe potential V_c. For probe potentials above the plasma potential, an electron sheath forms about the probe, and the probe current saturates at a value equal to the random electron current. As the probe potential is reduced below the plasma the electron sheath is replaced by an ion sheath, and the electron current decreases while the ion current increases. At the floating potential (about 4.6 to 9.7 volts negative with respect to the plasma potential) the electron and ion currents are equal and result in a zero probe current. Below the floating potential the probe current is predominantly ion current and is almost independent of the probe potential.

In order to determine the electron current component of the probe current, it is necessary to determine the ion current component and use it to correct the total probe current. In the ion current saturation range the probe current does not vary strongly with probe voltage, (about 1 per cent per volt) and when plotted on a semi-logarithmic scale ($\log_{10} i_p$ vs V_{probe}) can be linearly extrapolated to give the ion current correction. Since the saturation ion current is about 0.2 to 0.3 per cent of the saturation electron current, this correction is not large relatively except near the floating potential where the extrapolation itself is more valid.

A more satisfactory way of determining the electron current

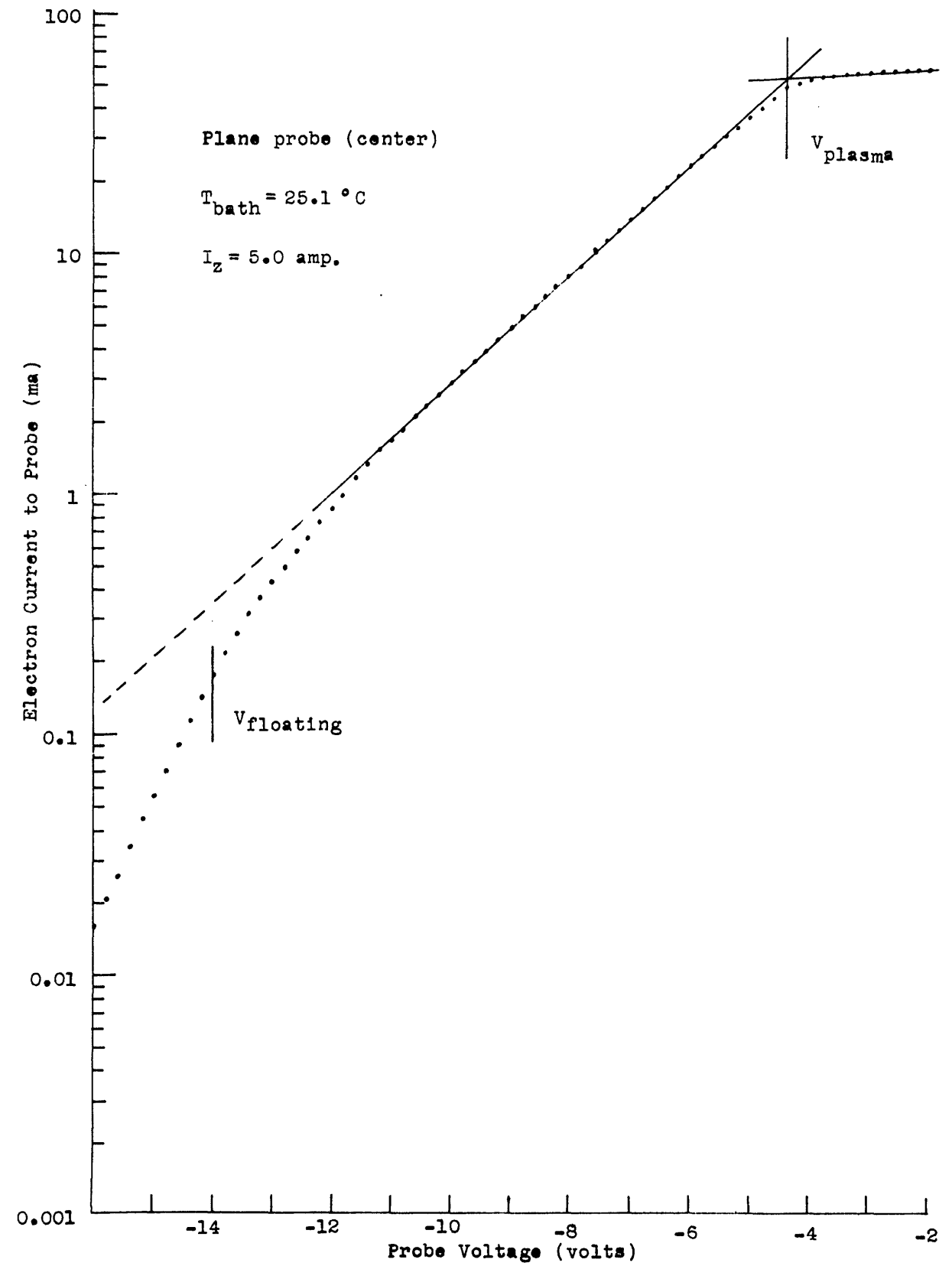

Fig. IV-1

Plane center probe curve

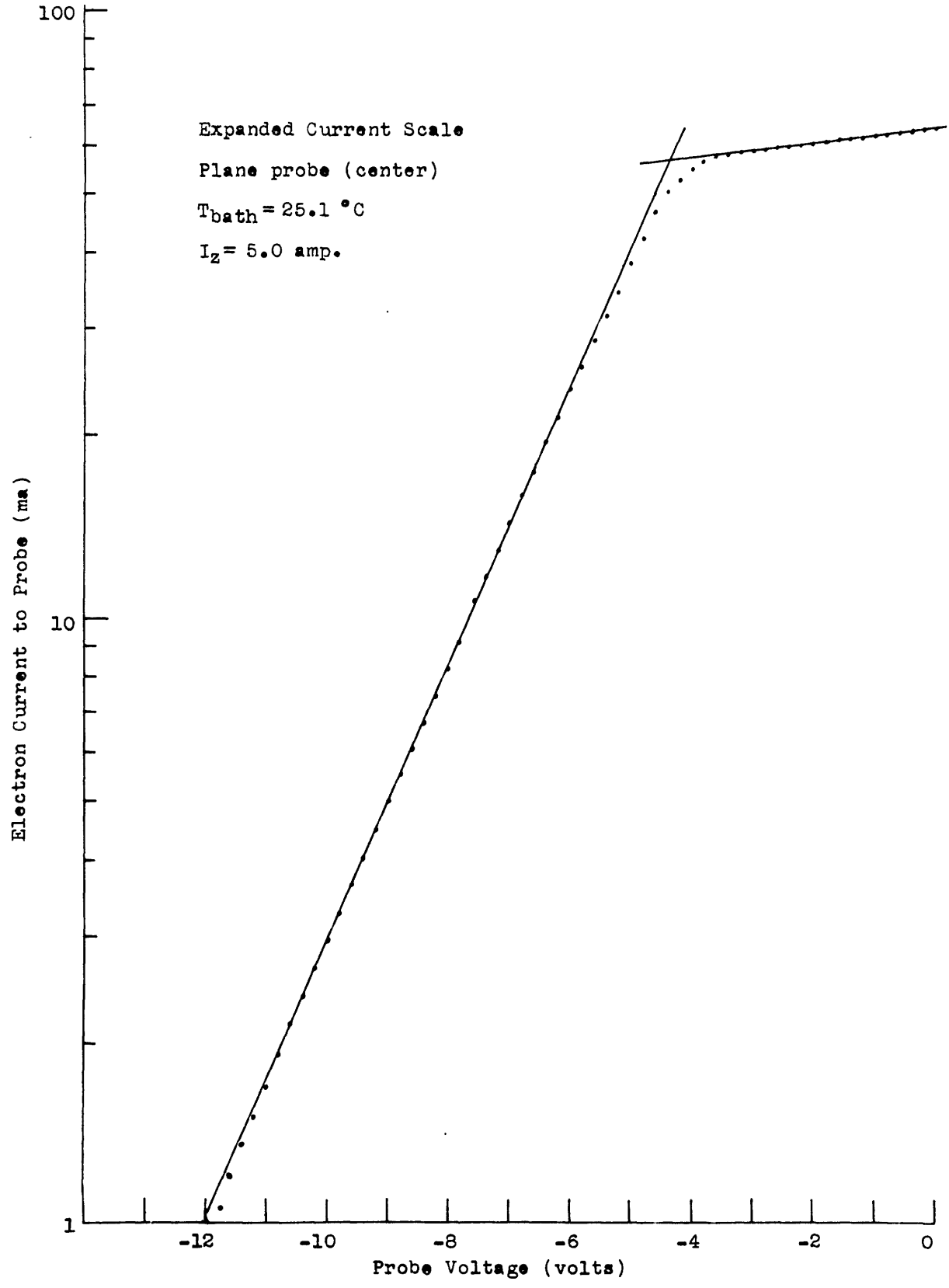

Fig. III-2

Expanded plane center probe curve

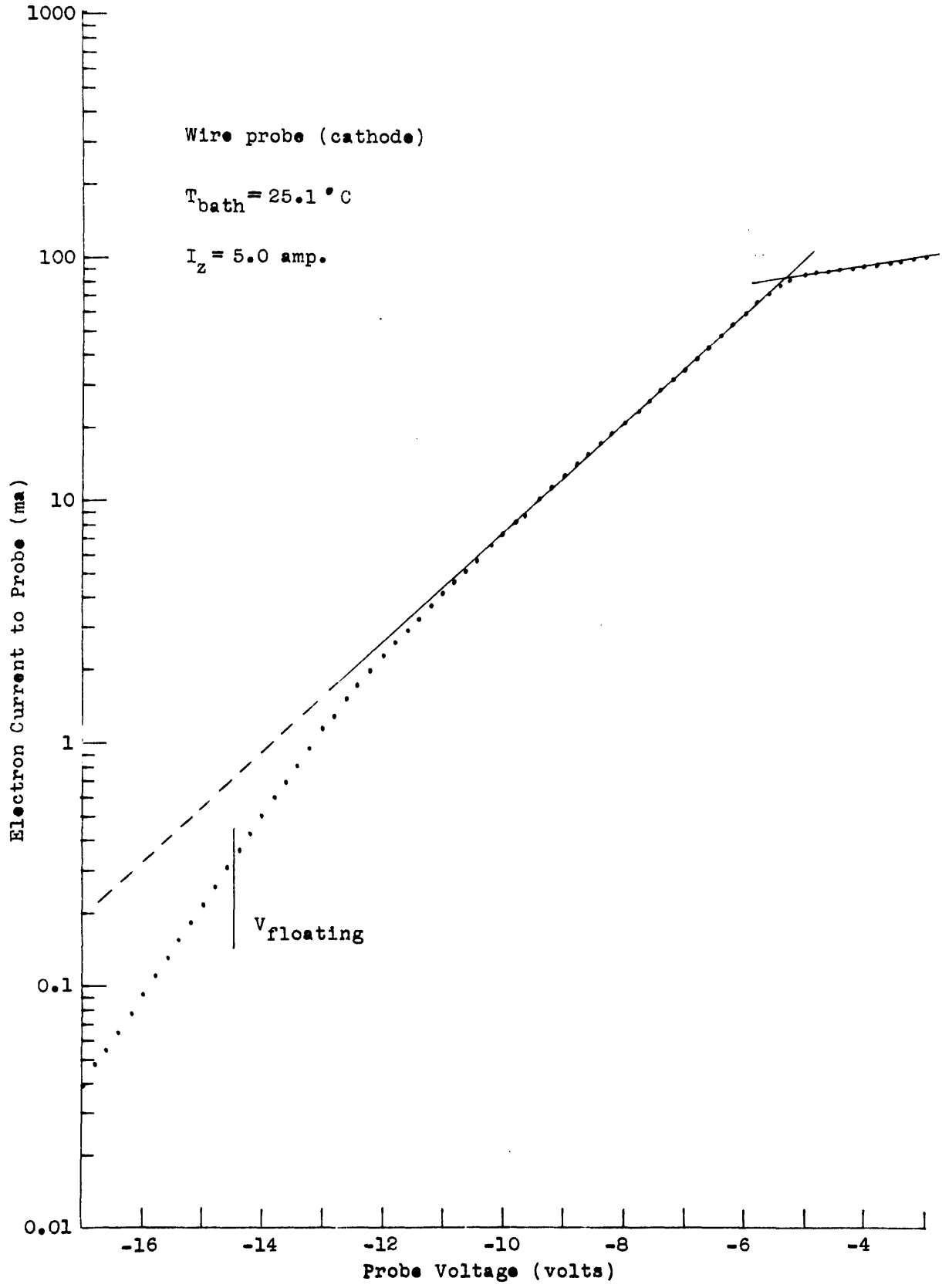

Fig. III-3

Wire probe curve

component is to use special probes designed to separate directly the electron and ion components. This has been done by others[22, 23] for other gases and would have been possible in this experiment except for the shorting of the internal cylinders of the multiple center probe.. In any event, the determination of the electron temperature, electron density, and plasma potential is dependent upon the body of the electron energy distribution and is relatively independent of the details of the high energy tail.

B. Determination of the electron temperature, electron density and plasma potential

After the electron current is plotted in the form $\log_{10} i_-$ vs the probe potential V_c, the resulting retarding potential characteristic is used to determine the electron temperature, the electron density, and the plasma potential. Typical plots are given in Figs. III-1 through III-21. The relation between the electron current density J_- and the probe potential V_c for a M-B distribution is given by:

$$J_- = \frac{n_-}{4}\left(\frac{8}{\pi}\frac{q}{m_-}\frac{kT_-}{q}\right)^{1/2} \exp\left(\frac{q(V_c - V_p)}{kT_-}\right) \qquad \text{(III-1)}$$

For $V_p > V_c$ the electron temperature, kT_-/q, in electron volts is obtained from the slope of the semi-logarithmic plot and from the relation:

$$\frac{d}{dV_c}\log_{10} J_- = 2.303\,\frac{q}{kT_-} \qquad \text{(III-2)}$$

This value of kT_-/q for each probe characteristic was obtained from an average of several determinations on a 5 cycle semi-logarithmic plot and from several determinations on a 2 cycle semi-log plot, in order to reduce the error introduced by plotting and slope measurements. In this

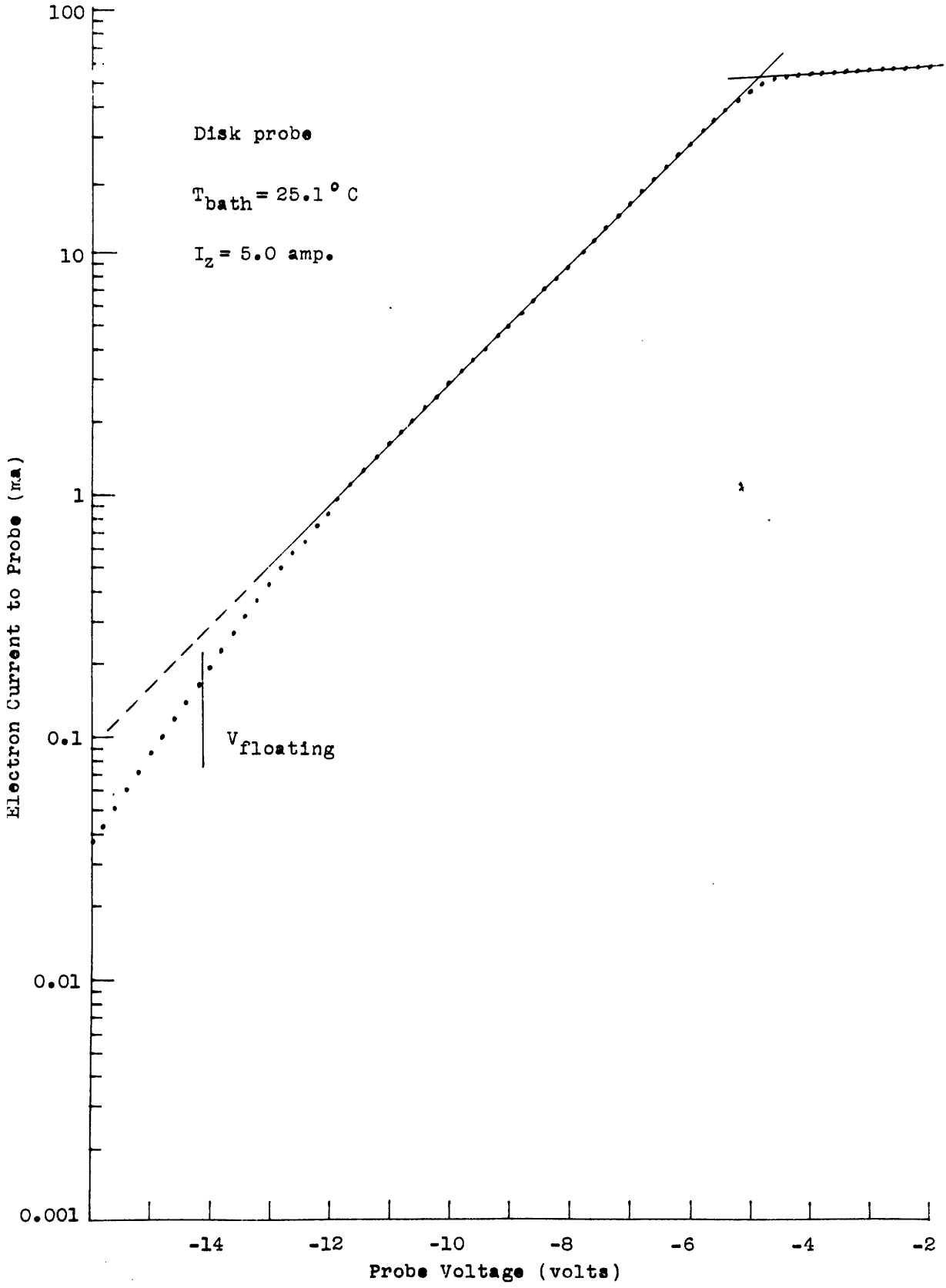

Fig. III-4

Disk probe curve

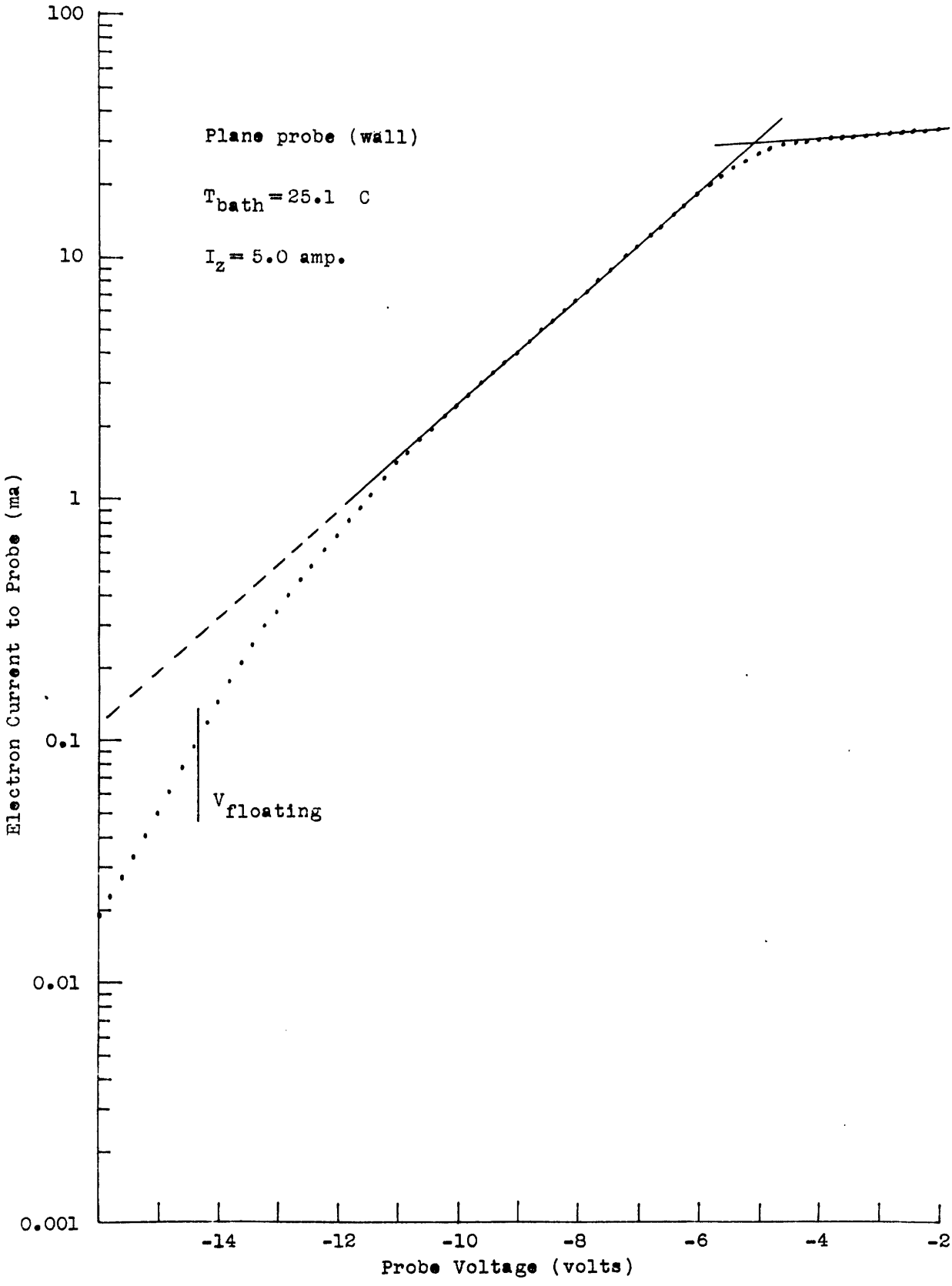

Fig. III-5

Plane wall probe curve

way, the agreement between successive determinations of electron temperature from the same data was about 1 per cent. In the calculation of the electron density, any uncertainty in the electron temperature is reduced by a factor of two since only the square root of the electron temperature is involved. To reduce the accumulated error due to rounding off figures, four significant figures were retained through all calculations. The latest values[24] of the basic physical constants were used in the calculations.

The value of the saturation electron current I_{-s} corresponding to the random electron current is obtained from the intersection of the extrapolated straight line characteristics of the retarded electron current and the saturated electron current. This intersection point is also used to determine the plasma potential. Again, repeated graphical determinations are used to reduce plotting error. The electron density is calculated from:

$$n_- = \frac{4}{\langle v_- \rangle} \frac{J_{-s}}{q} \qquad \text{(III-3)}$$

where the average electron velocity $\langle v_- \rangle$ for a M-B distribution is given by: $\langle v_- \rangle = 6.693 \times 10^5 (kT_-/q)^{1/2}$ meters/second. The depletion of the high energy electron is not significant in the determination of the electron density since the various retarding potential plots have a depletion potential $+(V_p - V_d)$ (with respect to the plasma potential) that is approximately related to the electron temperature by: $+(V_p - V_d) = 3.39\, kT_-/q$ which corresponds to an electron current of 3.4 per cent of the saturation current at the depletion potential thus indicating that the correction can be at the most this value of 3.4 per cent since this corresponds to a

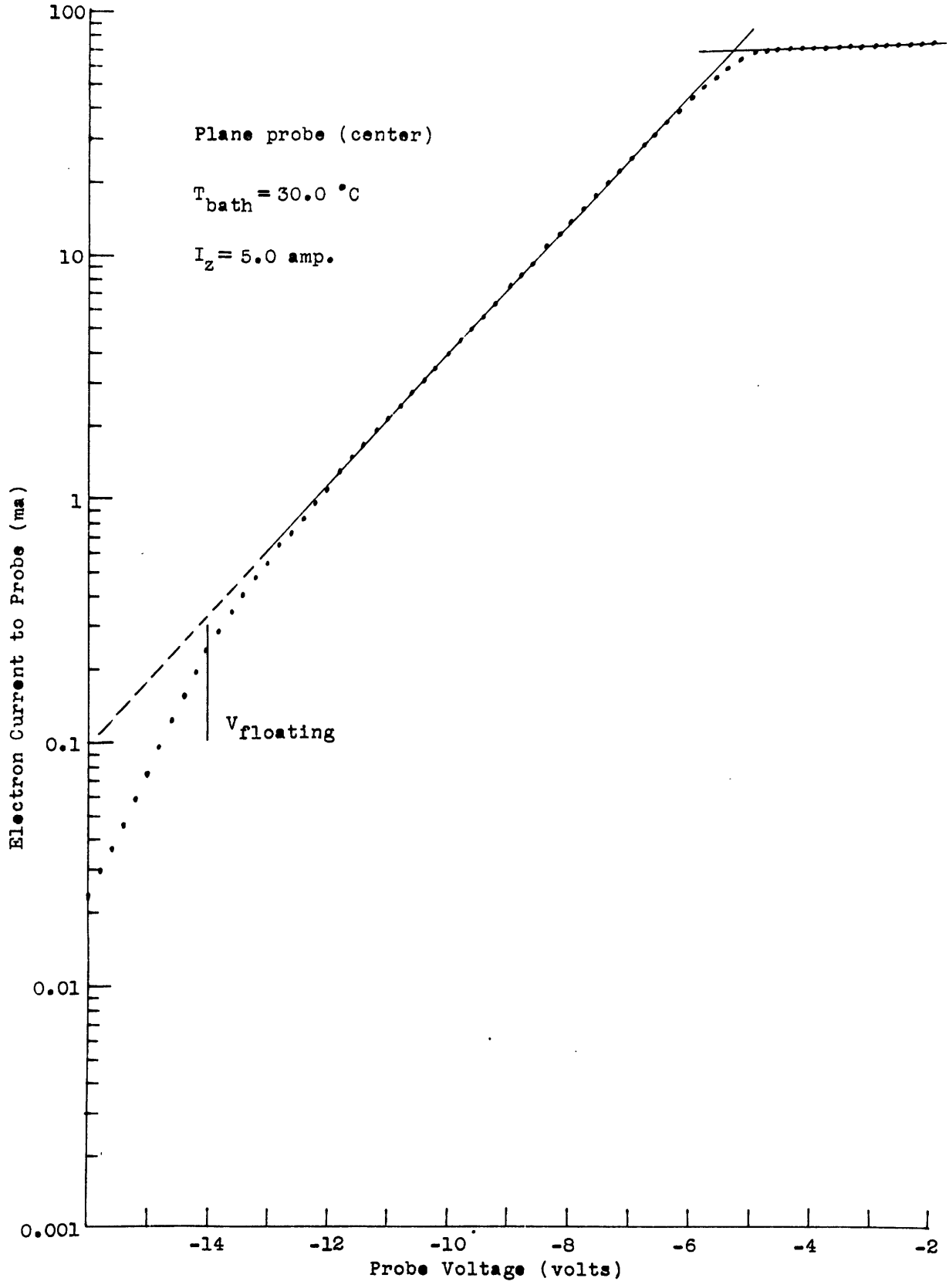

Fig. III-8

Plane center probe curve

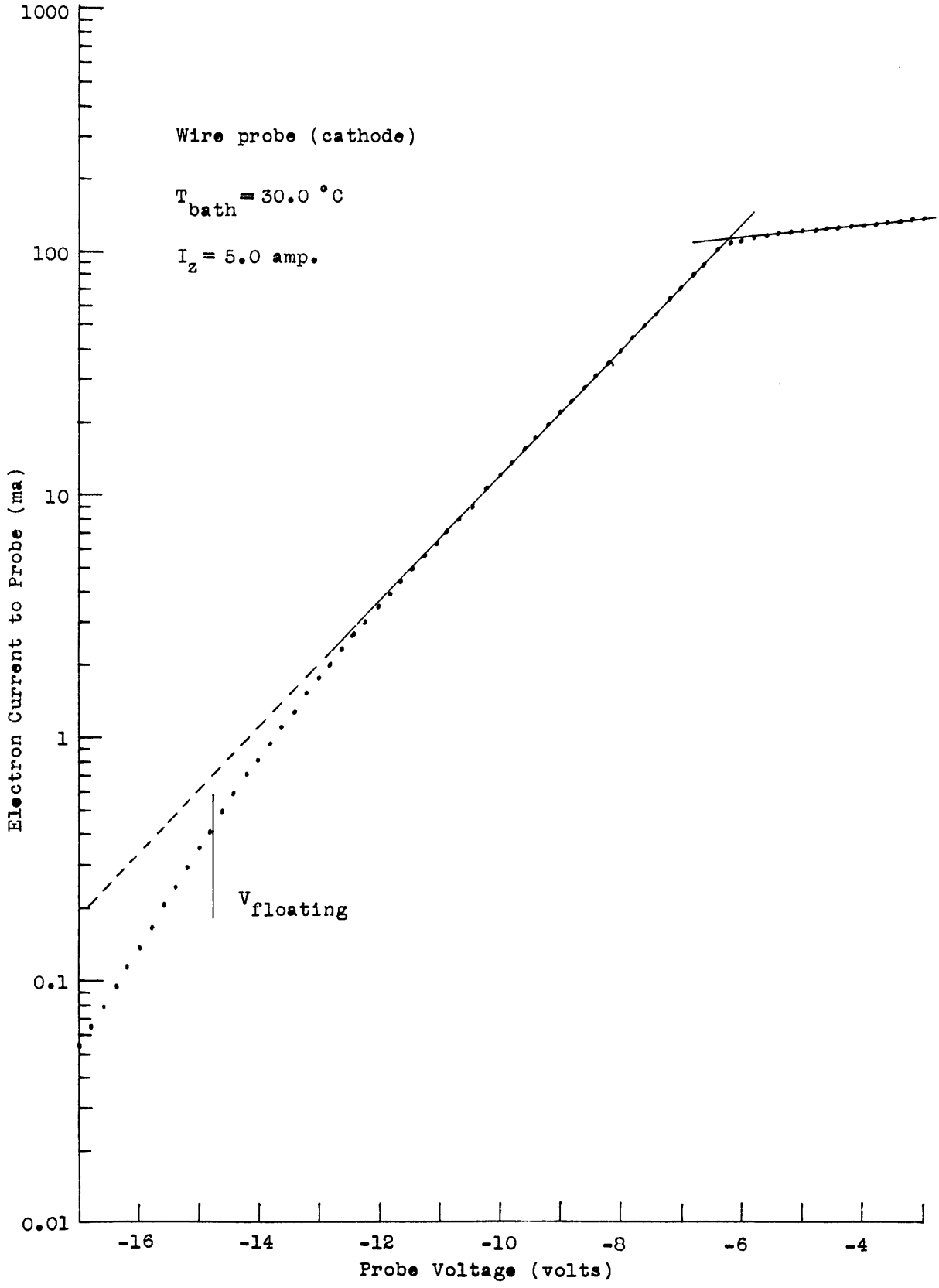

Fig. III-7

Wire probe curve

depletion of high energy electrons and not a complete absence of them.

The values of the electron temperature thus obtained are listed in Table I along with the electron density and plasma potentials. There are no significant systematic variations of the electron temperature with probe position, probe geometry or probe material, and therefore the average of the various electron temperatures for a given set (constant bath temperature and arc current) is used to give a characteristic electron temperature for the plasma. (See Table II.) The uncertainty of the mean electron temperature averaged over the 9 sets is 1.8 per cent and probably corresponds to the instability of the arc, bath temperature, and arc currents. The uniformity of the electron temperature for the low pressure arc is in agreement with the findings of Killian[5]. The average electron density at the axis of the plasma cylinder n_{-o}, is obtained from the average of the density measurements by the wire probes and the center plane probe. The small average uncertainty in n_{-0} (1.5 per cent on the average for the 9 sets) demonstrates the small axial charge density gradient and indicates that the charge density measurements are quite reliable.

Plasma potentials are not necessarily as accurate because of the uncertainty of the probe work-function due to the presence of surface gases. The tungsten probe measurements are more reliable, however, since the W probes were heated quite hot and made relatively clean. In addition, the axial potential gradient is obtained from differences of plasma potentials for the similar tungsten probes and therefore any systematic error in the tungsten work-function tends to cancel leaving

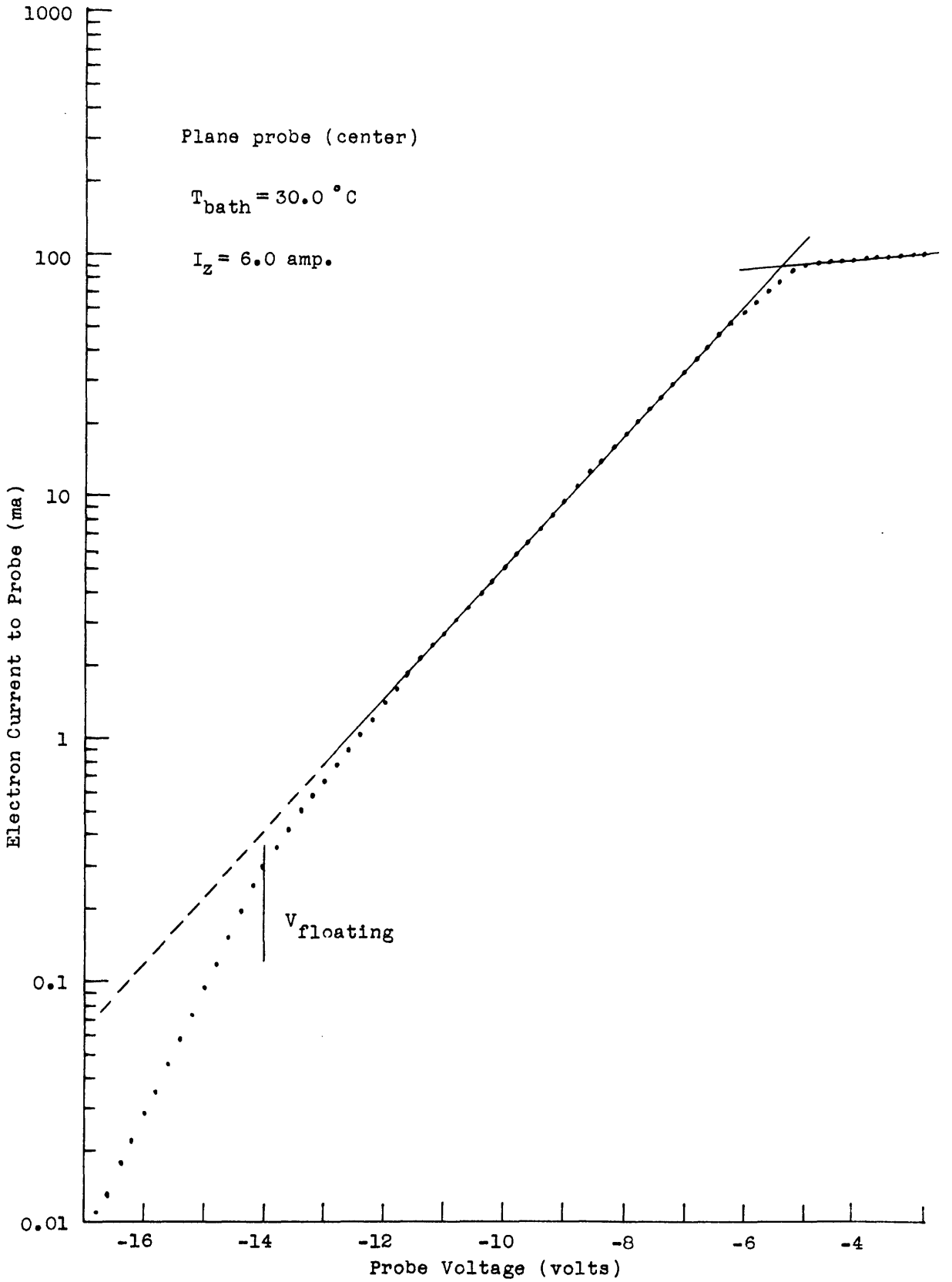

Fig. III-8

Plane center probe curve

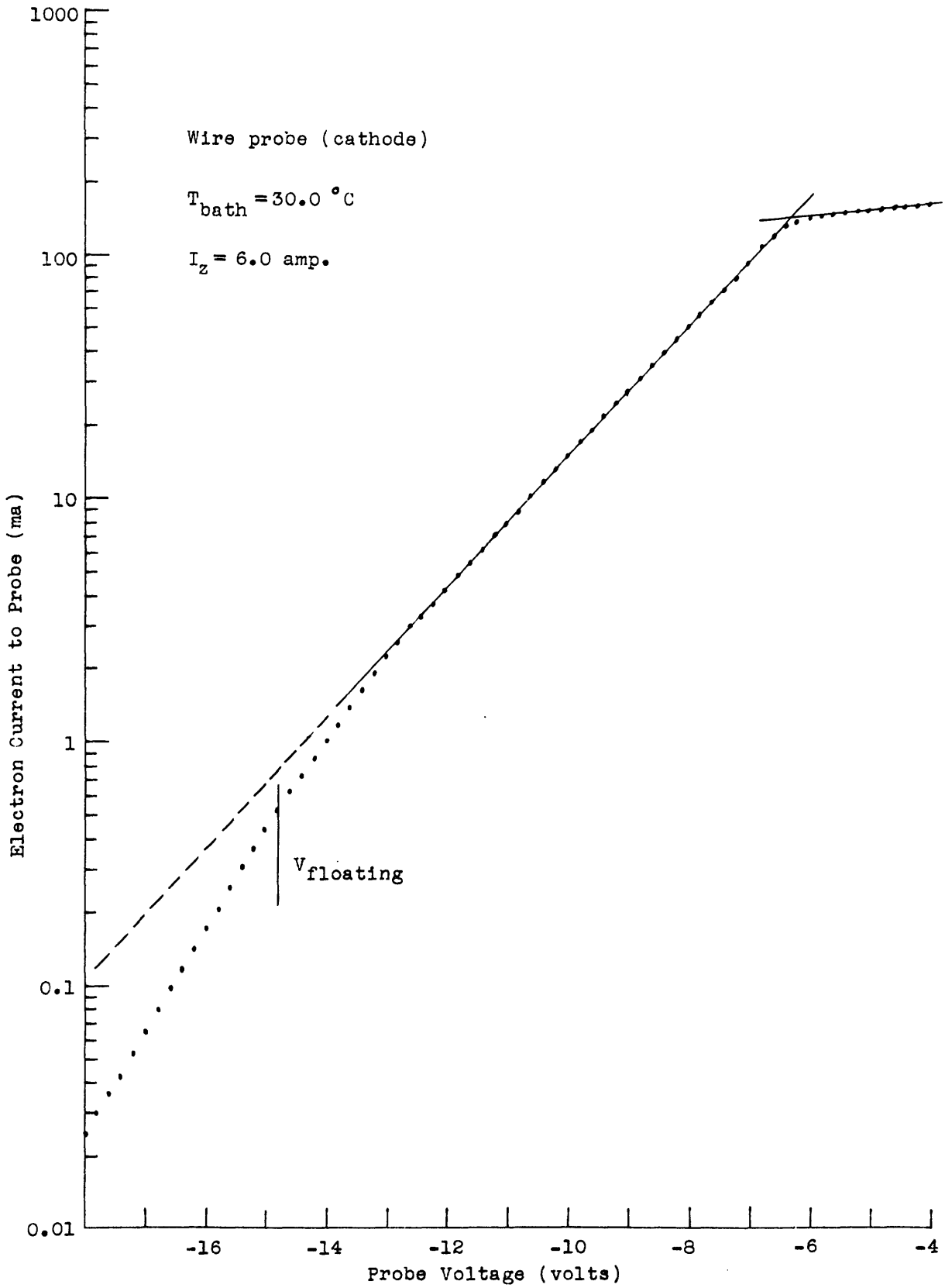

Fig. III-9

Wire probe curve

only second order errors. In several cases where wire probe measurements were repeated, the calculated values of the axial gradient are in agreement to an average of 1 per cent. The values of E_z are given in Table II. The potentials listed in Table I show that if the floating potentials V_f are used to calculate E_z rather than the plasma potentials V_p, there may be an error of up to a factor of 2 at the lower pressures. This difference occurs because the slight differences in the retarding potential plots for the wire probes become more important at the lower pressures where kT_-/q is larger.

C. Mercury vapor pressure and density

The density of mercury atoms in the plasma is an important parameter in the determination of the plasma processes. Mercury vapor pressure may be calculated as a function of the temperature of the inner glass wall provided that the discharge tube is submerged so that some mercury condenses on the wall to provide local equilibrium between the mercury and the mercury vapor. The need to submerge the whole discharge tube and not only the cathode pool area may be demonstrated by slowly raising the water level in the bath. When the water level reaches the horizontal arm, a drastic change in probe characteristic indicates a strong dependence of pressure upon the submersion of the tube.

The mercury vapor pressure is predominantly controlled by the water bath temperature T_b, but there is a correction of about 10 to 20 per cent in pressure corresponding to the temperature drop ΔT, in the pyrex wall, due to the conduction of heat outward to the water bath. The electrical energy input to the plasma can be calculated from the arc current I_z and the axial potential gradient E_z. It is assumed that

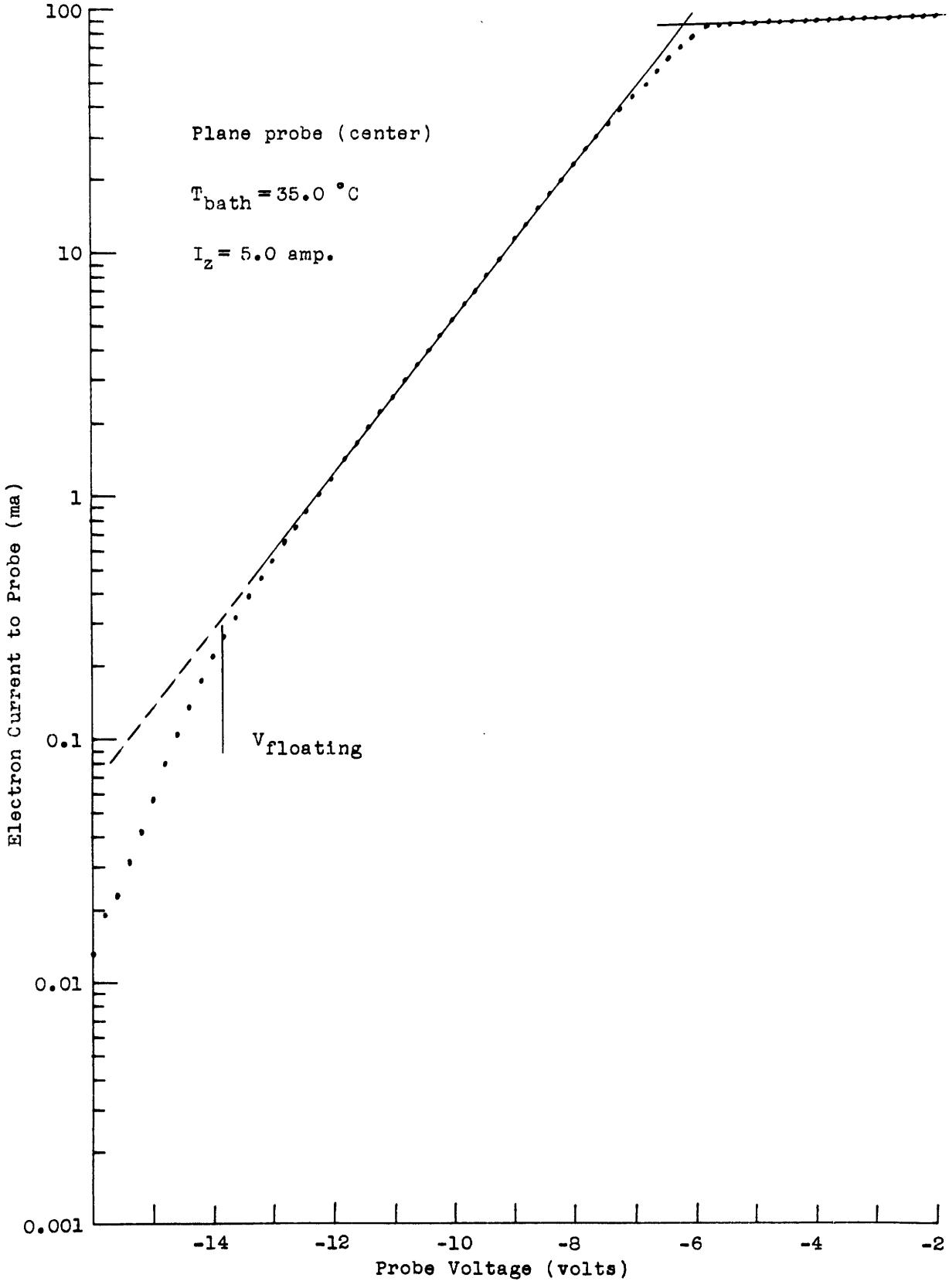

Fig. III-10

Plane center probe curve

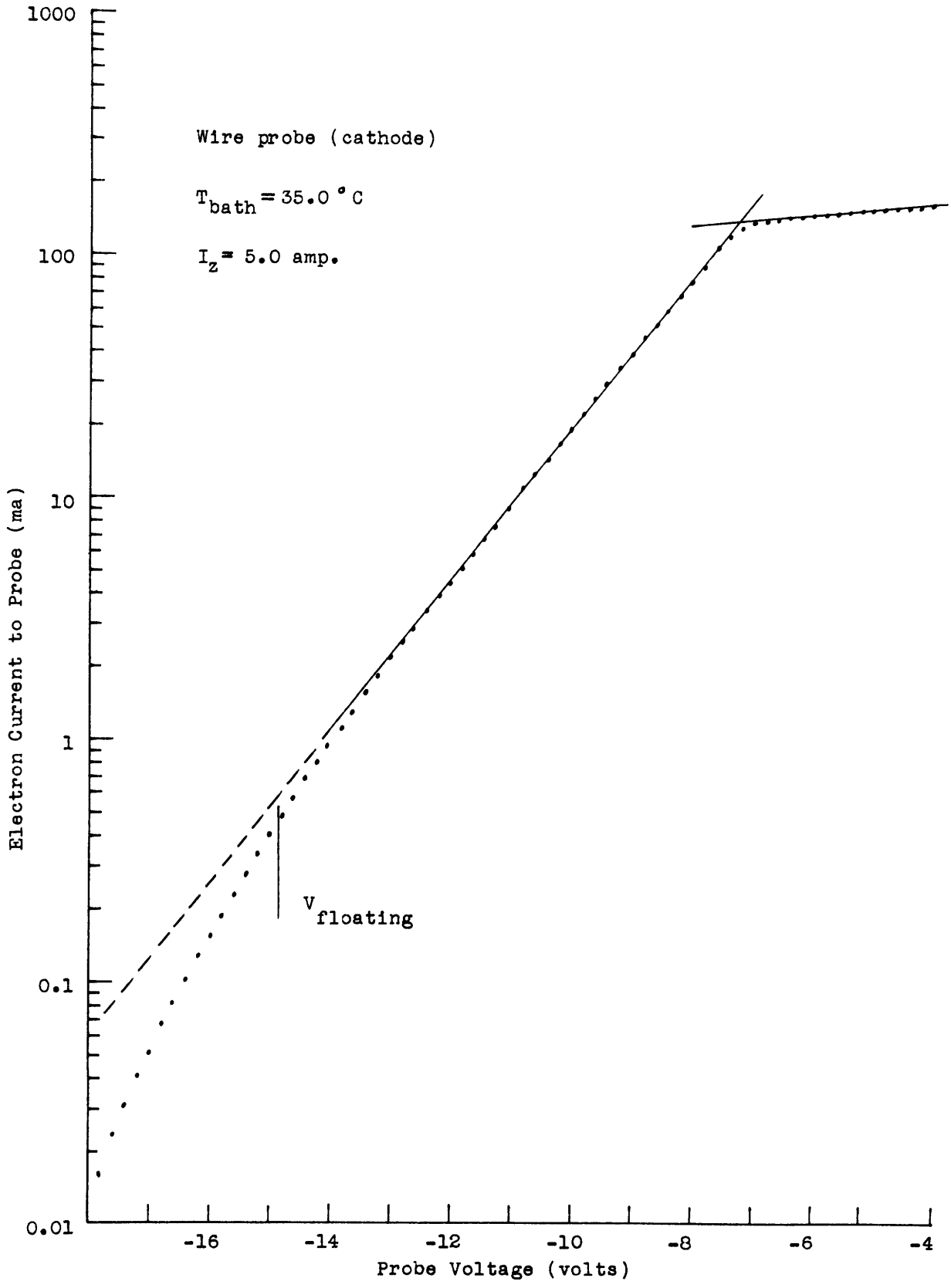

Fig. III-11

Wire probe curve

with the exception of a small fraction of this input which passes through the pyrex wall as electromagnetic radiation, this input energy must be removed by thermal conduction. From the tube geometry, the temperature drop ΔT, in the wall is given by:

$$\Delta T = \frac{E_z I_z}{2\pi K} \ln (r_2/r_1) \qquad \text{(III-4)}$$

where $I_z E_z$ is the electrical power input per unit length, r_2/r_1 is the ratio of outer tube radius to inner radius, and the thermal conductivity for Pyrex (chemical glass No. 7740) is given by: K = 0.0027 calories/sec x cm x ^{o}C. For the experimental tube used where the inner radius is 2.75 cm and the wall thickness is 0.24 cm, the temperature correction is:

$$\Delta T = 1.20\ E_z I_z \qquad \text{(III-5)}$$

where ΔT is in degrees C, E_z is in volts/cm, and I_z is in amperes. The significant values are given in Table II.

Very accurate data for the vapor pressure of mercury as a function of temperature are available in the International Critical Tables[25], and in slightly abbreviated form in recent editions of the Handbook of Chemistry and Physics[26]. The following empirical expression was calculated (using least squares) to describe the dependence of the vapor pressure p, on the temperature T^{o}K for the range between 0^{o}C and 100^{o}C:

$$\log_{10} p\,(\text{mm Hg}) = 8.0904 - \frac{3228.7}{T} \qquad \text{(III-6)}$$

This simple expression has an average magnitude of error of only 0.4 per cent with a maximum error of 1.2 per cent occurring at 0^{o}C, but in order not to introduce an avoidable error, this expression was used to

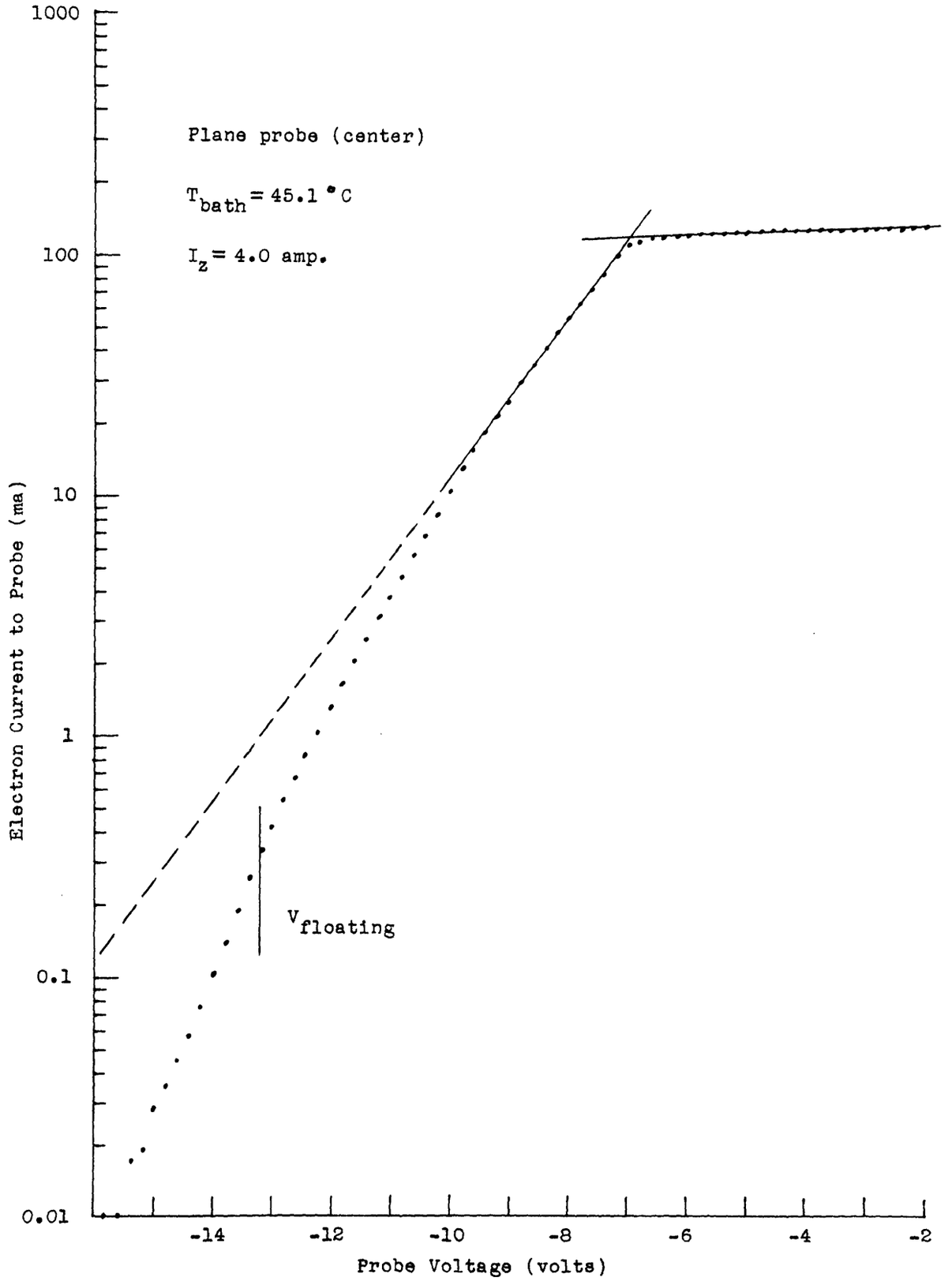

Fig. III-13

Plane center probe curve

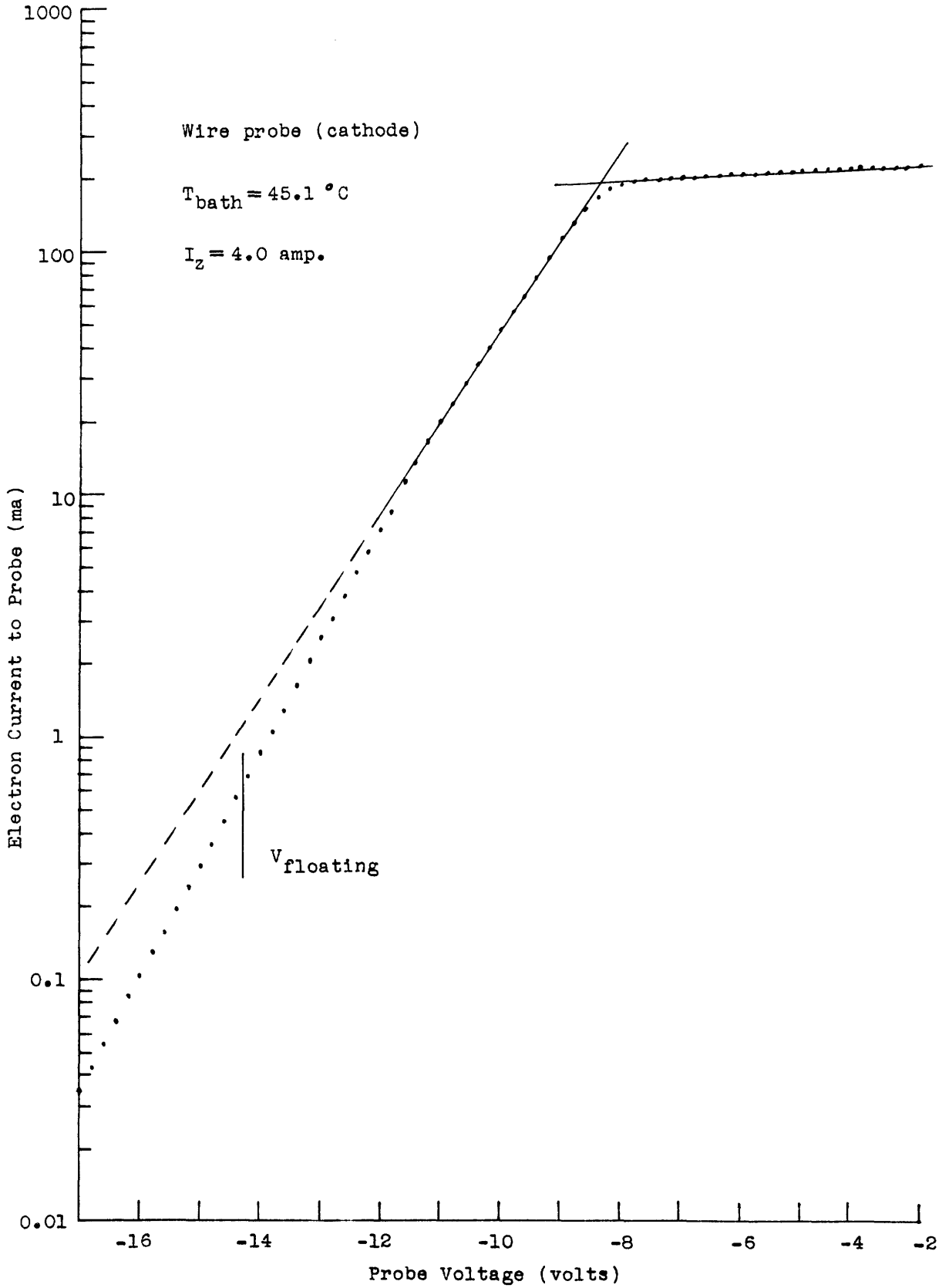

Fig. III-13

Wire probe curve

interpolate between the tabulated values rather than for direct calcuation. From this expression it can be seen that an uncertainty of $0.1^{o}C$ in the temperature corresponds to an error of less than 1 per cent in pressure for temperatures above $10^{o}C$.

What is really significant in the plasma is the mercury density rather than the vapor pressure. The perfect gas law ($P = nkT$), can be used to calculate the gas density n_g, from the vapor temperature T_g, and the vapor pressure p. In particular, one can calculate the reduced pressure p_o, which corresponds to the pressure for this same density at $0^{o}C$:

$$p_o = p \frac{273.2}{T_g \ ^{o}K} \qquad \text{(III-7)}$$

The reduced pressure is really only a unit of density with 3.536×10^{16} molecules/cm^3 equal to 1 mm Hg of reduced pressure. Calculated values of pressure, reduced pressure, and gas density are listed in Table II.

The mercury vapor temperature T_g, is assumed to be the same as the temperature $(T_b + \Delta T)$, of the inside of the pyrex envelope but actually the vapor temperature is slightly higher because of the "temperature jump"[27] associated with the conduction of heat from the gas to the wall. It will be shown that this temperature jump δT, is small. Chapman and Cowling[28] give the following expression for the temperature difference δT between a gas and a wall:

$$\delta T = \frac{2-\theta}{\theta} \mu' \lambda_g \frac{dT}{dr} \qquad \text{(III-8)}$$

where the accommodation coefficient θ, is a function of the gas and the wall material. The factor μ' is a constant of order unity, λ_g is the

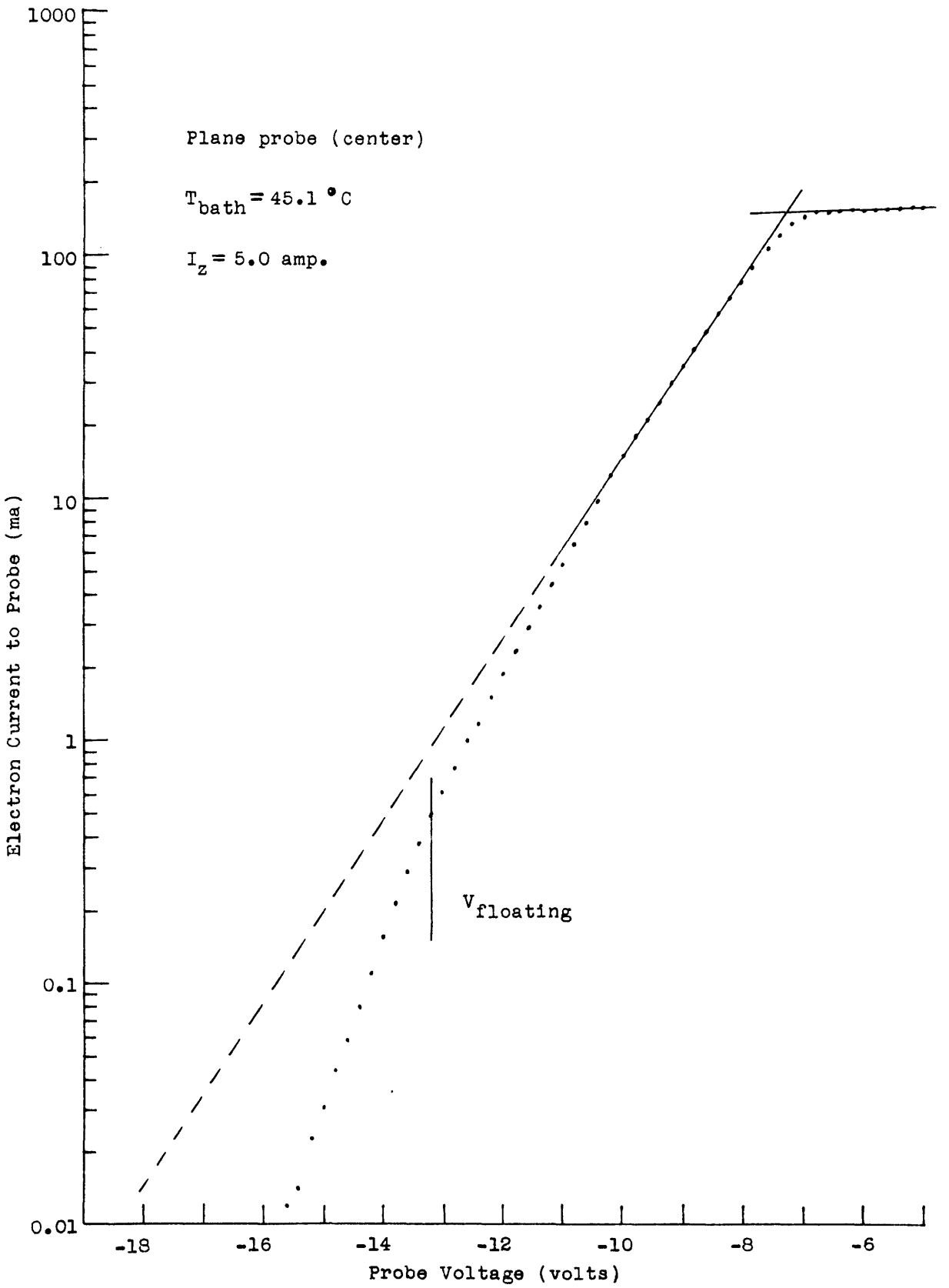

Fig. III-14

Plane center probe curve

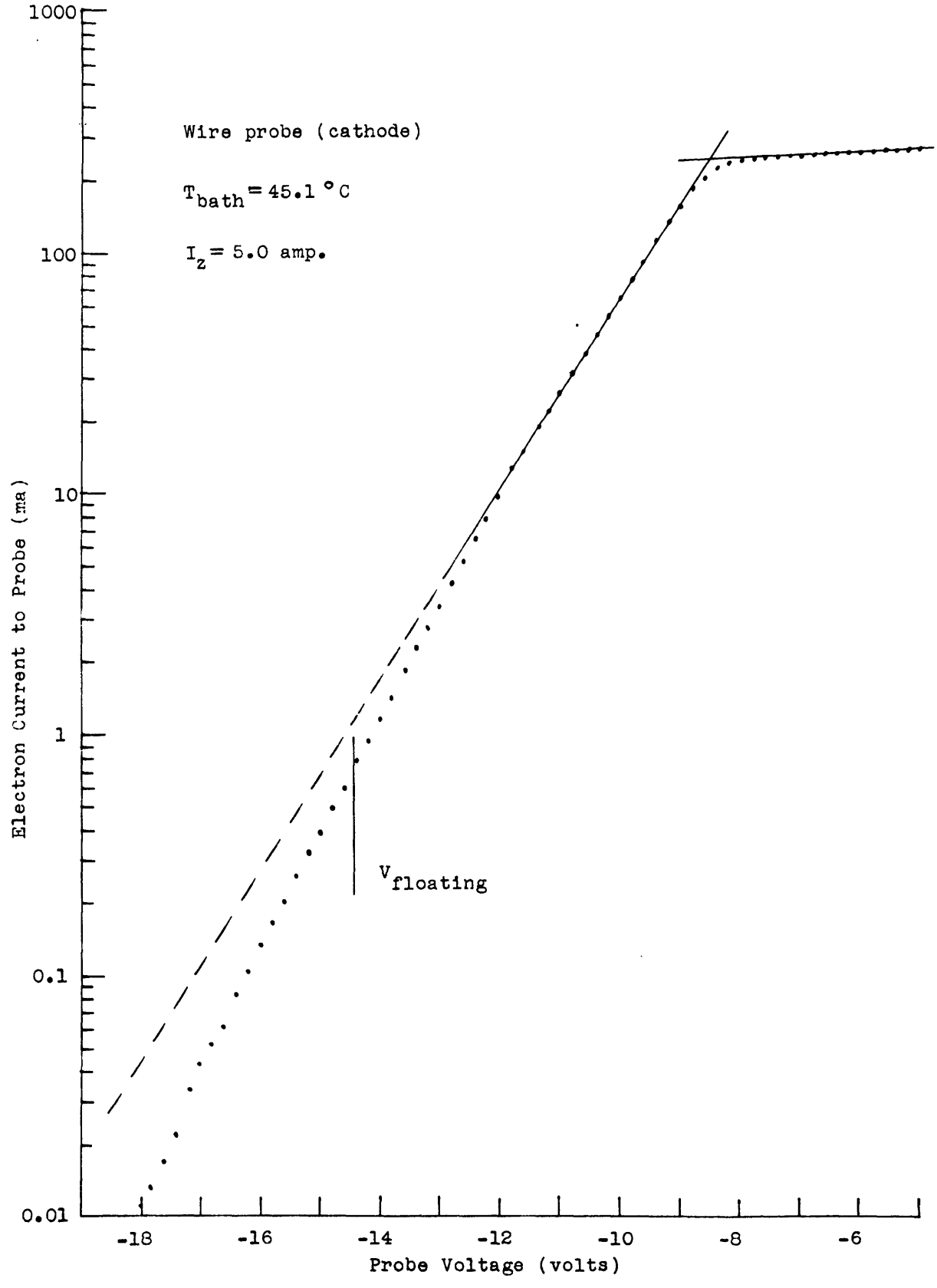

Fig. III-16

Wire probe curve

mean free path of the gas atoms and dT/dr is the temperature gradient in the gas. The accommodation coefficient can be interpreted[27] as the ratio of the actual energy transfer from gas to wall compared to the energy transfer that would occur if the gas atoms were emitted from the wall with the characteristic temperature of the wall. The International Critical Tables[29] give the accommodation coefficient for mercury atoms and liquid mercury as 1.00 ± 0.01. The mean free path for mercury atoms in mercury vapor can be calculated from data given in the Smithsonian Tables[30], and the value of $p_o \lambda_g$ obtained is 2.4×10^{-3} cm x mm Hg. For a mercury pressure of about 10 microns, the mean free path is about 0.24 cm which is small compared to the tube radius. It is somewhat difficult to determine the temperature gradient dT/dr in the gas but an estimate can be made of its value. The temperature drop in the pyrex wall has been calculated to be about 1 degree C for a thickness of 0.24 cm thus giving a temperature gradient of about 4 degrees C per cm for the pyrex wall. The thermal conductivity of pyrex is 2.7×10^{-3} calories/cm x sec x ^{o}C, while the thermal conducitivity of mercury vapor as calculated from data given by Elenbaas[31] is about 6×10^{-5} calories/cm x sec x ^{o}C for mercury vapor at 300^{o}K. The results given by Klarfeld[32] for a mercury arc indicate that for pressures below 100 microns, less than 1 per cent of the input power is converted into gas heat loss. With these figures it is calculated that the temperature gradient in the gas near the pyrex wall is about 2 degrees C per cm. When the value of the accommodation coefficient and the mean free path are introduced, the temperature jump δ T, is found to be about 0.5 ^{o}C. Since this approximate correction is only 0.2 per cent of the

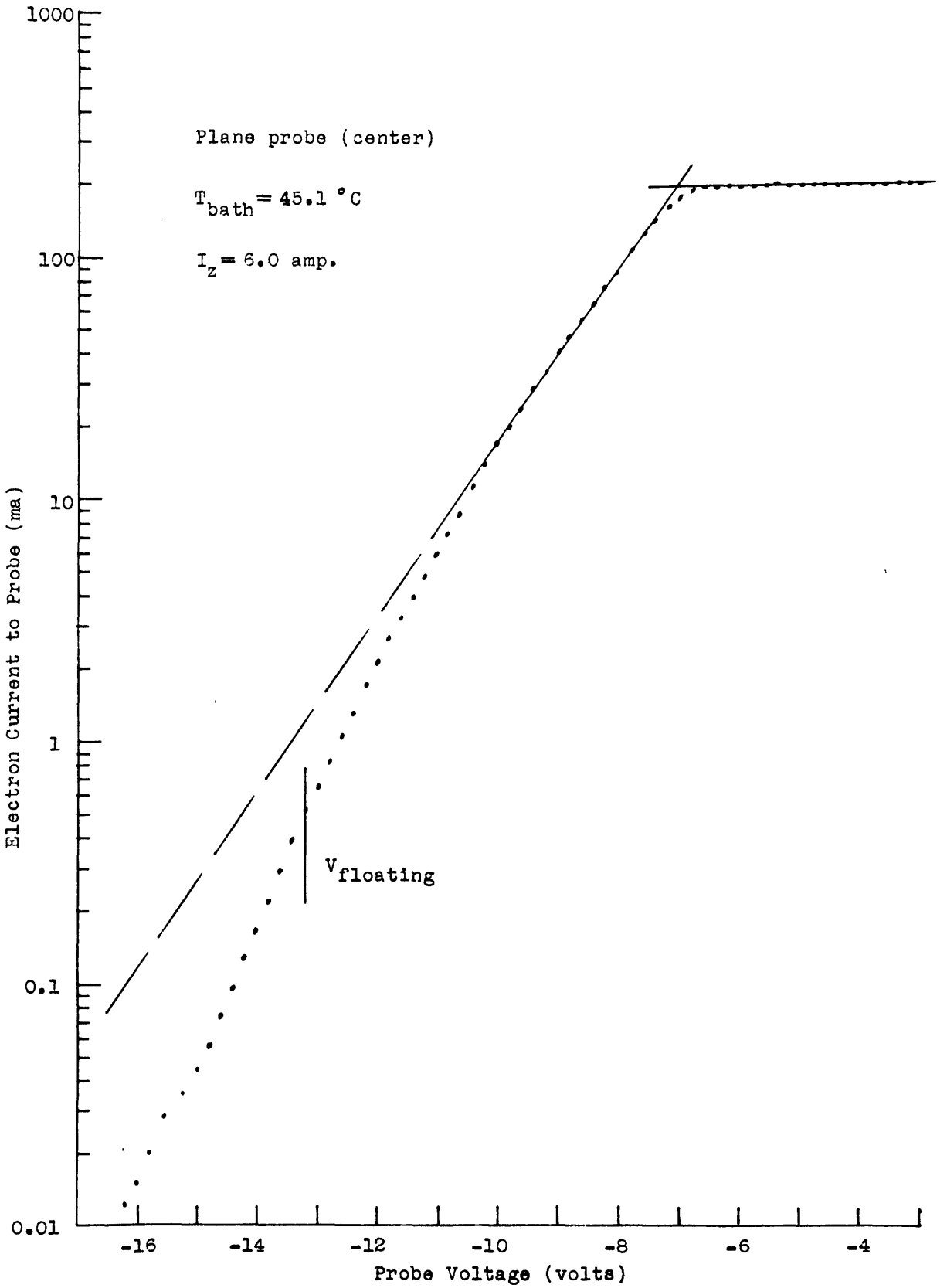

Fig. III-18

Plane center probe curve

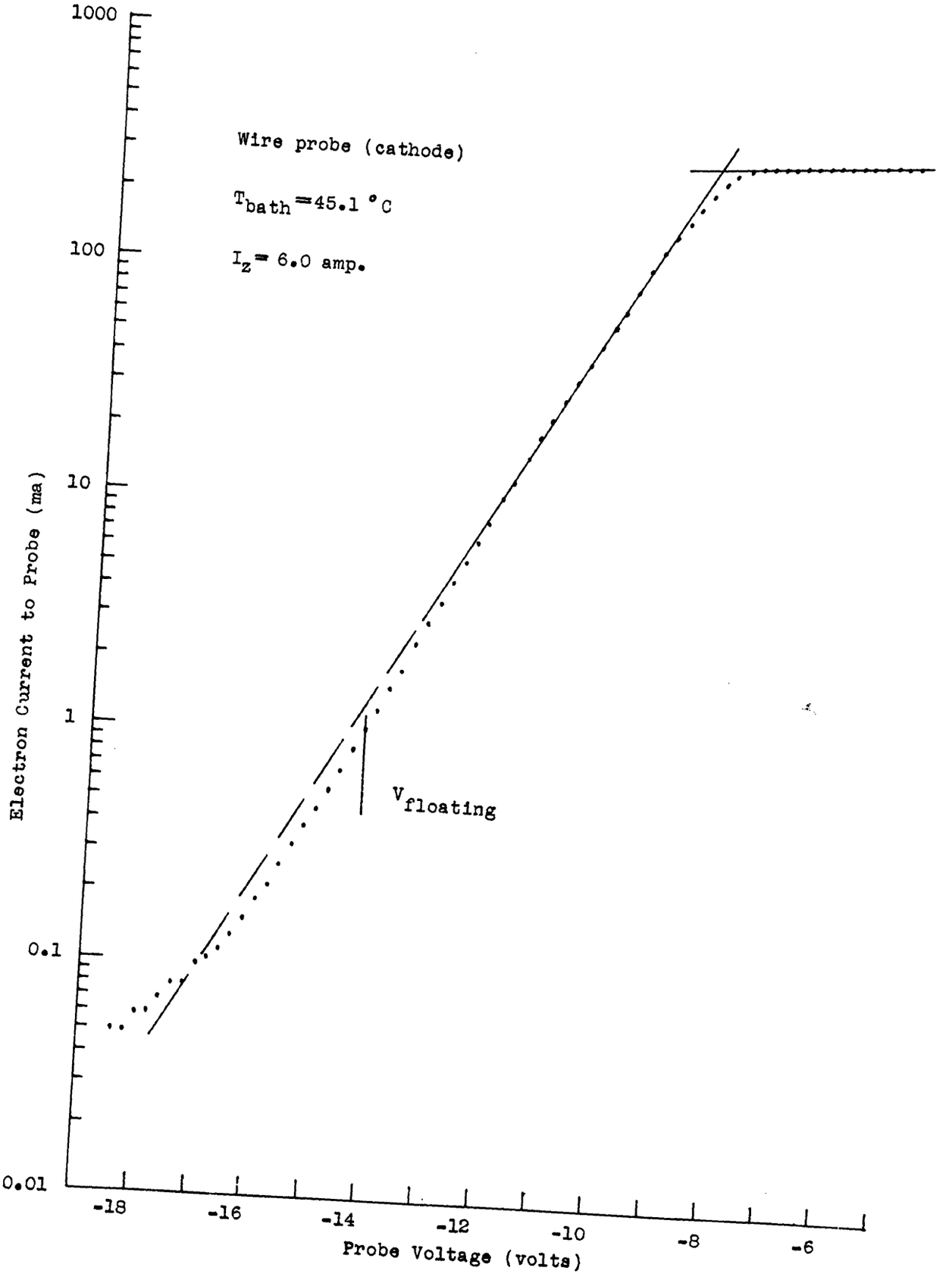

Fig. III-17

Wire probe curve

approximate vapor temperature of 300°K, the temperature jump will be neglected.

D. Wall sheath thickness

The diameter of the plasma does not correspond exactly to the inner diameter of the discharge tube because of the formation of an ion sheath on the insulating walls. In order to calculate the processes in the plasma, the plasma radius must be known and therefore the sheath thickness must be calculated. This sheath thickness Δr is calculated for the wall probe at floating potential and it is assumed that the floating potential of the tantalum probe is the same as the floating potential of the pyrex wall. The difference between the probe floating potential and the wall floating potential cannot be large because the electron current is a strong function of the collector potential.

Since the electron density in the ion sheath is small, the ion current flow to the wall is governed (in this region) by the Langmuir-Childs space charge law:

$$J_+ = \frac{4}{9}\epsilon_0 \left(\frac{2q}{M_+}\right)^{1/2} \frac{(\Delta V)^{3/2}}{(\Delta r)^2} \qquad \text{(III-9)}$$

where J_+ is the ion current density, ΔV is the potential difference between the plasma and the floating probe, Δr is the sheath thickness, and ϵ_o in rationalized MKS units is equal to 8.854×10^{-12} farad/m. This equation assumes that the plasma-sheath interface has a definite location, that the ions enter the sheath with zero velocity, and that the potential gradient is zero at the interface. Actually the ions enter with a directed energy of about $kT_-/2q$, and the potential gradient is approximately 1 volt/cm.

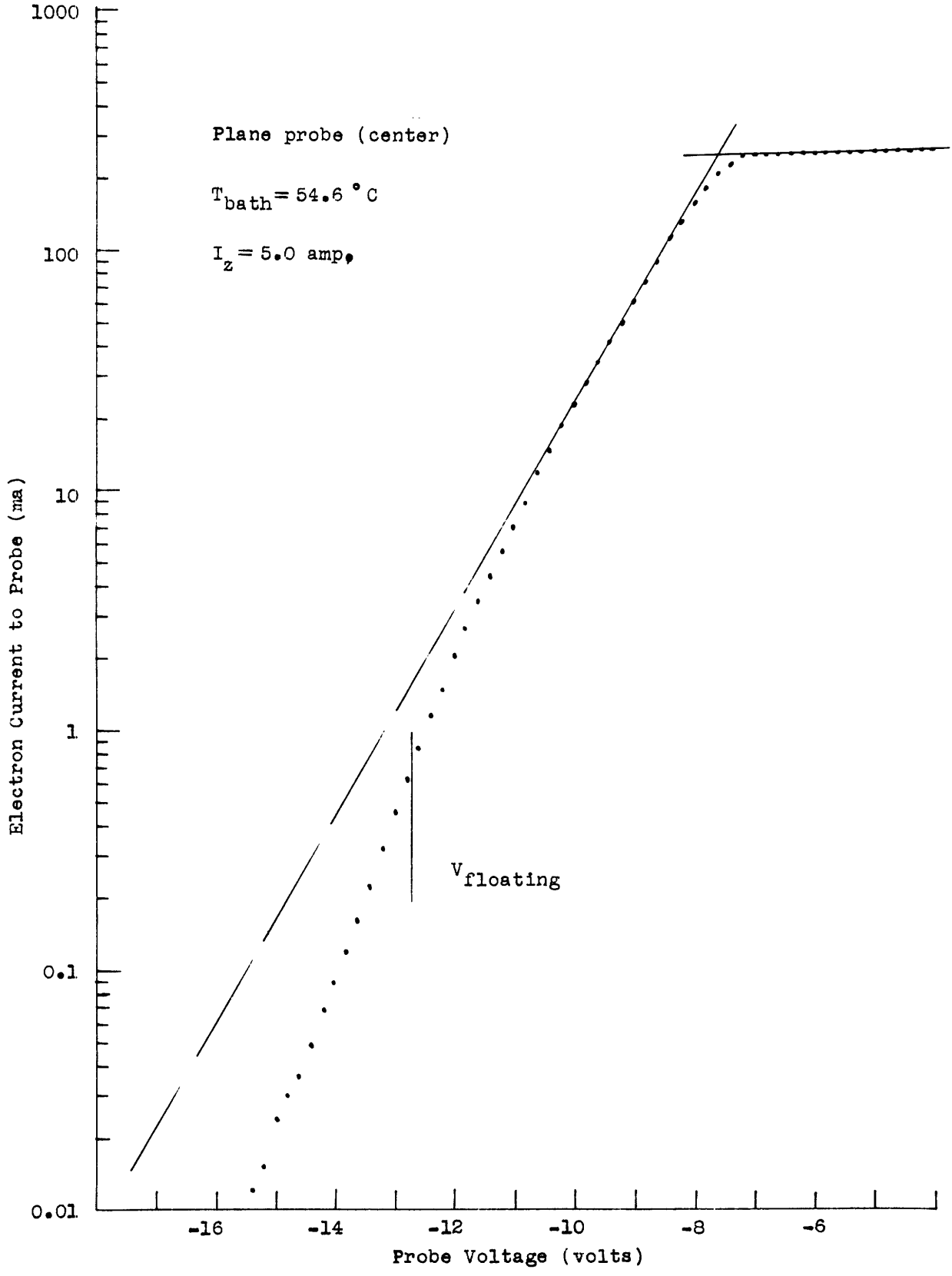

Fig. III-18

Plane center probe curve

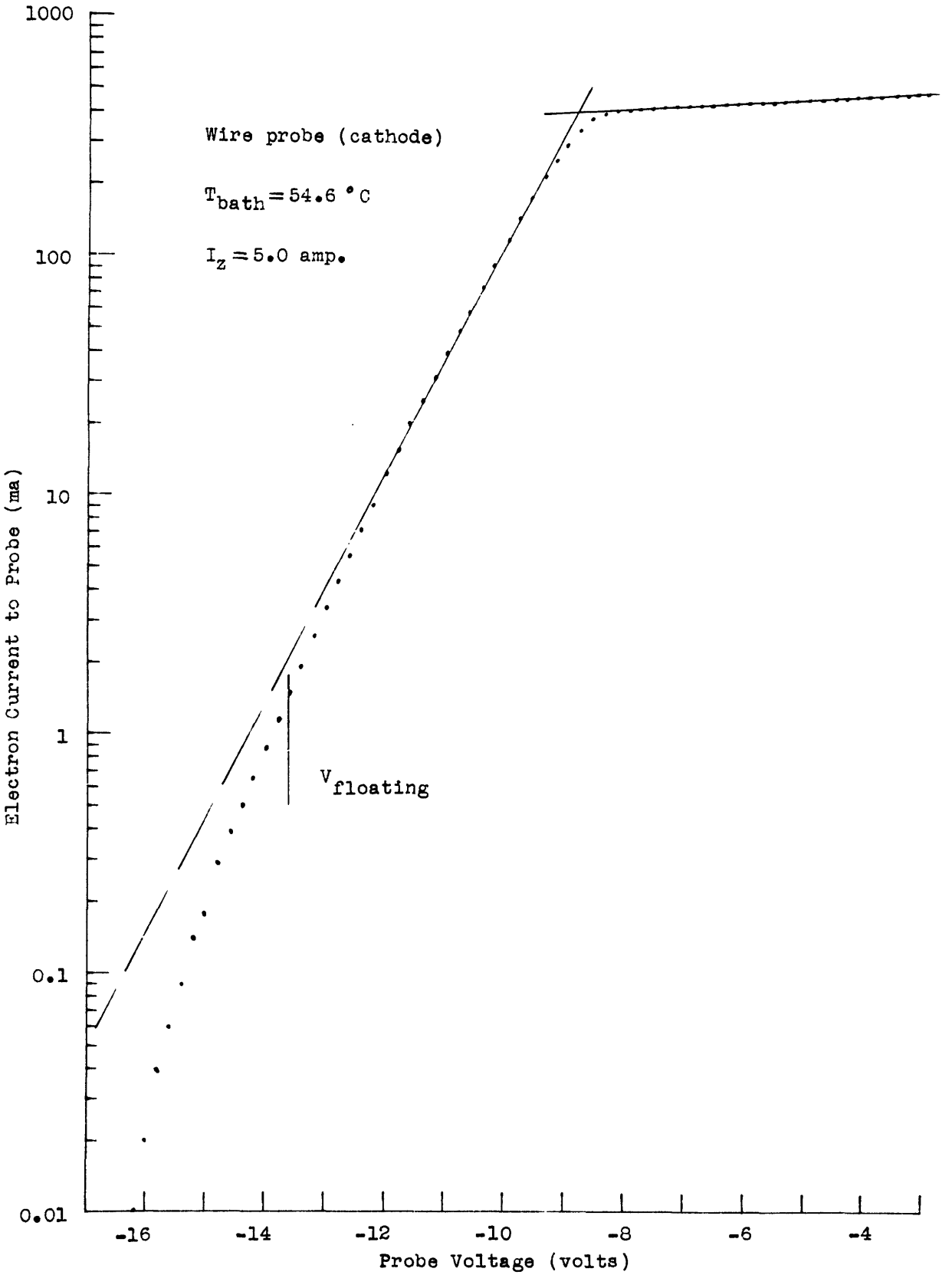

Fig. III-19

Wire probe curve

A first order correction has been calculated for the Langmuir-Childs space-charge equation, and results in a change in the calculated sheath thickness by the factor:

$$\frac{\Delta r\,(E_o, dV/dr)}{\Delta r} = 1 + \frac{3}{2}\left(\frac{E_o}{\Delta V}\right)^{1/2} + \frac{3}{4}\frac{E_o}{\Delta V} - \frac{27}{32}\left(\frac{\Delta r}{\Delta V}\right)^2\left(\frac{dV}{dr}\right)^2 \qquad \text{(III-10)}$$

where E_o is the initial directed energy of the ions in electron volts as they enter the sheath (assumed monoenergetic), ΔV is the potential difference between the plasma and the probe, dV/dx is the potential gradient at the interface, and Δr is the sheath thickness as calculated from the zeroth order Langmuir-Childs equation. When typical values are substituted in this expression, it is seen that the change in Δr caused by the interface potential gradient is quite small while the predominant correction is the $1.5\ (E_o/\Delta V)^{1/2}$ term which is about 38 per cent. Since the ion sheath results in a correction of less than 0.4 per cent of the radius which is comparable to the 0.4 per cent uncertainty in the measured tube diameter, any detailed correction is of small value. The calculated values of the ratio of plasma radius to inner wall radius r_p/r_w are listed in Table II.

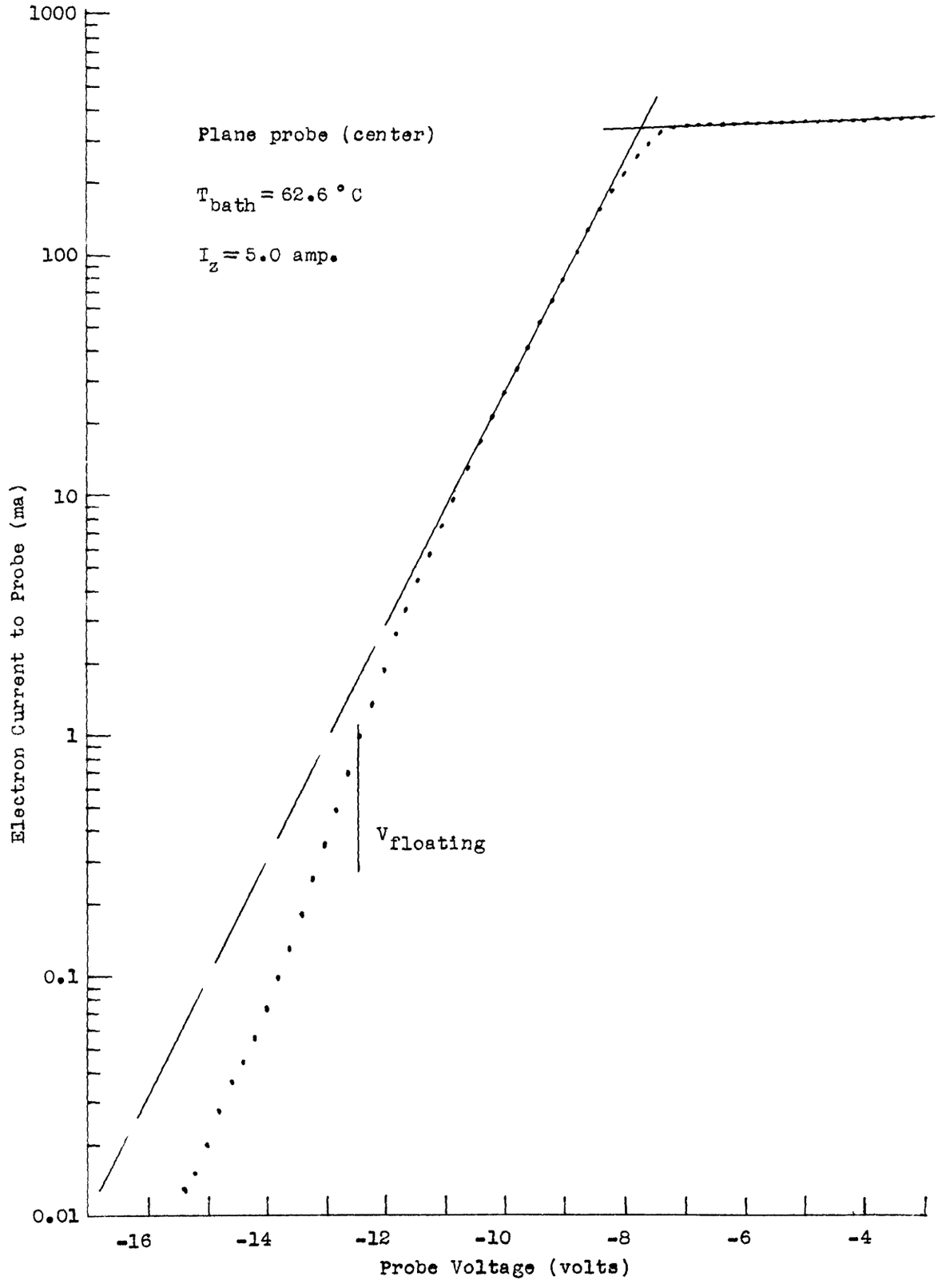

Fig. III-20

Plane center probe curve

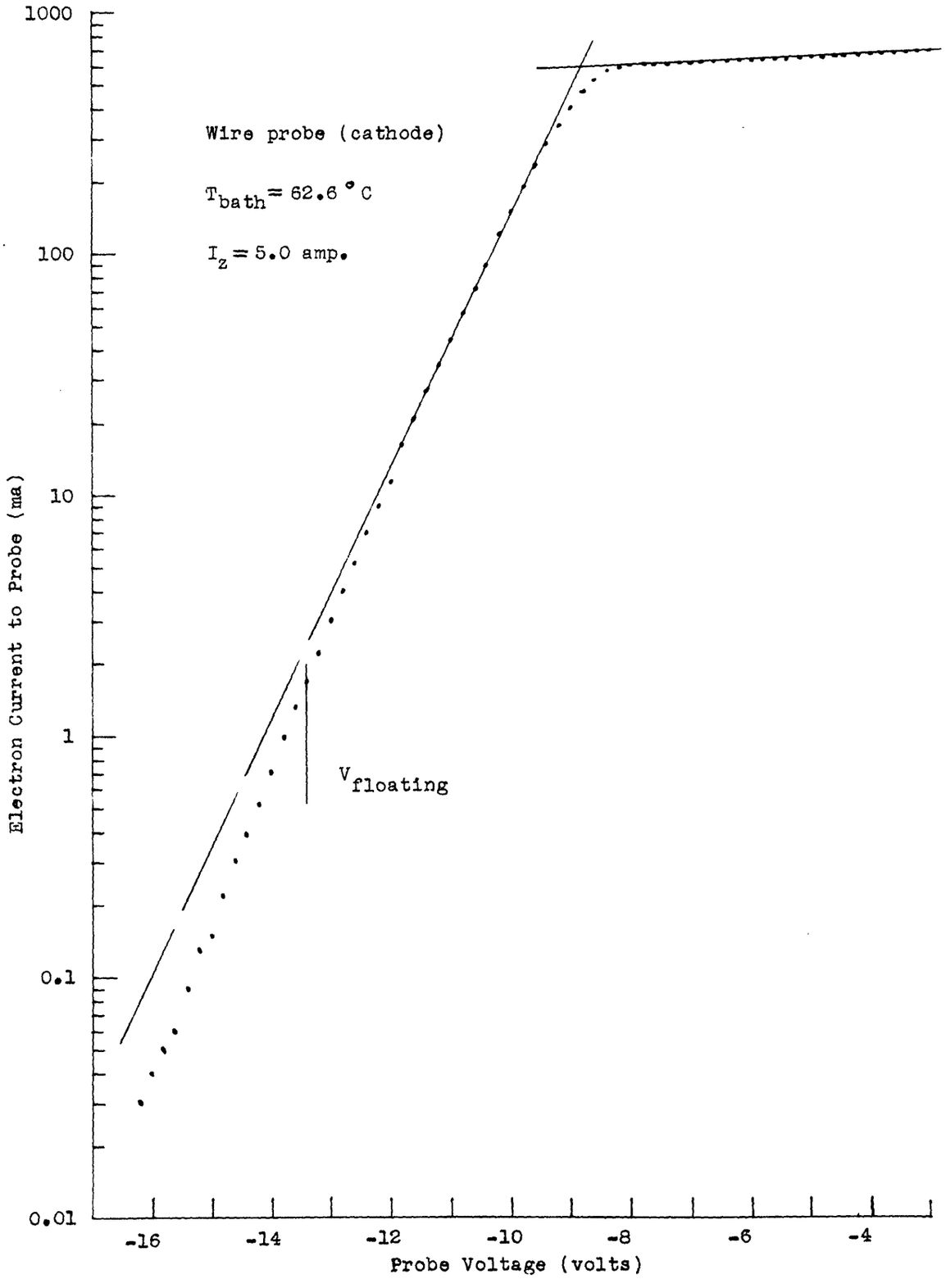

Fig. III-21

Wire probe curve

IV. Ionization Processes in the Plasma

A. Production of ions in the plasma

One of the important processes in the mercury arc plasma is the production of ions through the inelastic collisions of high energy electrons with mercury atoms. It is sometimes assumed that ions are generated predominantly by direct ionization of atoms in the ground state (6^1S_0). An alternative method of ionization involves the production of excited atoms ($6^3P_{0,1,2}$) and then the subsequent ionization of these excited atoms to form ions. Meissner and Miller[33] find that external irradiation of a positive column (He, Ne, A, Kr, Xe) results in a potential increase for a constant current. They show that practically the entire irradiation effect for the He plasma is due to the absorption of the 20,581 A line which raises the metastable 2^1S_0 state to the 2^1P_1 radiating state. Kenty[34] reports that for a discharge in a Hg and rare gas mixture, strong illumination by Hg radiation nearly doubles V and T_- (arc voltage and electron temperature). He concludes that the $^3P_2$ metastable state furnishes most of the ions. These experiments indicate that the ionization in a plasma is determined largely by the metastable density. In his microwave afterglow studies, Biondi[35] finds that collisions between pairs of metastable atoms also produce significant ionization in the decaying plasma. These ionization processes that take more than one step are called cumulative ionization.

It will be shown in this chapter that the ionization in the plasma under investigation proceeds predominantly by cumulative processes.

B. Measurement of the total ionization and the determination of the electron density distribution from ambipolar diffusion theory

It is necessary to measure the total ionization G, (ions generated per second per unit volume) as a function of the electron density n_-, the gas density n_g, and the electron temperature kT_-/q, in order to obtain the desired information about the fundamental processes involved in the production of ions. From consideration of charge conservation, when there is no significant volume recombination of ions and electrons, the ions and electrons produced in the steady state plasma will all travel to the wall where they will recombine. The ion current density to the wall probe when it is at floating potential $J_+(V_f)$, is therefore a measure of the total ionization averaged over a cross-section of the plasma G. This assumes that the effects of the secondary electron emission from the pyrex wall and from the tantalum wall probe are small.

There is very little information available for the secondary emission coefficients for Hg metastables, but a value for the secondary emission coefficient for Hg metastables on mercury has been reported by von Engle[36] to be about 0.01. This implies that the metastable induced electron emission from the pyrex wall (with condensed mercury on the surface) can be considered small. In addition, measurements on the ion current to a negative probe show that the difference between the ion current for a clean and dirty probe (Ta and W) is less than 2 per cent, for this mercury arc. Since Hagstrum[37] has shown that the secondary emission coefficients are very dependent upon the surface contamination, it is expected that if the secondary electron emission were contributing appreciably to the ion current measured by the wall probe, it should

be possible to influence this ion current by cleaning the probe by electron bombardment. The absence of such an effect implies that the secondary emission due to metastables is not significant. In addition, since the electrons ejected by metastable bombardment must again be collected by the wall, a net error is introduced only if the secondary emission coefficient for the pyrex-mercury wall is different from the secondary emission coefficient for the Ta wall probe. It can thus be seen that the secondary emission due to metastable atoms is only a second order effect in the measurement of the ambipolar ion current. Since the secondary emission coefficients appear to be only about 1 per cent for H_g, the second order effect due to metastable induced secondary emission will be neglected.

From the continuity equation div $(J_+/q) = G$, it can be shown that the average total ionization $\overline{G}$ (averaged over the cross-section of the long cylindrical plasma), is related to the wall ion particle current density Γ_{+w}, the plasma radius r_p, and the wall radius r_w, by the following expression:

$$\Gamma_{+w} = \frac{r_p}{2}\left(\frac{r_p}{r_w}\right)\overline{G} \qquad \text{(IV-1)}$$

The values of $\overline{G}$ calculated from the experimental data are listed in Table III.

In order to investigate the dependence of $\overline{G}/p_o\overline{n_-}$ upon kT_-/q, it is necessary to determine the value of $\overline{n_-}$ (averaged over a cross-section of the plasma) in terms of the central density n_{-o}, and the wall density n_{-w}. This makes it necessary to calculate the electron density distribution and requires a discussion of ambipolar diffusion theory.

If only electrons and singly charged ions are produced, the conservation of charge and the continuity equation for the steady state require that:

$$\operatorname{div} \vec{\Gamma}_+ = \sigma \tag{IV-2}$$

$$\operatorname{div} \vec{\Gamma}_- = \sigma \tag{IV-3}$$

In the range where mobility and diffusion processes determine the electron and ion flow,

$$\vec{\Gamma}_+ = D_+ \operatorname{grad} n_+ + \mu_+ n_+ \operatorname{grad} V \tag{IV-4}$$

$$\vec{\Gamma}_- = D_- \operatorname{grad} n_- - \mu_- n_- \operatorname{grad} V \tag{IV-5}$$

where D_+, μ_+, D_- and μ_- respectively are the ion diffusion coefficient, the ion mobility coefficient, the electron diffusion coefficient, and the electron mobility coefficient. The potential V, is related to the ion and electron density by Poisson's equation:

$$\operatorname{div} \operatorname{grad} V = -\frac{q}{\epsilon_0}(n_+ - n_-) \tag{IV-6}$$

where e_o is the permittivity in rationalized MKS units.

The diffusion coefficients D_+, and D_-, correspond to a net flow due to a density gradient. There is also a "temperature diffusion coefficient" which corresponds to a net flow resulting from a "temperature"

gradient, but it is assumed that the "temperature gradient" is small compared to the density gradient so that the thermal diffusion can be neglected.

There are now 5 independent equations relating the 5 variables $\vec{\Gamma}_+$, $\vec{\Gamma}_-$, n_-, n_+, and V (two vector and 3 scalar). Since the differential equations contain nonlinear terms it is necessary to resort to some simplification following Schottky's ambipolar diffusion theory[38] (but with a little more rigor in the derivation). The potential gradients in the plasma are quire small (about 1 volt per cm) and therefore according to Poisson's equation the ion density is very closely equal to the electron density and permits the elimination of one of the equations and one of the variables by allowing the approximation $n_- = n_+$. The ion and electron density gradients are also approximately equal although probably to a lesser extent. When the divergence of $\vec{\Gamma}_+$ and $\vec{\Gamma}_-$ are taken and the term div (n_- grad V) is eliminated, it is possible, without requiring any assumption about the equality of $\vec{\Gamma}_+$ and $\vec{\Gamma}_-$, to obtain the following expression which is valid for any geometry:

$$div\ (D_a\ grad\ n_-) + \sigma = 0 \qquad \text{(IV-7)}$$

where the ambipolar diffusion coefficient D_a, is defined by:

$$D_a \equiv \frac{D_+ \mu_- + D_- \mu_+}{\mu_- + \mu_+} \qquad \text{(IV-8)}$$

When D_a is assumed to be independent of position, the following results:

$$D_a\ div\ grad\ n_- + \sigma = 0 \qquad \text{(IV-9)}$$

This differential equation when solved with the appropriate boundary conditions will specify the density distribution of the electrons and ions

and will permit the average electron density $\bar{n}_-$, to be calculated.

Considerable information about the properties of the plasma can be obtained from the relationship between the currents and the potential and density gradients. Because div $\vec{\Gamma}_+$ = div $\vec{\Gamma}_-$, the vector currents $\vec{\Gamma}_+$ and $\vec{\Gamma}_-$, differ only by a constant vector term $\vec{B}$ and by a curl $\vec{A}$ term since in general div curl $\vec{A}$ = 0. For a long cylindrical plasma the radial component of the curl $\vec{A}$ term $\text{curl } A)_r = \frac{1}{r}\frac{\partial A_z}{\partial \phi} - \frac{\partial A_\phi}{\partial z}$ is zero because of the angular and axial symmetry. Since the radial components of the vectors $\vec{\Gamma}_+$ and $\vec{\Gamma}_-$ are equal at the wall (which is at floating potential), the radial component of the constant vector $\vec{B}$, is zero at the wall and is therefore zero throughout the plasma. This demonstrates that the radial components Γ_{+r} and Γ_{-r} are equal for all values of r in the plasma so that:

$$\Gamma_{+r} = \Gamma_{-r} = \Gamma_r \qquad \text{(IV-10)}$$

It should be noted that this is not necessarily true for all components of $\vec{\Gamma}_+$ and $\vec{\Gamma}_-$, as is sometimes stated or implicitly assumed. Elimination of Γ_r between the radial components of the vector equations results in the relationship between the radial density gradient and the radial potential gradient:

$$\frac{dV}{dr} = \frac{D_- - D_+}{\mu_- + \mu_+} \frac{d}{dr} \ln n_- \qquad \text{(IV-11)}$$

which has as a solution:

$$\frac{n_1}{n_2} = \exp\left[(V_1 - V_2) \frac{\mu_- + \mu_+}{D_- - D_+} \right] \qquad \text{(IV-12)}$$

It will be shown that this leads to the Einstein relation between the diffusion coefficient and the mobility coefficient.

An insulating surface placed in contact with the plasma will assume a potential with respect to the plasma such that the total current to the surface is zero. Since the electron and ion densities are equal, and the electron mass is much less than the ion mass, the random current to the probe will be predominantly electron current unless the ions are much more energetic than the electrons which is very unlikely. Thus the potential of the insulating surface will go negative with respect to the plasma until it repels all but a small fraction of the incident electrons. At the same time, this negative probe influences the plasma (in spite of the fact that the bulk of this potential difference appears across the small ion sheath) and draws additional ions to the surface in excess of the random flow. As a result of the negative wall, the radial flow of electrons due to the density gradient is very nearly compensated by the opposite flow due to the potential gradient. Since the negative wall considerably reduces the electron drain, the electrons are in approximate equilibrium and therefore their density may be described by the Boltzmann density distribution:

$$\frac{n_1}{n_2} = \exp\left[\frac{q(V_1 - V_2)}{kT_-}\right] \qquad \text{(IV-13)}$$

Since the mobility and diffusion coefficients for electrons are much larger than for ions, these equations lead to the Einstein relation:

$$\frac{D_-}{\mu_-} = \frac{kT_-}{q} \qquad \text{(IV-14)}$$

For the case where the distribution functions are not isotropic, the Einstein relation may be expressed in tensor form[39, 40].

Since the radial components of the flow vectors are equal, it is possible to eliminate dV/dr from the vector equations to obtain the following relation between the radial current flow and the radial density gradient without requiring any assumptions about the constancy of D_a:

$$\Gamma_{+r}(V_f) = - D_a \frac{dn_+}{dr} \qquad \text{(IV-15)}$$

This equation will be used in the next chapter to calculate the ambipolar diffusion coefficient from the measured value of $\Gamma_{+r}(V_f)$ and from the value of dn_-/dr calculated from the assumed density distribution. In addition, the average electron density $\bar{n}_-$, will be used in the calculation of the electron mobility.

Thus it can be seen that many interesting quantities can be calculated provided that the electron density distribution can be specified with reasonable accuracy. The partial differential equation for the electron density can be reduced to a differential equation in r if the plasma is long enough so that end effects are negligible and if advantage is taken of the cylindrical symmetry of the plasma to eliminate the angular dependence so that:

$$D_a \frac{1}{r} \frac{d}{dr}\left(r \frac{dn_-}{dr} \right) + \sigma = 0 \qquad \text{(IV-16)}$$

For the case where the ion generation is assumed constant throughout the plasma volume (only for the purpose of simplicity of solution), the electron density can be expressed in the following simple form:

$$\frac{n_-}{n_{-0}} = 1 - \frac{r^2}{R_0^2} \qquad \text{(IV-17)}$$

where the part of the solution that is singular at $r = 0$, is eliminated by the physical requirement that the electron density is finite and non-zero at all points in the plasma. This solution, although easily obtained is not an accurate description of the density distribution.

A much more accurate solution corresponds to the assumption that the ion generation is proportional to the electron density and can be written as

$$G = \nu_i n_- \tag{IV-18}$$

The ionization frequency ν_i (ions per second per electron) is a function of the electron energy distribution function and it is necessary to assume that ν_i contains no radial dependence in order to solve the differential equation. The resulting linear differential equation has solutions in the form of Bessel functions with the singular solutions excluded because of the finiteness requirement so that

$$\frac{n_-}{n_{-0}} = J_0\left(2.405 \frac{r}{R_0}\right) \tag{IV-19}$$

where as a result of the change of variable

$$\frac{\nu_i}{D_a} = \left(\frac{2.405}{R_0}\right)^2 \tag{IV-20}$$

Because negative values of n_- are not possible, the first zero of the Bessel function cannot be within the plasma. It is possible to determine R_0 by measuring the electron density at the center and at a particular radius (for convenience at the plasma edge). In this way, the quantity ν_i/D_a

can be calculated from the measured quantities.

The case where the ionization is assumed to be completely quadratic ionization ($G(n_-) = b(n_-)^2$), has been considered by Spenke[41] who solved the resulting nonlinear equation to give the density as a function of the radius:

$$\frac{n_-}{n_{-0}} = S\left(2.92\,\frac{r}{R_0}\right) \qquad \text{(IV-21)}$$

where 2.92 is the first zero of the Spenke function, and the values of S are tabulated by Spenke for the variable $2.92\,r/R_0$ in steps of 0.2 up to the first zero.

The difference between the density distribution given by the Bessel function and by the Spenke function is quite small (see Howe[15]) in view of the uncertainties of electron density measurements so that it is not easy to determine experimentally if the density distribution fits the Bessel function or the Spenke function better. Howe[15] has made measurements of the electron density distribution in the plasma of a low pressure mercury arc, and he obtained values of electron density (for 5 different radial positions) that could be fit somewhat better by the Spenke function than the Bessel function at the 3 highest pressures. On the basis of this and also in view of the fact that the direct ionization cannot account for the observed ionization, Howe concluded that the ionization in the plasma is quadratic cumulative ionization. Unfortunately the accuracy of Howe's experimental results are somewhat subject to question. Analysis of the experimental data given by Howe in his article shows that the electron density as measured by his wall probe is about 48 per cent (on the average) larger than the electron density as measured

by the element of his multiple probe nearest the wall. Since this is obviously impossible, the value of Howe's density measurements is reduced.

In any event, since the average of the electron density distribution is needed for the determination is the total ionization frequency, and for the electron mobility, the process of integration itself reduces any small difference between the assumed distribution and the actual distribution. To estimate the small differences resulting from the various assumed distributions, the average density (normalized to unity at the center) has been calculated for the parabolic distribution, the Bessel distribution, and the Spenke distribution, with the integration for each taken out to the zero since the averages differ the most at this value. The calculated values of $\bar{n}/n_o$ are: $\bar{n}/n_o$(parabolic) = 0.500, $\bar{n}/n_o$ (Bessel) = 0.432, and $\bar{n}/n_o$ (Spenke) = 0.374. The average value of the Spenke distribution was calculated by integration of the series solution given by Spenke. From the above results, it can be seen that the Bessel function can be used to evaluate the average electron density quite accurately with the uncertainty not more than 13.5 per cent if the actual density distribution falls between the Bessel distribution and the Spenke distribution. The properties of the Bessel function permit the average electron density $\bar{n}_-$, to be given by:

$$\frac{\bar{n}_-}{n_{-o}} = \frac{2J_1(x)}{x} \qquad \text{(IV-22)}$$

where the value of x is determined from the density at the center n_{-o}, and at the wall n_{-w}, by

$$\frac{n_{-w}}{n_{-o}} = J_o(x) \qquad \text{(IV-23)}$$

The values of $\bar{n}_-/n_{-o}$ calculated from n_{-w}/n_{-o} have been listed in Table III. It is now possible to calculate the total effective ionization frequency reduced to 1 mm Hg and 0^oC: $G/p_o\bar{n}_-$.

In order to analyze the dependence of the total ionization G, upon the electron density and the electron temperature, it is necessary to consider in some detail the general problem of the production of particles of type "B" as a result of collisions of electrons with particles of type "A". In general, the generation rate G (number per second per unit volume) is given by:

$$G(A\to B) = \int_{-\infty}^{\infty}\int_{-\infty}^{\infty}\int_{-\infty}^{\infty} n(A)\, v\, Q(A\to B) f(v)\, dv_x\, dv_y\, dv_z \qquad \text{(IV-24)}$$

where the velocity of the electron is assumed to be much larger than the velocity of particles "A" so that the relative velocity of the electrons and particles"A" can be assumed to be equal to that of the electrons v_-. When the differential cross-section $Q(A\to B)$, which is a function of the electron energy V, has a threshold energy V_θ, and when the velocity distribution function of the electrons is M-B with a characteristic temperature $V_T = kT_-/q$, the generation rate G, can be expressed in the form

$$G(A\to B) = n(A)\, n_-\, \langle v_-\rangle \int_{V_\theta}^{\infty} Q(A\to B)\, e^{-V/V_T} (V_T)^{-2} V\, dV \qquad \text{(IV-25)}$$

The effective cross-section $Q_o(A \rightarrow B)$, can be defined as that value of constant cross-section which when used to replace the differential cross-section in the integral will give the same value for $G(A \rightarrow B)$. Thus

$$G(A \rightarrow B) = n(A) n_- \langle \nu_- \rangle Q_o(A \rightarrow B) \left[1 + \frac{V_\theta}{V_T} \right] e^{-V_\theta / V_T} \qquad \text{(IV-26)}$$

and it is seen that the major dependence of G upon V_T is in the $\exp(-V_\theta/V_T)$ term since the effective cross-section Q_o is not a strong function of V_T.

This expression for the ion generation suggests that the quantity $\overline{G}/p_o\overline{n}_-$ when plotted (on a semi-log plot) as a function of q/kT_- will have a slope characteristic of the effective threshold energy V_θ, for the production of ions. It is assumed that the number of atoms of type "A" supplying the ions (atoms in the ground and excited states) is proportional to the reduced pressure p_o. The quantity $\log \overline{G}/p_o\overline{n}_-$ is plotted in Fig. IV-1 as a function of q/kT_- and it is seen that the points fall on a straight line as is implied by the previous equation.

The effective threshold voltage V_θ, is found to be 6.26 volts, and the average effective cross-section Q_o for ionization in the mercury plasma is calculated to be 0.41×10^{-16} cm^2 with a rms deviation of 10 per cent. Thus the actual ionization in the plasma can be described quite accurately by

$$\overline{G}(\text{IONS}) = n_g \overline{n}_- \langle \nu_- \rangle 0.41 \times 10^{-16} (cm^2) \left[1 + \frac{6.26}{V_T} \right] e^{-6.26/V_T} \qquad \text{(IV-27)}$$

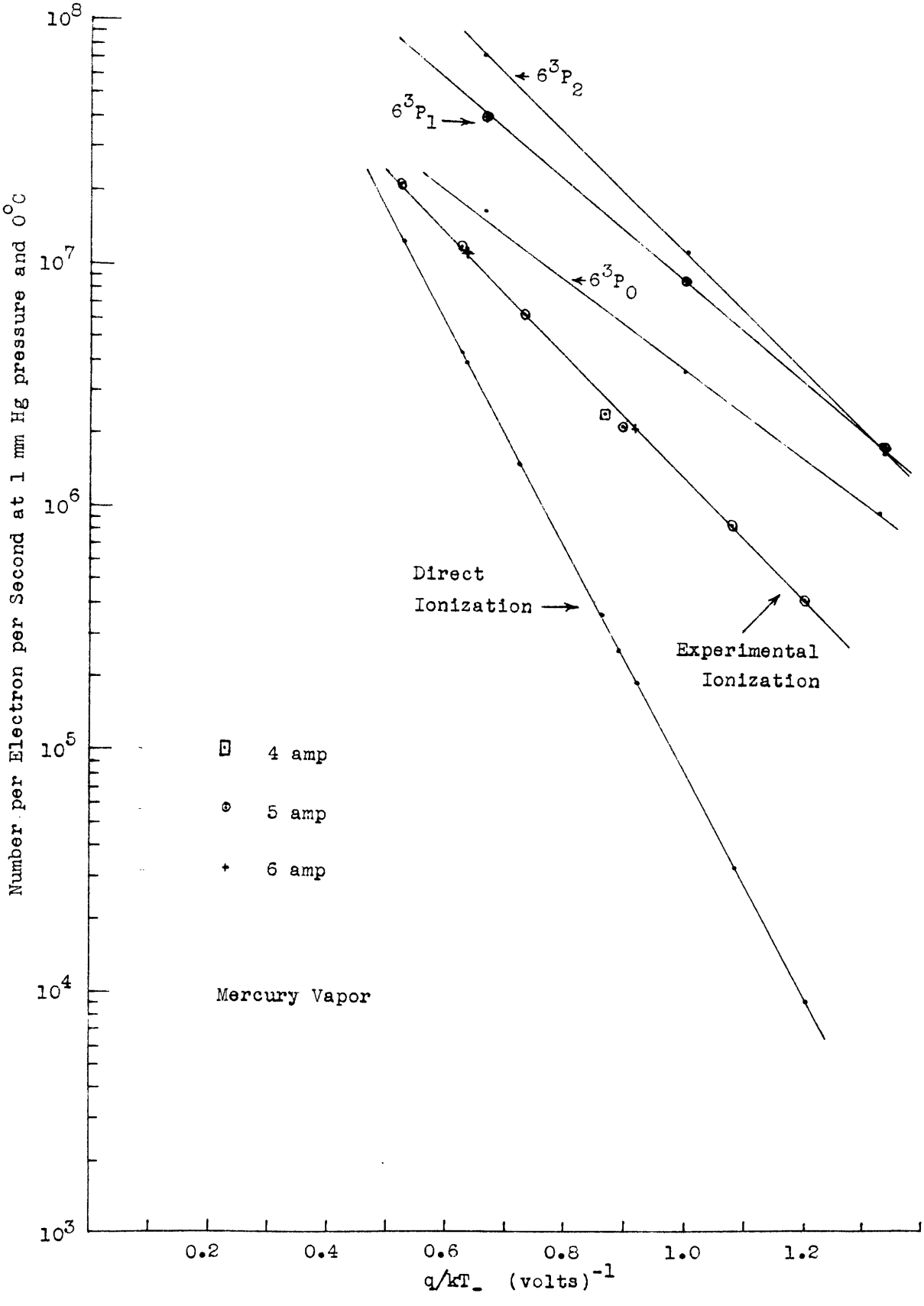

Fig. IV-1 Ion generation

If it can be assumed that the ions are produced through the ionization of the $6^3P_{0,1,2}$ states, and if an estimate can be made of the density of these states, an estimate can then be made of the cross-section for ionization of these states. This problem will be discussed in section D of chapter IV. First, however, it is necessary to demonstrate that the actual ionization is much larger than can be accounted for by direct ionization of atoms in the ground state. This will be done in the next section.

C. Calculation of the direct ionization component including the effect of the electron drift velocity

In order to compare the direct ionization with the total ionization, the value of ν_i/p_o was calculated from Nottingham's[42] data for the probability of direct ionization of mercury atoms by fast electrons. A M-B energy distribution for the electrons was assumed. The ionization frequency ν_i, (neglecting the atom velocity compared to the electron velocity) is given by

$$\nu_i = \langle v_- \rangle (V_T)^{-2} \int_{V_i}^{\infty} p_o P_i(V) e^{-V/V_T} V dV \qquad \text{(IV-28)}$$

The term V_T is the voltage equivalent of the electron temperature, V is the energy of the electron in electron volts, V_i is the ionization potential of 10.43 volts for mercury, and $\langle v_- \rangle$ is the magnitude of electron velocity averaged over the distribution function and is given by $\langle v_- \rangle = (8q/\pi m_-)^{1/2} (kT_-/q)^{1/2} = 6.693 \times 10^5 (kT_-/q)^{1/2}$ meters/second. The term $P_i(V)$ is Nottingham's probability of ionization (for electrons of energy V) measured in ions per electron per meter path

at 0^{o}C and 1 mm Hg pressure (for p_o equal to 1 mm Hg). The probability of ionization is related to the cross-section for ionization Q_i, by: $p_o P_i(V) = n_g Q_i(V)$, where the ratio n_g/p_o corresponds to a density of 3.536×10^{16} molecules per cm^3 for a reduced pressure p_o, of 1 mm Hg. Numerical integration yields values of the integral ν_i/p_o, which are tabulated in Table III and are plotted in Fig. IV-1 as a function of q/kT_- for comparison with the actual ionization frequency $\overline{G}/p_o\overline{n}_-$. Comparison of the experimental ionization frequency and the calculated ionization frequency for direct ionization shows that the actual ionization frequency is much larger than the direct ionization component.

It is logically necessary to demonstrate that the electron drift velocity superimposed upon the M-B velocity distribution does not significantly increase the direct ionization component. The distribution function for the electrons is taken to be a displaced M-B distribution of the form:

$$f(v)d\vec{v} = n_- \left(\frac{m_-}{2\pi kT_-}\right)^{3/2} \exp\left[-\frac{m_-\left(\left[v_z - v_\phi\right]^2 + v_x^2 + v_y^2\right)}{2kT_-}\right] dv \qquad \text{(IV-29)}$$

(where v_ϕ is the drift velocity). The direct ionization can be calculated by partial integration to be

$$\frac{\nu_i}{p_o} = \langle v_- \rangle \left(v_T\right)^{-2} \int_{V_i}^{\infty} e^{-\frac{V_\phi}{V_T}} \frac{\sinh\left[2\left(\frac{V_\phi}{V_T}\frac{V}{V_T}\right)^{1/2}\right]}{2\left(\frac{V_\phi}{V_T}\frac{V}{V_T}\right)^{1/2}} P_i(V) e^{-\frac{V}{V_T}} V dV \qquad \text{(IV-30)}$$

The drift energy - V_ϕ of the electrons is defined by: $qV_\phi = m_- v_\phi^2/2$. This integral was evaluated by numerical integration (again using Nottingham's data) for the lowest pressure data where the drift energy V_ϕ, is the largest fraction (4 per cent) of kT_-/q and where the effect of the drift energy on the direct ionization is the most important. It was found that even in this case the drift velocity has a small effect since it increases the direct ionization by only 16 per cent. The value of the drift velocity used in this calculation was obtained from the results of chapter V.

It is also necessary to point out that the actual probe curves indicate a depletion of high energy electrons above about 3.39 kT_-/q and therefore the assumption of a M-B distribution in the calculation of the direct ionization component is not quite accurate. This depletion strengthens the argument that the direct ionization is much smaller than the observed ionization since the calculated ionization for the M-B distribution case is an upper bound for the depleted distribution.

D. Determination of the important ionization processes in the plasma

It can be seen from Fig IV-1 that the actual ion generation in this experiment is much larger (up to a factor of 45.6 at the highest pressure) than the component that can be ascribed to direct ionization. This leads to the conclusion that the ions are produced predominantly through the ionization of excited and metastable atoms. It is first necessary to demonstrate that the rate of production of $6^3P_{0,1,2}$ states is large enough to supply the amount required by the observed ionization.

With the aid of the cross-sections for the production of $6^3P_{0,1,2}$

states in mercury as given by Kenty[43], it is possible to calculate the generation of such states by electrons with a M-B distribution:

$$G(6^1S_0 \rightarrow 6^3P) = n_- n_g \langle \nu_- \rangle (V_T)^{-2} \int_{V_0}^{\infty} Q(6^1S_0 \rightarrow 6^3P)\, e^{-\frac{V}{V_T}} V\, dV \qquad \text{(IV-31)}$$

where the threshold energies V_θ, for the $6^3P_{0,1,2}$ states are 4.67, 4.89, and 5.47 volts respectively. The results of these numerical integrations are given in Fig. IV-1 which shows that the production of these states is larger than the production of ions by about a factor of 10 and therefore can supply enough excited atoms to be ionized. The cross-section for ionization of these states has been given by Klarfeld[44] as about an order of magnitude (actually a factor of 30 was given by Klarfeld[44] in his original article) larger than the cross-section for ionization of the ground state. Waymouth and Bitter[45] report a factor of 3.3 for the ratio of the ionization cross-section for excited states to the cross-section for ionization of the ground state of mercury. It is possible to calculate from the data obtained in this experiment (with the aid of a few reasonable assumptions), a lower bound for the effective cross-section for ionization of the 6^3P states. This will be done later in this section.

It will be demonstrated that although the predominant ionization in the plasma is through the ionization of excited states (cumulative ionization), this cumulative ionization is a linear function of the electron density and not a quadratic function.

The loss of metastable states by diffusion is not the important factor in the determination of the density of these states. This can be

shown with the aid of the diffusion coefficient for 6^3P_2 metastable states in mercury which is given by Biondi[46] as: $D_m n_g = 1.5 \times 10^{18}$ ($\pm$ 10 per cent) $cm^2/sec \times cm^3$. The maximum density of 6^3P_2 states is given by Boltzmann's theorem:

$$\frac{n(6^3P_2)}{n(6^1S_0)} = \frac{g(6^3P_2)}{g(6^1S_0)} \exp\left(-\frac{5.47}{V_T}\right) \qquad \text{(IV-32)}$$

where the statistical weight ratio $g(6^3P_2)/g(6^1S_0)$, is equal to 5. This maximum value for the 6^3P_2 metastable density corresponds to the situation where the electrons and excited states are in equilibrium. According to some measurements made by Kenty[43] on a lower current mercury arc, the actual population of 6^3P_2 in his experiment is about 21 per cent of the maximum density given by the Boltzmann theorem. If the maximum value of the 6^3P_2 density is used together with the metastable diffusion coefficient given by Biondi, the resulting maximum loss by diffusion (assuming a Bessel function for the metastable radial density distribution) is given by

$$\text{MAXIMUM DIFFUSION LOSS}\left(\frac{\text{NUMBER}}{\text{SEC} - cm^3}\right) = \frac{n_m}{n_g} D_m n_g \left(\frac{2.405}{r_w}\right)^2 \qquad \text{(IV-33)}$$

If the actual metastable density distribution is more uniform than the Bessel function distribution, the diffusion loss will be even smaller. When the maximum diffusion loss of 6^3P_2 is compared to the generation of 6^3P_2 for set "D" of the data (corresponding to $kT_-/q = 0.920$ volts), it is found that the diffusion rate is less than the generation rate by a

factor of 3.4. Since the actual metastable density is lower than the maximum density calculated from Boltzmann's theorem, the loss of metastables by diffusion becomes even less significant.

The loss of metastables (at the higher pressures at least) is thus determined by collisions with electrons. Since the generation of excited states is proportional to the electron density, and the electron quenching rate is also proportional to n_-, the metastable density (for low D_m) should be independent of the electron density. An experiment by Kenty[43] has verified this statement. He measured the population of 6^3P_2 and 6^3P_0 metastable states by the absorption of 4047A and 5461A radiation as a function of arc current (and therefore as a function of n_-) and found that the absorption was essentially constant for arc currents ranging from about 0.1 to 0.45 amps. Thus for large electron densities and small D_m, the populations of metastables will be independent of n_-. If the ionization is predominantly produced through the ionization of metastables, the ion generation G should be a linear function of the electron density n_-, provided that the electron energy distribution function is relatively independent of n_-. As the pressure decreases the diffusion coefficient D_m for metastables (which is inversely proportional to p_o) increases and the diffusion loss of metastables becomes more important.

The results of this experiment show that $\overline{G}/p_o\overline{n}_-$ is independent of the electron density. For three of the nine sets of data, the arc current was changed by about 20 per cent with respect to the remaining 6 sets. If the cumulative ionization were quadratic as it is sometimes assumed, the value of $\overline{G}/p_o\overline{n}_-$ would be a linear function of $\overline{n}_-$ and would vary by 20 per cent for these three points. Such a variation is not observed and confirms the expectations.

As a result of the previous considerations, it is concluded that the ionization is proportional to the electron density, and therefore the cumulative ionization is linear ionization and not quadratic ionization. Any further investigation of the dependence of the ion generation upon electron density should also consider in some detail the electron energy distribution function, particularly for the high energy electrons. Unfortunately, at the present time, there is very little information available for the distribution functions.

It is possible to obtain limits for the effective cross-section for ionization of the 6^3P states if it is assumed that most of the ions are produced through ionization oı the 6^3P states, and if it is assumed that the $6^3P_{0,1,2}$ states have the same effective cross-section $Q_o(6^3P \rightarrow \text{ion})$. The method of calculation will be outlined below. Let 6^3P_j (where $j = 0, 1, 2$) represent any one of the $6^3P_{0,1,2}$ states. The density of the 6^3P_j state is given by:

$$\frac{n(6^3P_j)}{n(6^1S_0)} = S_j \frac{g(6^3P_j)}{g(6^1S_0)} \exp\left(-\frac{V_{0j}}{V_T}\right) \qquad \text{(IV-34)}$$

where the "saturation factor" s_j, is the ratio of the 6^3P_j density to the maximum density given by the Boltzmann theorem. The term $V_{\theta j}$ is the threshold energy for the j state. The multiplicity term $g(6^1S_0)$ is equal to 1, while the $g(6^3P_j)$ term is given by $(2j + 1)$. The generation of ions from the 6^3P_j state is now given by

$$G(6^3P_j \rightarrow \text{ion}) = n(6^3P_j)\, n_-(n_-)\, Q_o(6^3P_j \rightarrow \text{ion}) \left[1 + \frac{10.43 - V_{0j}}{V_T}\right] e^{-\frac{10.43 - V_{0j}}{V_T}} \qquad \text{(IV-35)}$$

The threshold energy for ionization of the 6^3P_j state is $(10.43 - V_{\theta j})$ volts. For the higher pressures where V_T is low, $n(6^1S_0) \approx n_g$, so that

$$\sigma(6^3P_j \rightarrow ion) = n_g n_- \langle v_- \rangle Q_o(6^3P \rightarrow ion) e^{-\frac{10.43}{V_T}} s_j(2j+1)\left[1 + \frac{10.43 - V_{\theta j}}{V_T}\right] \quad \text{(IV-36)}$$

At the higher pressures where the direct ionization is a small part of the total ionization, it may be assumed that

$$\sigma = \sum_{j=0,1,2} \sigma(6^3P_j \rightarrow ion) \quad \text{(IV-37)}$$

This observed ionization G, is thus related to the effective cross-section by

$$\sigma = n_g n_- \langle v_- \rangle Q_o(6^3P_j \rightarrow ion) e^{-\frac{10.43}{V_T}} \sum_{j=0,1,2} s_j(2j+1)\left[1 + \frac{10.43 - V_{\theta j}}{V_T}\right] \quad \text{(IV-38)}$$

If the values of s_j were known, then the value of Q_o $(6^3P \rightarrow ion)$ could be calculated from the known values of $V_{\theta j}$, and from the experimental values of G, n_g, n_-, $\langle v_- \rangle$, and V_T. Kenty's investigation [43] indicates that for his arc, s_0, s_1, s_2, are equal to 0.21, 0.047, 0.21 respectively. Since the

currents and electron densities in the present arc are much larger than in Kenty's arc, it is expected that the values of s_j in this experiment are closer to unity and that Kenty's values are a lower limit. When the maximum values of s_j (unity) are assumed, and the experimental values of G, n_g, n_-, $\langle v_- \rangle$, and V_T are introduced, a lower bound (minimum effective cross-section) is calculated for Q_o ($6^3P \rightarrow$ ion). The experimental values for the highest pressure (set E) give the greatest lower bound, and the corresponding minimum effective cross-section for ionization of the 6^3P states is found to be 8.1×10^{-16} cm^2. For the same electron temperature, the effective cross-section for ionization of the ground state is calculated from Nottingham's (42) data to be 0.90×10^{-16} cm^2. Thus the effective cross-section for ionization of a 6^3P_j state is a minimum of 9.0 times larger than the effective cross-section for ionization of the ground state. In addition, if the values of s_j given by Kenty for his arc are assumed to be approximately valid for this arc, the value of Q_o ($6^3P \rightarrow$ ion) calculated for the same set of date (highest pressure) is 53×10^{-16} cm^2 or about 58 times as large as the effective ionization cross-section for the ground state.

Since the values of s_j will probably be between unity and the values given by Kenty, the effective ionization cross-section for the 6^3P state will be between 9.0 and 58 times larger than the effective cross-section for ionization of the ground state, provided that the assumptions made in calculating these values are valid. When more definite values for s_j (or for the densities of the 6^3P_j states) are made available for a similar Hg arc, it will be possible to specify the cross-section Q_o ($6^3P \rightarrow$ ion) more closely.

V. Electron Mobility, Ambipolar Diffusion Coefficient, Ion Mobility Coefficient, Ion Diffusion Coefficient, and Cross-Section for Hg Ions in Their Parent Gas

A. Electron mobility

The mobility of electrons in the plasma can be obtained (from the results of the previous chapters) in terms of the axial current I_z, the plasma radius r_p, the axial potential gradient E_z, and the electron density averaged over a cross-section of the plasma $\overline{n_-}$. The axial drift current density $\overline{J_z}$, is given by

$$\overline{J_z} = q \mu_z \overline{n_-} \qquad \text{(V-1)}$$

where it is assumed that the axial potential gradient and the axial drift velocity (predominantly that of the electrons) are independent of the radial position in the plasma. Table IV contains values of $\overline{J_z}$ calculated from the axial current and the plasma radius. The average electron density $\overline{n_-}$, was calculated in chapter IV in conjunction with the determination of the ionization frequency, and is available from Table III. The resulting values of the axial drift velocity v_z are listed in Table IV and are plotted in Fig. V-1 as a function of E_z/p_o. This axial velocity is the sum of the drift velocity of the electrons and of the ions and is almost equal to the electron drift velocity. The ion mobility is very small compared to the electron mobility. This results in a correction of only about 0.2 per cent. The values of $p_o \mu_-$, defined by

$$p_o \mu_- = \frac{p_o v_z}{E_z} \qquad \text{(V-2)}$$

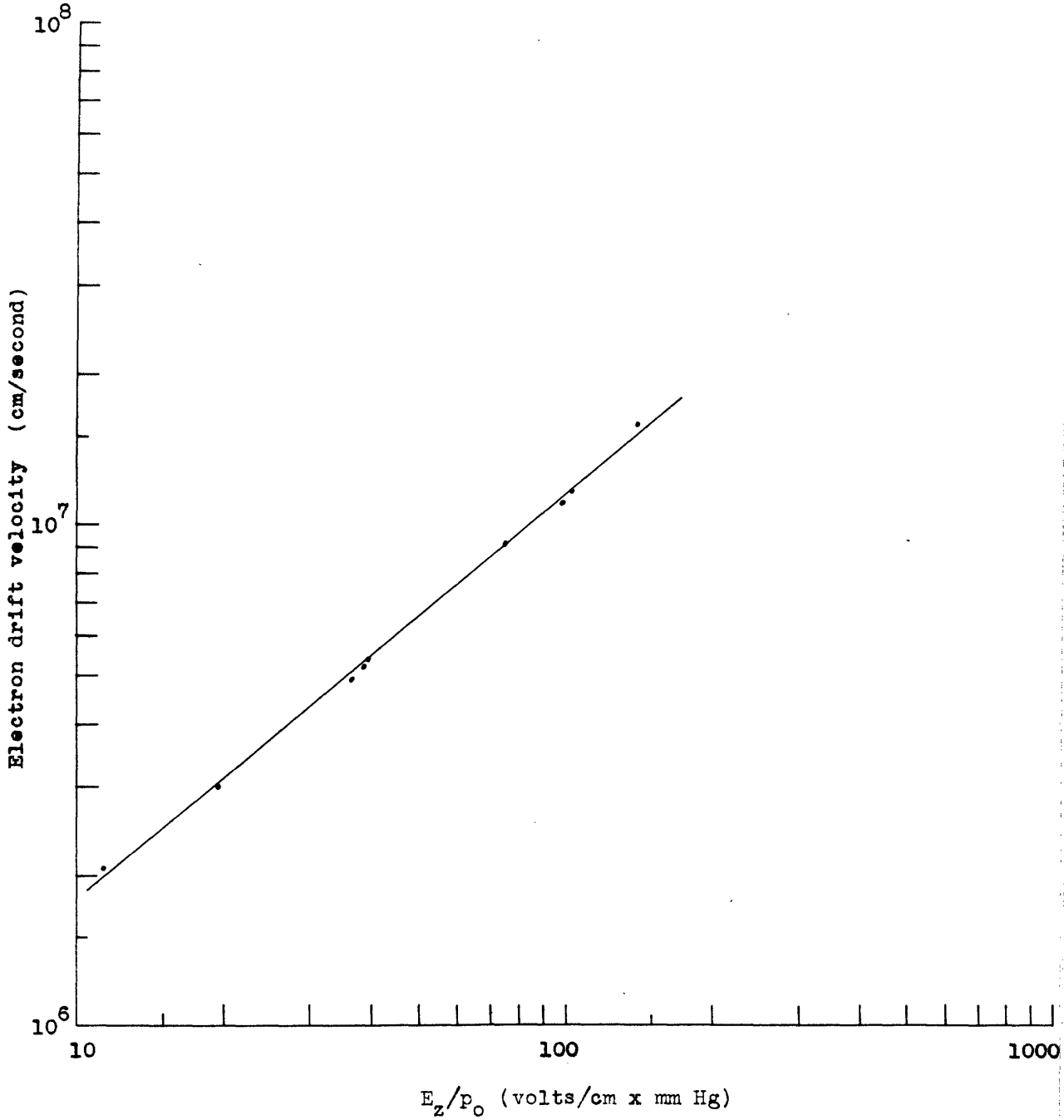

Fig. V-1

Electron drift velocity

are calculated from v_z and E_z and are listed in Table IV.

At the same time it is possible to obtain the ratio of the electron drift velocity to the average random velocity $v_{z-}/\langle v_- \rangle$, along with the ratio qV_z/kT_-, where kT_-/q is a measure of the random energy, and V_z is the axial drift energy defined by: $2qV_z = m_- v_{z-}^2$. In this experiment, the drift energy is at most 4 per cent of kT_-/q, and can be used to show that the effect of the drift energy on the direct ionization is not significant.

It is possible to calculate the effective mean free path for slow electrons in the mercury plasma from the relation between the electron mobility and the mean free path. Allis and Brown[47] give an accurate expression for the electron mobility in terms of a mean free path for electrons which is a general function of the electron velocity. Their expression was obtained by expanding the electron velocity distribution function into spherical harmonics in velocity space and then substituting it in the Boltzmann transport equation. If the effect of the drift velocity on the distribution function is small enough so that only the first two terms in the expansion need be retained, the electron mobility can be expressed as

$$\mu_- = \left\langle \frac{1}{3w^2} \frac{q}{m_-} \frac{d}{dw} (\lambda_m w^2) \right\rangle \qquad \text{(V-3)}$$

where λ_m is the momentum transfer mean free path for electrons. When it is assumed that the electrons have a M-B velocity distribution, this equation can be reduced by partial integration to give

$$\mu_- = \frac{1}{3} \frac{q}{kT_-} \langle \lambda_m w \rangle \qquad \text{(V-4)}$$

The momentum transfer mean free path λ_m, is related to the momentum transfer cross-section Q_m, by: $\lambda_m n_g Q_m = 1$, where n_g is the gas density. The momentum transfer cross-section Q_m, is related to the differential scattering cross-section $q(\theta)$, by:

$$Q_m = 2\pi \int_0^{\pi} q(\theta)(1 - \cos\theta) \sin\theta \, d\theta \qquad \text{(V-5)}$$

Electron scattering data is sometimes given in terms of the collision cross-section Q_c, which is related to the differential scattering cross-section by:

$$Q_c = 2\pi \int_0^{\pi} q(\theta) \sin\theta \, d\theta \qquad \text{(V-6)}$$

The probability of collision P_c is measured in collisions per centimeter at 1 mm Hg pressure and $0^{\circ}C$, and is related to the collision cross-section and the collision mean free path λ_c, by: $p_o P_c = n_g Q_c = (\lambda_c)^{-1}$. In order to permit the conversion of Q_c to Q_m, the values of Q_m/Q_c have been obtained by numerical integration of the angular scattering data given by Arnot[48] for electrons in mercury, and are tabulated for the following values of electron energy:

Electron energy		Q_m/Q_c
2 volts		0.783
4		0.817
6		0.823
7		0.802
8		0.834
	average	0.812 $\pm$ 1.6 per cent rms

Unfortunately there is no angular scattering data for electrons below 2 volts. According to Massey and Burhop[49], however, the angular distribution for elastically scattered slow electrons is uniform thus implying that Q_m/Q_c approaches unity as the electron energy is reduced.

The effective mean free path can be defined as that constant mean free path which when used to replace the velocity dependent mean free path will give the same mobility. The effective cross-section can be defined in the same way. In this experiment, it was found that the effective mean free path λ_m (eff.), is relatively independent of kT_-/q. For the case of a constant λ_m, (where λ_m now corresponds to the effective mean free path for momentum transfer) Eq. V-3 reduces to

$$\mu_- = \frac{q}{m_-}\frac{2}{3}\lambda_m\left\langle\frac{1}{v}\right\rangle \qquad \text{(V-7)}$$

It can be shown that for a Maxwell-Boltzmann velocity distribution:

$$\langle v^k\rangle = (v_{rms})^k\,\frac{\Gamma\left(\frac{k+3}{2}\right)}{\Gamma\left(\frac{3}{2}\right)}\left(\frac{2}{3}\right)^{k/2} \qquad \text{(V-8)}$$

where $\Gamma(k)$ is the complete gamma function. Thus:

$$\left\langle\frac{1}{v}\right\rangle\langle v\rangle = \frac{4}{\pi} \qquad \text{(V-9)}$$

so that

$$\mu_- = \frac{8}{3\pi}\frac{q}{m_-}\frac{\lambda_m}{\langle v_-\rangle} \qquad \text{(V-10)}$$

for the constant mean free path case. The Langevin[50] expression for the electron mobility

$$\mu_- = \frac{3}{4} \frac{q}{m_-} \frac{2\lambda_m}{\langle v_- \rangle} \qquad \text{(V-11)}$$

is lower by a factor of 1.132.

Equation V-10 implies that if the effective mean free path is independent of kT_-/q, the quantity $p_o \mu_e (kT_-/q)^{1/2}$ should be constant. This was found to be true since the average value of $p_o \mu_- (kT_-/q)^{1/2}$ is 1.49×10^5 $(cm^2/volt \times sec)$ (mm Hg) $(volt)^{1/2}$ with a small rms deviation from the mean of 5.6 per cent.

The effective momentum transfer cross-section for slow electrons in the mercury plasma (about 0.1 per cent ionized) was calculated and is plotted in Fig. V-2 as a function of kT_-/q, where it is seen that the cross-section is approximately constant. The average value of Q_m (eff.) is 42×10^{-16} cm^2 for electron temperatures ranging from 0.829 to 1.90 electron volts. The values of P_c given by Brode[51] for slow electrons in mercury indicate that Q_c decreases as the electron energy increases, and thus one would expect that Q_m (eff.) should decrease as kT_-/q increases. From Brode's[51,52] values of P_c, as a function of electron energy, it was calculated by numerical integration that the effective momentum transfer cross-section Q_m (eff.) is 58×10^{-16} cm^2 for electrons having a M-B distribution with a characteristic temperature of 1.00 electron volts in mercury. Elenbaas[53] has obtained cross-sections of 43 and 41×10^{-16} cm^2 for a high pressure mercury arc by using the Langevin equation and the energy transfer from electrons to atoms required to

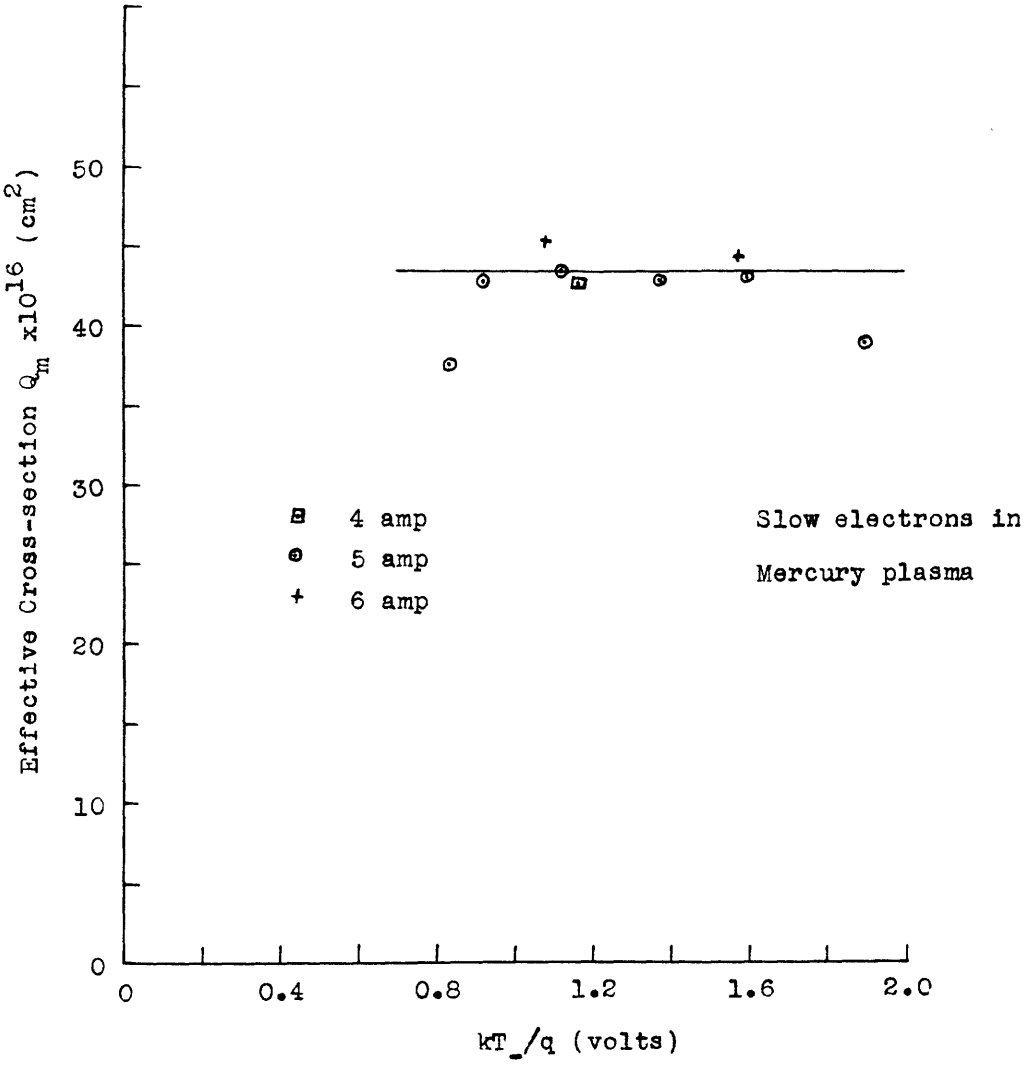

Fig. V-2

Effective cross-section for slow electrons

supply the heat and conduction loss. The electron temperature for his arc was about 0.43 electron volts. Adler and Margenau[54] have found (from microwave Measurements), that λ(effective) is constant and is equal to 9.5×10^{-3} cm at 1 mm Hg pressure. This corresponds to a cross-section of 30×10^{-16} cm^2 for electron temperatures in the range from 0.69 ev to 1.2 ev. The agreement of these cross-sections is good, particularly in view of the different values of kT_-/q and the different methods.

A survey of the literature was made for information about the cross-section for monoenergetic slow electrons in merucry. It was found that Brode[52] published results (prior to his review article) that indicated an increase in Q_c of only about 4 per cent as the electron energy was reduced from 1 volt to about 0.5 volts, thus indicating that the cross-section for very slow electrons in mercury is approximately constant and may even decrease for very slow electrons.

B. Ambipolar diffusion coefficient and ambipolar mobility coefficient

The ambipolar diffusion coefficient D_a can be calculated from the available experimental data subject, of course, to the assumption that the situation is describable in ambipolar diffusion terms. It was shown in chapter IV that the ambipolar diffusion coefficient is given by

$$\Gamma_{+r} = - D_a \frac{dn_-}{dr} \qquad \text{(V-12)}$$

where Γ_{+r} is the ion particle current density to the wall probe when it is at floating potential. The radial electron (and ion) density gradient dn_-/dr can be calculated from the assumed electron density distribution;

but, since a derivative is involved, any uncertainty in the form of the density distribution function results in a larger uncertainty in the gradient. A good representation for the density distribution (n_-/n_{-o}) is the Bessel function J_o (2.405 r/R_o) which was derived and discussed in chapter IV. With this representation, the density gradient

$$-\frac{dn_-}{dr}\Big)_{r_p} = n_{-o}\left(\frac{2.405}{R_o}\right) J_1\left(2.405\,\frac{r_p}{R_o}\right) \qquad \text{(V-13)}$$

was calculated at the plasma edge ($r = r_p$) in terms of the central electron density n_{-o}, and the wall density n_{-w}. The identical values for D_a may be obtained from the relation

$$D_a = v_i\left(\frac{R_o}{2.405}\right)^2 \qquad \text{(V-14)}$$

which was derived in the section on ambipolar diffusion. It is not surprising that these two expressions give the same result since they were both obtained from the same ambipolar diffusion assumptions, involve the same Bessel function solution and the same experimental data.

Since the electron mobility is much larger than the ion mobility, the ambipolar diffusion coefficient may be written as

$$D_a = \frac{kT_-}{q}\mu_+\left(1 + \frac{q}{kT_-}\frac{D_+}{\mu_+}\right) \qquad \text{(V-15)}$$

where the Einstein relation connecting the electron diffusion coefficient and the electron mobility coefficient has been used. An amb ipolar mobility coefficient μ_a will be defined here by:

$$D_a \equiv \frac{kT_-}{q}\mu_a \qquad \text{(V-16)}$$

Only for the case where the mobility flow of ions to the wall is much larger than the diffusion flow of ions to the wall (so that $D_+/\mu_+ \quad kT_-/q$) will the expression for the ambipolar diffusion coefficient reduce to the approximation

$$D_a \simeq \frac{kT_-}{q}\mu_+ \qquad \text{(V-17)}$$

The values of μ_a have been calculated and are shown in Fig. V-3 as a function of E_r/p_o, where E_r is the radial potential gradient at the plasma edge. The method for the determination of E_r will be described in the next section. With the help of the definition in Eq. V-16, values of D_a can be obtained from kT_-/q and μ_a.

There are very little data available for the purpose of comparison with the results of this experiment; this makes the present results even more important. Biondi[55] gives a value of $D_a n_g = 3.6 \times 10^{17}$ (cm^2/sec) (atoms/cm^3) for Hg ions and thermal electrons in mercury vapor at 350°K, which was obtained through afterglow measurements on a decaying plasma. This value is equivalent to $qD_a p_o/kT_- = 3.4 \times 10^2$ (cm^2/volt x sec)(mm Hg). In the present experiment, the corresponding value of $qD_a p_o/kT_-$ varied from 1.58×10^2 to 7.52×10^2 for an active plasma. The variation can be ascribed to the change of ion mobility and diffusion as a result of different arc conditions.

In the low pressure arc under consideration, the mobility and diffusion coefficients are functions of the electric field because the energy

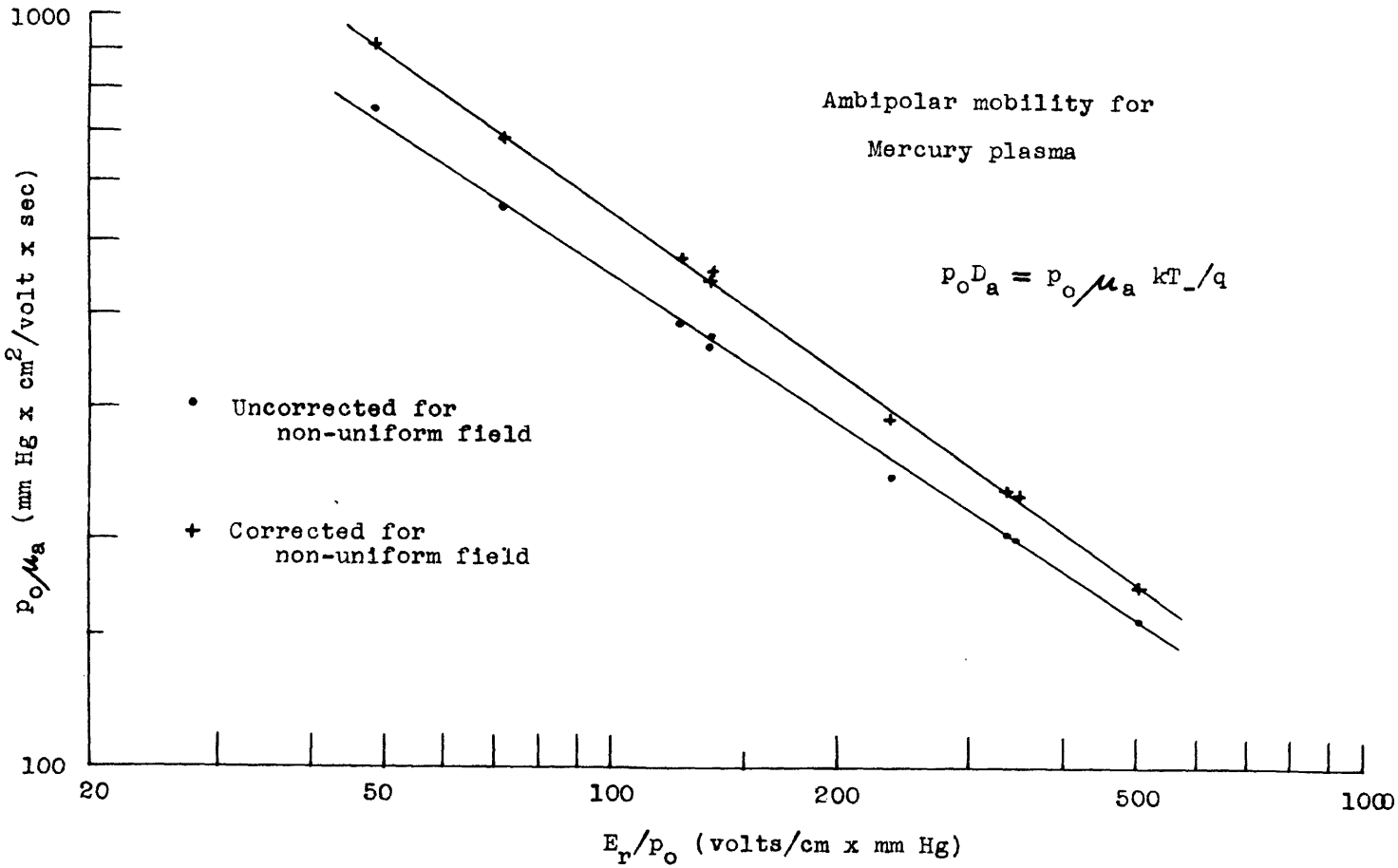

Fig. V-3 Ambipolar mobility coefficient

gained by an ion in a mean free path is large compared to the random energy thus making the mean free time of flight of the ion dependent upon the field. At the edge of the plasma, the radial electric field is much larger than the axial electric field so that the resultant electric field may be taken in the radial direction. At the low pressures in this arc, the diffusion flow of ions is not small enough to be neglected. Later in this chapter, the radial flow of ions will be decomposed into the mobility and diffusion components with the help of a special theory for ion mobility and diffusion in a strong electric field.

C. Ion velocity as a function of E_r/p_o

It is possible to calculate the radial potential gradient E_r from the radial density distribution of electrons and from the Boltzmann relation between the electron density and the plasma potential as follows:

$$E_r = -\frac{kT_-}{e}\frac{1}{n_-}\frac{dn_-}{dr} \qquad \text{(V-18)}$$

The directed ion velocity in the radial direction v_+ (at the plasma edge) can be obtained from the ion density ($n_{-w} = n_{+w}$) at the plasma-sheath interface and from the ion particle current density to the wall probe when it is at floating potential. Figure V-4 shows the ion velocity v_+, as a function of E_r/p_o, evaluated at the plasma edge.

There is very little other data available for the velocity of mercury ions in mercury. Kingdon and Lawton[56] in an abstract give the results of oscilloscopic transit time measurements for E/p ranging from 20 to 6000 (volts/cm x mm Hg), They state that the ion velocity

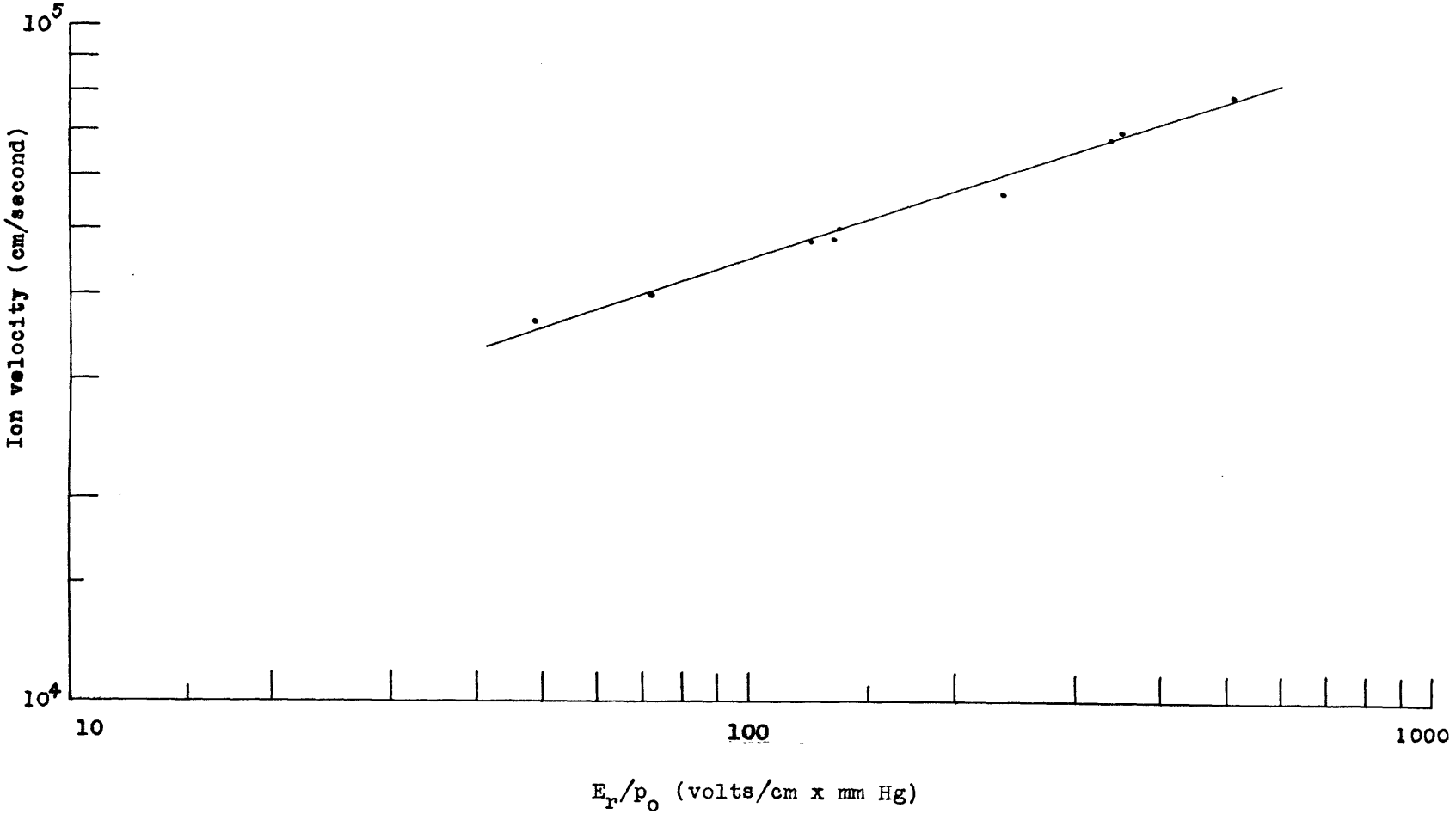

Fig. V-1 Ion radial drift velocity

was proportional to $(E/p)^{1/2}$ and they report an ion velocity of 10^5 cm/sec at an E/p of 1000 volts/cm x mm Hg. This corresponds to $v_+/(E/p)^{1/2} = 3.2 \times 10^3$ (cm/sec)/(volt/cm x mm Hg)$^{1/2}$. The accuracy involved was not specified nor was it demonstrated that the diffusion flow of ions across the drift space was negligible compared to the mobility flow. What is surprising about this result is the implication that the cross-section of mercury ions in mercury is independent of the ion energy, thus resulting in a constant mean free path.

For this experiment the relation between the ion velocity v_+, and E_r/p_o can be given by several representations of varying accuracy:

$v_+/(E_r/p_o)^{1/3} = 9.71 \times 10^3$ (cm/sec)(volt/cm x mm Hg)$^{1/3}$ $\pm$ 2.7 per cent rms

$v_+/(E_r/p_o)^{1/2} = 4.17 \times 10^3$ (cm/sec)(volt/cm x mm Hg)$^{1/2}$ $\pm$ 11 per cent rms

The difference between a variation of $(E_r/p_o)^{1/2}$ and one of $(E_r/p_o)^{1/3}$ is a factor of $(E_r/p_o)^{1/6}$ which is difficult to detect.

In order to separate the mobility and diffusion components of the ion flow so as to experimentally determine these coefficients, it is necessary to know the theoretical dependence of the ion mobility and diffusion coefficients upon the various arc parameters. Since in this experiment the energy gained by the ions in a mean free path is large compared to the random energy of the gas atoms, the mobility and diffusion coefficients will be a function of the electric field. There are no simple and satisfactory relations available for the diffusion and mobility of ions in a strong electric field. In the next section a simple theory will be developed for the ion mobility coefficient and the longitudinal diffusion coefficient for the case of a strong electric field.

D. Simple theory of ion mobility and diffusion coefficient for ions in a strong uniform electric field

In order to calculate the diffusion and mobility coefficients from the experimental data, it is necessary to make several assumptions to obtain a mathematically tractable model. It is assumed that the energy obtained by an ion in a free path is large, compared to the random energy of the ions, so that the motion of the ions between collisions is essentially determined by the field. If the scattering of the ions is by charge transfer processes, the new ion will have the kinetic energy of the gas atoms and therefore may be considered as starting at rest. The cross-section of the ion-gas interaction is assumed to be independent of the ion velocity. Near the plasma edge the radial electric field E_r is much larger than the axial electric field E_z and, therefore, the resulting electric field is taken as equal to the radial electric field. Since only the radial diffusion flow contributes to the radial ion current, it is only necessary to calculate the longitudinal diffusion coefficient for diffusion flow parallel to the strong electric field.

With the help of Professor W. P. Allis, it was possible to derive a simple yet reasonably accurate representation for the mobility and diffusion coefficients in a strong electric field.

Consider first the case of ions moving in a strong uniform electric field, and assume for the present that there is no density gradient of ions so that the diffusion flow may be neglected. It is desired to find the time average of the ion velocity for a single representative free flight. The time average velocity $\bar{v}$, is given by

$$\overline{v} = \frac{1}{\tau}\int_0^{\tau} v\,dt \qquad \text{(V-19)}$$

where τ is the time of flight. Assume the E field is very large so that the motion of the ion can be assumed to be parallel to the E field, and let "s" be the distance in the x direction (paralled to E) traversed in the time of flight. Then:

$$\overline{v} = \frac{1}{\tau}\int_0^{\tau} \frac{dx}{dt}\,dt = \frac{1}{\tau}\int_0^{s} dx = \frac{s}{\tau} \qquad \text{(V-20)}$$

It is desired to obtain $\overline{v}$ as a function of s and E. Assume that the ion has a terminal velocity (in the x direction) of v_f at the end of time τ, and that after the collision there is a persistence of velocity α, so that it starts the next free flight with velocity $\alpha\, v_f$. Assume also that it started the free flight under consideration with the same velocity $\alpha\, v_f$. It is seen that the final velocity is related to the time of flight by:

$$v_f(1-\alpha) = a\tau \qquad \text{(V-21)}$$

The acceleration "a" of the ion is given by

$$a = \frac{qE}{m_+} \qquad \text{(V-22)}$$

where q and m_+ are respectively the charge and mass of the ion. The time of flight τ is related to the distance of flight s by

$$s = \alpha v_f \tau + \frac{1}{2} a \tau^2 \qquad \text{(V-23}$$

Substitute v_f from Eq. V-21 in Eq. V-23 and solve for τ to get

$$\tau = \left(\frac{1-\alpha}{1+\alpha}\right)^{1/2}\left(\frac{2s}{a}\right)^{1/2} \qquad \text{(V-24)}$$

When τ is substituted in V-20, the time average velocity is found to be

$$\bar{v} = \left(\frac{1+\alpha}{1-\alpha}\right)^{1/2}\left(\frac{as}{2}\right)^{1/2} \qquad \text{(V-25)}$$

It is necessary to average over the mean free path distribution. In general,

$$\langle s^k \rangle_\lambda = \frac{1}{\lambda}\int_0^\infty s^k e^{-s/\lambda}\,ds = \lambda^k \Gamma(k+1) \qquad \text{(V-26)}$$

so that

$$\langle s^{1/2} \rangle_\lambda = \lambda^{1/2}\frac{(\pi)^{1/2}}{2} \qquad \text{(V-27)}$$

As a result, the average velocity is given by

$$\bar{v} = \left(\frac{\pi}{8}\right)^{1/2}\left(\frac{1+\alpha}{1-\alpha}\right)^{1/2}(a\lambda)^{1/2} \qquad \text{(V-28)}$$

for ion motion in a strong uniform electric field.

It is assumed that the motion of the Hg ions in the plasma is limited by charge transfer collisions where a fast ion exchanges identity with a gas atom. Since the velocity of the gas atom is very small compared

to that of the ion (and is also randomly directed), there is no persistence of velocity so that $a = 0$, and

$$\bar{v} = \left(\frac{\pi}{8}\right)^{1/2} (a\lambda)^{1/2} = 0.6267 (a\lambda)^{1/2} \qquad \text{(V-29)}$$

Sena[57] assumed charge transfer limited mobility and constant λ, and obtained the same result as Eq. V-29.

There are several other theories for the motion of ions in a strong electric field and they will be given for the purpose of comparison with the result (Eq. V-28) derived here. An early expression calculated by Tonks and Langmuir was

$$\bar{v} = 1.2 (a\lambda)^{1/2} \qquad \text{(V-30)}$$

They assumed a constant and a persistence of velocity of $a = 1/2$ for the fast ions. Wannier[58], in a more recent and much more detailed calculation which includes a constant λ (hard sphere), nearly isotropic scattering and persistence of velocity, obtains

$$\bar{v} = 1.147 (a\lambda)^{1/2} \qquad \text{(V-31)}$$

It will be shown that the simple theory developed here gives a value for $\bar{v}$ which is in good agreement with that of Wannier. According to Jeans[59], for the case of elastic scattering of a fast particle by a stationary hard sphere of equal mass, the persistence of velocity is 1/2, When $a = 1/2$ is substituted into Eq. V-28, there results

$$\bar{v} = \left(\frac{\pi}{8}\right)^{1/2} (3)^{1/2} (a\lambda)^{1/2} = 1.085 (a\lambda)^{1/2} \qquad \text{(V-32)}$$

which is very close to the value obtained by Wannier through a much more detailed calculation.

It is assumed that the Hg ions are scattered by charge transfer collisions so that in this case there is no persistence of velocity. Equation V-29 will therefore be used for the average ion velocity in a uniform electric field. In the plasma, ions will also flow to the wall because of the radial ion density gradient so that it is necessary to find a simple expression for the diffusion coefficient in a strong uniform field. Consider the particle current density for ions passing through a mathematical plane normal to the potential gradient E. The ion particle current density (ions per unit second per unit area) passing through the plane can be given by

$$\Gamma_+ = \int_0^\infty \bar{\nu} \left(n_0 - x \frac{dn}{dx}\right) \frac{1}{\lambda} e^{-x/\lambda} dx \qquad \text{(V-33)}$$

The term n_o is the density of ions at the plane, dn/dx is the density gradient of ions and exp (-x/) is the fraction of ions that will travel the distance "x" to the plane without a collision. This results in the following expression for Γ_+

$$\Gamma_+ = n_0 \bar{\nu} - \bar{\nu} \lambda \frac{dn}{dx} \qquad \text{(V-34)}$$

The ion mobility coefficient μ_+ is

$$\mu_+ = \frac{\bar{\nu}}{E} = \left(\frac{\pi}{8}\right)^{1/2} \left(\frac{q E \lambda}{m_+}\right)^{1/2} \frac{1}{E} \qquad \text{(V-35)}$$

while the longitudinal diffusion coefficient (for diffusion of ions in a direction parallel to the E field) is given by

$$D_{\parallel} = \left(\frac{\pi}{8}\right)^{1/2}\left(\frac{qE\lambda}{m_+}\right)^{1/2} \qquad \text{(V-36)}$$

From these two expressions, one can obtain a form similar to the Einstein relation

$$\frac{D_{\parallel}}{\mu_+} = E\lambda \qquad \text{(V-37)}$$

With the aid of the expressions for the ion mobility and diffusion coefficients, it is possible to obtain values of the effective for the ions in the plasma. Equations V-34 and V-29 yield

$$P_{+w} = n_{+w}\left(\frac{kT_-}{q}\right)^{1/2}\left(\frac{\pi}{8}\frac{q}{m_+}\right)^{1/2}\left(\frac{qE\lambda}{kT_-}\right)^{1/2}\left(1+\frac{qE\lambda}{kT_-}\right) \qquad \text{(V-38)}$$

where $dn_-/dr = dn_+/dr$ in the plasma was replaced by $-n_-qE/kT_-$, and the equation is evaluated at the wall. The only unknown, $qE\lambda/kT_-$, can be solved for by convergent approximation. This quantity, $qE\lambda/kT_-$, represents the relative importance of the diffusion flow of ions compared to the mobility flow. It ranged from 0.42 at the highest pressure to 0.65 at the lowest pressure. If the pressure were higher, the diffusion flow would be smaller.

The values of E_r (calculated in the previous section)plus the values of kT_-/q can be used to determine the values of λ from the calculated values of $qE\lambda/kT_-$. The ion mobility coefficient was

calculated and is plotted in Fig. V-5 as a function of E_r/p_o without a correction (at the present time) for the non-uniformity of the electric field. This correction will be calculated in the next section. The longitudinal diffusion coefficient is plotted in Fig. V-6. From the values of λ and the gas density, the cross-sections Q are calculated (from $\lambda n_g Q = 1$) and are shown in Fig. V-7 as a function of E_r/p_o and in Fig. V-8 as a function of $E\lambda$.

Although the values of λ for the ions ranged from 0.26 cm to 1.3 cm and were not very small compared to the radius (2.75 cm) of the plasma, the concept of ion mobility can still be applied. This is so because the charge transfer limited mobility requires only one collision rather than the many collisions needed for regular mobility flow.

In the range of ion energy about 1 electron volt, the cross-section increases with ion energy and is many times the cross-section of 8.29×10^{-16} cm^2 for Hg-Hg interactions which was obtained from viscosity[60] and x-ray[61] measurements. Very little data are available for scattering of low energy Hg ions in the parent gas. However, data available for other ions in the parent gas indicate that as the ion energy decreases, the cross-section increases up to a point and then decreases as the ion energy continues to decrease[62]. In this experiment the cross-section varied from 39 to 116×10^{-16} cm^2 for the case where the correction for the nonuniform electric field was not yet made. Massey and Burhop[63] give an approximate theoretical maximum value of 5×10^{-14} cm^2 for the charge transfer cross-section. Sena[64, 57] calculated a value of $Q = 5.3 \times 10^{-15}$ cm^2 for Hg ions of 1.6 ev energy in mercury vapor from the data given by Kingdon and Lawton[56]. Palyukh

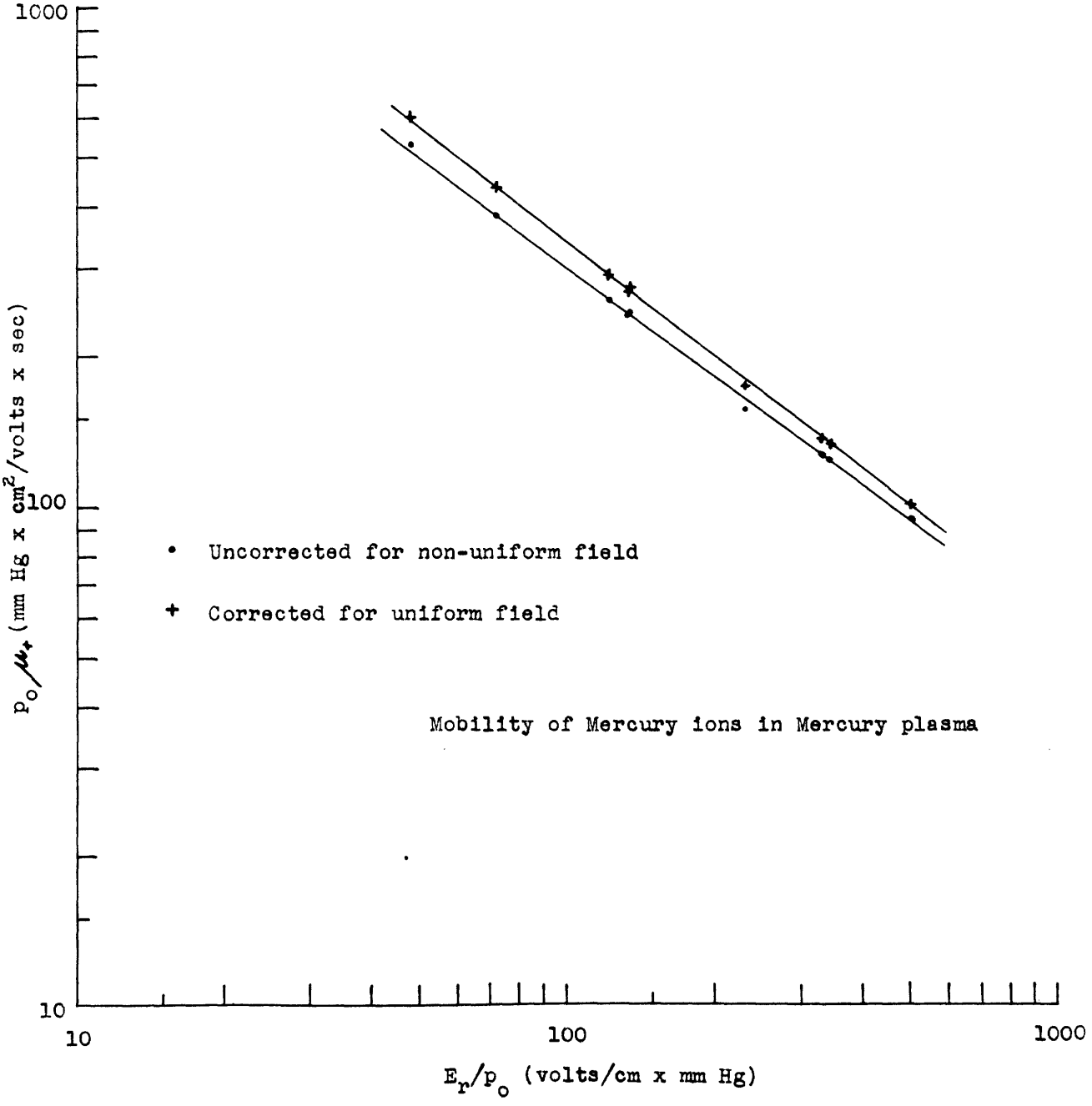

Fig. V-5

Ion mobility coefficient

and Sena[65] report values of the charge transfer cross-section for high energy Hg ions in mercury vapor. Their results give a charge transfer (at the extremes) of 1.1×10^{-14} cm^2 for 37 volt ions and 0.71×10^{-14} cm^2 for ions with an energy of about 1,000 volts. Varney[66] gives values of Q from drift velocity measurements of ions in the parent gas and reports values of 54, 65, 134, 157 and 192×10^{-16} cm^2 for He, Ne, A, Kr and Xe respectively.

In view of the agreement of the present results with the limited data given by others for the cross-section of mercury ions in mercury, it can be seen that the results of this experiment are of value, particularly since they are more detailed. In addition, the information was easily obtained from probe measurements in a dc discharge. This method may be applied to other gases to obtain information about the ion mobility and diffusion coefficients and the cross-section for low energy ions.

The ions are moving in a slightly nonuniform electric field so that it is necessary to refine the theory of ion mobility and diffusion to include this case. The next section will consider this correction.

E. First order theory for ion mobility and diffusion in a nonuniform strong electric field

If the ions are moving in a strong nonuniform electric field which has an appreciable change in a mean free path, it is necessary to take this into account in the calculation of the cross-section and the mobility and diffusion coefficients. The electric field will be expressed in the first order form as

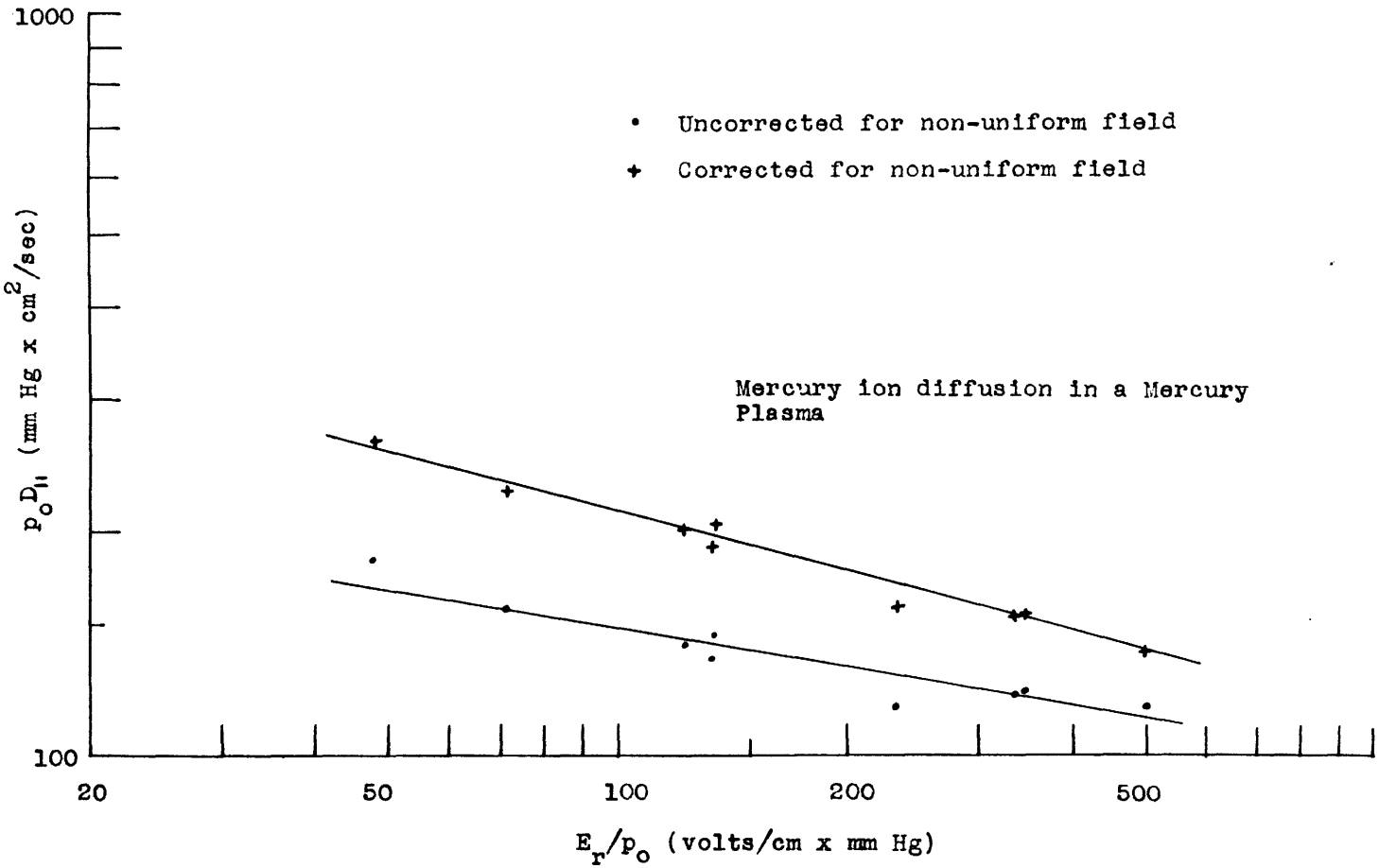

Fig. V-9 Longitudinal diffusion coefficient

$$E = E_\theta - (s - x)\frac{dE}{dx} \tag{V-39}$$

where E_θ is the value of E at the end of the free path. The time average ion velocity $\bar{v}$ is equal to s/τ. It is desired to express τ as a function of s, E_θ and dE/dx. Since the ions are assumed to start from rest, the time of flight τ is equal to

$$\tau = \int_0^s \frac{dx}{\left(\frac{2q}{M+}\right)^{1/2}(V_0 - V)^{1/2}} \tag{V-40}$$

where the ion has passed through the potential difference $(V_o - V_x)$. From the first order expansion for the E field, τ is given by

$$\tau = \int_0^s \frac{dx}{\left(\frac{2q}{M+}\right)^{1/2}(x)^{1/2}\left(E_\theta - s\frac{dE}{dx} + \frac{1}{2}x\frac{dE}{dx}\right)^{1/2}} \tag{V-41}$$

When this integral is evaluated in series form including terms up to the second order, it is found that the time average velocity is given by

$$\bar{v} = \left(\frac{1}{2}\right)^{1/2}\left(\frac{q}{M+}\right)^{1/2}(E_\theta s)^{1/2}\left[1 - \frac{5}{12}\frac{s}{E_\theta}\frac{dE}{dx} + \frac{203}{1140}\frac{s^2}{E_\theta^2}\left(\frac{dE}{dx}\right)^2\right] \tag{V-42}$$

After the terms containing "s" are averaged over the distribution in "s" (according to Eq. V-26) the following expression results for the average ion velocity in a nonuniform strong electric field:

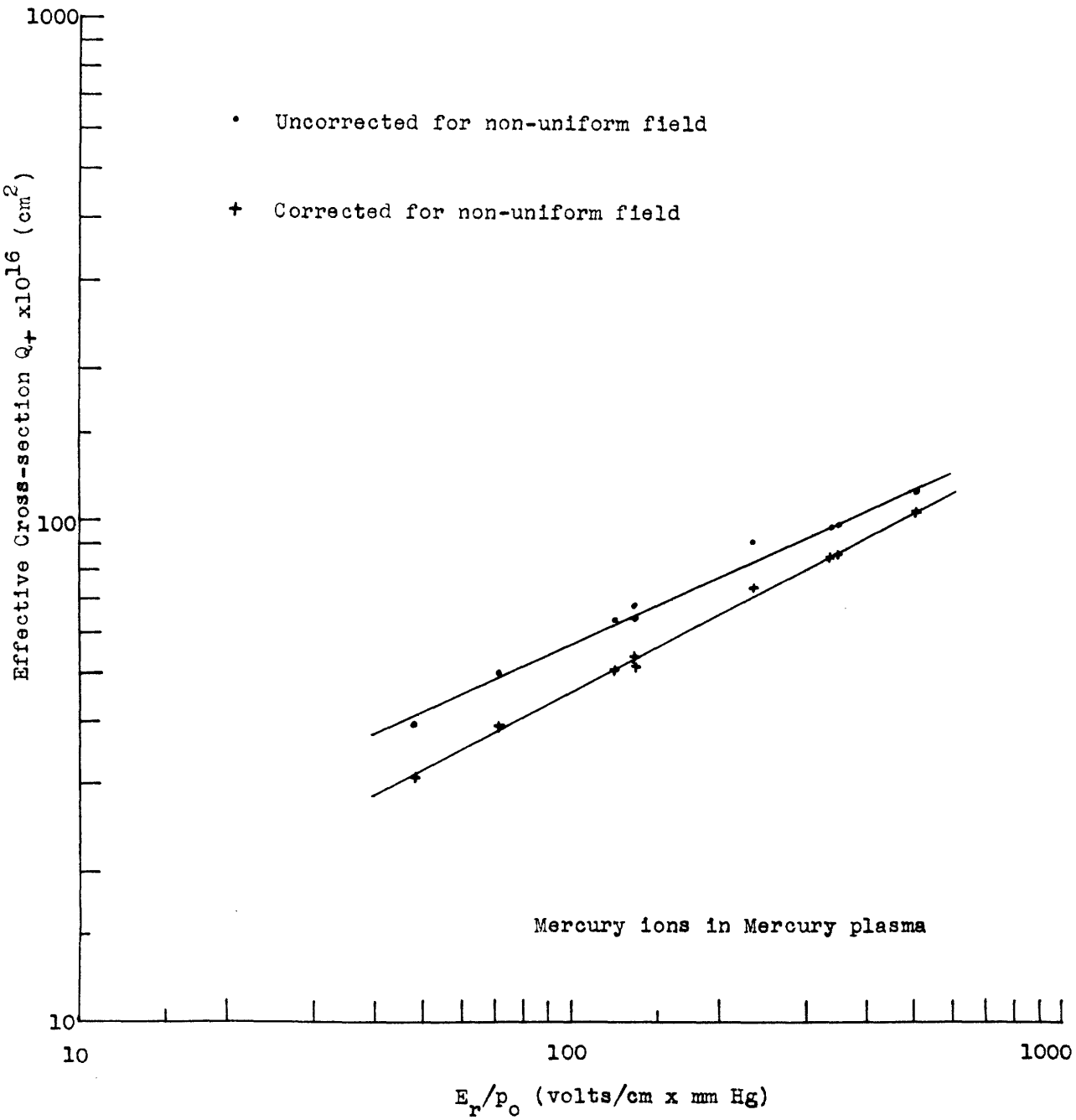

Fig. V-7

Cross-section for Hg ions in Hg vs E_r/p_o

$$\nu = \left(\frac{\pi}{8}\right)^{1/2}\left(\frac{q}{m_+}\right)^{1/2}\left(E_\ominus\lambda\right)^{1/2}\left[1 - \frac{5}{8}\frac{\lambda}{E_\ominus}\frac{dE}{dx} + \frac{609}{1152}\frac{\lambda^2}{E_\ominus^2}\left(\frac{dE}{dx}\right)^2\right] \qquad \text{(V-43)}$$

This is seen to reduce to the results of the previous section when $dE/dx = 0$.

The values of $(dE/dr)/E_\ominus$ can be calculated from the assumed Bessel function electron density distribution and the Boltzmann theorem relating the potential and density distribution. The following expression is obtained:

$$\frac{1}{E_\ominus}\frac{dE}{dr} = \frac{1}{r_p}\left(\chi_p\left[\frac{J_0(\chi_p)}{J_1(\chi_p)} + \frac{J_1(\chi_p)}{J_0(\chi_p)}\right] - 1\right) \qquad \text{(V-44)}$$

the quantity x_p is defined by

$$\frac{n-w}{n-o} = J_0(\chi_p) \qquad \text{(V-45)}$$

Equation V-38 in conjunction with Eq. V-43 gives

$$\Gamma_{+w} = n_+ w\left(\frac{kT_-}{q}\right)^{1/2}\left(\frac{\pi}{8}\frac{q}{m_+}\right)^{1/2}\left(\frac{qE_\ominus\lambda}{kT_-}\right)^{1/2}\left(1 + \frac{qE_\ominus\lambda}{kT_-}\right)\left(1 - \frac{5}{8}\frac{\lambda}{E_\ominus}\frac{dE}{dr} + \frac{609}{1152}\frac{\lambda^2}{E_\ominus^2}\left(\frac{dE}{dr}\right)^2\right) \qquad \text{(V-46)}$$

which can be solved for λ through self-consistant convergent approximations. From these new values of λ (which have been corrected for the nonuniform field), the cross-sections are calculated and are plotted

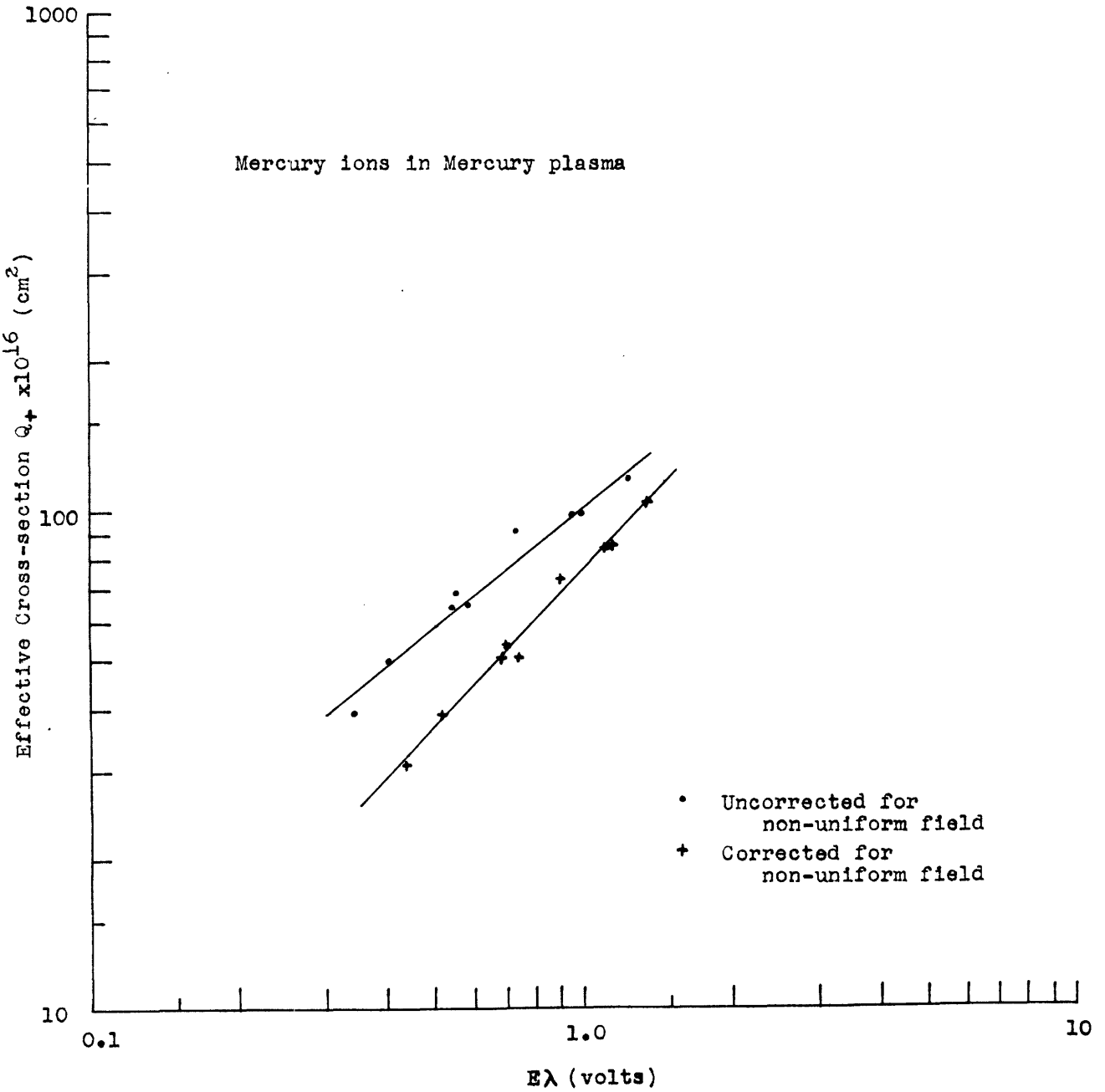

Fig. V-6

Cross-section for Hg ions in Hg

in Fig. V-7 as a function of E_r/p_o, and in Fig. V-8 as a function of $E\lambda$. The effective corrected cross-section increased from 31 to 104 x 10^{-16} cm^2 as the ion energy increased from 0.44 to 1.37 electron volts. The ion mobility and diffusion coefficients are calculated from the corrected and are plotted in Fig. V-5 and Fig. V-6 as a function of E_r/p_o. It was found that when the corrections for the diffusion flow and the nonuniform electric field were made, the ion velocity due to the field only can be described by

$$\mu_+ = Y_{1/2}\,(E_r/p_o)^{1/2} = 3.05 \times 10^3 (E_r/p_o)^{1/2} \text{ cm/sec} \pm 1\% \text{ rms} \qquad \text{(V-47)}$$

which is in good agreement with the value of $Y_{1/2} = 3.2 \times 10^3$ implied by the reported results of Kingdon and Lawton[56].

The accuracy of the results of this chapter is contingent on the validity of the assumed Bessel density distribution for the electrons and ions. Since the mobility and diffusion coefficients are dependent on the field, the next order of refinement involves the determination of the density distribution for the case of a variable ambipolar diffusion coefficient. This involves the numerical solution of a set of second order nonlinear differential equations, which cannot be made dimensionless because of the axial field parameter E_z. This problem will be left for a future paper.

VI. Electron Energy Distribution Function and Probe Measurements

A. Depletion of the high energy electrons and comparison with the Druyvesteyn distribution

It has been established in this experiment and in others[15,32], that there is a definite depletion from a M-B distribution for the high energy electrons in the low pressure mercury arc. This depletion can be seen in the typical experimental retarding potential plots given in chapter III. The depletion cannot be completely ascribed to incorrect extrapolation of the ion current component. The discrepancy between the probe current expected for a M-B distribution and the measured electron current is about equal to the ion current itself and would require that the actual ion current be larger than the measured ion current by about a factor of 2 to remove the depletion. On the other hand a depletion of high energy electrons is expected because of the various electron energy loss mechanisms.

Loss of electron energy through elastic collisions will lead the electron energy distribution towards a Druyvesteyn type distribution and will thus result in a depletion of high energy electrons. In addition, the inelastic collsions (which have an energy threshold) will result in a loss of high energy electrons alone. There is also a preferential loss of high energy electrons which have enough velocity to overcome the retarding potential of the negative wall.

The Druyvesteyn distribution gives a reasonable description of the probe curve expected for the elastic collisions although inclusion of the variation of the electron-atom cross-section with electron energy

would give a better description. In accordance with the expression for the retarding potential function obtained in chapter I, the normalized probe curve for the D-D has been plotted in dimensionless form in Fig. VI-1 along with a dimensionless curve for a M-B distribution of the same average energy and the same saturation current. These curves are plotted to show a variation of over 4 orders of magnitude and therefore do not show details for very low values of $V/\overline{V}$. For small values of $V/\overline{V}$, the quantity $J_-/J_{-sat.}$ is slightly above that for the M-B distribution. This difference has a maximum value of about 0.02 which occurs at $V/\overline{V}$ approximately equal to 0.2, and is so small that it is about equal to the plotting accuracy and is not apparent in the figure. As $V/\overline{V}$ increases, the probe current for the D-D falls below that of the M-B distribution. When $V/\overline{V}$ is about 4 the probe curve for the D-D is about 2 orders of magnitude below that for the M-B distribution.

A typical experimental curve for the central plane probe ($T_{bath} = 54.6^{o}C$, $I_z = 5.0$ amp) has been plotted in dimensionless form in the same figure for comparison, and it is seen that the low energy electrons have a distribution which is M-B while the higher energy electrons deviate towards the D-D in agreement with expectations.

It can be seen, from the values of the plasma potential V_p and the floating potential V_f listed in Table I for each probe, that the floating potential measured with respect to the plasma potential is proportional to kT_-/q. The quantity $V_f - V_p$ is equal to $5.32\ kT_-/q$ with a rms deviation of 3 per cent. The depletion potential V_d measured with respect to the plasma potential is also found to be proportional to kT_-/q although not as closely. The quantity $V_d - V_p$ is equal to 3.39

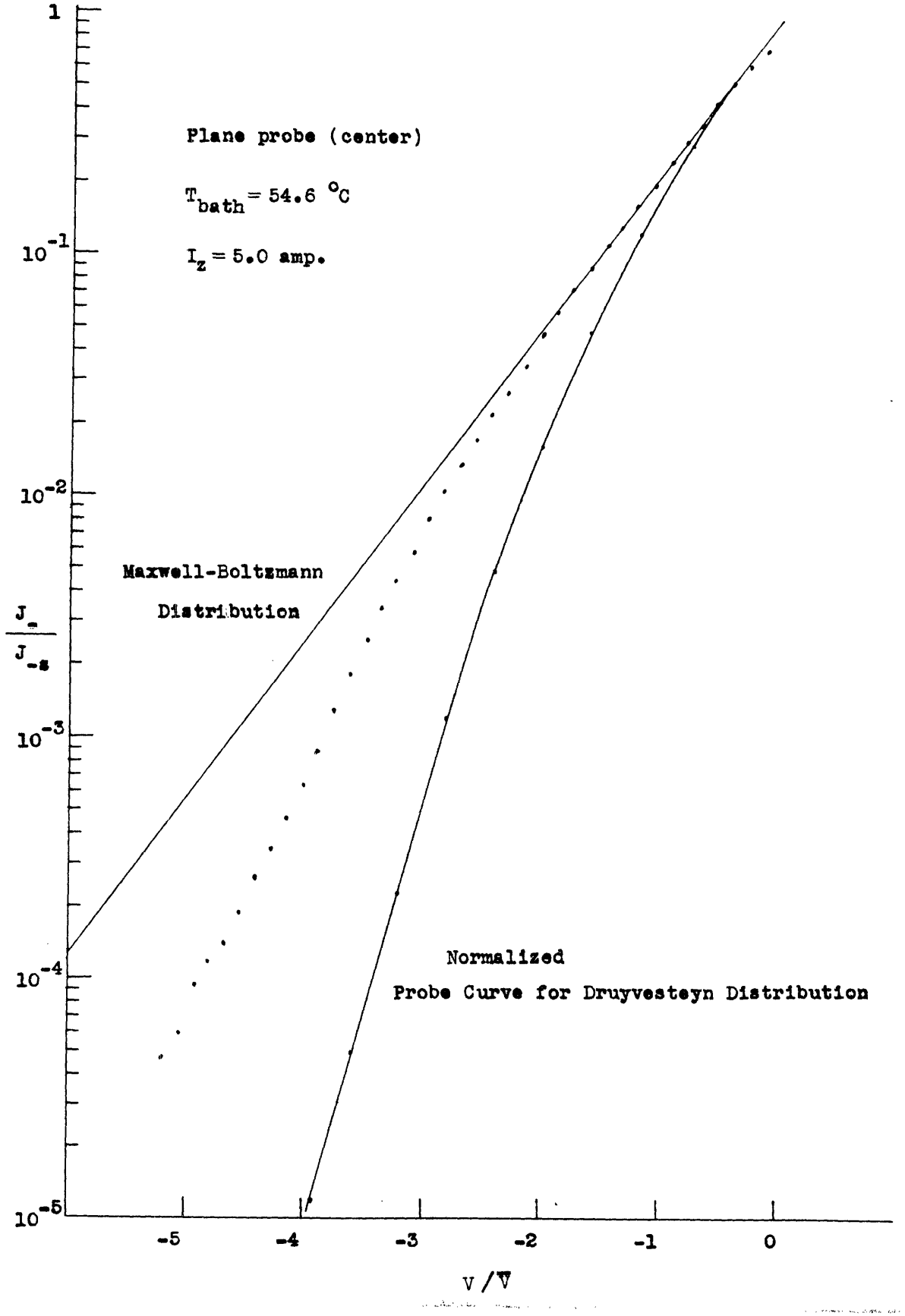

Fig. VI-1 Retarding potential plot

kT_-/q with an average deviation of 18 per cent. This depletion potential V_d is defined here as the probe potential at which the retarding potential plot for the high energy electrons begins to be depleted below the linear part characterized by the M-B distribution. These last observations may or may not be significant but they are included here for completeness.

It can be calculated, from the experimental values of ion generation, that at the lower pressure about 9 per cent of the input energy goes into the production of ions through inelastic collisions, while at the highest pressure about 18 per cent of the input energy goes into the production of ions. Thus a considerable fraction of the electron energy is lost through inelastic collisions. On the other hand, according to Klarfeld[32], the elastic losses in a low pressure mercury arc are less than 1 per cent of the input energy. This implies that the inelastic processes are more important than the elastic processes in the depletion of the high energy electrons.

It would be of considerable interest if the distribution function for the electrons were calculated taking into account the inelastic collisions and the electron-electron interactions. Since the degree of ionization is about 0.1 per cent, the electron-electron interactions should be considered in the calculation of the distribution function. Professor Allis has made available[67] most of the analysis necessary for this solution. The distribution function will not be determined in this research.

B. Theory of harmonic analysis of retarding potential plots and the effect of superimposed ac

It was shown in Chapter I that the velocity distribution for the electrons is related to the second derivative, (with respect to the probe potential), of the electron current to a plane probe. Numerical or graphical differentiation is inaccurate and tedious, so that various methods have been developed by others to increase the accuracy and convenience of the measurements. If a small monofrequency ac signal "A sin ωt" is added to the retarding potential V, the resulting probe current density, J, may be written as a Fourier series and may also be expanded as a power series in "A sin ωt". When the Fourier series is equated to the power series and multiplied by sin nωt (or cos nωt), integration plus the orthogonality properties of the sine and cosine functions will yield the Fourier coefficients. The complete result is given here for the dc term, the first harmonic, and the second harmonic:

$$J(V,A,\omega t) = \sum_{k=0}^{\infty} (\pi)^{-1/2} \frac{(A)^{2k}}{(2k)!} J^{(2k)}(V) \frac{\Gamma(k+1/2)}{\Gamma(k+1)}$$

$$+\sin \omega t \left[\sum_{k=0}^{\infty} 2(\pi)^{-1/2} \frac{(A)^{2k+1}}{(2k+1)!} J^{(2k+1)}(V) \frac{\Gamma(k+3/2)}{\Gamma(k+2)} \right] \qquad \text{(VI-1)}$$

$$-\cos 2\omega t \left[\sum_{k=0}^{\infty} 2(\pi)^{-1/2} \frac{(A)^{2k+2}}{(2k+2)!} J^{(2k+2)}(V) \frac{\Gamma(k+3/2)(k+1)}{\Gamma(k+2)(k+2)} \right]$$

where $J^{(k)}$ (V) is the k' th derivative of J(V). Note that the cos ωt and the sin $2\omega t$ terms do not appear.

Inspection of this expression indicates the various methods that may be used to determine the second derivative. In the increase in the dc current due to the ac signal is measured and if the amplitude "A" is small enough to permit the higher order terms to be neglected, this increase is proportional to the second derivative. In the experiments of Sloane and MacGregor[68] and of Pringle and Farvis[23], this increase is measured by balancing out the basic probe current with a constant current source and then measuring directly the change in the dc current when the ac signal is introduced. The disadvantage of this method is that the drift of the arc itself results in small fluctuations in the probe current that may be comparable to the measured increase.

The method of van Gorcum[64] eliminates the effect of the drift by measuring only the ac component corresponding to the sinωt term to obtain the first derivative. Subsequent differentiation of this result numerically or graphically gives the second derivative. The disadvantage of this method is, of course, the need for additional differentiation.

Another interesting method involves the measurement of the amplitude of the cos $2\omega t$ component since the leading term contains the second derivative directly. It should be noted that this term is incorrectly written as cos ωt by Sloane and MacGregor[68] instead of the correct form cos $2\omega t$ given here and originally by Landale[70]. This error is propagated in Loeb[71]. The advantage of the second harmonic method is that the second derivative may be measured directly with a tuned amplifier without the extreme sensitivity to drift that is implicit in the

incremental dc method. In addition, stray linear effects such as capacitance do not affect the measurement. On the other hand, the disadvantage of this method is that the source of the original ac voltage "A sin ωt" must have very small harmonic components.

In view of the disadvantages and limitations of these methods, a new method is proposed for future research. A small ac signal of frequency ω_2 is added to the probe voltage and the amplitude "A" of this signal is amplitude modulated at a much lower frequency ω_1 by a mechanical chopper switch. The resulting ac probe current is passed through a low pass filter to remove the high frequency components. It is then measured to give the amplitude of the increment in the dc current resulting from the small ac signal without the difficulties introduced by the drift of the arc. A synchronous mechanical or electronic rectifier operating at a frequency ω_1 plus an integrating circuit may be used to reduce the effect of stray signals. The above statements may be applied to the measurement of other nonlinear elements.

In conjunction with the discussion of the determination of the distribution function from the probe characteristics, there are several points worth mentioning.

The determination of the second derivative of the electron current from the second derivative of the probe current is valid for the range where the contribution to the second derivative by the ion current is negligible. If the distribution function is required for the high energy electrons, it is then necessary to use a special screened probe to separate the electron and ion components[23]. Harmonic analysis can then be used upon the electron component to determine the distribution function.

If the ac frequency is high enough so that the ions do not respond, then an ordinary probe may be used without the need for separating the ion current.

It can be shown that an upward "kink" in the retarding potential plot does not necessarily indicate that there are more high energy electrons than would be expected from the M-B body of the distribution function. For the range where the electron energy distribution is M-B, the electron current to the probe is an exponential function of qV/kT_-. The dc term in the Fourier series expansion of the probe current (Eq. VI-1) shows that when the electron current is an exponential function of the probe potential, the dc term separates into the same exponential term multiplied by a function of qA/kT_-. Thus, the slope as determined from a retarding potential plot is not changed as a result of a small monofrequency ac voltage, but the probe current is increased except above the plasma potential.

It is possible, however, for oscillations in the plasma to produce an upward "kink" in the retarding potential plot which may increase the apparent electron temperature and may increase the apparent number of high energy electrons. When the probe is slightly below plasma potential the dynamic impedance across the plasma-probe region is quite small (about 1 ohm) and only a small fraction of the ac voltage is superimposed upon the retarding potential. As the retarding potential is increased, the probe-plasma impedance becomes larger and comparable with the plasma impedance and the impedance of the external circuit. A larger fraction of the ac voltage is thus added to the regarding potential and results in an increase in the probe current and an upward "kink."

This upward "kink" was observed by Bailey[72] in a low pressure mercury arc where the oscillations were introduced inadvertently by the sheath around a "filtering" grid placed in the positive column.

C. Experimental ratio of saturation electron and saturation ion current and comparison with random current theory

There is a scarcity of published data for the ratio of saturation electron current J_{-s} to saturation ion current J_{+s}. The purpose of this and the following sections is to give accurate experimental values for this ratio and to compare them with the various theoretical values. A new theory will be advanced later to explain the results.

In this research the saturation ion current J_{+s} is defined in the following way. As the probe is made more negative with respect to the plasma potential, the electron current becomes smaller until the probe current is equal to the ion current. The value of probe current where the electron current first becomes small compared to the probe current (about 1 per cent or less) is defined as the saturation ion current. The probe current to a very negative probe is not a strong function of the probe potential (about 1 per cent per volt) while the electron current is a strong function (about 10 per cent per 0.1 volt for a kT_-/q of 1 electron volt).

The ratio J_{-s}/J_{+s} for each probe, calculated from the basic probe data of Table I, was broken into two groups: the planar probes and the wire probes. For a given set of arc parameters (T_{bath} and I_z), the ratios for the plane probes are in good agreement in spite of the different locations and orientations. When averaged, there is an average

uncertainty of 1.7 per cent in the ratios for the plane probes. Since the three plane probes have quite different edge surroundings and yet give almost the same saturation current ratios, it is concluded that the edge effects are probably not very significant for the plane probes used in this experiment. In particular, the wall probe, when it is measuring the ion current, is almost at the same potential as the floating potential of the negative wall which surrounds the wall probe. As a result, the tube wall at floating potential acts as a very large "guard ring" for the wall probe (when it is measuring ion current) and therefore no edge effects are expected for the wall probe measurements of the saturation ion current. Since the disk probe has no guard ring at all and yet gives about the same saturation current ratio as the wall probe, it is concluded that the edge effects are not very large. The same is true for the center plane probe. The average saturation current ratio for the plane probes is plotted in Fig. VI-3 as a function of p_o.

The situation for the wire probes is more complicated because of the different geometry. The ion collection area for the wire probe is larger than the geometric area because of the ion sheath around the negative probe. The values of J_{-s}/J_{+s} for the wire probes when averaged for each set have an average uncertainty of 0.9 per cent and are an average of 19 per cent below the ratios for the planar probes at the same pressure. The theories developed in this chapter will not be applied to the results for the wire probes.

A simple theory for the saturation electron and saturation ion current ratio assumes that the ratio of saturation currents is equal to the ratio of the random currents. Since the ion and electron densities

are equal, this simple theory predicts

$$\frac{J_{-s}}{J_{+s}} = \left(\frac{M_+}{m_-}\right)^{1/2}\left(\frac{T_-}{T_+}\right)^{1/2} \qquad \text{(VI-2)}$$

where the implicit assumption is made that the ions can be described by a M-B energy distribution with a characteristic temperature T_+. For mercury ions the factor $(M_+/m_-)^{1/2}$ is equal to 604.6. In conjunction with the experimental ratios of J_{-s}/J_{+s} ranging from 284 to 395, this requires that the ion temperature be about 4 times the electron temperature which is quite improbable from consideration of the basic processes in the plasma. In fact, the ion temperature should be very close to the gas temperature T_g because of the much lower ion mobility and the larger energy transfer for ion-atom collisions compared to that for electron-gas collisions. Carrying this one step further, if it is assumed that the ions have a characteristic temperature corresponding to random motion, and if this ion temperature is equal to the gas temperature T_g, the saturation current ratio J_{-s}/J_{+s} should be given by

$$\frac{J_{-s}}{J_{+s}} = \left(\frac{M_+}{m_-}\right)^{1/2}\left(\frac{T_-}{T_g}\right)^{1/2} \qquad \text{(VI-3)}$$

This quantity $(M_+/m_-)^{1/2}\,(T_-/T_g)^{1/2}$ is plotted in Fig. VI-3 as a function of p_o. It is seen that the random current model gives the wrong sense of variation of J_{-s}/J_{+s} with p_o and gives a value of 10 larger than experimental values. At the same time, the quantity T_-/T_g was calculated and is given in Fig. VI-2 for reference.

There are two types of explanation for the discrepancy between

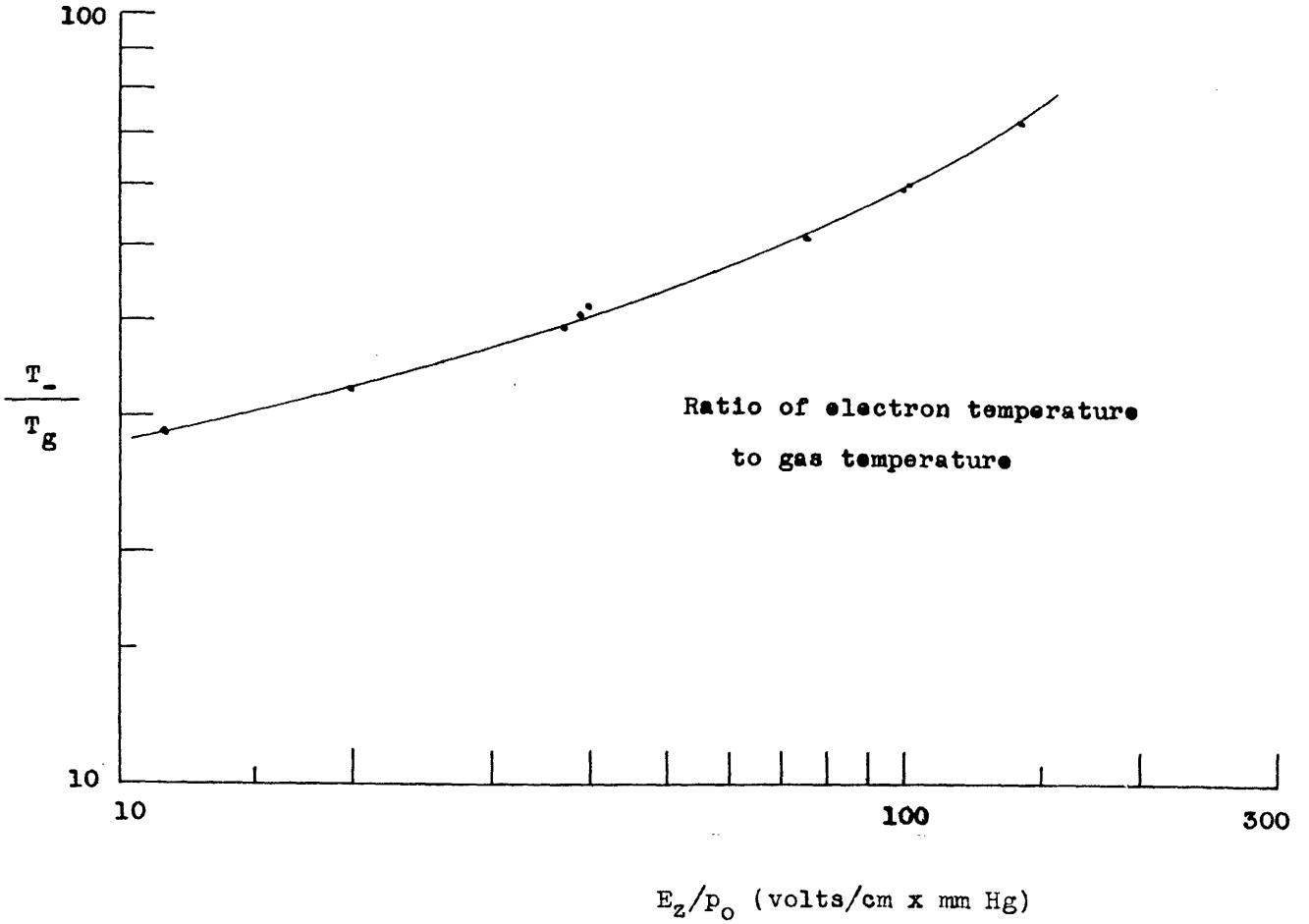

Fig. VI-2 Ratio of electron temperature to gas temperature

the experimental data and the simple random current model. One explanation is that the experimental value of J_{+s} does not correspond to the collection of ions but is related to the secondary emission of electrons from the negative probe. The other explanation is that the random current picture for the ions is not accurate. It can be shown that for this experiment the secondary processes are not able to explain the discrepancy and thus requires the abandonment of the random current model.

The electron emission from the negative probe can result from three fundamental processes: ion bombardment of the probe, metastable atoms striking the probe and radiation striking the probe. Induced electron emission resulting from the ion bombardment is not an acceptable explanation because the discrepancy between the experimental data and the simple theory would require that the ratio between the secondary electrons and the incident ions be larger than 10 which is not reasonable for such low energy ions. There are no experimental data available for the secondary yield coefficient γ for Hg ions on tantalum or tungsten, but for mercury ions on mercury the secondary yield coefficient is about 0.01 for 4 kV ions[21]. Experimental data for Hg metastables on Ta or W are not available but for Hg metastables on mercury the secondary yield is about 0.01[36]. Comparable values may be expected for the Ta and W surfaces. If the product of the secondary yield coefficient for metastable atoms and the metastable atom current to the probe is about 10 times the random ion current to the probe, the discrepancy may be explained in this way. The same argument holds for the radiation induced emission from the probes. Although it is possible that the electron emission effects are not completely negligible, they are not

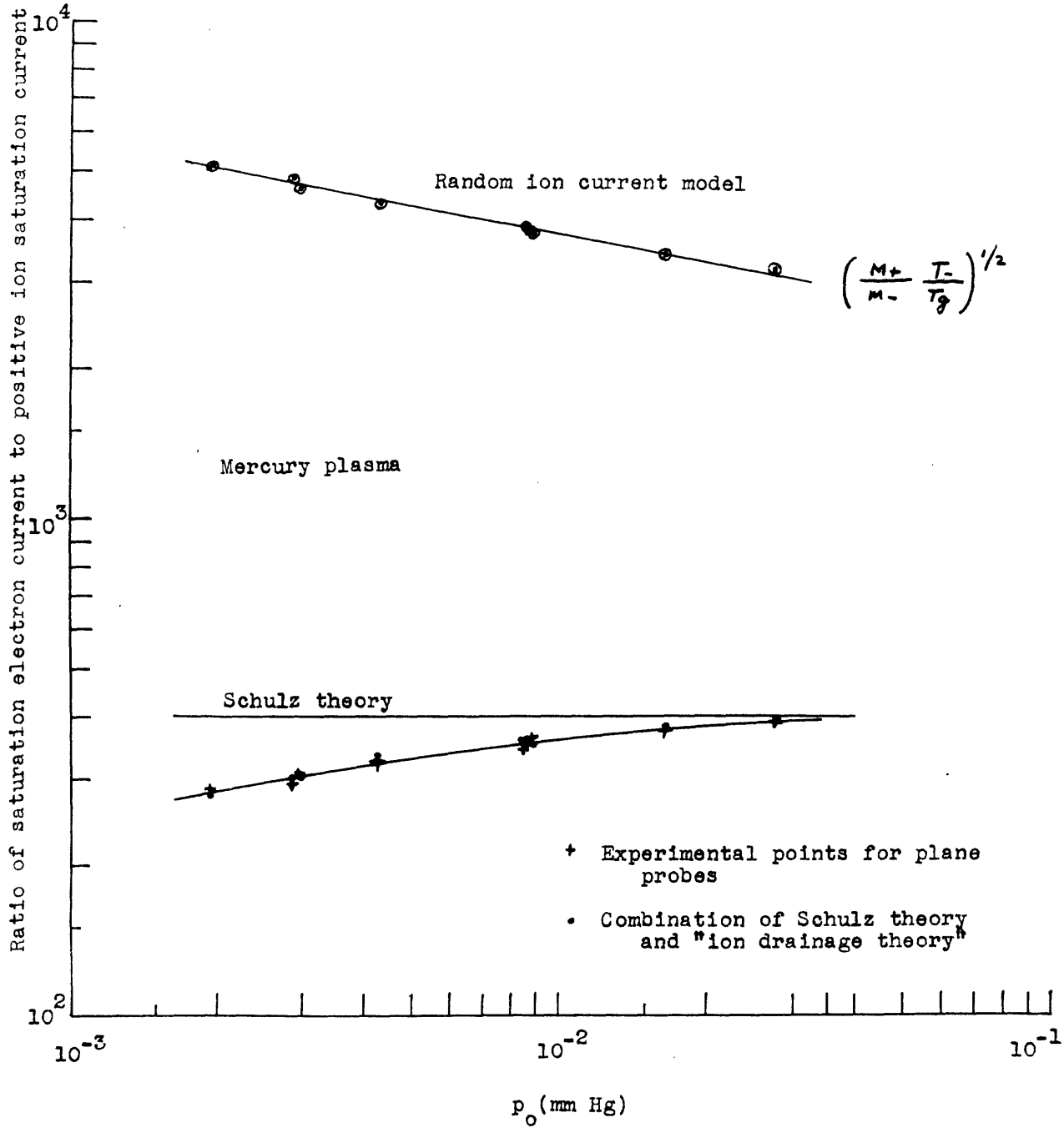

Fig. VI-3 Ratio of saturation electron current to saturation ion current

capable of completely explaining the difference of a factor of 10 between experiment and simple theory.

In addition, since Hagstrum[37] has shown that the secondary yield coefficients are strongly related to the surface conditions, it is expected that if the probe ion current contains a significant component of secondary processes the probe ion current should depend upon the time after the cleaning of the probe surface. Measurements of the probe ion current were made using the expanded scale meter and the recorder. It was found that the ion currents to the W and Ta probes remain constant to better than 2 per cent after the probes had been cleaned by electron bombardment. This indicates that the ion current is probably not predominantly electron emission current and it leads to the introduction of a more accurate theory and a better understanding of the process of ion collection by a negative probe.

D. Simplified form of Schulz's theory for the saturation current ratio and comparison with experiment

The assumption that the saturation ion current to the negative probe is equal to the random ion current has been observed here and elsewhere to be in considerable disagreement with experiment. If it is assumed that the ions in the plasma travel with a directed velocity towards the probe, much better agreement with experimental data can be obtained. This directed velocity in the plasma occurs because there is a small potential gradient in the plasma in spite of the fact that the major part of the potential difference between the probe and the plasma appears across the probe sheath. As early as 1929, Langmuir[73] stated that the ions enter the sheath with a directed velocity because the influence

of the negative probe extends into the plasma.

The collection of positive ions by a negative probe can be accurately described if several reasonable assumptions are made. The case of an infinite planar probe is considered in order to obtain an easily solvable model. The plasma is defined as the region where the ion and electron densities are approximately equal, while the ion sheath is defined as the region where the ion density is much larger than the electron density. Assume that the ions in the plasma enter the sheath with an arbitrary energy E_o (electron volts) in the direction normal to the plane probe and are accelerated toward the probe without appreciable collisions. The total energy is conserved so that

$$M_+ v_+^2 = 2q(E_o + V_b - V) \qquad \text{(VI-4)}$$

where $V_b - V$ is the potential in the sheath with respect to the potential V_b of the plasma-sheath interface. In the sheath the electron density is small so that there is no ionization, and the ion current is constant and

$$\frac{d}{dx}(n_+ v_+) = 0 \qquad \text{(VI-5)}$$

In the plasma the electron density is related to the plasma potential by the Boltzmann density law

$$\frac{n_-}{n_{-b}} = \exp\frac{q(V - V_b)}{kT_-} \qquad \text{(VI-6)}$$

The potential gradient dV/dx is assumed to be continuous at the interface and the electron and ion densities are assumed to be equal at the interface.

The last assumption that is needed may take either of two equivalent forms. It may be assumed that at the interface

$$\frac{1}{n_+}\left(\frac{dn_+}{dx}\right)_{SHEATH} = \frac{1}{n_-}\left(\frac{dn_-}{dx}\right)_{PLASMA} \qquad \text{(VI-7)}$$

or one may assume that at the interface

$$\frac{1}{n_+}\left(\frac{dn_+}{dx}\right)_{SHEATH} = \frac{1}{n_+}\left(\frac{dn_+}{dx}\right)_{PLASMA} \qquad \text{(VI-8)}$$

and

$$\frac{1}{n_+}\left(\frac{dn_+}{dx}\right)_{PLASMA} = \frac{1}{n_-}\left(\frac{dn_-}{dx}\right)_{PLASMA} \qquad \text{(VI-9)}$$

These statements can be made from knowledge of the processes in the plasma and the sheath and from the assumption that there is a gradual transition from the plasma to the sheath. In fact, it is difficult to define exactly where the plasma ends and the sheath begins. The validity of these assumptions will be tested by the agreement of the conclusions with experiment.

The previous equations can be combined in the following way to obtain the desired result. From Eq. VI-5 it is apparent that in the sheath

$$\frac{1}{n_+}\left(\frac{dn_+}{dx}\right)_s + \frac{1}{v_+}\left(\frac{dv_+}{dx}\right)_s = 0 \qquad \text{(VI-10)}$$

From Eq. VI-6

$$\frac{1}{n_-}\frac{dn_-}{dx} = \frac{q}{kT_-}\frac{dV}{dx} \qquad \text{(VI-11)}$$

Equation VI-7 shows that at the interface

$$\frac{q}{kT_-}\frac{dV}{dx} + \frac{1}{v_+}\frac{dv_x}{dx}\bigg|_s = 0 \qquad \text{(VI-12)}$$

When the logarithmic derivative of Eq. VI-4 is taken there results

$$2\frac{1}{v_+}\frac{dv_+}{dx} = -\frac{1}{E_o + V_b - V}\frac{dV}{dx} \qquad \text{(VI-13)}$$

When evaluated at the interface ($V = V_b$) and substituted in Eq. VI-12, the previous equation gives

$$\frac{q}{kT_-}\frac{dV}{dx} = \frac{1}{2}\frac{1}{E_o}\frac{dV}{dx} \qquad \text{(VI-14)}$$

Since the potential gradient at the interface dV/dx is not zero, the following result is obtained for E_o

$$E_o = \frac{1}{2}\frac{kT_-}{q} \qquad \text{(VI-15)}$$

This implies that the plasma and the sheath adjust themselves so that the ions enter the sheath with a directed energy E_o which is comparable to the random energy of the electrons, and is independent of the probe potential thus giving a saturation effect. The ion current to the probe is then obtained from the ion density at the interface and from the directed velocity where the directed velocity is related to E_o by

$$M_+ v_+^2 = 2qE_o \qquad \text{(VI-16)}$$

Since a potential gradient in the plasma is necessary to provide the ions with the initial energy E_o, the density of ions at the interface is less than the density in the plasma by a factor of about $\exp(qE_o/kT_-) = (e)^{1/2}$ from the Boltzmann density law. When combined with the random current density for the electrons (see chapter I), these considerations lead to the following ratio of saturation electron current to saturation ion current:

$$\frac{J_{-s}}{J_{+s}} = \left(\frac{M_+}{m_-}\right)^{1/2}\left(\frac{e}{2\pi}\right)^{1/2} \qquad \text{(VI-17)}$$

For the case of mercury ions the ratio is equal to 398. This result was given recently by Schulz and Brown[74] through similar reasoning. It was given even earlier in essentially the same form by Bohm, Burhop and Massey[75].

This constant value of 398 for the saturation current ratio is plotted in Fig. VI-3 for comparison with experiment, and it is seen that the agreement is good particularly for the higher pressures. At the lowest pressure, however, there is still a discrepancy since the value given by this simple theory is larger than the experimental value by a factor of 1.40. In addition, there is still a definite variation of the saturation current ratio with p_o that should be explained.

E. Basic theory for the prediction of the variation of the saturation current ratio with the arc parameters

It has been shown in the preceeding section that the ions enter the probe sheath with a directed energy E_o of from 0.5 to 1 electron volt. This result was obtained through certain assumptions about the matching of density gradients at the plasma-sheath interface and does not predict any variation of saturation current ratio with respect to the arc parameters. In this section a model will be developed which will also consider the rate of generation of ions in the plasma and the ion mobility limited flow of ions through the plasma towards the probe. The validity of the assumptions can be shown by the agreement of the results with the experimental values.

In order to obtain a solvable model, consider the one dimensional problem of a large planar probe in a large uniform plasma. When the probe is biassed negative with respect to the plasma potential, an ion sheath is formed near the surface of the probe. In this ion sheath the ion density is much larger than the electron density. Adjacent to this ion sheath is a region of the plasma where the ion and electron densities are about equal; but there is a potential and density gradient in the direction of the probe. Ions generated in this region of the plasma are formed with very small kinetic energy and, since they are in a potential well, they must eventually flow to the probe at a rate governed by the rate of generation of the ions. This region of plasma is called the ion drainage plasma. Adjacent to the ion drainage plasma is the relatively undisturbed plasma where the ion and electron densities are equal and where the density and potential gradients are small.

A number of statements can be made which apply to all parts of the plasma and sheath. From the conservation of charge in the steady state, the ion particle current is related to the generation of ions by

$$div\ \Gamma_+ = \nu_i\ n_- \qquad \text{(VI-18)}$$

where it is assumed that the ionization is proportional to the electron density. Poisson's equation relates the potential distribution to the electron and ion densities as follows:

$$div\ E = \frac{q}{\epsilon_0}(n_+ - n_-) \qquad \text{(VI-19)}$$

Since the negative probe draws very little electron current, the electron density in the plasma and the sheath can be related to the potential by the Boltzmann law

$$\frac{n_-}{n_{-0}} = exp\ \frac{q(V-V_0)}{kT_-} \qquad \text{(VI-20)}$$

From the above equations it is possible to obtain a differential equation relating Γ_+, n_- and n_+. Consider the one dimensional form of the divergence operator and use the following change of variable:

$$div\ \Gamma_+ = \frac{d\Gamma_+}{dx} = \frac{d\Gamma_+}{dn_-}\frac{dn_-}{dV}\frac{dV}{dx} \qquad \text{(VI-21)}$$

From Eqs. VI-18, VI-20, and VI-21, it follows that:

$$-E\ \frac{d\Gamma_+}{dn_-} = \nu_i \frac{kT_-}{q} \qquad \text{(VI-22)}$$

Equations VI-19, VI-20, and VI-21 give

$$-E\ \frac{q}{kT_-}(n_-)\frac{dE}{dn_-} = \frac{q}{\epsilon_0}(n_+ - n_-) \qquad \text{(VI-23)}$$

When E is eliminated between Eqs. VI-22 and VI-23 the following differential equation results:

$$-\frac{1}{2}\frac{qn_-}{kT_-}\left(v_i\frac{kT_-}{q}\right)^2\frac{d}{dn_-}\left(\frac{dr_+}{dn_-}\right)^{-2}=\frac{q}{\epsilon_0}(n_+-n_-) \qquad \text{(VI-24)}$$

This relates r_+ n_- and n_+. In order to obtain a differential equation in r_+, and n_- alone, it is necessary to eliminate n_+. This can be done if the ion velocity can be specified as a function of the potential distribution.

For the plasma in this experiment, the motion of the ions can be described in terms of the ion mobility. Kingdon and Lawton[56] have shown that for large values of E/p the velocity of Hg ions in mercury is given by

$$v_+ = 3.2\times10^3(E/p)^{1/2}\ \text{cm/sec} \qquad \text{(VI-25)}$$

In addition, the results of chapter V show that the ion velocity is given by

$$v_+ = \gamma_{1/2}(E/p_0)^{1/2} = 3.05\times10^3(E/p_0)^{1/2}\ \text{cm/sec} \pm 19\%\ \text{rms} \qquad \text{(VI-26)}$$

where the correction has been made for the diffusion flow and the nonuniform field. This formulation of mobility-limited ion flow to the probe is not necessarily accurate since the concept of charge transfer-limited mobility requires that the mean free path be as small as the distance travelled. The validity of this formulation and the relative importance of the inaccuracy will be tested by the agreement of the final results with the experimental values of the saturation current ratio.

Since $\Gamma_+ = n_+ v_+$, it is possible with the help of Eq. VI-26 to solve for n_+ as a function of Γ_+ and E to get the following:

$$n_+ = \frac{\Gamma_+}{v_+} = \frac{\Gamma_+}{\gamma_{1/2} (E/p_0)^{1/2}} \tag{VI-27}$$

When the value of E from Eq. VI-22 is substituted, there results

$$n_+ = \frac{\Gamma_+}{\gamma_{1/2}} \frac{1}{(\nu_i/p_0)^{1/2} (kT_-/q)^{1/2}} \left(- \frac{d\Gamma_+}{dn_-} \right)^{1/2} \tag{VI-28}$$

When n_+ from Eq. VI-28 is substituted into Eq. VI-24 it leads to a non-linear differential equation in Γ_+ and n_- which is difficult to solve.

An accurate simplification, however, can be made which makes a solution of the problem easy. Because the ion current in the sheath is constant (due to the much lower production of ions in the sheath), one can solve the problem by considering the equations that apply to the flow of ions in the plasma regions. Setting the ion density equal to the electron density permits considerable simplification of the problem. When E is eliminated from Eq. VI-22 and Eq. VI-27, and the ion density is set equal to the electron density, the following results directly:

$$-(\Gamma_+)^2 \frac{d\Gamma_+}{dn_-} = \frac{\nu_i}{p_0} \frac{kT_-}{q} (\gamma_{1/2})^2 (n_-)^2 \tag{VI-29}$$

This is a very simple differential equation which can be evaluated in the following way:

$$-\int_{\Gamma_+}^{C_1} (\Gamma_+)^2 \, d\Gamma_+ = \frac{\nu_i}{p_0} \frac{kT_-}{q} (\gamma_{1/2})^2 \int_{n_-}^{n_{-p}} (n_-)^2 \, dn_- \tag{VI-30}$$

The quantity Γ_+ is the ion current from the plasma to the sheath and it becomes equal to the saturation ion current Γ_{+s} as the electron density becomes smaller. It is seen that

$$(\Gamma_+)^3 = C_1 + \frac{\nu_i}{p_o}\frac{kT_-}{q}(\gamma_{1/2})^2(n-\rho)^3\left(1-\left[\frac{n_-}{n-\rho}\right]^3\right) \qquad \text{(VI-31)}$$

so that when n_-/n_{-p} is small, Γ_+ can be set equal to Γ_{+s}. The quantity n_{-p} is the electron density in the plasma. This gives

$$(\Gamma_{+s})^3 = C_1 + \frac{\nu_i}{p_o}\frac{kT_-}{q}(\gamma_{1/2})^2(n-\rho)^3 \qquad \text{(VI-32)}$$

where the constant of integration has yet to be evaluated.

From the value of Γ_{-s} obtained from chapter I, it can be seen that

$$\left(\frac{\Gamma_{+s}}{\Gamma_{-s}}\right)^3 = \left(\frac{J_{+s}}{J_{-s}}\right)^3 = C_2 + \left(\frac{2\pi m_-}{q}\right)^{3/2}\left(\frac{q}{kT_-}\right)^{1/2}\left(\frac{\nu_i}{p_o}\right)(\gamma_{1/2})^2 \qquad \text{(VI-33)}$$

Inspection of the factor $(q/kT_-)^{1/2}\ (\nu_i/p_o)$ shows that as the pressure increases the quantity J_{+s}/J_{-s} should decrease thus implying that the saturation current ratio J_{-s}/J_{+s} should increase as the pressure increases. This is in agreement with the experimental variation as can be seen from Fig. VI-3. The factor $(q/kT_-)^{1/2}\ (\nu_i/p_o)$ decreases as the pressure increases because the electron temperature decreases with increasing pressure and the quantity ν_i/p_o is a strong exponential function of the electron temperature. Physically this means that at the higher pressures

there is less ionization in the ion drainage region of the plasma and therefore the ion drainage component contributes less to the saturation ion current at the higher pressures.

In order to obtain numerical values of J_{-s}/J_{+s} for comparison with the experimental values, it is necessary to evaluate the constant C_2. When the contribution of the ion drainage plasma is small enough so that it can be neglected, the saturation ion current should be given by Schulz's theory so that, from Eq. VI-17, it is expected that

$$C_2 = \left(\frac{m_-}{M_+}\right)^{3/2}\left(\frac{2\pi}{6}\right)^{3/2} \qquad \text{(VI-34)}$$

Thus the results of this analysis predict the general relation

$$\left(\frac{p_{+s}}{p_{-s}}\right)^3 = \left(\frac{m_-}{M_+}\right)^{3/2}\left(\frac{2\pi}{6}\right)^{3/2} + \left(\frac{2\pi m_-}{q}\right)^{3/2}\left(\frac{q}{kT_-}\right)^{1/2}\left(\frac{\nu_i}{p_o}\right)\left(\gamma_{1/2}\right)^2 \qquad \text{(VI-35)}$$

which should be applicable to any discharge that satisfies the assumptions made. The validity of the assumptions made will be verified by the agreement of the predictions and the experimental values.

When the experimentally determined values of ν_i/p_o, kT_-/q, and $\gamma_{1/2}$ (which are available from the tables of basic data and from chapters IV and V) are substituted in Eq. VI-35, and the values of J_{-s}/J_{+s} are calculated, they are found to be in remarkable agreement with the experimental values. The calculated values are plotted in Fig. VI-3 for comparison with the experimental values. The difference between the theoretical values and the actual values is 3.4 per cent rms which is comparable with the experimental uncertainties. It can be concluded

either that the model and the assumptions are verified, or there is a strong coincidence.

In any event, if the assumptions and model are not acceptable, Eq. VI-35 can be proposed as an empirical expression relating the saturation current ratio, to the ion and electron mass, the electron temperature, the ionization frequency, the reduced pressure, and the mobility coefficient for large E/p_o. It would be of interest to test the applicability of Eq. VI-35 to probe measurements in other gases.

VII. Summary and Conclusions

Careful measurements have been made of the electron temperature, electron density, plasma potential, and probe currents for a set of probe measurements in the plasma of a low pressure mercury arc. As a result of the precautions used in the measurements, the results are accurate and reliable. Detailed analysis of the basic data yields considerable new information about the basic processes in the plasma.

It was shown that the actual ionization in the plasma is much larger ($_{up}$ to 45.6 times) than the direct ionization thus proving that the ionization in the plasma is predominantly cumulative ionization. The direct ionization was calculated for a Maxwell-Boltzmann electron energy distribution with the aid of Nottingham's data for the probability of direct ionization of mercury. A calculation of the effect on the direct ionization by the electron drift energy shows that this effect is small. The rate of production of the $6^3P_{o,1,2}$ excited states was calculated from the cross-sections given by Kenty, and it was shown that the rate of production of these excited states is larger than the ionization rate thus demonstrating that cumulative ionization through these excited states is possible. It was shown, with the aid of the diffusion coefficient for Hg metastables in mercury given by Biondi, that the maximum rate of diffusion loss (corresponding to the maximum metastable density given by the Boltzmann law) is lower than the rate of production of the metastables thus indicating that the predominant loss of metastables is the quenching by electron collision. This implies that the density of metastables should be relatively independent of electron density.

This indicates that the cumulative production of ions should be a linear function of electron density and not a quadratic one. The results of this experiment confirm this since $G/n_- p_o$ was found to be independent of n_- for a variation of n_- of 20 per cent.

Information was found about the electron mobility in the plasma. The average electron density, , the axial arc current, and the axial potential gradient gave the electron mobility. With the aid of the assumed Bessel function density distribution, the average electron density was found from the electron density at the center of the plasma and the electron density at the plasma edge. It was found that the mobility could be well represented by a velocity independent average cross-section for the slow electron body of the distribution. The electron mobility can be described by $\mu_- p_o (kT_-/q)^{1/2} = 1.49 \times 10^5$ $(cm^2/v\ sec)$ (mm Hg) $(volt)^{1/2}$ with an rms deviation from the mean of 6 per cent. The corresponding average cross-section is 42×10^{-16} cm^2 for electrons with kT_-/q ranging from 0.829 to 1.90 electron volts.

The ambipolar diffusion coefficient for an active plasma was obtained from the ion particle current density to the wall probe, and from the assumed Bessel function density distribution. The values obtained give more detailed information about D_a for a mercury plasma than has been reported before.

The Boltzmann theorem relating the density and potential distribution permits the radial electric field to be calculated from the assumed Bessel function density distribution. Values of the radial ion velocity were obtained from the radial ion current to the wall probe and from the ion density measures at the plasma edge. Thus the ion velocity v_+ was obtained as a function of E_r/p_o and could be expressed in the form

$$v_+ = 9.71 \times 10^3 (E_r/p_o)^{1/3} \text{ cm/sec} \pm 2.7\% \text{ rms}$$

or

$$v_+ = 4.17 \times 10^3 (E_r/p_o)^{1/2} \text{ cm/sec} \pm 11\% \text{ rms}$$

This indicates that the energy gained by the ion in one mean free path ($E\lambda$) is large compared to the random energy.

With the aid of a specially developed theory for the mobility and diffusion flow of ions in a strong field it was possible to calculate the mobility and longitudinal diffusion coefficients as well as the cross-section for slow Hg ions in mercury vapor. Since the ions are moving in a slightly nonuniform electric field, it was necessary to consider this nonuniformity. A first order theory was therefore developed for the mobility and diffusion coefficients in a strong nonuniform electric field. The mobility and diffusion coefficients and cross-sections were recalculated with this correction. The effect was small and resulted in a reduction for the cross-section of only 19 per cent on the average. The corrected cross-section for the mercury ions was found to increase from 31 to 104 x 10^{-16} cm^2 as $E\lambda$ increased from 0.44 to 1.37 electron volts. The methods and theories developed in this research may be used for the measurement of cross-sections for low energy ions in other gases.

The ion velocity corrected for the diffusion flow and the non-uniform field was calculated. It was found that this ion velocity could be described as proportional to $(E_r/p_o)^{1/2}$ with the average constant of proportionality equal to 3.05 x 10^3 cm/sec per (v/cm mm Hg)$^{1/2}$

with a rms deviation from the average of 19 per cent.

The retarding potential plots for the electrons were found to be intermediate between that for a Maxwell-Boltzmann and for a Druyvesteyn distribution. For the arc under consideration it was found that the depletion potential (the potential at which the depletion of high energy electrons started), measured with respect to the plasma potential, is approximately equal to 3.4 kT_-/q on the average. The same is true for the floating potential except that the numerical factor is 5.32.

The ratio of saturation electron current to saturation ion current was investigated both experimentally and theoretically. It was established that the ratios for the plane probes increase with p_o. In order to predict the observed variation of the saturation ration with the arc parameters, a model for ion collection by a negative planar probe has been proposed. This model includes the drainage of ions generated in the plasma near the probe. When combined with the Schulz theory for the saturation current ratio, this ion drainage theory gives values for the saturation current ratio which are in very good agreement with the experimental values.

Various new experimental techniques were developed to increase the accuracy and convenience of the measurements. The retarding potential was accurately supplied by a specially designed low impedance voltage source which features a high degree of negative feedback. The partial pressure of residual gases was kept in the 10^{-8} to 10^{-7} mm Hg range and was measured while the arc was in operation in the water bath. The probe surface was automatically cleaned by electron

bombardment before each probe current reading in order to keep the probe work-function constant. A new method was developed to permit the change of probe work-function to be directly recorded, and may prove useful in future experiments.

Appendix

Table I Basic Probe Data

T_b C	I_z amp.	Probe	I_{-s} ma	I_{+s} ma	kT_-/q volts	V_p volts	V_f volts	n_- per $m^3 \times 10^{17}$
25.1	5.0	wire(a)	86.5	0.375	1.91	2.58	13.13	1.03
		wire(a)	92.8	0.400	1.92	2.68	13.28	1.10
		center	56.0	0.202	1.91	4.37	13.98	1.10
		wire(c)	86.4	0.370	1.93	5.30	14.46	1.02
		wall	30.3	0.108	1.96	5.10	14.35	0.590
		disk	55.4	0.189	1.74	4.87	14.10	0.560
30.0	5.0	wire(a)	115	0.466	1.65	3.35	12.87	1.47
		center	73.9	0.255	1.59	5.38	13.98	1.60
		wire(c)	117	0.465	1.67	6.25	14.77	1.49
		wall	35.3	0.120	1.60	6.17	14.42	0.761
		disk	70.2	0.238	1.46	5.87	13.97	0.774
30.0	6.0	wire(a)	146	0.570	1.63	3.46	12.85	1.88
		center	95.3	0.317	1.63	5.34	13.98	2.03
		wire(c)	146	0.550	1.63	6.33	14.82	1.88
		wall	44.2	0.149	1.56	6.25	14.38	0.963
		disk	89.0	0.288	1.41	5.97	13.91	1.00
35.0	5.0	wire(a)	136	0.490	1.42	4.04	12.27	1.88
		wire(a)	142	0.530	1.44	4.10	12.30	1.95
		center	89.3	0.271	1.36	6.21	13.85	2.09
		wire(c)	143	0.512	1.40	7.22	14.84	1.99
		wall	39.5	0.119	1.40	6.99	14.52	0.909
		disk	81.9	0.250	1.23	6.74	13.88	0.984
45.1	4.0	wire(a)	187	0.652	1.14	5.05	11.02	2.88
		center	121	0.355	1.29	7.00	13.20	2.90
		wire(c)	197	0.660	1.14	8.41	14.30	3.04
		wall	41.3	0.125	1.05	8.20	13.87	1.10
		disk	108	0.303	1.18	7.48	13.14	1.33
45.1	5.0	wire(a)	231	0.790	1.07	5.20	11.06	3.67
		center	154	0.430	1.17	7.30	13.15	3.88
		center	158	0.445	1.23	7.09	13.22	3.87
		wire(c)	250	0.815	1.11	8.57	14.39	3.89
		wall	51.4	0.149	1.04	8.36	14.03	1.37
		disk	135	0.365	1.09	7.65	13.24	1.72
45.1	6.0	wire(a)	297	0.970	1.09	5.17	11.08	4.67
		center	202	0.568	1.20	7.11	13.18	5.03
		wire(c)	308	1.04	1.06	8.49	14.22	4.91
		wall	65.0	0.193	0.994	8.36	13.86	1.78
		disk	173	0.445	1.07	7.51	13.10	2.22
54.6	5.0	wire(a)	403	1.28	0.929	5.61	10.55	6.87
		center	256	0.698	1.01	7.64	12.77	6.96
		wire(c)	411	1.31	0.906	8.88	13.63	7.10
		wall	72.4	0.192	0.855	8.68	13.43	2.13
		disk	217	0.560	0.906	7.97	12.71	3.04
62.6	5.0	wire(a)	584	1.73	0.818	5.74	10.27	10.6
		center	351	0.908	0.891	7.71	12.47	10.1
		wire(c)	614	1.83	0.825	8.84	13.37	11.1
		wall	88.7	0.223	0.785	8.79	13.06	2.73
		disk	300	0.748	0.828	7.97	12.41	4.39

Table II

Basic Discharge Parameters

Set	T_b °C	I_z amp.	E_z V/cm	ΔT °C	$\bar{p}$ x10^3 mm Hg	p_o x10^3 mm Hg	n_g x10^{-14} per cm^3	r_p/r_w	Average kT_-/q volts	Average T_- °K	Average n_{-o} x10^{-11} #/cm^3
A	25.1	5.0	0.267	1.6	2.12	1.93	0.682	0.996	1.90	22,000	1.06
G	30.0	5.0	0.290	1.7	3.18	2.85	1.01	0.996	1.59	18,500	1.52
H	30.0	6.0	0.287	2.1	3.29	2.94	1.04	0.997	1.57	18,200	1.93
B	35.0	5.0	0.315	1.9	4.80	4.22	1.49	0.996	1.37	15,900	1.98
I	45.1	4.0	0.336	1.6	9.98	8.52	3.01	0.997	1.16	13,400	2.94
C	45.1	5.0	0.337	2.0	10.3	8.77	3.10	0.997	1.12	13,000	3.83
F	45.1	6.0	0.332	2.4	10.6	9.01	3.19	0.998	1.08	12,600	4.87
D	54.6	5.0	0.327	2.0	20.0	16.6	5.87	0.998	0.920	10,700	6.98
E	62.6	5.0	0.310	1.9	34.0	27.5	9.71	0.998	0.829	9,630	10.6

Table III Ion Generation in the Plasma

Set	n_{w-}/n_{o-}	$\overline{n_-}/n_{o-}$	$J_w(V_f)$ amp./m^2	G_{total} x 10^{-15} (#/sec.)/cm^3	ν_i/p_o (direct) (#/sec.)/mm	$\frac{\nu_i(total)}{\nu_i(direct)}$
A	0.554	0.767	7.52	3.43	1.27 x10^7	1.71
G	0.502	0.738	8.54	3.89	4.41 x10^6	2.76
H	0.499	0.737	10.5	4.79	4.00 x10^6	2.86
B	0.460	0.715	8.25	3.76	1.50 x10^6	4.21
I	0.374	0.666	8.83	4.02	3.55 x10^5	6.80
C	0.358	0.657	10.6	4.82	2.60 x10^5	8.42
F	0.364	0.660	13.7	6.21	1.87 x10^5	11.4
D	0.306	0.626	13.7	6.21	3.27 x10^4	26.2
E	0.257	0.597	15.8	7.20	9.08 x10^3	45.6

Table IV Electron Mobility and Electron Drift Energy

Set	J_z $\times 10^{-3}$ amp./m^2	v_z $\times 10^{-5}$ m/s	$p_o \mu_-$ $\times 10^{-5}$ (cm/s)/(V/cm)mm	$\frac{\langle v_- \rangle}{v_z}$	$\frac{V_z}{kT_-/q}$
A	2.12	1.62	1.17	5.68	0.0395
G	2.12	1.18	1.16	7.16	0.0248
H	2.54	1.12	1.14	7.52	0.0225
B	2.12	0.936	1.26	8.38	0.0182
I	1.69	0.541	1.37	13.3	0.00719
C	2.12	0.525	1.37	13.5	0.00700
F	2.54	0.492	1.34	14.2	0.00636
D	2.11	0.302	1.53	21.3	0.00282
E	2.11	0.208	1.84	29.3	0.00149

Glossary

a acceleration of ion, p. 68

A amplitude of small ac signal, p. 81

C_1 constant of integration, p. 97

C_2 constant of integration, p. 98

D_a ambipolar diffusion coefficient, p. 39

D_m diffusion coefficient for metastables, p. 52

D_+ ion diffusion coefficient, p. 38

D_- electron diffusion coefficient, p. 38

D_{11} longitudinal ion diffusion coefficient, p. 72

e_o permittivity in rationalized MKS units, p. 33

E_o directed energy of ion in electron volts, p. 34

E_r radial electric field (evaluated at plasma edge), p. 65

E_z axial electric field, p. 29

E_θ electric field at end of free path for ion, p. 75

$f(\vec{v})$ density of electrons in phase space, p. 2

$f_o(v)$ spherically symmetric part of the distribution function, p. 3

g statistical weight of a state, p. 52

G total ionization in ions generated per second per unit volume, p. 36

$\overline{G}$ total ionization averaged over the cross-section of the plasma, p. 37

i_p current to the probe, p. 1

i_- electron current to probe, p. 2

i_+ ion current to probe, p. 25

I_v current in vertical arm of discharge, p. 9

I_z axial arc current in horizontal arm of discharge, p. 9

I_{-s} saturation electron current, p. 27

J_z axial current density in horizontal plasma averaged over the plasma averaged over the plasma cross-section, (same as $\overline{J_z}$) p. 57

J_- electron current density, p. 26

J_{-s} saturation electron current density, p. 3

J_{+s} saturation ion current density, p. 85

$J_{+w}(V_f)$ ion current density to floating wall probe, p. 36

J_0 Bessel function of the first kind, p. 43

J_1 Bessel function of the first kind, p. 45

k Boltzmann's constant, p. 2

K thermal conductivity of pyrex, p. 30

m_- mass of electron, p. 2

M_+ mass of ion, p. 68

n_g density of mercury atoms, p. 49

n_m density of metastable atoms, p. 52

n_- electron density in number per unit volume, p. 1

n_+ ion density in number per unit volume, p. 1

$\overline{n}_-$ electron density averaged over a cross-section of the cylindrical plasma p. 45

n_{-o} electron density at the center of the plasma, p. 45

n_{-w} electron density at the edge of the plasma, p. 45

p vapor pressure of mercury, p. 30

p_o reduced pressure, p. 31

P_c probability of collision in number per unit length, p. 59

P_i probability of ionization in number per unit length, p. 48

q magnitude of electron charge, p. 2

$q(\theta)$ differential scattering cross-section, p. 59

Q_c collision cross-section, p. 59

Q_i cross-section for ionization, p. 49

Q_m cross-section for momentum transfer, p. 59

Q_o effective cross-section, p. 47

$Q(A \rightarrow B)$ cross-section for the production of species B from species A, p. 46

r_p radius of the plasma, p. 33

r_w radius of the wall, p. 30

r_1 inner radius of pyrex wall (same as r_w), p. 30

r_2 outer radius of pyrex wall, p. 30

Δr thickness of ion sheath on wall, p. 33

R_o radial location of zero of electron distribution, p. 43

s distance of flight of ion, p. 68

s_j saturation factor for the j'th state - ratio of the density of the state to the maximum density given by the Boltzmann theorem, p. 54

S Spenke function, p. 44

T_b temperature of water bath, p. 29

T_g temperature of mercury vapor, p. 31

T_- electron temperature in degrees K, p. 1

T_+ "temperature of ions", p. 87

ΔT temperature drop in the pyrex wall, p. 30

δT temperature jump from the mercury vapor to wall, p. 31

v magnitude of velocity vector, p. 3

v_f terminal velocity of ion at end of flight, p. 68

v_o minimum velocity required to overcome retarding potential, p. 2

v_x velocity in the "x" direction, p. 2

v_z axial drift velocity of electrons, p. 57

v_{rms} root mean square velocity of electrons, p. 6

v_+ ion velocity in the radial direction ($\Gamma_{+w} = n_+ v_+$), p. 65

$\overline{v}$ time average velocity, p. 67

v_ϕ drift velocity of electrons, p. 49

$\langle v \rangle$ electron velocity averaged over the distribution function, p. 3

V retarding potential of the probe with respect to the plasma potential, p. 2

V_c potential of the collector (probe), p. 26

V_d potential at which the depletion of high energy electrons starts, p. 80

V_f floating potential of probe, p. 79

V_i ionization potential, p. 48

V_p plasma potential, p. 27

V_T voltage equivalent of T_- (equal to kT_-/q), p. 46

V_z axial drift energy of electrons, p. 58

$\overline{V}$ average energy in electron volts, p. 79

V_ϕ drift energy of electrons in electron volts, p. 49

V_θ threshold energy in electron volts, p. 46

$V_{\theta j}$ threshold energy for the j'th state, p. 54

x 2.405 r/R (evaluated at the plasma edge where $x_p = 2.405\ r_p/R_p$) p. 45

y_o $0.7397\ V/\overline{V}$, p. 5

$Y_{1/2}$ ratio of average ion velocity to $(E/p_o)^{1/2}$, p. 77

a persistence of velocity, p. 68

$\Gamma(k)$ complete gamma function, p. 5

Γ_{+w} ion particle current density to the wall, p. 42

$\vec{\Gamma}_+$ particle current density of ions, p. 38

$\vec{\Gamma}_-$ particle current density of electrons, p. 38

λ_g mean free path of the mercury atoms, p. 31

λ mean free path for the mercury ions, p. 69

λ_c mean free path for collisions, p. 59

λ_m mean free path for momentum transfer, p. 58

μ_a ambipolar mobility coefficient, p. 64

μ_- mobility coefficient for electrons, p. 38

μ_+ mobility coefficient for ions, p. 38

θ accommodation coefficient for mercury atoms on pyrex, p. 31

τ time of flight, p. 68

ν_i ionization frequency in number per electron per second, p. 43

$\Delta\phi$ change of work-function, p. 17

References

1. I. Langmuir, Gen. Elec. Rev. 26, 731 (1923)
2. I. Langmuir and H. M. Mott-Smith, Gen. Elec. Rev. 27, 449, 538, 616, 762, 810 (1924)
3. H. M. Mott-Smith and I. Langmuir, Phys. Rev. 28, 727 (1926)
4. L. Tonks and I. Langmuir, Phys. Rev. 34, 876 (1929)
5. T. J. Killian, Phys. Rev. 35, 1238 (1930)
6. M. J. Druyvesteyn and F. M. Penning, Rev. Mod. Phys. 12, 87, (1940)
7. P. M. Morse, W. P. Allis, and E. S. Lamar, Phys. Rev. 48, 412 (1935)
8. S. Chapman and T. G. Cowling, The Mathematical Theory of Non-Uniform Gases, second edition, The University Press, (Cambridge), 1953, p. 346
9. R. F. Post, Rev. Mod. Phys. 28, 338 (1956)
10. M. J. Druyvesteyn, Z. Physik, 64, 791 (1930)
11. G. Medicus, J. Appl. Phys. 27, 1242 (1956)
12. R. T. Bayard and D. Alpert, Rev. Sci. Instr. 21, 571 (1950)
13. T. A. Anderson, Phil. Mag. 38, 179 (1947)
14. M. A. Easley, J. Appl. Phys. 22, 590 (1951)
15. R. M. Howe, J. Appl. Phys. 24, 881 (1953)
16. G. Wehner and G. Medicus, J. Appl. Phys. 23, 1035 (1952)
17. A. L. Reimann, Phil. Mag. 20, 594 (1935)
18. G. L. Weissler and T. N Wilson, J. Appl. Phys. 24, 472 (1953)
19. G. L. Weissler and R. W. Kotter, Phys. Rev. 73, 538 (A) (1948)
20. C. W. Oatley, Phys. Soc. Proc. 51, 318 (1939)
21. P. F. Little, Handbuch der Physik, Vol. XXI, 1956, p. 639
22. R. L. F. Boyd, Proc. Roy. Soc. (London) A201, 329 (1950)
23. D. H. Pringle and W. E. J. Farvis, Phys. Soc. Proc. B68, 836 (1955)
24. E. R. Cohen, J. W. M. DuMond, T. W. Layton, and J. S. Rollett, Rev. Mod. Phys. 27, 363 (1955)
25. International Critical Tables, Vol. III, McGraw-Hill, (New York), 1928, p. 206
26. Handbook of Chemistry and Physics, 38 ed. Chemical Rubber Publishing Co., (Cleveland), 1956-57, p. 2150
27. E. H. Kennard, Kinetic Theory of Gases, McGraw-Hill (New York), 1938, p. 311

28. Chapman and Cowling, p. 104

29. International Critical Tables, Vol. V, 1929, p. 53

30. Smithsonian Physical Tables, 9th ed. Smithsonian Institute, (Washington), 1954, p. 638

31. W. Elenbaas, The High Pressure Mercury Vapor Discharge, Interscience Publishers, (New York), 1951 p. 42

32. B. Klarfeld, Jour. Phys. U.S.S.R. 5, 173 (1941)

33. K. W. Missner and W. F. Miller, Phys. Rev. 92, 896 (1953)

34. C. Kenty, Phys. Rev. 80, 95 (L) (1950)

35. M. A. Biondi, Phys. Rev. 88, 660 (1952)

36. A. von Engel, Ionized Gases, Clarendon Press, (Oxford), 1955, p. 84

37. H. D. Hagstrum, Phys. Rev. 104, 1516 (1956)

38. W. Schottky, Physik. Z. 25, 342 635 (1924)

39. W. P. Allis, Handbuch der Physik, Vol. XXI, 1956

40. J. O. Hirschfelder, C. F. Curtis and B. R. Bird, Molecular Theory of Gases and Liquids, 1954, p. 441

41. E. Spenke, Z. Physik, 127, 221 (1950)

42. W. B. Nottingham, Phys. Rev. 55, 203 (1939)

43. C. Kenty, J. Appl. Phys. 21, 1309 (1950)

44. B. Klarfeld, Tech. Phys. U.S.S.R. 5, 913 (1938)

45. J. F. Waymouth and F. Bitter, J. Appl. Phys. 27, 122 (1956)

46. M. A. Biondi, Phys. Rev. 90, 730 (1953)

47. W. P. Allis and S. C. Brown, Phys. Rev. 87, 419 (1952)

48. F. L. Arnot, Proc. Roy . Soc. (London), A130, 655 (1930)

49. H. S. W. Massey and E. H. S. Burhop, Electronic and Ionic Impact Phenomena, The Clarendon Press, (Oxford), 1956, p. 121

50. K. K. Darrow, Electrical Phenomena in Gases, The Williams and William Co., (Baltimore) 1932, p. 200

51. R. B. Brode, Rev. Mod. Phys. 5, 257 (1932)

52. R. B. Brode, Proc. Roy. Soc. (London) A125, 134 (1929)

53. W. Elenbaas, Phillips Res. Reports, 2, 20 (1947)

54. F. P. Adler and H. Margenau, Phys. Rev. 79, 970 (1950)

55. M. A. Biondi, Phys. Rev. 90, 730 (1953)

56. K. H Kingdon and E. J Lawton, Phys. Rev. 56, 215 (A) (1939)

57. L. Sena, Jour. Phys. U.S.S.R. 10, 179 (1946)

58. G. H. Wannier, The Bell System Tech. Jour. 32, 170 (1953)

59. J. H. Jeans, The Dynamical Theory of Gases, Dover Publications, (New York) 1954, p. 263

60. L. F Epstein and M. D. Powers, Jour. Phys. Chem. 57, 336 (1953)

61. J. S. Lukesh, W. H. Howland, L. F. Epstein and M. D. Powers, Jour. Chem. Phys. 23, 1923 (1955)

62. Massey and Burhop, p. 526

63. Massey and Burhop, p. 444

64. Massey and Burhop, p. 413

65. B. M. Palyukh and L. A. Sena, J. Exp. Theor. Phys. U.S.S.R. 20, 481 (1950)

S. C Brown and W. P. Allis, Technical Report 283, Research Laboratory of Electronics, M.I.T. 1954, p. 21

American Institute of Physics Handbook, McGraw-Hill, (New York) (1957), p. 7-174

66. R. N. Varney, Phys. Rev. 88, 362 (1952)

67. W. P. Allis, Handbuch der Physik, Vol. XXI, 1956, p. 90

68. R. H Sloane and E. I. R. MacGregor, Phil. Mag. 18, 193 (1934)

69. A. H. van Gorcum, Physica, (Hauge), 207, 1936

70. S. E. A Landale, Proc. Camb. Phil. Soc. 25, 355 (1929)

71. L. B. Loeb, Basic Processes of Gaseous Electronics, University of California Press (Berkeley) 1955, p. 345

72. J. M. Bailey, Unpublished M.S. Thesis, Department of Physics, M.I.T. May 1951

73. I. Langmuir, Phys. Rev. 33, 954 (1929)

74. G. J. Schulz and S. C Brown, Phys. Rev. 98, 1642 (1955)

G. J. Schulz, PhD Thesis, Department of Physics, M.I.T. 1954

75. D. Bohm, E H. S Burhop, and H. S. W. Massey, "Uses of Probes for Plasma Explorations", in The Characteristics of Electrical Discharges in Magnetic Fields, ed. by A. Guthrie and R. K. Wakerling, McGraw-Hill, (New York) 1949, p. 13

Acknowledgement

I would like to thank Professor Wayne B. Nottingham for all the help and advice he has given me. I am grateful to Professor W. P. Allis for valuable aid with the theory. The interest shown by Professor S. C. Brown and Professor F. Bitter was very encouraging.

I would also like to thank the members, past and present, of the Physical Electronics group and the Microwave Gaseous Discharge group for many enlightening discussions.

Thanks are due to Mr. L. W. Ryan and Mr. A. J. Velluto for their expert glass-blowing, Mr. A. Berg and his wiring shop for the construction of the electronic circuits, Mr. L. E. Sprague for drawing some of the figures, and Miss Anne F. Crimmings for typing the thesis.

The encouragement of my wife, Dr. Ruth Aisenberg, is gratefully acknowledged.

Biographical Note

Sol Aisenberg was born in New York City on August 26, 1928. He was educated in the New York public schools and graduated from Brooklyn Technical High School. He entered Brooklyn College in 1947 where he majored in physics. In 1951 he received his B.S. cum laude with honors in physics, and was admitted to the graduate school of the Massachusetts Institute of Technology. From July 1951 to September 1956, he held a research assistantship in the Research Laboratory of Electronics and the Physics Department of the Massachusetts Institute of Technology.

He is a member of the American Physical Society, Sigma Xi, Pi Mu Epsilon, and Phi Beta Kappa.

He was married on February 12, 1956.

Basic Retarding Potential Data

The following 48 pages of data which represent the original measurements for 43 retarding potential plots are not a necessary part of this thesis but are included at the request of Professors W. P. Allis, S. C. Brown, and W. B. Nottingham. The significant quantities which were calculated from the data for use in this thesis are listed in tables I and II. These quantities include the electron temperature, the electron density, the plasma potential, and the saturation electron and ion currents for each probe.

The current to the probe was measured as a function of the probe potential V, where this potential is measured with respect to the anode in the horizontal arm of the discharge tube. Since there is a small voltage drop in the probe current meter, the probe potential V, must be increased according to the following:

50 milivolts full scale for the 100 to 1000 miliampere range,
50 milivolts full scale for the 10 to 100 miliampere range,
50 milivolts full scale for the 1 to 10 miliampere range,
50 milivolts full scale for the 0.1 to 1 miliampere range,
and 5 milivolts full scale for the 0 to 0.1 muliampere range.

WIRE PROBE (CATHODE)

T_b = 25.1 °C ± 0.1 °C

I_g = 5.0 AMP ± 1%

I_v = 5.0 AMP ± 1%

A1

7/19/56

V (VOLTS)	i_p (MA)	i_+	i_-
2.0	112	0.3	112.3
.2	110		110.3
.4	109		109.3
.6	108		108.3
.8	107		107.3
3.0	105		105.3
	104		104.3
	102		102.3
	101		101.3
	97.2		97.5
4.0	96.2		96.5
	94.8		95.1
	93.1		93.4
	91.0		91.3
	89.8		90.1
5.0	87.2		87.5
	83.5		83.8
	79.0		79.3
	72.3		72.6
	67.5		67.8
6.0	60.5		60.8
	54.5		54.8
	47.8		48.1
	43.8		44.1
	39.5		39.8
7.0	35.3		35.6
	32.2		32.5
	29.0		29.3
	25.9		26.2
	23.6		23.9
8.0	21.1		21.4
	19.3		19.6
	17.5		17.8
	15.6		15.9
	14.3		14.6
9.0	12.8		13.1
	11.5	0.3	11.8
	9.70	0.33	10.03
	8.42		8.75
	7.91		8.24
10.0	7.18		7.51
	6.48		6.81
	5.48	0.33	5.81
	4.86	0.34	5.20
	4.35		4.69
11.0	3.82		4.16
	3.38		3.72
	2.98		3.32
	2.62		2.96
	2.27	0.34	2.61

V	i_p	i_+	i_-
12.0	1.97	0.34	2.31
	1.68	0.34	2.02
	1.42	0.341	1.76
	1.19	0.342	1.53
	0.915	0.342	1.257
13.0	0.782	0.343	1.125
	0.608	0.344	0.952
	0.473	0.345	0.818
	0.355	0.346	0.701
	0.255	0.347	0.602
14.0	0.165	0.347	0.512
	0.078	0.348	0.426
	0.018	0.349	0.367
	0.038	0.349	0.311
	0.091	0.350	0.260
15.0	0.130	0.351	0.221
	0.169	0.352	0.183
	0.198	0.352	0.154
	0.221	0.353	0.132
	0.243	0.354	0.111
16.0	0.262	0.355	0.093
	0.278	0.356	0.078
	0.292	0.357	0.065
	0.302	0.357	0.055
	0.311	0.358	0.047
17.0	0.319	0.358	0.039
	0.327	0.359	0.032
	0.332	0.360	0.028
	0.338	0.361	0.023
	0.343	0.362	0.019
18.0	0.348	0.363	0.015
19.0	0.362		
20.0	0.370		

Σ POINTS = 83

18 CHECK POINTS

AVERAGE CHANGE = 2.5%

DISK PROBE

T_b = 25.1 °C

I_z = 5.0 A

I_v = 5.0 A

A_2

7/19/56

V (VOLTS)	i_p (MA)	i_+	i_-
1.0	63.8	0.2	64.0
	63.3		63.5
	63.2		63.64
	62.5		62.7
	62.0		62.2
2.0	61.8		62.0
	61.4		61.6
	61.1		61.3
	60.8		61.0
	60.0		60.2
3.0	59.8		60.0
	59.3		59.5
	59.3		59.5
	58.3		58.5
	58.2		58.5
4.0	57.0		57.2
	57.0		57.2
	55.7		55.9
	54.2		54.4
	52.0		52.2
5.0	48.2		48.4
	44.3		44.5
	39.8		40.0
	35.9		36.1
	32.2		32.4
6.0	28.9		29.1
	25.7		25.9
	22.9		23.1
	20.5		20.7
	18.2		18.4
7.0	16.3		16.5
	14.6		14.8
	12.8		13.0
	11.4		11.6
	10.3	0.2	10.5
8.0	8.75	0.18	8.93
	7.78		7.96
	6.95		7.13
	6.22		6.40
	5.52		5.70
9.0	4.92		5.10
	4.40		4.58
	3.92		4.10
	3.45		3.63
	3.12		3.30
10.0	2.76		2.94
	2.42		2.60
	2.18		2.36
	1.92		2.10
	1.69	0.18	1.87

V	i_p	i_+	i_-
11.0	1.48	0.18	1.66
	1.29	0.18	1.47
	1.12	0.18	1.30
	0.930	0.180	1.11
	0.795	0.181	0.976
12.0	0.679	0.181	0.860
	0.579	0.181	0.760
	0.480	0.182	0.662
	0.395	0.182	0.577
	0.320	0.182	0.502
13.0	0.252	0.182	0.434
	0.191	0.182	0.373
	0.138	0.183	0.321
	0.089	0.183	0.272
	0.050	0.183	0.233
14.0	0.015	0.183	0.198
	0.015	0.183	0.168
	0.0415	0.183	0.141
	0.0625	0.184	0.121
	0.0805	0.184	0.103
15.0	0.0970	0.184	0.087
	0.112	0.185	0.073
	0.123	0.185	0.062
	0.133	0.185	0.052
	0.142	0.185	0.043
16.0	0.149	0.186	0.037
	0.156	0.186	0.030
	0.160	0.186	0.026
	0.163	0.187	0.024
	0.169	0.187	0.018
17.0	0.172	0.187	0.015
18.0	0.182	0188	0.006
19.0	0.189		
20.0	0.191		

Σ = 84 POINTS

18 CHECK POINTS

AVERAGE CHANGE = 0.7%

ANODE WIRE PROBE [w(a)]

T_b = 25.1 °C ± 0.1°C

I_y = 5.0 AMP

I_v = 5.0 AMP

A3

7/19/56

V (VOLTS)	i_p (MA)	i^+ (MA)	i^- (MA)
0.0	108	0.3	108.3
0.2	106		106.3
0.4	104		104.3
0.6	103		103.3
0.8	102		102.3
1.0	98.2		98.5
	96.8		97.1
	95.5		95.8
	93.8		94.1
	92.3		92.6
2.0	91.1		91.4
	89.2		89.5
	86.2		86.5
	82.9		83.2
	77.2		77.5
3.0	70.6		70.9
	63.5		63.8
	56.2		56.5
	50.6		50.9
	45.4		45.7
4.0	40.6		40.9
	36.5		36.8
	32.5		32.8
	29.6		29.9
	26.3		26.6
5.0	23.8		24.1
	21.2		21.5
	19.3		19.5
	17.2		17.5
	15.8		16.1
6.0	14.3		14.6
	13.1		13.4
	11.9		12.2
	10.8	0.3	11.1
	9.15	0.29	9.44
7.0	8.32		8.61
	7.62		7.91
	6.93		7.22
	6.31		6.60
	5.83	0.29	6.12
8.0	5.24	0.30	5.54
	4.84		5.14
	4.33		4.63
	3.95		4.25
	3.59		3.89
9.0	3.25		3.55
	2.97	0.30	3.27
	2.69	0.31	3.00
	2.40	0.31	2.71
	2.16	0.31	2.47

V (VOLTS)	i_p (MA)	i^+ (MA)	i^- (MA)
10.0	1.92	0.310	2.23
	1.72	0.311	2.03
	1.52	0.313	1.83
	1.34	0.314	1.65
	1.16	0.316	1.48
11.0	1.02	0.318	1.34
	0.812	0.319	1.131
	0.695	0.320	1.015
	0.582	0.322	0.904
	0.482	0.323	0.805
12.0	0.382	0.325	0.707
	0.298	0.327	0.625
	0.223	0.328	0.551
	0.155	0.330	0.485
	0.083	0.332	0.415
i^- 13.0	0.030	0.334	0.364
i^+	0.018	0.335	0.317
	0.063	0.337	0.274
	0.106	0.338	0.232
	0.138	0.340	0.202
14.0	0.172	0.341	0.169
	0.201	0.343	0.142
	0.224	0.344	0.120
	0.246	0.347	0.101
	0.263	0.348	0.085
15.0	0.281	0.350	0.069
	0.293	0.351	0.058
	0.305	0.353	0.048
	0.315	0.354	0.039
	0.324	0.357	0.033
16.0	0.332	0.358	0.026
	0.339	0.359	0.020
	0.347	0.361	0.014
	0.352	0.363	0.011
	0.353	0.364	0.011
17.0	0.358	0.367	0.009
18.0	0.372	0.375	0.003
19.0	0.384	0.385	0.001

Σ = 88 POINTS

18 CHECK POINTS

AVERAGE CHANGE = 1.7%

WALL - PLANE PROBE

T_b = 25.0°C

I_z = 5.0 AMP

I_v = 5.0 AMP

A4

7/19/56

V	i_p MA	N_+	i_-
0.0	35.3	0.1	35.4
0.2	35.6		35.7
0.4	35.4		35.5
0.6	35.2		35.3
0.8	35.0		35.1
1.0	34.8		34.9
	34.7		34.8
	34.6		34.7
	34.4		34.5
	34.2		34.3
2.0	33.9		34.0
	33.8		33.9
	33.5		33.6
	33.3		33.4
	33.3		33.4
3.0	33.0		33.1
	32.8		32.9
	32.5		32.6
	32.2		32.3
	31.9		32.0
4.0	31.8		31.9
	31.2		31.3
	30.8		30.9
	29.9		30.0
	28.9		29.0
5.0	27.5		27.6
	25.9		26.0
	24.2		24.3
	22.1		22.2
	20.5		20.6
6.0	18.7		18.8
	17.1		17.2
	15.3		15.4
	14.0		14.1
	12.8		12.9
7.0	11.6		11.7
	10.4	0.1	10.5
	9.10	0.09	9.19
	8.22		8.31
	7.46		7.55
8.0	6.78	0.09	6.87
	6.13		6.22
	5.50		5.59
	4.98		5.07
	4.48		4.55
9.0	4.02	0.10	4.12
	3.62		3.72
	3.28		3.38
	2.95		3.05
	2.66		2.76

V	i_p MA.	N_+	i_-
10.0	2.38	0.10	2.48
	2.12		2.22
	1.89		1.99
	1.68		1.78
	1.48	0.10	1.58
11.0	1.31	0.097	1.41
	1.14	0.10	1.24
	0.953	0.098	1.052
	0.829	0.098	0.927
	0.722	0.099	0.821
12.0	0.620	0.099	0.719
	0.528	0.099	0.627
	0.443	0.100	0.543
	0.371	0.100	0.471
	0.306	0.100	0.406
13.0	0.248	0.100	0.348
	0.198	0.100	0.298
	0.150	0.101	0.251
	0.109	0.101	0.210
	0.0722	0.102	0.174
14.0	0.0425	0.102	0.145
i_-	0.0165	0.102	0.119
i_+	0.006	0.102	0.096
	0.025	0.102	0.077
	0.0408	0.103	0.062
15.0	0.0528	0.103	0.050
	0.0625	0.103	0.040
	0.0702	0.103	0.033
	0.0762	0.103	0.027
	0.0809	0.104	0.023
16.0	0.0845	0.104	0.019
	0.0878	0.104	0.016
	0.0909	0.105	0.014
	0.0929	0.105	0.012
	0.0950	0.105	0.010
17.0	0.0962	0.105	0.009
	0.0978	0.106	0.008
	0.0989	0.106	0.007
	0.103	0.107	0.004
	0.103	0.107	0.004
18.0	0.104	0.107	0.003
	0.104		
	0.105		
	0.106		
	0.107		
19.0	0.108		
20.0	0.109		

$\leq$ = 97 POINTS

20 CHECK POINTS

AVERAGE CHANGE 1.0%

CENTER – PLANE PROBE

T_b = 25.0 °C

I_z = 5.0 AMP

I_v = 5.0 AMP

A5

7/17/56

V (VOLTS)	i_p (MA)	i_+	i_-
0.0	63.2	0.2	63.4
	63.2		63.4
	63.0		63.2
	62.9		63.1
	62.5		62.7
1.0	61.9		62.1
	61.9		62.1
	61.4		61.6
	61.0		61.2
	60.6		60.8
2.0	60.3		60.5
	59.9		60.0
	59.5		59.7
	59.1		59.3
	58.9		59.1
3.0	58.3		58.5
	58.2		58.4
	57.5		57.7
	57.2		57.4
	56.2		56.7
4.0	54.8		55.0
	52.6		52.8
	50.2		50.4
	45.9		46.1
	41.9		42.1
5.0	38.2		38.4
	34.5		34.7
	31.3		31.5
	28.6		28.8
	25.9		26.1
6.0	23.6		23.8
	21.2		21.4
	19.3		19.5
	17.4		17.6
	15.8		16.0
7.0	14.2	0.2	14.4
	12.8	0.2	13.0
	11.6	0.2	11.8
	10.6	0.2	10.8
	8.94	0.16	9.10
8.0	8.08	0.164	8.24
	7.32	0.16	7.48
	6.60	0.17	6.77
	5.94	0.17	6.11
	5.34	0.17	5.51
9.0	4.81	0.17	4.98
	4.32	0.17	4.49
	3.88	0.17	4.05
	3.47	0.17	3.64
	3.12	0.17	2.39

V (VOLTS)	i_p (MA)	i_+	i_-
10.0	2.78	0.17	2.95
	2.48	0.17	2.65
	2.22	0.17	2.39
	1.98	0.17	2.15
	1.73	0.17	1.90
11.0	1.52	0.17	1.69
	1.33	0.17	1.50
	1.17	0.18	1.35
	1.02	0.19	1.20
	0.828	0.176	1.004
12.0	0.702	0.177	0.879
	0.604	0.177	0.781
	0.503	0.178	0.681
	0.416	0.179	0.595
	0.332	0.180	0.512
13.0	0.262	0.180	0.442
	0.198	0.181	0.379
	0.139	0.182	0.321
	0.084	0.182	0.266
i_-	0.039	0.183	0.222
14.0 i_+	0.004	0.184	0.180
	0.039	0.185	0.146
	0.0685	0.186	0.117
	0.0928	0.186	0.093
	0.114	0.186	0.072
15.0	0.130	0.186	0.056
	0.142	0.187	0.045
	0.153	0.188	0.035
	0.162	0.188	0.026
	0.169	0.190	0.021
16.0	0.174	0.190	0.016
17.0	0.189	0.194	0.005
18.0	0.198		
19.0	0.203		
20.0	0.207		

Σ = 85 POINTS

20 CHECK POINTS

AVERAGE CHANGE = 0.7%

ANODE WIRE PROBE (W (a))

T_b = 25.1°C

I_z = 5.0 AMP

I_v = 5.0 AMP

AC

9/5/56

V (VOLTS)	i_p (MA)	i_+	i_-
0.0	110	0.4	110.4
	109		109.4
	109		109.4
	108		108.4
	107		107.5
1.0	105	0.4	105.4
	104		104.4
	102		102.4
	101		101.4
	97.2		97.6
2.0	95.1	0.4	95.5
	93.6		94.0
	91.2		91.6
	88.5		88.9
	83.9		84.3
3.0	78.2	0.4	78.6
	71.3		71.7
	64.3		64.7
	57.2		57.6
	51.2		51.6
4.0	46.0	0.4	46.4
	41.2		41.6
	37.0		37.4
	33.2		33.6
	30.0		30.4
5.0	27.2	0.4	27.6
	24.2		24.6
	21.8		22.2
	19.8		20.2
	17.9		18.3
6.0	16.2	0.44	16.6
	14.6		15.0
	13.1		13.5
	11.9		12.3
	10.8		11.2
7.0	9.42	0.35	9.77
	8.57	0.35	8.92
	7.83		8.13
	7.15		7.50
	6.50		6.95
8.0	5.88	0.35	6.23
	5.33	0.36	5.69
	4.82	0.36	5.18
	4.42	0.36	4.78
	4.02	0.36	4.38
9.0	3.62	0.36	3.98
	3.28	0.36	3.64
	2.95	0.36	3.31
	2.65	0.36	3.01
	2.39	0.36	2.75

V	i_p	i_+	i_-
10.0	2.15	0.36	2.51
	1.91	0.36	2.27
	1.69	0.36	2.05
	1.50	0.37	1.87
	1.31	0.37	1.68
11.0	1.15	0.37	1.52
	1.00	0.37	1.37
	0.812	0.367	1.179
	0.692	0.367	1.059
	0.578	0.368	0.946
12.0	0.473	0.368	0.841
	0.378	0.369	0.747
	0.292	0.370	0.662
	0.220	0.371	0.591
	0.142	0.372	0.514
13.0	0.079	0.372	0.451
i_-	0.022	0.373	0.395
i_+	0.033	0.374	0.341
	0.075	0.375	0.300
	0.120	0.375	0.255
14.0	0.156	0.376	0.220
	0.183	0.377	0.194
	0.214	0.388	0.174
	0.237	0.388	0.151
	0.260	0.389	0.129
15.0	0.278	0.380	0.102
	0.294	0.380	0.086
	0.308	0.381	0.073
	0.318	0.382	0.064
	0.331	0.383	0.052
16.0	0.337	0.383	0.047
	0.342	0.384	0.042
	0.351	0.385	0.034
	0.355	0.386	0.031
	0.361	0.387	0.026
17.0	0.365	0.387	0.022
	0.369	0.388	0.019
	0.372	0.388	0.016
	0.375	0.389	0.014
	0.379	0.390	0.011
18	0.380	0.391	0.011
	0.383	0.392	0.009
	0.384		
	0.387		
	0.388		
19	0.390	0.395	0.005
20	0.398		
22	0.409		
24	0.419		
26	0.427		
28	0.433		

Σ = 101 POINTS 24 CHECK POINTS AVERAGE CHANGE = 0.7%

CATHODE WIRE PROBE

T_b = 35.0 °C

I_z = 5.0 Amp

I_v = 5.0 Amp

B1

7/20/56

V (VOLTS)	i_p (MA)	i_+	i_-
4.0	163	0.5	163.5
	162		162.5
	161		161.5
	160		160.5
	161		161.5
5.0	159		159.5
	158		158.5
	156		156.5
	153		153.5
	152		152.5
6.0	152		152.5
	151		151.5
	149		149.5
	146		146.5
	143		143.5
7.0	140		140.5
	133		133.5
	123		123.5
	109		109.5
	91.8		92.3
8.0	79.3		79.8
	69.5		70.0
	60.8		61.3
	52.2		52.7
	46.8		47.3
9.0	39.7		40.2
	34.6		35.1
	29.9		30.4
	26.0		26.5
	22.3		22.8
10.0	19.6		20.1
	16.8		17.3
	14.2		14.7
	12.3		12.8
	10.7	0.5	11.2
11.0	8.61	0.~~47~~47	9.08
	7.30		7.77
	6.42		6.89
	5.52		6.99
	4.73		5.20
12.0	4.04		4.51
	3.44		3.91
	2.94		3.41
	2.49		2.96
	2.08		2.55
13.0	1.72		2.19
	1.40		1.97
	1.14	0.~~47~~47	1.61
	0.845	0.~~47~~.473	1.318
	0.660	.476	1.136

V		i_p	i_+	i_-
14.0		0.495	0.478	0.973
		0.352	0.480	0.832
		0.221	0.480	0.701
		0.112	0.481	0.593
	i_-	0.015	0.481	0.496
15.0	i_+	0.065	0.482	0.417
		0.138	0.485	0.347
		0.198	0.486	0.288
		0.252	0.488	0.236
		0.298	0.490	0.192
16.0		0.331	0.490	0.159
		0.361	0.491	0.130
		0.389	0.492	0.103
		0.410	0.494	0.084
		0.429	0.497	0.068
17.0		0.446	0.498	0.052
		0.458	0.500	0.042
		0.468	0.500	0.032
		0.478	0.502	0.024
		0.487	0.503	0.016
18.0		0.492	0.505	0.013
19.0		0.512		
20.0		0.522		

73 points

16 check points

Average change = 1.6%

DISK PROBE

T_b = 35.0 °C

I_z = 5.0 AMP

I_v = 5.0 AMP

B_z

7/20/56

V (VOLTS)	i_p (MA)	i_+	i_-
3.0	92.2	0.2	92.4
	88.5		88.7
	88.8		89.0
	88.2		88.4
	88.1		88.3
4.0	87.2		87.4
	86.5		86.7
	86.3		86.5
	87.2		87.4
	86.6		86.8
5.0	85.6		85.8
	85.2		85.4
	84.7		84.9
	84.0		84.2
	83.5		83.7
6.0	82.9		83.1
	81.0		81.2
	77.1		77.3
	71.2		71.4
	64.7		64.9
7.0	56.8		57.0
	49.8		50.0
	43.5		43.7
	37.7		37.9
	32.6		32.8
8.0	28.4		28.6
	24.4		24.6
	21.2		21.4
	18.1		18.3
	15.6		15.8
9.0	13.2		13.4
	11.2	0.2	11.4
	8.90	0.23	9.13
	7.64		7.87
	6.45		6.68
10.0	5.55		5.78
	4.69		4.92
	3.94		4.17
	3.34		3.57
	2.82		3.05
11.0	2.46		2.69
	1.99		2.22
	1.66		1.89
	1.37		1.60
	1.12	0.23	1.35
12.0	0.860	0.232	1.092
	0.712	0.232	0.944
	0.573	0.233	0.806
	0.458	0.233	0.691
	0.354	0.234	0.588

V	i_p	i_+	i_-
13.0	0.269	0.235	0.504
	0.192	0.235	0.427
	0.125	0.236	0.361
	0.0658	0.237	0.303
	0.0171	0.238	0.255
14.0	0.0248	0.238	0.213
	0.0602	0.239	0.179
	0.0902	0.239	0.149
	0.118	0.240	0.122
	0.140	0.240	0.100
15.0	0.159	0.240	0.081
	0.175	0.241	0.066
	0.188	0.242	0.054
	0.200	0.242	0.042
	0.208	0.242	0.034
16.0	0.215	0.242	0.027
	0.222	0.243	0.021
	0.228	0.243	0.015
	0.232	0.245	0.013
	0.236	0.245	0.009
17.0	0.238	0.247	0.009
18.0	0.249	0.249	—
19.0	0.252		
20.0	0.257		

Σ = 74 POINTS

17 CHECK POINTS

AVERAGE CHANGE = 1.2%

WALL - PLANE PROBE

$T_b = 35.0$ °C

$I_z = 5.0$ AMP.

$I_v = 5.0$ AMP.

B3

7/20/56

V (VOLTS)	i_p (MA)	i_+	i_-
3.0	43.5	0.1	43.6
	44.2		44.3
	43.9		44.0
	43.5		43.6
	43.1		43.2
4.0	42.8		42.9
	42.3		42.4
	41.7		41.8
	41.5		41.6
	41.4		41.5
5.0	41.0		41.1
	40.8		40.9
	40.8		40.9
	41.1		41.2
	40.7		40.8
6.0	40.2		40.3
	39.5		39.6
	38.5		38.6
	37.1		37.2
	35.1		35.2
7.0	32.4		35.5
	29.3		29.4
	26.2		26.3
	23.4		23.5
	21.2		21.3
8.0	18.6		18.7
	16.5		16.6
	14.3		14.4
	12.5		12.6
	11.0	0.1	11.1
9.0	9.10	0.11	9.21
	7.89		8.00
	6.93		7.04
	6.02		6.13
	5.18		5.29
10.0	4.52		4.63
	3.89		4.00
	3.30		3.41
	2.85		2.96
	2.47		2.58
11.0	2.13		2.24
	1.83		1.94
	1.58		1.69
	1.34		1.45
	1.16	0.11	1.27
12.0	0.933	0.108	1.041
	0.798		0.906
	0.664		0.772
	0.559		0.667
	0.454	0.108	0.562

V	i_p	i_+	i_-
13.0	0.370	0.108	0.478
	0.298	0.108	0.406
	0.234	0.108	0.342
	0.178	0.109	0.287
	0.129	0.110	0.239
14.0	0.0858	0.111	0.197
	0.0494	0.112	0.161
	0.0175	0.112	0.130
	0.0115	0.113	0.101
	0.0355	0.113	0.077
15.0	0.0569	0.114	0.057
	0.0728	0.114	0.041
	0.0822	0.115	0.033
	0.0908	0.115	0.024
	0.0975	0.116	0.018
16.0	0.106	0.117	0.011
	0.109	0.117	0.008
	0.112	0.118	0.006
	0.115	0.118	0.003
	0.117	0.118	0.001
17.0	0.119	0.119	
	0.120	0.120	
	0.121		
	0.121		
	0.121		
18.0	0.122		
19.0	0.125		
20.0	0.128		

Σ POINTS = 78

17 CHECK POINTS

AVERAGE CHANGE = 0.90%

ANODE WIRE PROBE

T_b = 35.0 °C

I_z = 5.0 AMP

I_v = 5.0 AMP.

B4

7/20/56

V (VOLTS)	i_p (MA)	i_+	i_-
1.0	159	0.4	159.4
	158		158.4
	156		156.4
	154		154.4
	152		152.4
2.0	152		152.4
	150		150.4
	149		149.4
	148		148.4
	145		145.4
3.0	143		143.4
	142		142.4
	140		140.4
	138		138.4
	135		135.4
4.0	132		132.4
	128		128.4
	114		114.4
	93.5		93.9
	80.2		80.6
5.0	71.2		71.6
	61.0		61.4
	50.1		50.5
	43.2		43.6
	38.0		38.4
6.0	32.6		33.0
	28.5		28.9
	24.8		25.2
	21.6		22.0
	19.0		19.4
7.0	16.3		16.7
	14.2		14.6
	12.2		12.6
	10.7	0.4	11.1
	8.65	0.44	9.09
8.0	7.48		7.92
	6.52		6.96
	5.61		6.05
	4.87		5.31
	4.22		4.66
9.0	3.65		4.09
	3.12		3.56
	2.72		3.16
	2.32		2.76
	1.98		2.42
10.0	1.70		2.14
	1.42		1.86
	1.19	0.44	1.63
	0.928	0.436	1.364
	0.762	0.436	1.20

V	i_p	i_+	i_-
11.0	0.622	0.436	1.06
	0.488		0.924
	0.374		0.810
	0.270		0.706
	0.178		0.614
12.0	0.0922	0.436	0.528
	0.0232	0.439	0.462
	0.0410	0.441	0.400
	0.0982	0.443	0.345
	0.152	0.448	0.296
13.0	0.195	0.450	0.255
	0.232	0.451	0.219
	0.269	0.453	0.184
	0.301	0.458	0.157
	0.324	0.459	0.135
14.0	0.348	0.460	0.112
	0.367	0.462	0.095
	0.386	0.465	0.079
	0.402	0.469	0.067
	0.418	0.470	0.052
15.0	0.430	0.471	0.041
	0.442	0.475	0.033
	0.452	0.478	0.026
	0.461	0.480	0.019
	0.469	0.481	0.012
16.0	0.474	0.484	0.010
17.0	0.498	0.495	
18.0	0.509		
19.0	0.521		

Σ points = 79

18 check points

Average change = 1.0%

CENTER - PLANE PROBE

T_b = 35.0 °C

I_z = 5.0 AMP.

I_v = 5.0 AMP

B5

7/20/56

V (VOLTS)	i_p (MA)	i_+	i_-
1.0	97.5	0.3	97.8
	97.8		98.1
	97.8		98.1
	97.4		97.7
	97.3		97.6
2.0	97.2		97.5
	96.8		97.1
	96.1		96.4
	96.1		96.4
	95.8		96.1
3.0	95.7		96.0
	95.3		95.6
	95.2		95.5
	94.8		95.1
	94.4		94.7
4.0	94.0		94.3
	93.9		94.2
	93.3		93.6
	92.8		93.1
	92.3		92.6
5.0	92.2		92.5
	91.4		91.7
	90.8		91.1
	89.4		89.7
	86.2		86.5
6.0	79.9		80.2
	72.8		73.1
	65.3		65.6
	57.5		57.8
	51.2		51.5
7.0	45.2		45.5
	39.8		40.1
	34.9		35.1
	30.8		31.1
	26.8		27.1
8.0	23.4		23.7
	20.5		20.8
	17.8		18.1
	15.4		15.7
	13.2		13.5
9.0	11.5	0.3	11.8
	9.32	0.25	9.57
	8.08		8.33
	7.05		7.30
	6.08		6.33
10.0	5.18		5.43
	4.46		4.71
	3.82		4.07
	3.28		3.53
	2.80	0.25	3.05

V	i_p	i_+	i_-
11.0	2.37	0.25	2.62
	2.03		2.28
	1.72		1.97
	1.44		1.69
	1.21		1.46
12.0	0.938	0.247	1.19
	0.772	0.248	1.02
	0.629	0.249	0.878
	0.499	0.250	0.749
	0.392	0.251	0.643
13.0	0.298	0.252	0.550
	0.213	0.252	0.465
	0.139	0.254	0.393
	0.0695	0.255	0.325
	0.0130	0.256	0.269
14.0	0.373	0.257	0.220
	0.0820	0.258	0.176
	0.122	0.259	0.137
	0.155	0.260	0.105
	0.182	0.261	0.079
15.0	0.205	0.262	0.057
	0.220	0.262	0.042
	0.232	0.264	0.032
	0.242	0.265	0.023
	0.248	0.267	0.019
16.0	0.255	0.268	0.013
17.0	0.272	0.271	0.001
18.0	0.277	0.277	
19.0	0.282		

62 POINTS = 79

17 CHECK POINTS

AVERAGE CHANGE = 0.7%

ANODE WIRE PROBE

T_b = 35.0 °C

I_z = 5.0 AMP

I_v = 5.0 AMP

BC

9/6/56

V (VOLTS)	i_p (MA)	i_+	i_-
0.0	169	0.5	169.5
	169		169.5
	168		168.5
	167		167.5
	165		165.5
1.0	164		164.5
	162		162.5
	161		161.5
	160		160.5
	160		160.5
2.0	158		158.5
	155		155.5
	154		154.5
	152		152.5
	151		151.5
3.0	149		149.5
	148		148.5
	145		145.5
	142		142.5
	140		140.5
4.0	137		137.5
	128		128.5
	115		115.5
	102		102.5
	83.8		84.3
5.0	73.8		74.3
	64.9		65.4
	56.3		56.8
	49.3		49.8
	42.9		43.4
6.0	37.2		37.87
	32.4		32.9
	28.2		28.7
	24.5		25.0
	21.2		21.7
7.0	18.3		18.8
	15.9		16.4
	13.8		14.3
	11.9		12.4
	10.3	0.5	10.8
8.0	8.43	0.48	8.91
	7.43		7.91
	6.32		6.80
	5.45		5.93
	4.72	0.48	5.20
9.0	4.03	0.49	4.52
	3.45		3.94
	2.99		3.48
	2.58		3.07
	2.19	0.49	2.68

V	i_p	i_+	i_-
10.0	1.87	0.49	2.36
	1.58		2.07
	1.32		1.81
	1.09	0.49	1.58
	0.839	0.494	1.333
11.0	0.685	0.495	1.18
	0.538	0.496	1.034
	0.413	0.497	0.910
	0.302	0.498	0.800
	0.202	0.499	0.701
12.0	0.112	0.500	0.612
	0.034	0.501	0.535
	0.034	0.501	0.467
	0.095	0.503	0.408
	0.151	0.504	0.353
13.0	0.199	0.505	0.306
	0.238	0.506	0.268
	0.275	0.507	0.232
	0.305	0.508	0.203
	0.334	0.509	0.175
14.0	0.357	0.510	0.153
	0.380	0.511	0.131
	0.398	0.512	0.114
	0.416	0.513	0.097
	0.431	0.514	0.083
15.0	0.443	0.515	0.072
	0.456	0.517	0.061
	0.465	0.518	0.053
	0.475	0.519	0.044
	0.481	0.520	0.039
16.0	0.489	0.521	0.032
	0.496	0.522	0.026
	0.501	0.523	0.022
	0.505	0.524	0.019
	0.512	0.526	0.014
17.0	0.513	0.527	0.014
	0.517	0.528	0.011
	0.521	0.529	0.008
	0.524	0.530	0.006
	0.527	0.531	0.004
18.0	0.530	0.532	0.002
	0.531		
	0.532		
	0.534		
	0.537		
19.0	0.538		
20.0	0.542		
22.0	0.558		
24.0	0.568		
26.0	0.579		
28.0	0.588		

Σ POINTS = 101 25 CHECK POINTS AVERAGE CHANGE = 0.69%

ANODE WIRE PROBE

T_b = 45.1 °C

I_z = 5.0 AMP

I_v = 5.0 AMP

C1

7/27/56

V (VOLTS)	i_p (MA)	i_+	i_-
2.0	266	0.7	266.7
	262		262.7
	260		260.7
	258		258.7
	256		256.7
3.0	254		254.7
	252		252.7
	248		248.7
	247		247.7
	244		244.7
4.0	242		242.7
	240		240.7
	238		238.7
	234		234.7
	229		229.7
5.0	222		222.7
	207		207.7
	182		182.7
	153		153.7
	131		131.7
6.0	112		112.7
	84.1		84.8
	71.6		72.3
	60.2		60.9
	50.2		50.9
7.0	41.9		42.6
	34.9		35.6
	29.2		29.9
	24.2		24.9
	19.9		20.6
8.0	16.3		17.0
	13.2		13.9
	10.9	0.7	11.6
	8.11	0.73	8.84
	6.65		7.38
9.0	5,31		6.04
	4.20		4.93
	3.31		4.04
	2.58		3.31
	1.98	0.73	2.71
10.0	1.47	0.74	2.21
	1.05	0.74	1.79
	0.660	0.739	1.399
	0.410	0.740	1.15
	0.210	0.741	0.951
11.0	0.037	0.743	0.780
	0.098	0.745	0.647
	0.218	0.747	0.529
	0 312	0.748	0.436
	0.392	0.749	0357

V	i_p	i_+	i_-
12.0	0.458	0.750	0.292
	0.510	0.751	0.241
	0.557	0.753	0.196
	0.589	0.757	0.168
	0.621	0.759	0.138
13.0	0.646	0.760	0.114
	0.670	0.760	0.090
	0.688	0.761	0.073
	0.700	0.762	0.062
	0.715	0.764	0.049
14.0	0.725	0.766	0.041
	0.737	0.768	0.031
	0.744	0.769	0.025
	0.750	0.770	0.020
	0.754	0.771	0.017
15.0	0.761	0.772	0.011
	0.763	0.775	0.012
	0.765	0.778	0.013
	0.768	0.779	0.011
	0.771	0.780	0.009
16.0	0.772	0.780	0.008
17.0	0.789		
18.0	0.796		
19.0	0.802		
20.0	0.810		

Σ POINTS = 75

18 CHECK POINTS

AVERAGE CHANGE = 0.9 %

9

DISK PROBE

T_b = 45.1 °C

I_z = 5.0 A

I_v = 5.0 A

C_2

7/27/56

V (VOLTS)	i_p (MA)	i_+	i_-
4.0	148	0.3	148.3
	148		148.3
	147		147.3
	146		146.3
	145		145.3
5.0	144		144.3
	143		143.3
	143		143.3
	142		142.3
	142		142.3
6.0	141		141.3
	140		140.3
	140		140.3
	139		139.3
	138		138.3
7.0	137		137.3
	136		136.3
	132		132.3
	122		122.3
	110		110.3
8.0	90.6		90.9
	77.8		78.1
	66.5		66.8
	56.4		56.7
	47.2		47.5
9.0	39.5		39.8
	32.9		33.2
	27.2		27.5
	22.5		22.8
	18.4		18.7
10.0	15.2		15.5
	12.2	0.3	12.5
	9.19	0.34	9.53
	7.46		7.80
	6.00		6.34
11.0	4.73		5.07
	3.71		4.05
	2.91		3.25
	2.22	0.34	2.56
	1.69	0.35	2.04
12.0	1.24	0.35	1.59
	0.832	0.347	1.179
	0.589	0.348	0.937
	0.395	0.348	0.743
	0.240	0.348	0.588
13.0	0.117	0.349	0.466
	0.0167	0.350	0.367
	0.0600	0.350	0.290
	0.121	0.351	0.230
	0.169	0.352	0.183

V	i_p	i_+	i_-
14.0	0.209	0.353	0.144
	0.241	0.353	0.112
	0.267	0.354	0.087
	0.287	0.355	0.068
	0.301	0.356	0.055
15.0	0.315	0.357	0.042
	0.324	0.358	0.034
	0.333	0.359	0.026
	0.341	0.359	0.018
	0.345	0.360	0.015
16.0	0.351	0.360	0.009
	0.353	0.361	0.008
	0.357	0.362	0.005
	0.359	0.363	0.004
	0.360	0.363	0.003
17.0	0.362	0.364	0.002
	0.363	0.365	0.002
	0.366	0.366	
	0.368		
	0.369		
18.0	0.369		
19.0	0.374		
20.0	0.377		

Σ POINTS = 73

17 CHECK POINTS

AVERAGE CHANGE = 0.447

WALL - PLANE PROBE

T_b = 45.1 °C

I_z = 5.0 A

I_v = 5.0 A.

C3

7/27/96

V (VOLTS)	i_p (MA)	i_+	i_-
5.0	55.8	0.1	55.9
	55.7		55.8
	55.4		55.5
	55.2		55.3
	54.9		55.0
6.0	54.4		54.5
	54.1		54.2
	53.8		53.9
	53.4		53.5
	53.1		53.2
7.0	52.8		52.9
	52.2		52.3
	51.6		51.7
	51.0		51.1
	49.7		49.8
8.0	46.2		46.3
	41.4		41.5
	36.9		37.0
	32.8		32.9
	28.6		28.7
9.0	24.8		24.9
	21.2		21.3
	17.9		18.0
	15.1		15.2
	12.7		12.8
10.0	10.6	0.1	10.7
	8.34	0.14	8.48
	6.99		7.13
	5.77		5.93
	4.72		4.86
11.0	3.87		4.01
	3.12		3.26
	2.52		2.66
	2.03		2.17
	1.61		1.75
12.0	1.28	0.14	1.42
	0.938	0.143	1.081
	0.738	0.144	0.882
	0.574	0.144	0.718
	0.439	0.144	0.583
13.0	0.329	0.144	0.473
	0.239	0.144	0.383
	0.162	0.144	0.306
	0.0995	0.144	0.244
	0.0482	0.145	0.193
14.0	0.0050	0.146	0.150
	0.0300	0.145	0.115
	0.0588	0.146	0.087
	0.0830	0.146	0.063
	0.0988	0.147	0.048

V	i_p	i_+	i_-
15.0	0.112	0.147	0.035
	0.121	0.147	0.026
	0.128	0.147	0.019
	0.132	0.148	0.016
	0.135	0.148	0.013
16.0	0.138	0.148	0.010
	0.140	0.148	0.008
	0.142	0.148	0.006
	0.143	0.148	0.005
	0.145	0.148	0.003
17.0	0.148	0.149	0.001
18.0	0.151		
19.0	0.152		
20.0	0.154		

Σ POINTS = 68

15 CHECK POINTS

AVERAGE CHANGE = 0.6%

2

CENTER – PLANE PROBE

T_b = 45.1°C

I_y = 5.0 A

I_v = 5.0 A.

C4

7/27/56

V (VOLTS)	i_p (MA)	i_+	i_-
5.0	162	0.4	162.4
	161		161.4
	159		159.4
	159		159.4
	158		158.4
6.0	158		158.4
	157		157.4
	157		157.4
	155		155.4
	154		154.4
7.0	149		149.4
	138		138.4
	125		125.4
	110		110.4
	90.2		90.6
8.0	78.3		78.7
	67.9		68.3
	58.1		58.5
	49.4		49.8
	42.1		42.5
9.0	35.7		36.1
	30.2		30.6
	25.4		25.8
	21.4		21.7
	17.9		18.3
10.0	14.8		15.2
	12.2	0.4	12.6
	9.35	0.40	9.75
	7.68		8.08
	6.29		6.69
11.0	5.06	0.40	5.46
	4.07	0.41	4.48
	3.22		3.63
	2.55		2.96
	1.99		2.40
12.0	1.52		1.93
	1.13	0.41	1.54
	0.771	0.410	1.181
	0.547	0.411	0.958
	0.355	0.412	0.767
13.0	0.203	0.413	0.616
	0.0700	0.415	0.485
	0.0375	0.416	0.378
	0.129	0.418	0.289
	0.204	0.419	0.215
14.0	0.264	0.419	0.155
	0.311	0.420	0.109
	0.340	0.420	0.080
	0.362	0.421	0.059
	0.378	0.422	0.044

V	i_p	i_+	i_-
15.0	0.392	0.423	0.031
	0.401	0.424	0.023
	0.409	0.425	0.014
	0.415	0.427	0.012
	0.419	0.428	0.009
16.0	0.423	0.429	0.006
	0.428	0.430	0.002
	0.429	0.430	0.001
	0.430		
	0.432		
17.0	0.433		
18.0	0.439		
19.0	0.442		
20.0	0.444		

Σ POINTS = 64

14 CHECK POINTS

AVERAGE CHANGE = 0.4%

CATHODE WIRE PROBE

$T_b = 45.1\ ^{\circ}C$

$I_z = 5.0\ A$

$I_v = 5.0\ A$

C5

7/27/56

V (VOLTS)	i_p (MA)	i_+	i_-
5.0	281	0.7	281.7
	280		280.7
	279		279.7
	278		278.7
	276		276.7
6.0	274		274.7
	273		273.7
	272		272.7
	270		270.7
	268		268.7
7.0	265		265.7
	262		262.7
	260		260.7
	258		258.7
	254		254.7
8.0	251		251.7
	246		246.7
	235		235.7
	213		213.7
	189		189.7
9.0	162		162.7
	138		138.7
	119		119.7
	92.8		93.5
	78.0		78.7
10.0	66.5		67.2
	55.9		56.6
	46.5		47.2
	38.8		39.5
	32.3		33.0
11.0	26.8		27.5
	22.2		22.9
	18.1		18.8
	14.9	0.7	15.6
	12.0	0.75	12.8
12.0	9.00	0.75	9.75
	7.25	0.76	8.01
	5.85	0.76	6.61
	4.60	0.76	5.36
	3.58	0.76	4.34
13.0	2.75	0.76	3.51
	2.09	0.76	2.85
	1.55	0.76	2.31
	1.09	0.76	1.86
	0.650	0.770	1.42
14.0	0.395	0.771	1.166
	0.175	0.771	0.946
	0.005	0.772	0.767
	0.162	0.774	0.612
	0.275	0.775	0.500

V	i_p	i_+	i_-
15.0	0.375	0.778	0.403
	0.451	0.780	0.329
	0.519	0.782	0.263
	0.576	0.785	0.209
	0.619	0.787	0.168
16.0	0.652	0.788	0.136
	0.686	0.790	0.104
	0.706	0.791	0.085
	0.731	0.793	0.062
	0.743	0.795	0.052
17.0	0.756	0.799	0.043
	0.768	0.800	0.034
	0.778	0.800	0.022
	0.785	0.802	0.017
	0.791	0.804	0.013
18.0	0.797	0.808	0.011
19.0	0.815		
20.0	0.828		
21.0	0.835		
22.0	0.845		
23.0	0.851		

Σ POINTS = 71

18 CHECK POINTS

AVERAGE CHANCE = 0.5%

CENTER – PLANE PROBE

T_b = 45.1 °C

I_y = 5.0 A

I_u = 5.0 A

C6

8/31/56

V (VOLTS)	i_p (MA)	i_+	i_-
3.0	171	0.4	171.4
	170		170.4
	169		169.4
	168		168.4
	167		167.4
4.0	165		165.4
	165		165.4
	164		164.4
	163		163.4
	163		163.4
5.0	162		162.4
	162		162.4
	161		161.4
	161		161.4
	160		160.4
6.0	160		160.4
	159		159.4
	158		158.4
	157		157.4
	153		153.4
7.0	147		147.4
	133		133.4
	119		119.4
	104		104.4
	85.0		85.4
8.0	73.5		73.9
	63.9		64.3
	54.5		54.9
	46.3		46.7
	39.5		39.9
9.0	33.7		34.1
	28.5		28.9
	23.8		24.2
	19.9		20.3
	16.5		16.9
10.0	13.7		14.1
	11.3	0.4	11.7
	8.62	0.43	9.05
	7.09	0.43	7.52
	5.76	0.43	6.19
11.0	4.61	0.43	5.04
	3.69	0.43	4.12
	2.93	0.43	3.36
	2.31	0.43	2.74
	1.79	0.43	2.22
12.0	1.35	0.43	1.78
	0.918	0.432	1.35
	0.668	0.433	1.101
	0.457	0.433	0.884
	0.282	0.434	0.716

V	i_p	i_+	i_-
13.0	0.135	0.435	0.570
	0.012	0.435	0.447
	0.088	0.436	0.348
	0.182	0.437	0.255
	0.252	0.438	0.186
14.0	0.305	0.439	0.134
	0.340	0.439	0.099
	0.364	0.439	0.075
	0.382	0.439	0.057
	0.398	0.440	0.042
15.0	0.409	0.440	0.031
	0.415	0.440	0.025
	0.421	0.441	0.020
	0.424	0.442	0.018
	0.429	0.442	0.013
16.0	0.432	0.443	0.011
	0.434	0.444	0.010
	0.437	0.444	0.007
	0.439	0.445	0.006
	0.441		
17.0	0.442		
18.0	0.448		
19.0	0.451		
20.0	0.455		
22.0	0.459		
24.0	0.465		
26.0	0.470		
28.0	0.474		

$\leq$ POINTS = 78

21 CHECK POINTS

AVERAGE CHANGE = 0.60%

WIRE PROBE (CATHODE)

$T_b = 54.6\ ^\circ C$

$I_z = 5.0\ A$

$I_v = 5.0\ A$

D1

8/3/56

V (VOLTS)	i_p (MA)	i_+	i_-
0.0	508	1.2	509
	512		513
	508		509
	505		506
	502		503
1.0	503		504
	501		502
	498		499
	498		499
	498		499
2.0	498		499
	495		496
	492		493
	492		493
	491		492
3.0	490		491
	488		489
	485		486
	482		483
	481		482
4.0	479		480
	479		480
	478		479
	472		473
	472		473
5.0	470		471
	468		469
	465		466
	461		462
	458		459
6.0	453		454
	452		453
	448		449
	445		446
	442		443
7.0	439		440
	435		436
	432		433
	430		431
	428		429
8.0	421		422
	416		417
	407		408
	387		388
	348		349
9.0	301		302
	258		259
	217		218
	179		180
	147	1.2	148

V	i_p	i_+	i_-
10.0	119	1.2	120
	90.2		91.4
	73.8		75.0
	59.2		60.4
	48.0		49.2
11.0	38.2		39.4
	30.3		31.5
	24.1		25.3
	19.0		20.2
	14.5		15.7
12.0	11.0	1.2	12.2
	7.82	1.23	9.05
	5.93	1.24	7.17
	4.35	1.24	5.59
	3.14	1.25	4.39
13.0	2.13	1.25	3.38
	1.32	1.25	2.57
	0.63	1.26	1.89
	0.22	1.26	1.48
	0.120	1.26	1.14
14.0	0.390	1.27	0.88
	0.605	1.27	0.66
	0.768	1.27	0.50
	0.890	1.28	0.39
	0.990	1.28	0.29
15.0	1.10	1.28	0.18
	1.14	1.28	0.14
	1.19	1.28	0.09
	1.22	1.28	0.06
	1.25	1.29	0.04
16.0	1.27	1.29	0.02
	1.28	1.29	0.01
	1.30		
	1.31		
	1.31		
17.0	1.32		
18.0	1.33		
19.0	1.34		
20.0	1.37		
22.0	1.39		
24.0	1.40		
26.0	1.41		
28.0	1.43		
30.0	1.45		

Σ POINTS = 94

24 CHECK POINTS

AVERAGE CHANGE = 0.99%

DISK PROBE

$T_b = 54.6°C$

$I_z = 5.0\ A$

$I_v = 5.0\ A$

D2

8/3/56

V (VOLTS)	i_p (MA)	i_+	i_-
4.0	234	0.5	234.5
	233		233.5
	232		232.5
	231		231.5
	232		232.5
5.0	231		231.5
	230		230.5
	229		229.5
	227		227.5
	227		227.5
6.0	226		226.5
	225		225.5
	222		222.5
	222		222.5
	221		221.5
7.0	220		220.5
	219		219.5
	217		217.5
	210		210.5
	198		198.5
8.0	175		178.5
	152		152.5
	128		128.5
	108		108.5
	82.2		82.7
9.0	67.8		68.3
	55.5		56.0
	44.6		45.1
	36.0		36.5
	28.8		29.3
10.0	22.8		23.3
	17.9		18.4
	13.9		14.4
	10.9	0.5	11.4
	7.63	0.54	8.17
11.0	5.86	0.54	6.40
	4.39	0.54	4.93
	3.22	0.54	3.76
	2.32	0.54	2.86
	1.61	0.54	2.15
12.0	1.08	0.54	1.62
	0.582	0.542	1.124
	0.303	0.543	0.846
	0.085	0.544	0.629
	0.077	0.545	0.468
13.0	0.204	0.546	0.342
	0.292	0.547	0.255
	0.358	0.548	0.190
	0.404	0.549	0.145
	0.441	0.549	0.108

V	i_p	i_+	i_-
14.0	0.470	0.550	0.080
	0.490	0.550	0.060
	0.501	0.551	0.050
	0.512	0.552	0.040
	0.522	0.553	0.031
15.0	0.532	0.553	0.021
	0.538	0.553	0.015
	0.540	0.554	0.014
	0.549	0.555	0.006
	0.549	0.557	0.008
16.0	0.552	0.558	0.006
	0.556		
	0.558		
	0.559		
	0.559		
17.0	0.561		
18.0	0.565		
19.0	0.569		
20.0	0.575		
22.0	0.580		
24.0	0.588		
26.0	0.595		
28.0	0.602		
30.0	0.611		

Σ POINTS = 74

21 CHECK POINTS

AVERAGE CHANGE 0.6%

WIRE PROBE (ANODE)

T_b = 54.6 °C

I_g = 5.0 A

I_v = 5.0 A

D3

8/3/56

V (VOLTS)	i_p (MA)	i_+	i_-
1.0	453	1.2	454
	452		453
	450		451
	450		451
	448		449
2.0	446		447
	442		443
	440		441
	438		439
	433		434
3.0	432		433
	428		429
	424		425
	422		423
	419		420
4.0	417		418
	413		414
	410		411
	406		407
	401		402
5.0	398		399
	377		378
	363		364
	327		328
	282		8283
6.0	239		240
	201		202
	168		169
	138		139
	112		113
7.0	84.8		86.4
	69.1		70.3
	56.1		57.3
	45.0		46.2
	36.0		37.2
8.0	28.9		30.1
	23.7		23.9
	17.8		19.0
	13.7		14.9
	10.5	1.2	11.7
9.0	7.45	1.24	8.69
	5.62		6.86
	4.17		5.41
	2.99		4.23
	2.04		3.28
10.0	1.30		2.54
	0.641		1.88
	0.238		1.48
	0.091		1.15
	0.346	1.24	0.89

V	i_p	i_+	i_-
11.0	0.546	1.26	0.71
	0.702	1.26	0.55
	0.820	1.26	0.44
	0.916	1.26	0.34
	0.981	1.27	0.29
12.0	1.07	1.27	0.20
	1.11	1.27	0.16
	1.13	1.27	0.14
	1.17	1.27	0.10
	1.19	1.27	0.08
13.0	1.20	1.27	0.07
	1.22	1.27	0.05
	1.22	1.27	0.05
	1.23	1.27	0.04
	1.24	1.27	0.03
14.0	1.25	1.28	0.03
	1.25	1.28	0.03
	1.25	1.28	0.03
	1.27	1.28	0.01
	1.27	1.28	0.01
15.0	1.27	1.28	0.01
16.0	128		
17.0	129		
18.0	130		
19.0	131		
20.0	132		
22.0	133		
24.0	135		
26.0	138		
28.0	138		
30.0	140		

Σ POINTS = 81

25 CHECK POINTS

AVERAGE CHANGE = 0.7 %

CENTER - PLANE PROBE

T_b = 54.6°C

I_y = 5.0 A

I_x = 5.0 A

D4

8/3/56

V (VOLTS)	i_p (MA)	i_+	i_-
4.0	270	0.7	270.7
	270		270.7
	269		269.7
	268		268.7
	267		267.7
5.0	265		265.7
	264		264.7
	263		263.7
	263		263.7
	262		262.7
6.0	261		261.7
	260		260.7
	259		259.7
	258		258.7
	258		258.7
7.0	255		255.7
	250		250.7
	237		237.7
	213		213.7
	187		187.7
8.0	160		160.7
	135		135.7
	113		113.7
	89.8		90.5
	74.8		75.5
9.0	62.1		62.8
	50.9		51.6
	42.0		42.7
	34.2		34.9
	27.9		28.6
10.0	22.4		23.1
	18.0		18.7
	14.2		14.9
	11.2	0.7	11.9
	8.21	0.67	8.88
11.0	6.43		7.13
	4.92		5.59
	3.71		4.38
	2.76		3.43
	2.02		2.69
12.0	1.38	0.67	2.05
	0.807	0.672	1.479
	0.467	0.673	1.14
	0.192	0.674	0.866
	0.032	0.675	0.643
13.0	0.214	0.676	0.462
	0.351	0.677	0.326
	0.451	0.678	0.227
	0.518	0.679	0.161
	0.561	0.679	0.118

V	i_p	i_+	i_-
14.0	0.591	0.680	0.089
	0.612	0.680	0.068
	0.633	0.681	0.048
	0.645	0.681	0.036
	0.652	0.682	0.030
15.0	0.659	0.683	0.024
	0.668	0.683	0.015
	0.672	0.684	0.012
	0.672	0.685	0.013
	0.676	0.686	0.010
16.0	0.679	0.687	0.008
	0.682	0.688	0.006
	0.682	0.688	0.006
	0.685	0.689	0.004
	0.687	0.689	0.002
17.0	0.687	0.690	0.003
	0.688		
	0.688		
	0.691		
	0.691		
18.0	0.689		
19.0	0.687		
20.0	0.700		
22.0	0.708		
24.0	0.713		
26.0	0.719		
28.0	0.722		
30.0	0.728		

Σ POINTS = 78

21 CHECK POINTS

AVERAGE CHANGE = 0.6%

WALL – PLANE PROBE

T_b = 54.6 °C

I_g = 5.0 A

I_v = 5.0 A

D5

8/3/5C

V (VOLTS)	i_p (MA)	i_+	i_-
3.0	80.5	0.2	80.7
	80.7		80.9
	80.3		80.5
	80.1		80.3
	79.9		80.1
4.0	79.4		79.6
	79.0		79.2
	78.8		79.0
	78.5		78.7
	78.2		78.4
5.0	77.8		78.0
	77.5		77.7
	77.2		77.4
	76.9		77.1
	76.8		77.0
6.0	76.2		76.4
	76.1		76.3
	75.7		75.9
	75.2		75.4
	74.9		75.1
7.0	75.0		75.2
	74.5		74.7
	74.3		74.5
	73.4		73.6
	72.4		72.6
8.0	71.3		71.5
	67.6		67.8
	60.7		60.9
	53.2		53.4
	46.0		46.2
9.0	39.7		39.9
	33.3		33.5
	28.0		28.2
	23.2		23.4
	18.9		19.1
10.0	15.5		15.7
	12.5	0.2	12.7
	9.32	0.18	9.50
	7.51	0.18	7.69
	6.02	0.18	6.20
11.0	4.73	0.18	4.91
	3.71	0.18	3.89
	2.88	0.18	3.06
	2.21	0.18	2.39
	1.68	0.18	1.86
12.0	1.23	0.18	1.41
	0.835	0.184	1.019
	0.602	0.184	0.786
	0.418	0.185	0.603
	0.275	0.185	0.460

V	i_p	i_+	i_-
13.0	0.163	0.185	0.348
	0.0732	0.186	0.259
	0.007	0.186	0.193
	0.0442	0.187	0.143
	0.0832	0.187	0.104
14.0	0.118	0.187	0.069
	0.139	0.187	0.048
	0.152	0.188	0.036
	0.161	0.188	0.027
	0.169	0.188	0.019
15.0	0.173	0.188	0.015
	0.178	0.188	0.010
	0.181	0.188	0.007
	0.183	0.189	0.006
	0.184	0.190	0.006
16.0	0.188	0.190	0.002
	0.188	0.191	0.003
	0.189	0.191	0.002
	0.190	0.191	0.001
	0.191	0.192	0.001
17.0	0.191	0.192	0.001
	0.192		
	0.192		
	0.192		
	0.193		
18.0	0.193		
19.0	0.193		
20.0	0.198		
22.0	0.198		
24.0	0.202		
26.0	0.205		
28.0	0.209		
30.0	0.211		

Σ POINTS = 83

23 CHECK POINTS

AVERAGE CHANGE = 0.90%

WIRE PROBE (CATHODE)

$T_b = 62.6\ ^\circ C$

$I_y = 5.0\ A$

$I_v = 5.0\ A$

E1

8/6/56

V (VOLTS)	i_p (MA)	i_+	i_-
3.0	702	2	704
	701		703
	698		700
	690		692
	683		6985
4.0	682		684
	680		682
	684		686
	677		679
	675		677
5.0	673		675
	668		670
	663		665
	661		663
	659		661
6.0	654		656
	652		654
	652		654
	648		650
	643		645
7.0	638		640
	633		635
	631		633
	628		630
	619		621
8.0	613		615
	604		606
	583		585
	540		542
	478		480
9.0	413		415
	349		351
	291		293
	238		2840
	192		194
10.0	154		156
	122	2	124
	89.3	1.8	91.1
	71.0		72.8
	55.9		57.7
11.0	43.3		45.1
	33.5		35.3
	25.8		27.6
	19.5		21.3
	14.6		16.4
12.0	10.8	1.8	11.6
	7.35	1.77	9.12
	5.25	1.77	7.02
	3.58	1.77	5.35
	2.30	1.77	4.07

V	i_p	i_+	i_-
13.0	1.29	1.77	3.06
	0.442	1.77	2.21
	0.0685	1.78	1.71
	0.470	1.78	1.31
	0.778	1.78	1.00
14.0	1.08	1.78	0.70
	1.26	1.79	0.53
	1.40	1.79	0.39
	1.49	1.80	0.31
	1.58	1.80	0.22
15.0	1.65	1.80	0.15
	1.68	1.81	0.13
	1.72	1.81	0.09
	1.75	1.81	0.06
	1.77	1.82	0.05
16.0	1.78	1.82	0.04
	1.79	1.82	0.03
	1.79	1.82	0.03
	1.80	1.83	0.03
	1.81	1.83	0.02
17.0	1.82	1.83	0.01
18.0	1.83		
19.0	1.84		
20.0	1.87		
22.0	1.89		
24.0	1.90		
26.0	1.92		
28.0	1.94		
30.0	1.98		

Σ POINTS = 79

23 CHECK POINTS

AVERAGE CHANGE = 0.40%

WIRE PROBE (ANODE)

T_b = 62.6°C

I_g = 5.0 A

I_v = 5.0 A

E2

8/6/56

V (VOLTS)	i_p (MA)	i_+	i_-
2.0	638	2	640
	634		636
	632		634
	628		630
	628		630
3.0	622		624
	618		620
	618		620
	612		614
	608		610
4.0	605		607
	601		603
	598		600
	592		594
	585		587
5.0	579		581
	565		567
	530		532
	476		478
	412		414
6.0	350		352
	293		295
	242		244
	198		200
	158		160
7.0	125	2	127
	92.5	1.7	94.2
	73.8		75.5
	58.1		59.8
	45.2		46.9
8.0	35.3		37.0
	27.2		28.9
	20.8		22.5
	15.6		17.3
	11.7	1.7	13.4
9.0	7.85	1.67	9.52
	5.70	1.67	7.37
	3.95	1.67	5.62
	2.65	1.68	4.33
	1.60	1.68	3.28
10.0	0.660	1.68	2.34
	0.140	1.68	1.82
	0.270	1.69	1.42
	0.620	1.69	1.07
	0.860	1.70	0.84
11.0	1.12	1.70	0.58
	1.28	1.70	0.42
	1.38	1.70	0.32
	1.46	1.71	0.25
	1.52	1.71	0.19

V	i_p	i_+	i_-
12.0	1.58	1.71	0.13
	1.61	1.72	0.11
	1.63	1.72	0.09
	165	1.72	0.07
	168	1.72	0.04
13.0	1.69	1.72	0.03
	1.70	1.72	0.02
	1.71	1.73	0.02
	1.71	1.73	0.02
	1.72	1.73	0.01
14.0	1.73	1.73	
15.0	1.75		
16.0	1.76		
17.0	1.77		
18.0	1.78		
19.0	1.80		
20.0	1.81		
22.0	1.82		
24.0	1.83		
26.0	1.86		
28.0	1.89		
30.0	1.90		

Σ POINTS = 72

24 CHECK POINTS

AVERAGE CHANGE = 1.1%

DISK PROBE

T_b = 62.6°C

I_z = 5.0 A

I_v = 5.0 A

E3

8/6/56

V (VOLTS)	i_p (MA)	i_+	i_-
4.0	319	0.7	319.7
	318		318.7
	317		317.7
	316		316.7
	313		313.7
5.0	313		313.7
	312		312.7
	312		312.7
	311		311.7
	310		310.7
6.0	308		308.7
	308		308.7
	308		308.7
	307		307.7
	304		304.7
7.0	302		302.7
	300		300.7
	293		293.7
	282		282.7
	261		261.7
8.0	231		231.7
	199		199.7
	167		167.7
	138		138.7
	111		111.7
9.0	83.2		83.9
	66.2		66.9
	52.8		53.5
	41.7		42.4
	32.4		33.1
10.0	25.3		26.0
	19.4		20.1
	14.7		15.4
	11.0	0.7	11.7
	7.58	0.72	8.30
11.0	5.62	0.72	6.34
	4.03	0.72	4.75
	2.86	0.73	3.59
	1.93	0.73	2.66
	1.22	0.73	1.95
12.0	0.621	0.728	1.349
	0.270	0.729	0.999
	0.01	0.730	0.740
	0.201	0.730	0.529
	0.348	0.731	0.383
13.0	0.453	0.732	0.297
	0.534	0.732	0.198
	0.588	0.733	0.145
	0.628	0.734	0.106
	0.652	0.736	0.084

V	i_p	i_+	i_-
14.0	0.673	0.737	0.064
	0.690	0.737	0.047
	0.702	0.738	0.036
	0.711	0.739	0.028
	0.719	0.740	0.021
15.0	0.723	0.740	0.017
	0.729	0.741	0.012
	0.732	0.741	0.009
	0.731	0.742	0.011
	0.732	0.743	0.011
16.0	0.738	0.744	0.006
17	0.747		
18	0.752		
19	0.758		
20	0.763		
22	0.769		
24	0.771		
26	0.781		
28	0.786		
30	0.801		

Σ POINTS = 70

21 CHECK POINTS

AVERAGE CHANGE = 0.5%

WALL – PLANE PROBE

T_b = 62.6 °C

I_y = 5.0 A

I_w = 5.0 A

E4

8/6/56

V (VOLTS)	i_p (MA)	i_+	i_-
4.0	96.8	0.2	97.0
	96.3		96.5
	96.1		96.3
	95.1		95.7
	95.0		95.2
5.0	94.8		95.0
	94.2		94.4
	94.0		94.2
	93.8		94.0
	93.3		93.5
6.0	93.3		93.5
	92.8		93.0
	92.5		92.7
	92.5		92.7
	92.0		92.2
7.0	91.8		92.0
	91.2		91.4
	90.9		91.1
	90.8		91.0
	89.5		89.7
8.0	88.8		90.0
	85.8		86.0
	77.9		78.1
	68.3		68.5
	59.3		59.5
9.0	50.3		50.5
	42.0		42.2
	34.8		35.0
	28.3		28.5
	22.9		23.1
10.0	18.3		18.5
	14.5		14.7
	11.4	0.2	11.6
	8.32	0.21	8.53
	6.53	0.21	6.74
11.0	5.03	0.21	5.24
	3.84	0.21	4.05
	2.93	0.21	3.14
	2.18	0.21	2.39
	1.58	0.21	1.79
12.0	1.12	0.22	1.34
	0.710	0.215	0.925
	0.472	0.215	0.687
	0.275	0.216	0.491
	0.129	0.216	0.345
13.0	0.0223	0.217	0.239
	0.0521	0.217	0.165
	0.103	0.217	0.114
	0.135	0.218	0.083
	0.159	0.218	0.059

V	i_p	i_+	i_-
14.0	0.173	0.218	0.045
	0.187	0.218	0.031
	0.194	0.218	0.024
	0.202	0.219	0.017
	0.202	0.219	0.017
15.0	0.209	0.220	0.011
	0.212	0.220	0.008
	0.215	0.221	0.006
	0.218	0.221	0.003
	0.219	0.221	0.002
16.0	0.220	0.222	0.002
	0.220	0.222	0.002
	0.221	0.222	0.001
	0.222	0.223	0.001
	0.222	0.223	0.001
17.0	0.223		
18.0	0.225		
19.0	0.227		
20.0	0.228		
22.0	0.232		
24.0	0.237		
26.0	0.239		
28.0	0.242		
30.0	0.244		

Σ POINTS = 74

21 CHECK POINTS

AVERAGE CHANGE = 0.7%

CENTER — PLANE PROBE

T_b = 62.6°C

I_z = 5.0 A

I_v = 5.0 A

E_5

8/6/56

V (VOLTS)	i_p (MA)	i_+	i_-
3.0	379	0.9	380
	378		379
	375		376
	373		374
	372		373
4.0	371		372
	370		371
	369		370
	368		369
	368		369
5.0	368		369
	366		367
	366		367
	364		365
	364		365
6.0	363		364
	361		362
	359		360
	359		360
	357		358
7.0	353		354
	348		349
	332		333
	299		300
	263		264
8.0	225		226
	189		190
	158		159
	129		130
	106		107
9.0	79.5		80.4
	64.8		65.7
	52.0		52.9
	41.6		42.5
	33.1		34.0
10.0	26.2		27.1
	20.7		21.6
	15.9		16.8
	12.2	0.9	13.1
	8.59	0.89	9.48
11.0	6.58		7.47
	4.88		5.77
	3.58		4.47
	2.52		3.41
	1.70		2.69
12.0	1.03	0.89	1.92
	0.465	0.889	1.354
	0.108	0.890	0.998
	0.182	0.890	0.708
	0.378	0.891	0.493

V	i_p	i_+	i_-
13.0	0.535	0.891	0.356
	0.635	0.892	0.257
	0.712	0.893	0.181
	0.762	0.894	0.132
	0.798	0.896	0.098
14.0	0.822	0.896	0.074
	0.842	0.897	0.055
	0.854	0.898	0.044
	0.862	0.899	0.037
	0.872	0.900	0.028
15.0	0.880	0.900	0.020
	0.885	0.900	0.015
	0.888	0.901	0.013
	0.892	0.901	0.009
	0.890	0.902	0.012
16.0	0.894	0.903	0.009
	0.900	0.904	0.004
	0.901	0.905	0.004
	0.902	0.906	0.004
	0.902	0.907	0.005
17.0	0.905	0.908	0.003
18.0	0.912		
19.0	0.915		
20.0	0.917		
22.0	0.925		
24.0	0.931		
26.0	0.943		
28.0	0.949		
30.0	0.953		

Σ POINTS = 79

22 CHECK POINTS

AVERAGE CHANGE = 0.6[illegible]

WIRE PROBE (ANODE)

T_b = 45.1 °C

I_z = 6.0 A

I_v = 5.0 A

F1

8/24/56

V (VOLTS)	i_p (MA)	i_+	i_-
0.0	342	1.00	343
	341		342
	339		340
	339		340
	338		339
1.0	337		338
	333		334
	331		332
	330		331
	328		329
2.0	328		329
	327		328
	323		324
	322		323
	320		321
3.0	317		318
	313		314
	311		312
	311		312
	310		311
4.0	307		308
	304		305
	302		303
	299		300
	291		292
5.0	277		278
	249		250
	218		219
	189		190
	162		163
6.0	137		138
	117		118
	91.2		92.2
	76.4		77.4
	64.9		65.9
7.0	54.2		55.2
	45.0		46.0
	37.5		38.5
	31.2		32.2
	25.7		26.7
8.0	21.1		22.1
	17.3		18.3
	14.0		15.0
	11.3	1.0	12.3
	8.54	.99	9.53
9.0	6.92	.99	7.91
	5.51	.99	6.50
	4.32	.99	5.31
	3.35	1.00	4.35
	2.58	1.00	3.58

V	i_p	i_+	i_-
10.0	1.93	1.00	2.93
	1.38	1.00	2.38
	0.852	1.00	1.852
	0.552	1.00	1.552
	0.298	1.00	1.298
11.0	0.074	1.00	1.074
	0.109	1.00	0.891
	0.267	1.00	0.733
	0.389	1.00	0.611
	0.488	1.01	0.522
12.0	0.568	1.01	0.442
	0.635	1.01	0.375
	0.693	1.01	0.317
	0.743	1.01	0.267
	0.781	1.02	0.239
13.0	0.810	1.02	0.210
	0.832	1.02	0.188
	0.852	1.02	0.168
	0.870	1.02	0.150
	0.888	1.02	0.132
14.0	0.901	1.02	0.119
	0.913	1.02	0.107
	0.923	1.02	0.097
	0.932	1.025	0.093
	0.938	1.025	0.087
15.0	0.943	1.025	0.082
	0.952	1.025	0.073
	0.953	1.025	0.072
	0.961	1.025	0.064
	0.968	1.03	0.062
16.0	0.968	1.03	0.062
	0.975	1.03	0.055
	0.975	1.03	0.055
	0.977	1.03	0.053
	0.982	1.033	0.048
17.0	0.980	1.03	0.05
18.0	0.995		
19.0	1.04		
20.0	1.05		
22.0	1.07		
24.0	1.07		
26.0	1.09		
28.0	1.09		
30.0	1.11		

Σ POINTS = 94

25 CHECK POINTS

AVERAGE CHANGE = 0.8%

DISK PROBE

T_b = 45.1°C

I_y = 6.0 A

I_w = 5.0 A

F_2

8/21/5C

V (VOLTS)	i_p (MA)	i_+	i_-
0.0	200	0.4	200.4
	200		200.4
	199		199.4
	198		198.4
	197		197.4
1.0	197		197.4
	197		197.4
	196		196.4
	195		195.4
	194		194.4
2.0	194		194.4
	194		194.4
	193		193.4
	192		192.4
	191		191.4
3.0	190		190.4
	190		190.4
	190		190.4
	189		189.4
	188		188.4
4.0	187		187.4
	185		185.4
	185		185.4
	184		184.4
	183		183.4
5.0	183		183.4
	182		182.4
	181		181.4
	180		180.4
	179		179.4
6.0	179		179.4
	178		178.4
	178		178.4
	177		177.4
	174		174.4
7.0	172		172.4
	170		170.4
	161		161.4
	146		146.4
	128		128.4
8.0	110		110.4
	88.1		88.5
	75.3		75.7
	63.2		63.6
	52.8		53.2
9.0	44.0		44.4
	36.3		36.7
	30.2		30.6
	24.9		25.3
	20.4	0.4	20.8

V	i_p	i_+	i_-
10.0	16.5	0.4	16.9
	13.3	0.4	13.7
	10.8	0.4	11.2
	7.97	0.42	8.39
	6.37	0.42	6.79
11.0	5.02	0.42	5.44
	3.92	0.42	4.34
	3.01	0.42	3.43
	2.30	0.42	2.72
	1.72	0.42	2.14
12.0	1.26	0.42	1.68
	0.808	0.424	1.232
	0.555	0.425	0.980
	0.348	0.425	0.773
	0.183	0.426	0.609
13.0	0.051	0.427	0.478
	0.048	0.428	0.380
	0.132	0.429	0.297
	0.198	0.429	0.231
	0.247	0.430	0.183
14.0	0.287	0.430	0.143
	0.328	0.431	0.103
	0.342	0.432	0.090
	0.363	0.433	0.070
	0.379	0.434	0.055
15.0	0.396	0.435	0.039
	0.403	0.435	0.032
	0.412	0.436	0.024
	0.418	0.437	0.019
	0.423	0.438	0.015
16.0	0.428	0.438	0.010
	0.433	0.439	0.006
	0.436	0.440	0.004
	0.437	0.441	0.004
	0.439	0.442	0.003
17.0	0.440	0.443	0.003
	0.443	0.444	0.001
	0.442	0.445	0.003
	0.445	0.445	—
	0.445	0.446	0.001
18.0	0.447	0.447	—
19.0	0.450		
20.0	0.455		
22.0	0.463		
24.0	0.472		
26.0	0.477		
28.0	0.481		
30.0	0.487		

Σ POINTS = 98

25 CHECK POINTS

AVERAGE CHANGE = 1.7%

CENTER-[redacted] PLANE PROBE

T_b = 45.1 °C

I_z = 6.0 A

I_v = 5.0 A

F3

8/24/56

V (VOLTS)	i_p (MA)	i_+	i_-
2.0	215	0.5	215.5
	215		215.5
	214		214.5
	215		215.5
	214		214.5
3.0	213		213.5
	213		213.5
	213		213.5
	212		212.5
	211		211.5
4.0	211		211.5
	210		210.5
	210		210.5
	210		210.5
	209		209.5
5.0	208		208.5
	207		207.5
	207		207.5
	205		205.5
	204		204.5
6.0	203		203.5
	203		203.5
	202		202.5
	201		201.5
	197		197.5
7.0	183		183.5
	166		166.5
	147		147.5
	128		128.5
	110		110.5
8.0	89.8		90.3
	76.3		76.8
	65.8		66.3
	56.2		56.7
	47.8		48.3
9.0	40.6		41.1
	34.2		34.7
	28.8		29.3
	24.0		24.5
	20.2		20.7
10.0	16.5		17.0
	13.6		14.1
	11.2	0.5	11.7
	8.42	0.54	8.96
	6.88	0.54	7.42
11.0	5.54	0.54	6.08
	4.41	0.54	4.95
	3.49	0.54	4.03
	2.73	0.55	3.28
	2.22	0.55	2.77

V	i_p	i_+	i_-
12.0	1.60	0.55	2.15
	1.19	0.55	1.74
	0.779	0.548	1.327
	0.532	0.548	1.080
	0.308	0.549	0.857
13.0	0.130	0.549	0.679
	0.0180	0.550	0.532
	0.150	0.550	0.400
	0.258	0.550	0.292
	0.334	0.551	0.217
14.0	0.390	0.552	0.162
	0.431	0.553	0.122
	0.460	0.553	0.093
	0.482	0.554	0.072
	0.502	0.555	0.053
15.0	0.512	0.555	0.043
	0.514	0.556	0.042
	0.521	0.557	0.036
	0.529	0.558	0.029
	0.539	0.559	0.020
16.0	0.544	0.559	0.015
	0.548	0.560	0.012
	0.550	0.560	0.010
	0.552	0.561	0.009
	0.552	0.562	0.010
17.0	0.552	0.562	0.010
	0.556	0.563	0.007
	0.558	0.564	0.006
	0.560	0.565	0.005
	0.562	0.566	0.004
18.0	0.563	0.566	0.003
19.0	0.569		
20.0	0.572		
22.0	0.579		
24.0	0.582		
26.0	0.588		
28.0	0.590		
30.0	0.595		

Σ POINTS = 88

23 CHECK POINTS

AVERAGE CHANGE = 0.5[redacted]

WIRE PROBE (CATHODE)

T_b = 45.1 °C

I_y = 6.0 A

I_v = 5.0 A

F4

8/24/56

V (VOLTS)	i_p (MA)	i_+	i_-
3.0	358	1.0	359
	358		359
	354		355
	353		354
	353		354
4.0	353		354
	352		353
	352		353
	350		351
	348		349
5.0	346		347
	342		343
	340		341
	338		339
	335		336
6.0	333		334
	331		332
	329		330
	327		328
	323		324
7.0	322		323
	321		322
	318		319
	314		315
	311		312
8.0	303		304
	292		293
	268		269
	236		237
	206		207
9.0	178		179
	152		153
	129		130
	109		110
	85.1		86.1
10.0	71.2		72.2
	59.9		60.9
	49.9		50.9
	41.3		42.3
	34.0		35.0
11.0	28.3		29.3
	23.2		24.2
	19.0		20.0
	15.4		16.4
	11.5		12.4
12.0	10.0	1.0	11.0
	7.43	1.00	8.43
	5.90	1.00	6.90
	4.65	1.00	5.65
	#3.58	1.00	4.58

V	i_p	i_+	i_-
13.0	2.74	1.00	3.74
	2.04	1.00	3.04
	1.46	1.00	2.46
	0.882	1.00	1.882
	0.544	1.00	1.544
14.0	0.262	1.00	1.26
	0.02	1.01	1.03
	0.162	1.01	0.86
	0.318	1.01	0.69
	0.441	1.01	0.57
15.0	0.542	1.01	0.47
	0.622	1.02	0.40
	0.692	1.02	0.33
	0.751	1.02	0.27
	0.798	1.02	0.22
16.0	0.832	1.02	0.19
	0.869	1.025	0.156
	0.892	1.025	0.133
	0.910	1.025	0.115
	0.925	1.03	0.105
17.0	0.932	1.03	0.098
	0.945	1.03	0.08
	0.954	1.03	0.08
	0.962	1.03	0.07
	0.973	1.03	0.06
18.0	0.983	1.04	0.06
	0.990	1.04	0.05
	0.991	1.04	0.05
	1.02	1.04	0.03
	1.03	1.05	0.02
19.0	1.04	1.05	0.01
	1.04	1.05	0.01
	1.04		
	1.04		
	1.04		
20.0	1.05		
22.0	1.07		
24.0	1.08		
26.0	1.09		
28.0	1.10		
30.0	1.12		

Σ POINTS = 91

22 CHECK POINTS

AVERAGE CHANGE = 0.70%

WALL – PLANE PROBE

T_b = 45.1 °C

I_g = 6.0 A

I_v = 5.0 A

F5

8/24/66

V (VOLTS)	i_p (MA)	i_+	i_-
3.0	72.9	0.2	73.1
	73.0		73.2
	72.9		73.1
	72.6		72.8
	~~72.4~~		72.6
4.0	71.8		72.0
	71.1		71.3
	71.0		71.32
	70.7		70.9
	70.5		70.7
5.0	70.1		70.3
	69.8		70.0
	69.7		69.9
	69.4		69.6
	69.1		69.3
6.0	68.8		69.0
	68.3		68.5
	68.0		68.2
	67.8		68.0
	67.2		67.4
7.0	66.8		67.0
	66.2		66.4
	65.8		66.0
	64.7		64.9
	61.8		62.0
8.0	56.9		57.1
	50.8		51.0
	45.0		45.2
	39.5		39.7
	34.2		34.4
9.0	29.4		29.6
	25.1		25.3
	21.2		21.4
	17.8		18.0
	14.8		15.0
10.0	12.3		12.5
	10.2	0.2	10.4
	7.88	0.18	8.06
	6.51		6.69
	5.32		5.50
11.0	4.33		4.51
	3.49		3.67
	2.82		3.00
	2.24		2.42
	1.78		1.96
12.0	1.40		1.58
	1.10	0.18	1.28
	0.785	0.185	0.970
	0.605	0.185	0.790
	0.452	0.185	0.637

V	i_p	i_+	i_-
13.0	0.332	0.186	0.518
	0.232	0.186	0.418
	0.148	0.186	0.334
	0.0730	0.187	0.260
	0.014	0.187	0.201
14.0	0.0352	0.187	0.152
	0.0725	0.187	0.114
	0.105	0.188	0.083
	0.126	0.188	0.062
	0.141	0.188	0.047
15.0	0.152	0.188	0.036
	0.160	0.188	0.028
	0.168	0.188	0.020
	0.172	0.189	0.017
	0.177	0.189	0.012
16.0	0.179	0.190	0.011
	0.182	0.190	0.008
	0.183	0.190	0.007
	0.185	0.190	0.005
	0.186	0.191	0.005
17.0	0.188	0.191	0.003
	0.188	0.192	0.004
	0.189	0.192	0.003
	0.190	0.192	0.002
	0.190	0.192	0.002
18.0	0.192	0.193	0.001
	0.192		
	0.192		
	0.192		
	0.192		
19.0	0.193		
20.0	0.195		
22.0	0.199		
24.0	0.202		
26.0	0.203		
28.0	0.207		
30.0	0.209		

Σ POINTS = 87

22 CHECK POINTS

AVERAGE CHANGE = 0.4%

WIRE PROBE (ANODE)

T_b = 30.0 °C

I_z = 5.0 A

I_v = 5.0 A

F1

9/7/56

V (VOLTS)	i_p (MA)	i_+	i_-
0.0	137	0.4	137.4
	137		137.4
	135		135.4
	134		134.4
	133		133.4
1.0	132		132.4
	130		130.4
	129		129.4
	128		128.4
	127		127.4
2.0	125		125.4
	123		123.4
	122		122.4
	121		121.4
	119		119.4
3.0	117		117.4
	113		113.4
	109		109.4
	101		101.4
	86.8		87.2
4.0	77.1		77.5
	68.4		69.8
	60.9		61.3
	53.9		54.3
	47.5		47.9
5.0	42.1		42.5
	37.1		37.5
	33.1		33.5
	29.3		29.8
	26.0		26.4
6.0	22.9		23.3
	20.3		20.7
	18.1		18.5
	16.0		16.4
	14.1		14.5
7.0	12.5		12.9
	11.1	0.4	11.5
	9.35	0.41	9.76
	8.25		8.66
	7.37		7.78
8.0	6.57		6.98
	5.84	0.41	6.25
	5.20	0.42	5.62
	4.59		5.01
	4.10		4.52
9.0	3.62		4.04
	3.21		3.63
	2.85		3.27
	2.53		2.95
	2.21	0.42	2.63

V	i_p	i_+	i_-
10.0	1.96	0.42	2.38
	1.70	0.42	2.12
	1.48	0.42	1.90
	1.28	0.42	1.70
	1.10	0.43	1.53
11.0	0.885	0.426	1.311
	0.749	0.426	1.175
	0.627	0.427	1.054
	0.508	0.428	0.936
	0.403	0.429	0.832
12.0	0.313	0.429	0.742
	0.229	0.430	0.659
	0.152	0.431	0.583
	0.082	0.432	0.514
	0.020	0.433	0.453
13.0	0.037	0.434	0.397
	0.084	0.435	0.351
	0.132	0.435	0.303
	0.173	0.436	0.263
	0.209	0.437	0.228
14.0	0.240	0.438	0.198
	0.267	0.439	0.172
	0.292	0.440	0.148
	0.312	0.440	0.128
	0.331	0.441	0.110
15.0	0.348	0.442	0.094
	0.360	0.443	0.083
	0.374	0.444	0.070
	0.385	0.445	0.060
	0.395	0.446	0.051
16.0	0.403	0.447	0.044
	0.411	0.447	0.036
	0.416	0.448	0.032
	0.422	0.449	0.027
	0.428	0.450	0.022
17.0	0.431	0.451	0.020
	0.434	0.452	0.018
	0.439	0.453	0.014
	0.441	0.453	0.012
	0.443	0.454	0.011
18.0	0.448	0.455	0.007
19.0	0.454		
20.0	0.462		
22.0	0.473		
24.0	0.482		
26.0	0.492		
28.0	0.502		

Σ POINTS = 97

24 CHECK POINTS

AVERAGE CHANGE = 0.40

CENTER – PLANE PROBE

T_b = 30.0 °C

I_g = 5.0 A

I_v = 5.0 A

G2

9/7/56

V (VOLTS)	i_p (MA)	i_+	i_-
1.0	81.1	0.2	81.3
	80.8		81.0
	81.0		81.2
	8x0.2		80.4
	80.0		80.2
2.0	79.8		80.0
	79.2		79.4
	79.3		79.5
	78.8		79.0
	78.7		78.9
3.0	78.3		78.5
	77.8		78.0
	77.3		77.5
	76.9		77.1
	76.3		76.5
4.0	76.2		76.4
	75.7		75.9
	75.2		75.4
	75.0		75.2
	74.1		74.3
5.0	72.1		72.3
	68.5		68.7
	62.8		63.0
	57.3		57.5
	52.0		52.2
6.0	46.2		46.4
	41.1		41.3
	36.9		37.1
	32.6		32.8
	29.3		29.5
7.0	26.2		26.4
	23.2		23.4
	20.8		21.0
	18.4		18.6
	16.3		16.5
8.0	14.3		14.5
	12.8		13.0
	11.2	0.2	11.4
	9.42	0.24	9.66
	8.26		8.50
9.0	7.23		7.47
	6.32		6.56
	5.61		5.85
	4.93		5.17
	4.34		4.58
10.0	3.81		4.05
	3.35		3.59
	2.94		3.18
	2.59		2.83
	2.25	0.24	2.49

V	i_p	i_+	i_-
11.0	1.97	0.24	2.21
	1.71		1.95
	1.48		1.72
	1.27		1.51
	1.08	0.24	1.32
12.0	0.863	0.241	1.104
	0.733	0.241	0.974
	0.613	0.241	0.854
	0.500	0.242	0.742
	0.405	0.242	0.647
13.0	0.311	0.242	0.553
	0.238	0.242	0.480
	0.163	0.243	0.406
	0.103	0.243	0.346
	0.046	0.244	0.290
14.0	0.005	0.244	0.239
	0.048	0.244	0.196
	0.086	0.245	0.159
	0.121	0.245	0.124
	0.149	0.245	0.096
15.0	0.172	0.246	0.074
	0.187	0.246	0.059
	0.200	0.246	0.046
	0.210	0.247	0.037
	0.217	0.247	0.030
16.0	0.223	0.247	0.024
	0.228	0.247	0.019
	0.232	0.248	0.016
	0.235	0.248	0.013
	0.239	0.249	0.010
17.0	0.240	0.249	0.009
	0.242	0.250	0.008
	0.243	0.250	0.007
	0.244	0.251	0.007
	0.246	0.251	0.005
18.0	0.248	0.252	0.004
	0.248	0.252	0.004
	0.249	0.252	0.003
	0.250	0.252	0.002
	0.251	0.2525	0.0015
19.0	0.252	0.253	0.001
20.0	0.255		
22.0	0.259		
24.0	0.263		
26.0	0.267		
28.0	0.270		

Σ POINTS = 100

23 CHECK POINTS

AVERAGE CHANGE = 0.5%

DISK PROBE

T_b = 30.0 °C

I_y = 5.0 A

I_U = 6.0 A

G-3

9/7/56

V (VOLTS)	i_p (MA)	i_+	i_-
1.0	81.6	0.2	81.8
	81.3		81.5
	81.0		81.2
	81.0		81.2
	80.3		80.5
2.0	79.9		80.1
	79.2		79.4
	78.5		78.7
	78.6		78.8
	77.9		78.1
3.0	77.8		78.0
	77.0		77.2
	76.5		76.7
	76.3		76.5
	75.5		75.7
4.0	75.3		75.5
	74.9		75.1
	74.5		74.7
	73.6		73.8
	73.2		73.4
5.0	72.8		73.0
	71.9		72.1
	70.4		70.6
	67.3		67.5
	62.5		62.7
6.0	56.9		57.1
	50.3		50.5
	44.6		44.8
	39.8		40.0
	35.2		35.4
7.0	31.0		31.2
	27.2		27.4
	23.9		24.1
	21.1		21.3
	18.4		18.6
8.0	16.2		16.4
	14.2		14.4
	12.3		12.5
	10.8	0.2	11.0
	8.85	0.22	9.07
9.0	7.67		7.89
	6.74		6.96
	5.80		6.02
	5.09		5.31
	4.41		4.63
10.0	3.83		4.05
	3.31		3.53
	2.88		3.10
	2.49		2.71
	2.17	0.22	2.39

V	i_p	i_+	i_-
11.0	1.88	0.219	2.10
	1.61	0.219	1.83
	1.38	0.220	1.60
	1.17	0.220	1.39
	1.00	0.220	1.22
12.0	0.783	0.221	1.004
	0.655	0.221	0.876
	0.543	0.222	0.765
	0.438	0.223	0.661
	0.352	0.223	0.575
13.0	0.272	0.223	0.495
	0.202	0.223	0.425
	0.138	0.223	0.361
	0.083	0.224	0.307
	0.035	0.224	0.259
14.0	0.006	0.224	0.218
	0.042	0.225	0.183
	0.071	0.225	0.154
	0.096	0.225	0.129
	0.120	0.226	0.106
15.0	0.139	0.226	0.087
	0.155	0.227	0.072
	0.168	0.227	0.059
	0.177	0.227	0.050
	0.187	0.228	0.041
16.0	0.193	0.228	0.035
	0.201	0.228	0.027
	0.205	0.228	0.023
	0.210	0.229	0.019
	0.213	0.229	0.016
17.0	0.216	0.230	0.014
	0.218	0.230	0.012
	0.221	0.230	0.009
	0.222	0.231	0.009
	0.223	0.231	0.008
18.0	0.225	0.232	0.007
	0.227	0.232	0.005
	0.228	0.232	0.004
	0.229	0.2325	0.0035
	0.229	0.233	0.004
19.0	0.230	0.233	0.003
20.0	0.231		
22.0	0.238		
24.0	0.242		
26.0	0.246		
28.0	0.250		

Σ POINTS = 96

24 CHECK POINTS

AVERAGE CHANGE = 0.30%

WIRE PROBE (CATHODE)

T_b = 30.0 °C

I_g = 5.0 A

I_v = 5.0 A

G-4

7/7/56

V (VOLTS)	i_p (MA)	i_+	i_-
0.0	151	0.4	151.4
	151		151.4
	150		150.4
	150		150.4
	149		149.4
1.0	148		148.4
	148		148.4
	147		147.4
	146		146.4
	143		143.4
2.0	142		142.4
	141		141.4
	140		140.4
	140		140.4
	139		139.4
3.0	138		138.4
	137		137.4
	135		135.4
	135		135.4
	133		133.4
4.0	132		132.4
	131		131.4
	130		130.4
	129		129.4
	127		127.4
5.0	125		125.4
	122		122.4
	121		121.4
	120		120.4
	118		118.4
6.0	114		114.4
	110		110.4
	104		104.4
	91.2		91.6
	81.7		82.1
7.0	73.1		73.5
	64.1		64.5
	56.9		57.3
	50.3		50.7
	44.6		45.0
8.0	39.9		40.3
	35.3		35.7
	31.2		31.6
	27.8		28.2
	24.6		25.0
9.0	21.9		22.3
	19.5		19.9
	17.1		17.5
	15.1		15.5
	13.3	0.4	13.8

V	i_p	i_+	i_-
10.0	11.9	0.4	12.3
	10.4	0.4	10.8
	8.79	0.41	9.20
	7.70	0.41	8.11
	6.79	0.41	7.20
11.0	5.99	0.41	6.40
	5.25	0.42	5.67
	4.60	0.42	5.02
	4.03	0.42	4.45
	3.51	0.42	3.93
12.0	3.06	0.42	3.48
	2.65	0.42	3.07
	2.28	0.42	2.70
	1.94	0.42	2.36
	1.63	0.42	3.05
13.0	1.37	0.42	1.79
	1.13	0.42	1.55
	0.855	0.42	1.28
	0.690	0.426	1.116
	0.529	0.427	0.956
14.0	0.393	0.428	0.821
	0.275	0.429	0.704
	0.170	0.430	0.600
	0.072	0.430	0.502
	0.011	0.431	0.420
15.0	0.079	0.432	0.353
	0.139	0.433	0.294
	0.189	0.434	0.245
	0.232	0.435	0.203
	0.269	0.436	0.167
16.0	0.298	0.436	0.138
	0.321	0.437	0.116
	0.343	0.438	0.095
	0.360	0.439	0.079
	0.374	0.440	0.066
17.0	0.388	0.441	0.053
	0.398	0.442	0.044
	0.404	0.443	0.037
	0.413	0.445	0.032
	0.419	0.445	0.026
18.0	0.423	0.446	0.023
19.0	0.442		
20.0	0.450		
22.0	0.465		
24.0	0.475		
26.0	0.485		
28.0	0.495		

Σ POINTS = 97

24 CHECK POINTS

AVERAGE CHANGE = 0.5%

WALL - PLANE PROBE

T_b = 30.0 °C

I_y = 5.0 A

I_v = 5.0 A.

G-5

9/7/56

V (VOLTS)	i_p (MA)	i_+	i_-
1.0	40.2	0.1	40.3
	40.1		40.2
	40.1		40.2
	39.9		40.0
	39.8		39.9
2.0	39.7		39.8
	39.4		39.5
	39.2		39.3
	39.0		39.1
	38.8		38.9
3.0	38.3		38.4
	38.2		38.3
	38.2		38.3
	38.0		38.1
	37.8		37.9
4.0	37.6		37.7
	37.4		37.5
	37.4		37.5
	37.1		37.2
	36.9		37.0
5.0	36.5		36.6
	36.2		36.3
	35.7		35.8
	34.7		34.8
	34.3		34.4
6.0	31.8		31.9
	29.8		29.9
	27.3		27.4
	24.9		25.0
	22.4		22.5
7.0	20.2		20.3
	18.1		18.2
	16.3		16.4
	14.5		14.6
	12.9		13.0
8.0	11.5		11.6
	10.2	0.1	10.3
	8.52	0.11	8.63
	7.49		7.60
	6.35		6.46
9.0	5.88		5.99
	5.18		5.29
	4.58		4.69
	4.14		4.25
	3.57		3.68
10.0	3.13		3.24
	2.77		2.88
	2.41		2.52
	2.12		2.23
	1.87	0.11	1.98

V	i_p	i_+	i_-
11.0	1.62	0.11	1.73
	1.41	0.11	1.52
	1.23	0.11	1.34
	1.08	0.11	1.19
	0.870	0.113	0.983
12.0	0.745	0.113	0.858
	0.632	0.113	0.745
	0.535	0.113	0.648
	0.445	0.114	0.559
	0.369	0.114	0.483
13.0	0.299	0.114	0.413
	0.238	0.114	0.352
	0.188	0.115	0.303
	0.139	0.115	0.254
	0.0949	0.115	0.210
14.0	0.058	0.116	0.174
	0.028	0.116	0.144
	0.002	0.116	0.118
	0.023	0.117	0.094
	0.0432	0.117	0.074
15.0	0.0598	0.117	0.057
	0.0730	0.117	0.044
	0.0825	0.117	0.034
	0.0899	0.117	0.027
	0.0960	0.117	0.021
16.0	0.100	0.118	0.018
	0.107	0.118	0.011
	0.110	0.118	0.008
	0.112	0.118	0.006
	0.113	0.118	0.005
17.0	0.114	0.118	0.004
	0.116	0.118	0.002
	0.117	0.118	0.001
	0.118	0.119	0.001
	0.118	0.119	0.001
18.0	0.119	0.120	0.001
	0.120		
	0.120		
	0.120		
	0.121		
19.0	0.121		
20.0	0.122		
22.0	0.125		
24.0	0.128		
26.0	0.130		
28.0	0.131		

Σ POINTS = 96

24 CHECK POINTS

AVERAGE CHANGE = 0.90%

WIRE PROBE (ANODE)

T_b = 30.0 °C

I_z = 6.0 A.

I_v = 5.0 A.

H1

9/10/56

V (VOLTS)	i_p (MA)	i_+	i_-
0.0	172	0.5	172.5
	171		171.5
	170		170.5
	169		169.5
	168		168.5
1.0	167		167.5
	163		163.5
	162		162.5
	161		161.5
	160		160.5
2.0	159		159.5
	156		156.5
	154		154.6
	153		153.5
	151		151.5
3.0	149		149.5
	145		145.5
	140		140.5
	132		132.5
	120		120.5
4.0	108		108.5
	90.3		90.8
	79.6		80.1
	70.4		70.9
	62.2		62.7
5.0	55.4		55.9
	49.0		49.5
	43.3		43.8
	38.2		38.7
	33.5		34.0
6.0	29.8		30.3
	26.3		26.8
	23.4		23.9
	20.8		21.3
	18.2		18.7
7.0	16.1		16.6
	14.1		14.6
	12.6		13.1
	11.1	0.5	11.6
	9.39	0.51	9.90
8.0	8.31	0.51	8.82
	7.40	0.51	7.91
	6.58	0.52	7.10
	5.82	0.52	6.34
	5.17	0.52	5.69
9.0	4.58	0.52	5.10
	4.02	0.52	4.54
	3.55	0.52	4.07
	3.13	0.52	3.65
	2.77	0.52	3.29

V	i_p	i_+	i_-
10.0	2.42	0.52	2.94
	2.11	0.52	2.63
	1.82	0.52	2.38
	1.58	0.52	2.10
	1.35	0.52	1.87
11.0	1.14	0.53	1.67
	0.909	0.528	1.437
	0.757	0.529	1.286
	0.613	0.530	1.143
	0.484	0.531	1.015
12.0	0.371	0.532	0.903
	0.272	0.533	0.805
	0.178	0.534	0.712
	0.090	0.535	0.625
	0.015	0.536	0.551
13.0	0.051	0.537	0.486
	0.114	0.538	0.424
	0.169	0.539	0.370
	0.216	0.540	0.324
	0.259	0.541	0.298
14.0	0.296	0.542	0.246
	0.329	0.543	0.214
	0.358	0.544	0.186
	0.384	0.545	0.170
	0.409	0.546	0.137
15.0	0.428	0.547	0.119
	0.446	0.548	0.102
	0.462	0.549	0.087
	0.478	0.549	0.071
	0.490	0.550	0.060
16.0	0.498	0.550	0.052
	0.505	0.551	0.046
	0.515	0.552	0.037
	0.522	0.553	0.031
	0.529	0.555	0.026
17.0	0.535	0.556	0.021
	0.541	0.557	0.016
	0.544	0.558	0.014
	0.548	0.559	0.011
	0.551	0.560	0.009
18.0	0.553	0.560	0.007
	0.552		
	0.556		
	0.559		
	0.560		
19.0	0.562		
20.0	0.571		
22.0	0.581		
24.0	0.593		
26.0	0.603		
28.0	0.614		

Σ POINTS = 101 24 CHECK POINTS AVERAGE CHANGE = 0.4%

WIRE PROBE (CATHODE)

$T_b = 30.0\ ^\circ C$

$I_z = 6.0\ A$

$I_u = 5.0\ A$

H_2

9/10/56

V (VOLTS)	i_p (MA)	i_+	i_-
1.0	180	0.5	180.5
	180		180.5
	180		180.5
	179		179.5
	178		178.5
2.0	177		177.5
	177		177.5
	175		175.5
	173		173.5
	172		172.5
3.0	171		171.5
	170		170.5
	170		170.5
	169		169.5
	168		168.5
4.0	164		164.5
	163		163.5
	162		162.5
	160		160.5
	159		159.5
5.0	158		158.5
	156		156.5
	153		153.5
	151		151.5
	149		149.5
6.0	145		145.5
	140		140.5
	133		133.5
	122		122.5
	110		110.5
7.0	93.2		93.7
	81.1		81.6
	72.8		73.3
	65.2		65.7
	57.8		58.3
8.0	50.8		51.3
	49.9		50.4
	39.8		40.3
	35.4		35.9
	31.3		31.8
9.0	27.9		28.4
	24.8		25.3
	21.8		22.3
	19.2		19.7
	16.9		17.4
10.0	14.9		15.4
	13.1		13.6
	11.6		12.1
	10.2	0.5	10.7
	8.48	0.50	8.98

V	i_p	i_+	i_-
11.0	7.49	0.50	7.99
	6.58	0.50	7.08
	5.75	0.50	6.25
	4.99	0.50	5.49
	4.34	0.50	4.84
12.0	3.78	0.50	4.28
	3.27	0.50	3.77
	2.82	0.50	3.32
	2.42	0.51	2.93
	2.07	0.51	2.58
13.0	1.72	0.51	2.23
	1.42	0.51	1.93
	1.16	0.51	1.67
	0.862	0.511	1.373
	0.675	0.512	1.187
14.0	0.507	0.514	1.021
	0.358	0.515	0.873
	0.225	0.517	0.742
	0.116	0.518	0.634
	0.008	0.519	0.527
15.0	0.073	0.520	0.447
	0.152	0.521	0.369
	0.213	0.522	0.309
	0.269	0.523	0254
	0.314	0.524	0.210
16.0	0.352	0.525	0.173
	0.384	0.527	0.143
	0.411	0.528	0.117
	0.431	0.529	0.098
	0.450	0.530	0.080
17.0	0.466	0.531	0.065
	0.480	0.532	0.052
	0.491	0.533	0.042
	0.499	0.535	0.036
	0.507	0.537	0.030
18.0	0.513	0.538	0.025
	0.519	0.539	0.020
	0.524	0.540	0.016
	0.529	0.541	0.012
	0.529	0.542	0.013
19.0	0.533	0.543	0.010
20.0	0.549		
22.0	0.562		
24.0	0.573		
26.0	0.588		
28.0	0.598		

Σ POINTS = 96

23 CHECK POINTS

AVERAGE CHANGE = 0.4%

CENTER-PLANE PROBE

T_b = 30.0 °C

I_z = 6.0 A

I_U = 5.0 A

H_3

9/10/5 C

V (VOLTS)	i_p (MA)	i_+	i_-
0.0	110	0.3	110.3
	110		110.3
	110		110.3
	110		110.3
	110		110.3
1.0	108		108.3
	108		108.3
	108		108.3
	108		108.3
	107		107.3
2.0	106		106.3
	106		106.3
	105		105.3
	104		104.3
	104		104.3
3.0	104		104.3
	103		103.3
	103		103.3
	103		103.3
	102		102.3
4.0	101		101.3
	98.3		98.6
	97.2		98.0
	96.8		97.1
	95.4		95.7
5.0	93.2		93.5
	88.8		89.1
	81.4		81.7
	73.9		74.2
	66.2		66.5
6.0	59.9		60.2
	53.9		54.2
	47.8		48.1
	42.8		43.1
	37.8		38.1
7.0	33.4		33.7
	29.9		30.2
	26.4		26.7
	23.6		23.9
	20.9		21.2
8.0	18.5		18.8
	16.2		16.5
	14.3		14.6
	12.8		13.1
	11.1	0.3	11.4
9.0	9.33	0.30	9.63
	8.17		8.47
	7.23		7.53
	6.38		6.68
	5.58	0.30	5.88

V	i_p	i_+	i_-
10.0	4.89	0.30	5.19
	4.30		4.60
	3.74		4.04
	3.27		3.57
	2.85		3.15
11.0	2.49		2.79
	2.18		2.48
	1.85		2.15
	1.56		1.86
	1.34		1.64
12.0	1.14	0.30	1.44
	0.902	0.301	1.203
	0.742	0.302	1.044
	0.618	0.302	0.920
	0.486	0.303	0.789
13.0	0.373	0.303	0.676
	0.284	0.304	0.588
	0.200	0.304	0.504
	0.125	0.305	0.430
	0.055	0.305	0.360
14.0	0.006	0.305	0.299
	0.057	0.306	0.249
	0.109	0.306	0.197
	0.152	0.307	0.155
	0.188	0.307	0.119
15.0	0.213	0.308	0.095
	0.234	0.308	0.074
	0.251	0.309	0.058
	0.263	0.309	0.046
	0.274	0.309	0.035
16.0	0.281	0.310	0.029
	0.288	0.310	0.022
	0.292	0.310	0.018
	0.298	0.311	0.013
	0.301	0.312	0.011
17.0	0.302	0.312	0.010
	0.304	0.312	0.008
	0.307	0.313	0.006
	0.308	0.313	0.005
	0.310	0.314	0.006
18.0	0.311	0.315	0.004
19.0	0.317		
20.0	0.319		
22.0	0.323		
24.0	0.328		
26.0	0.333		
28.0	0.338		

Σ POINTS = 97

24 CHECK POINTS

AVERAGE CHANGE = 0.8%

WALL – PLANE PROBE

T_b = 30.0 °C

I_y = 6.0 A

I_v = 5.0 A

H4

9/10/56

V (VOLTS)	i_p (MA)	i_+	i_-
1.0	49.9	0.1	50.0
	49.8		49.9
	49.5		46.6
	49.3		49.4
	49.2		49.3
2.0	49.0		49.1
	48.8		48.9
	48.5		48.5
	48.1		48.2
	48.0		48.1
3.0	47.8		47.9
	47.4		47.5
	47.3		47.4
	47.2		47.3
	46.8		46.9
4.0	46.5		46.6
	46.5		46.6
	46.1		46.2
	45.8		45.9
	45.6		45.7
5.0	45.2		45.3
	44.5		44.6
	44.0		44.1
	43.1		43.2
	41.8		41.9
6.0	39.9		40.0
	36.9		37.0
	33.9		34.0
	31.0		31.1
	28.2		28.3
7.0	25.6		25.7
	22.8		22.9
	20.4		20.5
	18.2		18.3
	16.1		16.2
8.0	14.3		14.4
	12.8		12.9
	11.2	0.1	11.3
	9.35	0.14	9.49
	8.22		8.36
9.0	7.30		7.44
	6.42		6.56
	5.64		5.78
	4.96		5.10
	4.37		4.51
10.0	3.83		3.97
	3.35		3.49
	2.95		3.09
	2.59		2.73
	2.27	0.14	2.41

V	i_p	i_+	i_-
11.0	1.99	0.14	2.13
	1.72		1.86
	1.51		1.65
	1.30		1.44
	1.11	0.14	1.25
12.0	0.890	0.142	1.032
	0.765	0.142	0.897
	0.641	0.142	0.783
	0.538	0.143	0.681
	0.441	0.143	0.584
13.0	0.359	0.143	0.502
	0.289	0.143	0.432
	0.220	0.143	0.363
	0.166	0.143	0.309
	0.113	0.144	0.257
14.0	0.0680	0.144	0.212
	0.0302	0.144	0.174
	0.004	0.144	0.140
	0.0331	0.145	0.112
	0.590	0.145	0.086
15.0	0.0782	0.145	0.067
	0.0426	0.145	0.052
	0.107	0.145	0.038
	0.115	0.145	0.030
	0.122	0.146	0.024
16.0	0.127	0.146	0.019
	0.132	0.146	0.014
	0.134	0.146	0.012
	0.138	0.147	0.009
	0.139	0.147	0.008
17.0	0.140	0.147	0.007
	0.141	0.147	0.006
	0.142	0.148	0.006
	0.143	0.148	0.005
	0.144	0.148	0.004
18.0	0.145	0.148	0.003
19.0	0.149		
20.0	0.150		
22.0	0.152		
24.0	0.155		
26.0	0.158		
28.0	0.159		

Σ POINTS = 96

23 CHECK POINTS

AVERAGE CHANGE = 0.6%

DISK PROBE

$T_b = 30.0$ °C

$I_z = 6.0$ A

$I_v = 5.0$ A

H5

9/10/56

V (VOLTS)	i_p (MA)	i_+	i_-
0.0	109	0.3	109.3
	109		109.3
	108		108.3
	108		108.3
	107		107.3
1.0	106		106.3
	105		105.3
	105		105.3
	104		104.3
	104		104.3
2.0	103		103.3
	103		103.3
	103		103.3
	102		102.3
	102		102.3
3.0	102		102.3
	101		101.3
	96.87		97.0
	96.2		96.5
	95.88		96.1
4.0	94.9		95.2
	94.5		94.8
	94.2		94.5
	94.0		94.3
	93.2		93.5
5.0	92.1		92.4
	91.1		91.4
	89.8		90.1
	86.2		86.5
	80.3		80.6
6.0	73.2		73.5
	65.2		65.5
	58.2		58.5
	51.6		51.9
	45.5		45.8
7.0	39.9		40.2
	35.0		35.3
	30.9		31.2
	27.2		27.5
	23.8		24.1
8.0	20.8		21.1
	18.0		18.3
	15.5		15.8
	13.7		14.0
	11.9		12.2
9.0	10.2	0.3	10.5
	8.38	0.27	8.65
	7.29	0.27	7.56
	6.38	0.27	6.66
	5.45	0.27	5.72

V	i_p	i_+	i_-
10.0	4.65	0.27	4.92
	4.02	0.27	4.29
	3.49	0.27	3.76
	3.02	0.27	3.29
	2.59	0.27	2.86
11.0	2.22	0.27	2.49
	1.91	0.27	2.18
	1.62	0.27	1.89
	1.38	0.27	1.65
	1.17	0.27	1.44
12.0	0.909	0.273	1.182
	0.752	0.273	1.025
	0.621	0.274	0.895
	0.501	0.274	0.775
	0.393	0.274	0.667
13.0	0.303	0.275	0.578
	0.219	0.275	0.494
	0.146	0.275	0.421
	0.080	0.276	0.356
	0.025	0.276	0.301
14.0	0.022	0.277	0.255
	0.0635	0.277	0.213
	0.100	0.278	0.178
	0.129	0.278	0.149
	0.155	0.278	0.123
15.0	0.176	0.279	0.103
	0.195	0.279	0.084
	0.210	0.280	0.070
	0.222	0.280	0.058
	0.233	0.280	0.047
16.0	0.241	0.281	0.040
	0.249	0.281	0.032
	0.255	0.282	0.027
	0.260	0.282	0.022
	0.264	0.282	0.019
17.0	0.267	0.283	0.016
	0.270	0.283	0.013
	0.272	0.284	0.012
	0.275	0.284	0.009
	0.277	0.285	0.008
18.0	0.279	0.285	0.006
19.0	0.283		
20.0	0.288		
22.0	0.293		
24.0	0.298		
26.0	0.302		
28.0	0.307		

Σ POINTS = 97

25 CHECK POINTS

AVERAGE CHANGE = 0.3 %

WIRE PROBE (ANODE)

T_b = 45.1 °C

I_z = 4.0 A

I_v = 5.0 A

I,

9/11/5C

V (VOLTS)	i_p (MA)	i_+	i_-
0.0	222	0.6	222.6
	221		221.6
	221		221.6
	220		220.6
	219		219.6
1.0	218		218.6
	217		217.6
	215		215.6
	214		214.6
	212		212.6
2.0	211		211.6
	211		211.6
	209		209.6
	208		208.6
	207		207.6
3.0	203		203.6
	202		202.6
	201		201.6
	200		200.6
	198		198.6
4.0	195		195.6
	193		193.6
	190		190.6
	188		188.6
	182		182.6
5.0	171		171.6
	152		152.6
	132		132.6
	114		114.6
	92.0		92.6
6.0	78.5		79.1
	66.7		67.3
	56.2		56.8
	47.0		47.6
	39.5		40.1
7.0	32.9		33.5
	27.6		28.1
	23.0		23.6
	19.0		19.6
	15.8		16.4
8.0	12.9		13.5
	10.5	0.6	11.1
	8.09	0.60	8.69
	6.62	0.60	7.22
	5.34	0.61	5.95
9.0	4.28	0.61	4.89
	3.38	0.61	3.99
	2.65	0.61	3.26
	2.06	0.61	2.67
	1.56	0.61	2.17

V	i_p	i_+	i_-
10.0	1.14	0.61	1.75
	0.759	0.612	1.371
	0.520	0.612	1.133
	0.321	0.614	0.935
	0.155	0.616	0.771
11.0	0.013	0.617	0.630
	0.100	0.618	0.518
	0.195	0.619	0.424
	0.274	0.619	0.345
	0.331	0.620	0.289
12.0	0.379	0.621	0.242
	0.420	0.622	0.202
	0.454	0.623	0.169
	0.482	0.624	0.142
	0.508	0.626	0.118
13.0	0.529	0.627	0.098
	0.546	0.628	0.082
	0.562	0.629	0.067
	0.576	0.630	0.054
	0.583	0.631	0.048
14.0	0.593	0.632	0.039
	0.599	0.633	0.034
	0.605	0.634	0.029
	0.608	0.635	0.027
	0.612	0.636	0.024
15.0	0.618	0.637	0.019
	0.619	0.638	0.019
	0.625	0.639	0.014
	0.628	0.640	0.012
	0.630	0.641	0.011
16.0	0.632	0.642	0.010
	0.635	0.643	0.008
	0.638	0.644	0.006
	0.638	0.645	0.007
	0.639	0.646	0.007
17.0	0.641	0.647	0.006
	0.643	0.648	0.005
	0.645	0.649	0.004
	0.647	0.650	0.003
	0.651		
18.0	0.651		
19.0	0.658		
20.0	0.661		
22.0	0.672		
24.0	0.685		
26.0	0.698		
28.0	0.706		

Σ POINTS = 97

24 CHECK POINTS

AVERAGE CHANGE = 0.60%

WIRE PROBE (CATHODE)

T_b = 45.1°C

I_z = 4.0 A

I_v = 5.0 A

I_2

9/11/56

V (VOLTS)	i_p (MA)	i_+	i_-
2.0	238	0.6	239.6
	238		238.6
	238		238.6
	237		237.6
	235		235.6
3.0	235		235.6
	233		233.6
	231		231.6
	231		231.6
	230		230.6
4.0	230		230.6
	228		228.6
	228		228.6
	226		226.6
	224		224.6
5.0	222		222.6
	222		222.6
	220		220.6
	219		219.6
	218		218.6
6.0	214		214.6
	213		213.6
	212		212.6
	211		211.6
	208		208.6
7.0	206		206.6
	204		204.6
	203		203.6
	203		203.6
	199		199.6
8.0	195		195.6
	189		189.6
	174		174.6
	156		155.6
	136		136.6
9.0	118		118.6
	94.0		94.6
	79.8		80.4
	67.9		68[illegible]5
	57.2		57.8
10.0	48.1		48.7
	40.3		40.9
	33.9		34.5
	28.3		28.9
	23.6		24.2
11.0	19.4		20.0
	16.0		16.6
	13.1		13.7
	10.7	0.6	11.3
	8.11	0.61	8.72

V	i_p	i_+	i_-
12.0	6.59	0.62	7.21
	5.30	0.62	5.92
	4.21	0.62	4.83
	3.30	0.62	3.92
	2.57	0.63	3.20
13.0	1.97	0.63	2.60
	1.45	0.63	2.08
	1.04	0.63	1.67
	0.672	0.629	1.301
	0.428	0.631	1.059
14.0	0.232	0.632	0.864
	0.060	0.633	0.693
	0.065	0.634	0.569
	0.178	0.635	0.457
	0.269	0.636	0.367
15.0	0.339	0.637	0.298
	0.399	0.638	0.239
	0.443	0.639	0.196
	0.485	0.640	0.155
	0.511	0.642	0.131
16.0	0.540	0.643	0.103
	0.559	0.644	0.085
	0.577	0.646	0.069
	0.592	0.647	0.055
	0.605	0.648	0.043
17.0	0.616	0.649	0.033
	0.6[illegible]23	0.650	0.027
	0.6[illegible]30	0.651	0.021
	0.638	0.652	0.014
	0.6[illegible]40	0.653	0.013
18.0	0.642	0.655	0.013
	644	0.656	0.012
	650	0.657	0.007
	652	0.658	0.006
	658	0.660	0.002
19.0	0.660	0.660	
20.0	0.668		
22.0	0.682		
24.0	0.692		
26.0	0.705		
28.0	0.718		

Σ POINTS = 95

23 CHECK POINTS

AVERAGE CHANGE = 0.5%

WALL - PLANE PROBE

$T_b = 45.1\ ^\circ C$

$I_z = 4.0\ A$

$I_u = 5.0\ A$

I_3

9/11/56

V (VOLTS)	i_p (MA)	i_+	i_-
3.0	46.9	0.1	47.0
	47.2		47.3
	47.0		47.1
	46.8		46.9
	46.3		46.4
4.0	46.2		46.3
	46.1		46.2
	45.9		46.0
	45.6		45.7
	45.4		45.5
5.0	45.1		45.2
	44.9		45.0
	44.7		44.8
	44.4		44.5
	44.2		44.3
6.0	44.2		44.3
	43.8		43.9
	43.6		43.7
	43.3		43.4
	42.9		43.0
7.0	42.8		42.9
	42.2		42.3
	41.8		41.9
	41.0		41.1
	39.1		39.2
8.0	35.6		35.7
	32.0		32.1
	28.5		28.6
	24.9		25.0
	21.8		21.9
9.0	18.2		18.3
	15.86		15.7
	13.2		13.3
	11.1	0.1	11.2
	8.79	0.12	8.91
10.0	7.30		7.42
	6.19		6.31
	5.02		5.14
	4.14		4.26
	3.38		3.50
11.0	2.75		2.87
	2.21		2.33
	1.79		1.91
	1.41		1.53
	1.11	0.12	1.23
12.0	0.818	0.118	0.936
	0.642	0.118	0.760
	0.499	0.119	0.618
	0.380	0.119	0.499
	0.288	0.119	0.407

V	i_p	i_+	i_-
13.0	0.213	0.120	0.333
	0.148	0.120	0.268
	0.0908	0.120	0.211
	0.0464	0.120	0.166
	0.011	0.121	0.132
14.0	0.021	0.121	0.100
	0.0452	0.121	0.076
	0.0648	0.121	0.056
	0.0792	0.122	0.043
	0.0892	0.122	0.033
15.0	0.0969	0.122	0.025
	0.105	0.122	0.017
	0.109	0.122	0.013
	0.112	0.1225	0.0105
	0.115	0.123	0.008
16.0	0.117	0.123	0.006
	0.119	0.123	0.004
	0.120	0.123	0.003
	0.120	0.123	0.003
	0.121	0.1235	0.0025
17.0	0.121	0.1235	0.0025
	0.122	0.124	0.002
	0.123	0.124	0.001
	0.123	0.1245	0.0015
	0.124	0.125	0.001
18.0	0.125	0.125	
	0.126		
	0.125		
	0.125		
	0.126		
19.0	0.127		
	0.127		
	0.127		
	0.127		
	0.128		
20.0	0.128		
21.0	0.129		
22.0	0.130		
24.0	0.131		
26.0	0.134		
28.0	0.137		

Σ POINTS = 95

22 CHECK POINTS

AVERAGE CHANGE = 0.3%

CENTER - PLANE PROBE

T_b = 45.1°C

I_z = 4.0 A

I_v = 5.0 A

I_4

9/11/56

V (VOLTS)	i_p (MA)	i_+	i_-
1.0	135	0.3	135.3
	135		135.3
	135		135.3
	134		134.3
	134		134.3
2.0	133		133.3
	133		133.3
	132		132.3
	132		132.3
	132		132.3
3.0	131		131.3
	131		131.3
	131		131.3
	130		130.3
	130		130.3
4.0	129		129.3
	129		129.3
	130		130.3
	129		129.3
	129		129.3
5.0	128		128.3
	127		127.3
	126		126.3
	125		125.3
	124		124.3
6.0	123		123.3
	123		123.3
	122		122.3
	120		120.3
	112		112.3
7.0	112		112.3
	111		111.3
	84.5		84.8
	73.3		73.6
	64.1		64.4
8.0	55.8		56.1
	47.9		48.2
	~~44.7~~ 41.1		41.4
	35.2		35.5
	30.0		30.3
9.0	25.3		25.6
	21.4		21.7
	18.0		18.3
	15.1		15.4
	12.5		12.8
10.0	10.3	0.3	10.6
	8.02	0.34	8.36
	6.60	0.34	6.94
	5.39	0.34	5.73
	4.34	0.34	4.68

V	i_p	i_+	i_-
11.0	3.48	0.34	3.82
	2.78	0.34	3.12
	2.19	0.34	2.53
	1.72	0.34	2.06
	1.32	0.34	1.66
12.0	0.918	0.340	1.258
	0.682	0.340	1.022
	0.488	0.340	0.828
	0.332	0.341	0.673
	0.202	0.342	0.544
13.0	0.085	0.342	0.427
	0.000	0.343	0.343
	0.081	0.344	0.263
	0.151	0.344	0.193
	0.205	0.345	0.140
14.0	0.243	0.345	0.102
	0.269	0.345	0.076
	0.288	0.345	0.057
	0.301	0.346	0.045
	0.311	0.346	0.035
15.0	0.319	0.347	0.028
	0.328	0.347	0.019
	0.331	0.348	0.017
	0.338	0.348	0.010
	0.339	0.349	0.010
16.0	0.341	0.349	0.008
	0.341	0.349	0.008
	0.343	0.350	0.007
	0.345	0.350	0.005
	0.347	0.350	0.003
17.0	0.347	0.351	0.004
	0.350	0.352	0.002
	0.351	0.352	0.001
	0.352	0.352	
	0.352	0.353	
18.0	0.352	0.353	
19.0	0.355		
20.0	0.359		
22.0	0.362		
24.0	0367		
26.0	0.372		
28.0	0.375		

Σ POINTS = 92

23 CHECK POINTS

AVERAGE CHANGE = 0.5%

DISK PROBE

$T_b = 48.1\ ^\circ C$

$I_z = 4.0\ A$

$I_v = 5.0\ A$

I5

9/11/56

V (VOLTS)	i_p (MA)	i_+	i_-
3.0	122	0.3	122.3
	121		121.3
	120		120.3
	120		120.3
	120		120.3
4.0	119		119.3
	119		119.3
	118		118.3
	118		118.3
	117		117.3
5.0	116		116.3
	115		115.3
	114		114.3
	113		113.3
	113		113.3
6.0	112		112.3
	112		112.3
	111		111.3
	110		110.3
	110		110.3
7.0	109		109.3
	107		107.3
	102		102.3
	87.1		87.4
	76.5		76.8
8.0	66.6		66.9
	57.2		57.5
	48.8		49.1
	41.2		41.5
	34.9		35.2
9.0	29.2		29.5
	24.1		24.4
	20.0		20.3
	16.7		17.0
	13.4		13.7
10.0	11.1	0.3	11.4
	8.32	0.29	8.61
	6.76		7.05
	5.42		5.71
	4.33		4.62
11.0	3.42		3.71
	2.68		2.97
	2.08		2.37
	1.59		1.88
	1.19	0.29	1.48
12.0	0.795	0.297	1.092
	0.572	0.298	0.870
	0.395	0.298	0.693
	0.254	0.298	0.552
	0.142	0.299	0.441

V	i_p	i_+	i_-
13.0	0.050	0.289	0.339
	0.019	0.290	0.271
	0.0725	0.290	0.217
	0.118	0.291	0.173
	0.153	0.291	0.138
14.0	0.183	0.292	0.109
	0.208	0.292	0.084
	0.225	0.293	0.068
	0.238	0.293	0.055
	0.250	0.293	0.043
15.0	0.260	0.294	0.034
	0.269	0.295	0.026
	0.275	0.295	0.020
	0.279	0.295	0.016
	0.284	0.296	0.012
16.0	0.288	0.297	0.009
	0.288	0.297	0.009
	0.291	0.297	0.006
	0.293	0.298	0.005
	0.294	0.298	0.004
17.0	0.295	0.299	0.004
	0.298	0.299	0.001
	0.299	0.300	0.001
	0.299	0.300	0.001
	0.300	0.301	0.001
18.0	0.300	0.302	0.002
	0.301		
	0.302		
	0.302		
	0.303		
19.0	0.303		
20.0	0.307		
22.0	0.311		
24.0	0.318		
26.0	0.321		
28.0	0.325		

Σ POINTS = 90

21 CHECK POINTS

AVERAGE CHANGE = 0.7%